Chemical and Biochemical Studies of Dityrosine Cross-link Formation in Amyloidogenic Peptides

Youssra Kareem Al-Hilaly

A thesis submitted for the degree of Doctor of Philosophy
Supervised by Professor Louise C Serpell
Department of Biochemistry
University of Sussex
January 2014

Declaration

I hereby declare that this thesis is my own work and to the best of my knowledge it contains no materials previously published or written by another person, or substantial proportions of material which have been accepted for the award of any other degree at any other University, except where due acknowledgement is made in the thesis. Any contribution made to the research by others, with whom I have worked at University or elsewhere, is explicitly acknowledged in the thesis.

Signature: ....

Youssra Kareem Al-Hilaly

Acknowledgements

Firstly, I thank GOD for every thing, thank Lord for every gift you have given me; my parents, life, husband, daughters, sisters, brothers, and friends. Thank you God for blessing me much more than I deserve and for being with me all the way.

This work was supported in part by grants from the Iraqi Government, Ministry of Higher Education and Scientific Research, a big thank you for this gift.

I would like to express my sincere thanks and deep appreciation to my supervisor, Professor Louise Serpell, for all her ideas, guidance, constant support, encouragement, and love throughout my project. Louise has been, and continues to be a first-class scientific mentor for me in my development as a research scientist, with unfailing patience and dedication to me as her student and friend.

I would like to express my thanks and appreciation to Dr. Alaa Abdul Sada, my second supervisor for all his encouragement and technical advice that have been invaluable throughout my studies. I would especially like to thank him for allowing me to freely use the facilities in his laboratory.

Special thanks to my co-worker, Dr. Kyle Morris for all his generosity of time and expertise in biophysical techniques and for his collaboration on the collection and analysis of X-ray fibre diffraction, CD and LD data. Kyle's collaboration and willingness to share material and expertise has been pivotal to the success of this study.

I am very grateful to Dr. Tom Williams for his help, idea, experiment planning, and for performing SDS-PAGE analysis of Aβ in Chapter five.

My sincere thanks to Dr. Julian Thorpe, Electron Microscopy Academic Research Manager, for all his guidance. I would especially like to thank him for his help in arranging samples for this study and for his helpful critique of my manuscripts and for preparing of sections of human brain tissue and neuroblastoma cells.

I am grateful to Professor Mark Bagley for his help in analysis of all NMR data and his critical reading of and valuable comments on Chapter three. I would like to thank Dr. Darren Thompson for his help in the gel electrophoresis training and for letting me use his equipment. Many thanks for Dr. Ian Day from the chemistry department for the NMR training and for his help in dityrosine NMR analysis.

I am grateful to my co-worker Maris, PhD student for her collaboration in the preparing of cultured neuroblastoma cells, and also for her support. Many thanks for Dr. Shahin Zibaee for providing the recombinant α-synuclein and for his critical reading and helpful comments on chapter six.

My special thanks and appreciation to Dr. Mathew Stanley for introducing me to organic chemistry field and for his help in the synthesis of dityrosine. I would like to express my appreciation to Raghad and Dr. Camilla from Professor Hill lab for their advice and help in mass spectrometry, thanks a lot.

I gratefully acknowledge Asma and Majid for their supporting and help throughout my project. They have been always there whenever I need them.

I would like to acknowledge the assistance and support I have received from all of my friends, colleagues and fellow students at the university of Sussex, Dr. Wendy Doyle, Dr. Karen Marshall, Liza, Lenzi, Zahraa and Zainab, my sincere thanks to everyone.

Finally, I would like to thank all of my family for their support and encouragement throughout my PhD candidature. In particular my lovely parents for their love and support. I would like to thank my husband, Basim, and my daughters, Zainab, Bara'a and Fatima for all their love, patience and loyalty and for their understanding of my need for time to work and study. Fatima born in the first days of my PhD study, and has been an enduring, unquestioning source of love. Moving forward from thesis submission, it is my foremost intention to spend more time with all of you (Basim, Zainab, Bara'a and Fatima).

" And Ootim of science only slightly"

Al-Israa Sura, Aya 85

You have been given only a little of the knowledge

University of Sussex
Youssra Kareem Al-Hilaly
A thesis submitted for the degree of Doctor of Philosophy

Chemical and Biochemical Studies of Dityrosine Cross-link Formation in Amyloidogenic Peptides

SUMMARY

Amyloid fibrils are associated with a large number of diseases in which proteins and peptides abnormally assemble to form insoluble amyloid that deposit in the tissues. However, oxidative stress has been implicated in the pathogenesis of a number of neurodegenerative diseases and is believed to play an important role in the amyloid deposition through protein cross-linkings. Under oxidative stress conditions, tyrosyl radicals can be formed and coupled to form dityrosine cross-linkage. The formation of dityrosine cross-linked oligomers is one of the oxidative modifications that may mediate the toxicity of amyloid β (Aβ) and α-synuclein (α-syn) in Alzheimer's disease (AD) and Parkinson's disease (PD) respectively. In this thesis, I explored the oxidative modification of two short peptides, HYFNIF and VIYKI, using a Cu^{2+}/H_2O_2 oxidation system, and studied the morphological and conformational changes of these amyloid fibrils during the oxidation process. These peptides were selected as simple amyloid model systems that have been previously structurally characterised, to better understand the dityrosine formation at a structural level and to optimise the oxidation conditions.

Oxidative stress has been implicated in AD. Here, I have explored the formation of dityrosine cross-linked Aβ42 *in vitro*. We have shown that dityrosine is generated in internalised Aβ in cell cultures. Results also revealed the prevalence of dityrosine crosslinks in amyloid plaques in brain tissue and cerebrospinal fluid from AD patients, indicating that dityrosine could be used as a biomarker of oxidative stress in AD.

The ability of the Cu^{2+} ion to promote the formation of *in vitro* dityrosine cross-linked α-syn was also explored and the effect on α-syn fibrillogenesis and conformation induced by Cu^{2+} was investigated. The results revealed the possibility of involvement

the dityrosine cross-linked α-syn dimer as a nucleus to initiate the polymerisation process of α-syn to form amyloid fibrils.

Dityrosine cross-linkages can be generated *in vitro* using oxidation system of Cu^{2+}/H_2O_2, and might play an important role in the solubility and assembly of amyloidogenic peptides and proteins that are associated in the pathogenesis of many neurodegenerative disease including AD and PD. Dityrosine cross-linkages can lend a further stability to the already stable amyloid fibrils, and this may explain their protease resistance. Dityrosine cross-links formation represents one of the possible pathways by which oligomers can be formed. Dityrosine cross-linked oligomers represent a good bio-index of oxidatively coupled tyrosine-contained proteins due to their high stability.

Table of Contents

Abbreviations

a.u.	Arbitrary Units
Aβ	Amyloid β
AD	Alzheimer's disease
AICD	APP intracellular domain
APP	Amyloid precursor protein
CD	Circular dichroism
CSF	Cerebrospinal fluid
DMSO	Dimethyl sulfoxide
ELISA	Enzyme-linked immunosorbent assay
EM	Electron microscopy
EtOAc	Ethyl acetate
HFPI	1,1,1,3,3,3-hexafluoro-2-propanol
HRP	Horseradish peroxidase
LC-ESIMS	Liquid chromatography-electrospray ion source mass spectrometry
LD	Linear dichroism
m/z	Mass charge ratio
MCO	Metal-catalysed oxidation
MeOH	Methanol
MPTP	1-methyl-4-phenyl-1,2,3,6- tetrahydropyridine
MRM	Multiple reaction monitoring
NAC	Non-Ab component of plaques
NMR	Nuclear magnetic resonance
PD	Parkinson's disease
pI	Isoelectric point
PICUP	Photo-induced cross-linking of unmodified protein
PMT	Photo multiplier tube
PrP	Prion protein
Q	Quadrupole
ROS	Reactive oxygen species
RP-HPLC	Reverse phase –high performance liquid chromatography
SDS-PAGE	Sodium dodecyl sulphate-poly acryl amide gel electrophoresis
SEM	Scanning electron microscope
SRCD	Synchrotron radiation CD
ssNMR	Solid-state nuclear magnetic resonance
STM	Scanning tunneling electron microscope
TEM	Transmission electron microscopy
TFA	Trifluoroacetic acid
Tg	Transgenic
ThT	Thioflavin T
TTR	Transthyretin
XRFD	X-ray fibre diffraction
ZnT3	Zinc transporter 3
α-syn	Alpha-synuclein

List of Figures

List of tables

1 Introduction

1.1 **Amyloid (an over view)**

Rudolf Virchow first used "amyloid" term in 1854 to describe a structure observed in human brain tissue (Cohen 1986; Virchow 1854; Westermark 2005). Virchow observed that wax-like deposits in brain tissue displayed a starch-like reaction with iodine and subsequently concluded that these inclusions were composed of carbohydrate and called them amyloid which is derived from the Latin *amylum*, meaning starch. Later, Friedrich and Kekule refuted the hypothesis of the cellulose nature of amyloid by discovering that these wax-like deposits were mainly composed of protein, and this was further confirmed by Hanssen, who revealed that amyloid is digestible with pepsin (Westermark 2005). Using electron microscopy (EM), Cohen and Calkins were able to identify the ultrastructure of amyloid *in vivo*, which has characteristic fine fibrillar morphology (Cohen and Calkins 1959). This was followed by *ex-vivo* EM study of amyloid fibres (Cohen 1982), showing that amyloid fibres have a width of 75 – 100 Å and indeterminate length. Connors *et al.* revealed the formation of *in vitro* amyloid fibrils from intact β-microglobulin, demonstrating that they are non-branching fibrils of indeterminate length with 8 – 10 nm in diameter by EM (Connors et al. 1985). These findings contributed early insights toward an understanding of amyloid structure.

The knowledge of the biochemical and structural nature of amyloid fibrils has increased over the time. By definition, amyloids are *in vivo* filamentous protein deposits, which are composed of self-assembled peptides formed of β-sheets that showed a typical cross-β X-ray diffraction pattern arising from cross-β structure (Harrison et al. 2007; Serpell et al. 1997; Westermark et al. 2007). Also, amyloid fibrils display an apple-green birefringence under cross-polarised lighted when binding to Congo red dye (Figure 1-1, A), and are found to be long, straight and unbranched by EM (Figure 1-1, B) (Rambaran and Serpell 2008; Serpell et al. 1997). Although amyloid proteins are biochemically different, they share distinct features: the ability to bind Congo red dye, fibril ultrastructure and typical cross-β X-ray diffraction pattern.

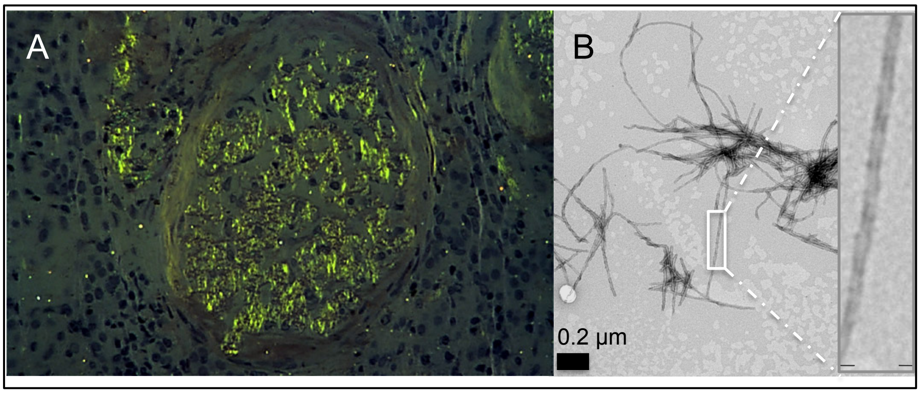

Figure 1-1: Characterisation of amyloid fibrils. A) Glomerulus from renal biopsy stained with Congo red and visualised by polarisation microscopy showing the classic apple-green birefringence characteristic of amyloid, adapted from (http://www.pathology.vcu.edu/education/). B) Negative stain electron micrograph of synthetic amyloid fibrils made from Aβ peptide that displays long, straight unbranched fibrils.

Although amyloid fibrils can be formed from many pathogenic precursor proteins implicated in a wide range of diseases, many non-pathogenic proteins including those that are naturally occurring or designed can produce amyloid fibrils, and this consequently added more criteria to define amyloid. A recent amyloid definition states: " to be included in the list, the protein has to be a major fibril protein in extracellular deposits, which have the characteristics of amyloid, including affinity for Congo Red with resulting green birefringence. Synthetic fibrils with amyloid properties are best named 'amyloid-like' " (Westermark 2005). Later on, it has been found that many proteins can form intracellular inclusions with typical amyloid structure (Westermark et al. 2007). Thus, the definition of amyloid has expanded to involve these intracellular amyloids, and also exclude any extracellular and intracellular deposits that do not fulfill the criteria of amyloid identity such as binding with Congo red dye and showing the typical green birefringence. Additional criteria have been added, including the ability bind Thioflavin T (ThT) dye giving enhanced fluorescence, although this is not necessarily fundamental (Pepys 2006). However, one criterion that has been accepted is that fibrils must display a cross-β structure to be called amyloid or amyloid-like (Meinhardt and Fandrich 2009; Sunde et al. 1997).

A diverse group of diseases of acquired or hereditary origin are associated with insoluble amyloid fibril deposition in the affected organs and are called "amyloidoses" (Westermark et al. 2007). The main component of amyloid deposits is the amyloid fibril, where a specific precursor protein is deposited in each kind of amyloidosis

(Westermark 2005). It has been revealed that amyloid toxicity is independent of polypeptide amino acid sequence, length and chirality (Pastor et al. 2008). However, it is clear that amyloid deposits in tissue contain other common components including glycosaminoglycans, apolipoprotein E and serum amyloid P-component (Uversky et al. 2006b; Westermark 2005). Amyloidoses are discussed in more detail below.

In contrast to their pathogenic role, it has been found that some amyloids have a functional role in many organisms, from bacteria to mammals, without observable toxic effect (Fowler et al. 2006; Maji et al. 2009; Maury 2009). Furthermore, amyloid fibres have recently been applied for industrial purpose, and this due to their high stability and strength (Sawada et al. 2013; Smith et al. 2006b).

1.2 Protein folding and misfolding

Proteins represent one of the most important biological molecules in the cells due to their biological role in controlling and regulating the majority of cellular processes. Proteins are synthesised on ribosomes where a linear sequence of amino acids can be produced through a specific translation process. For each newly synthesised protein to be functionally active, it needs to fold into a three-dimensional structure (Figure 1-2), which is a unique complex structure called the native state.

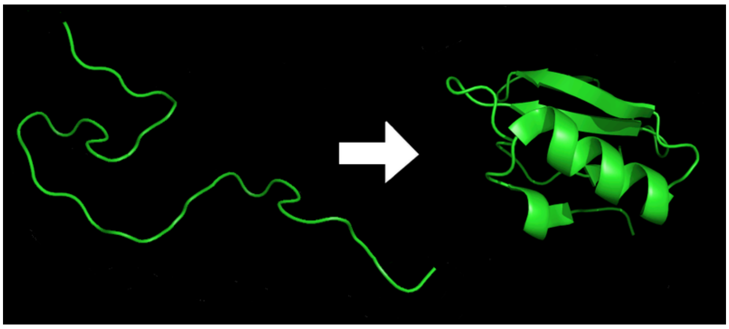

Figure 1-2: Folding of a linear amino acid sequence into a three-dimension structure. Reproduced from (http://physics.stackexchange.com).

Essentially, there are 20 different native amino acids that can be combined via peptide bonds to form an enormous number of different sized proteins. However, the native proteins consist of a specific amino acid sequences that encoded to fold into a native protein state. In 1973, Anfinsen had observed that ribonuclease A folded spontaneously into its native state *in vitro*, concluding that all required information for the native fold are contained within the primary amino acid sequence (Anfinsen 1973). Many experimental and theoretical studies have been designed to investigate the protein folding mechanism (Anfinsen 1973; Bartlett and Radford 2009; Dobson 2004; Lee et al. 2006; Radford and Dobson 1999; Vabulas et al. 2010). The Levinthal paradox highlighted that the folding of any polypeptide chain into its native state can not occur by a random search of all possible conformations, as this would take an unrealistic time compared with that actually observed for protein folding (Lenvinthal 1968). It has been suggested that protein folding is driven initially by hydrophobic collapse followed by formation of secondary structure forms within a polypeptide, and then formation of covalent bonds, such as S-S bond under oxidising conditions, that help to stabilise the final native state (Gething and Sambrook 1992).

Intermediate formation has observed to accompany the folding mechanism, and considered as the rule for larger proteins (> 100 amino acid), which have a high tendency to rapidly collapse in aqueous solution into compact non-native conformations (Bartlett and Radford 2009; Brockwell and Radford 2007). The polypeptide chain may fold by many routes, likely adopting multiple folded intermediates on-path to the native state (Onuchic and Wolynes 2004). A multidimensional energy landscape has been used to describe the protein folding pathway (Dobson 2003; Radford 2000), explaining that there are likely an enormous number of pathways to reach the native state and the pathway will depend on the details of the protein being studied, such as the amino acid sequence and the experimental conditions. Generally, proteins fold either on a relatively smooth landscape or a rough, rugged landscape (Bartlett and Radford 2009). A relatively smooth landscape (Figure 1-3, A), can be produced when a protein folds via a two-state transition (from denatured state to native state), and this transition is rare (Brockwell and Radford 2007). By contrast, when a protein is funneled to the native state through multiple routes that might be involved intermediate formation, a rugged landscape is produced (Figure 1-3, B).

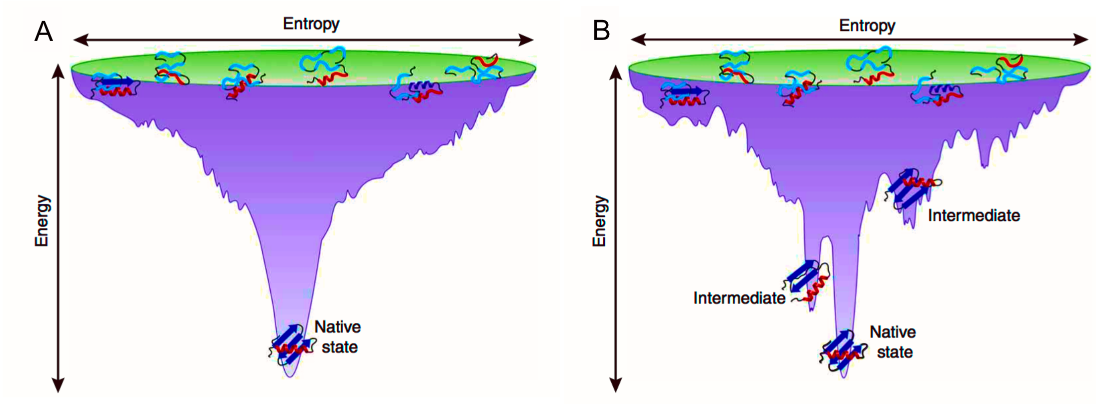

Figure 1-3: Schematic representation of energy folding funnels. Two different types of folding funnels can be occupied by proteins: (A) smooth energy landscape, in which a protein is effectively funneled to the native structure via a two-state transition, (B) rough, rugged landscape, through which the protein has to navigate, possibly via one or more populated intermediates, to the native state. In both types, the denatured state occupies several structures containing elements of both native and non-native interactions. Adapted with permission from (Bartlett and Radford 2009).

Recently, it has been demonstrated that even small proteins that fold on a subsecond timescale may pass through structural intermediates on their way toward native state (Bartlett and Radford 2009), explaining that such intermediates are either ‘stepping stones’ on-pathway toward the native state, or kinetically stable, misfolded intermediates that may need fundamental reorganisation to reach the final native state. However, incorrectly folded protein can result in a wide range of protein misfolding diseases (Dobson 2003). Many of these diseases display pathologies in which insoluble amyloid fibrils are formed from soluble and often functional proteins. It has been shown that partially folded or misfolded intermediates, that formed en route to the native state, often tend to aggregate, especially when they represent major kinetic traps in the folding route (Bartlett and Radford 2009). In these conformational forms, the hydrophobic amino acid residues and regions of unstructured polypeptide backbone are exposed, whereas in native state they are mostly buried. Like intramolecular folding, aggregation, which represents intermolecular interaction between two or more non-native protein molecules, is highly driven by hydrophobic interactions and leads to formation of either amorphous structures or amyloid fibrils that are thermodynamically highly stable, ordered forms and show a common structural feature of cross-β structure (Figure 1-4) (Bartlett and Radford 2009; Hartl and Hayer-Hartl 2009; Relini et al. 2014). It has been illustrated that amyloid formation is an inherent feature of the polypeptide chain, and can be enhanced using an appropriate *in vitro* denatured conditions (Chiti and Dobson 2006; Dobson 2003).

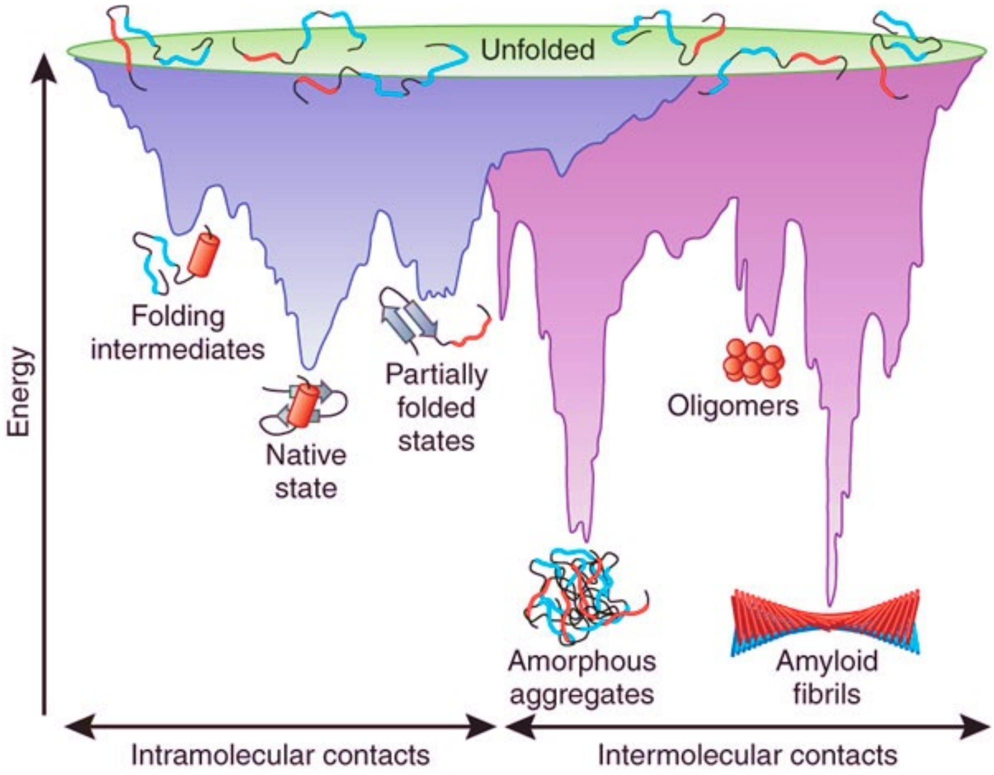

Figure 1-4: Schematic diagram showing protein folding and aggregation funnel landscape. Protein folding occurs when intermediate fold into more ordered native state via intramolecular interactions and this is showed by the purple surface. The pink area shows the multitude conformations moving toward amorphous aggregates or amyloid fibrils via intermolecular interactions. Cell-toxic oligomers may represent on or off-pathway intermediates of amyloid fibril formation. Reused with permission from (Hartl and Hayer-Hartl 2009).

Amyloid fibrils are extremely stable and exhibit a resistance to many denaturation agents such as urea, SDS and formic acid compared to native state globular proteins. However, they can be dissolved using very strong chaotropic agents or organic solvents such as phenol (Masters et al. 1985). Furthermore, the core is highly protease resistant, a common characteristic of amyloid fibres (Hartley et al. 2008; Hill et al. 1999). These observations together indicate that amyloid fibres are the lowest energy state that a protein can adopt, and have the lowest energy minima in the folding funnel landscape (Chiti and Dobson 2006; Hartl and Hayer-Hartl 2009) as shown in Figure 1-4.

Oxidative modifications of protein have been reported to promote protein misfolding both *in vivo* and *in vitro*, and eventually aggregation formation (Campioni et al. 2010; Scheinost et al. 2010). Reactive oxygen species (ROS) are generated as a by-product of normal metabolism and/or by exogenous stimuli such as ultraviolet light (Andreyev et al. 2005). ROS can attack all biological macromolecules, including proteins and causing oxidative damage (Campioni et al. 2010). Oxidation of a protein *in vitro* can induce its aggregation via multiple mechanisms such as destabilisation of the native state (Granata et al. 2007). Similarly, *in vivo* protein oxidation can also promote aggregation by additional mechanisms, such as protein cross-linking (Atwood et al. 2004; Zhang et al. 2004).

1.3 **Amyloid fibril structure**

The structure of amyloid fibrils can not usually be determined using commonly used structural techniques due to the insolubility and heterogeneity of amyloid fibrils. Instead, structural techniques including X-ray fibre diffraction (XRFD), solid-state nuclear magnetic resonance (ssNMR) and electron microscopy are often used to determine amyloid fibril structure. Many morphological and macromolecular structural analyses have been carried out using both electron and atomic force microscopy, revealing that amyloid fibrils are long, straight and unbranched (Goldsbury et al. 1999; Makin and Serpell 2005; Stromer and Serpell 2005; Sunde et al. 1997) (Figure 1-6, A). Moreover, it has been demonstrated that amyloid fibrils are made up of twisted individual subunits called “protofilaments” that can vary in number in different fibrils (Rambaran and Serpell 2008; Serpell et al. 2000b). Synthetic amyloid fibrils that are formed by amyloid β (Aβ), insulin and lysozyme were analysed using cryo-electron microscopy and showed to be composed of several protofilaments (2-6) twisted around one another (Figure 1-5, K) (Jimenez et al. 2001; Jimenez et al. 2002).

Amyloid fibrils that are generated from the same amyloidogenic protein are reported to show different fibril morphologies, i.e structural polymorphism (Figure 1-5, L) (Meinhardt et al. 2009), and this is attributed to different factors including different numbers of protofilaments (Goldsbury et al. 2000; Jimenez et al. 2002), different protofilament arrangements (Chamberlain et al. 2000), or different peptide conformations (Petkova et al. 2005). The structure of Aβ40 fibrils that were formed under agitation or quiescent conditions have been analysed using ssNMR, and a high-resolution structural model was constructed (Figure 1-5, H) (Paravastu et al. 2008; Petkova et al. 2006). More structural details for amyloid fibrils obtained using different structural techniques are shown in Figure 1-5.

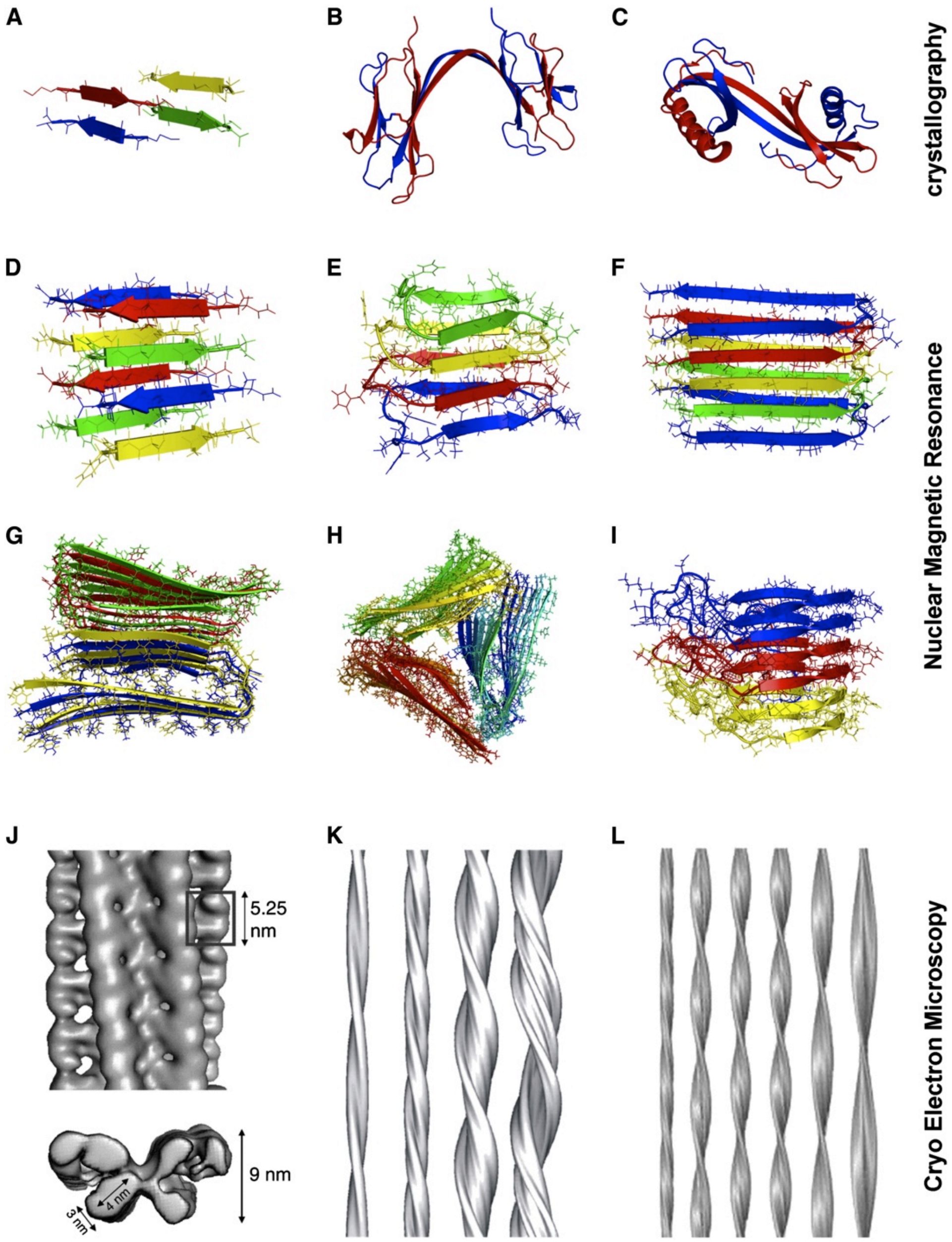

Figure 1-5: Diversity of cross-β structures that are characterised using X-ray crystallography, ssNMR, and cryo-EM. (A) The atomic structure of Aβ (35-40) segment with amino acid sequence of MVGGVV has been identified using X-ray microcrystallography and showed steric zipper conformation (Sawaya et al. 2007). (B) Crystal structure of β2-microglobulin (β_2m) dimer cross linked via disulfide linkages and formed in three-dimensional domain-swapped amyloid fibrils (Liu et al. 2011). (C) Crystal structure stefin B in a domain-swapped dimer conformation implicated as pre-fibril oligomers in amyloid formation (Jenko Kokalj et al. 2007). (D, E) Three-dimensional structures of cross-β parallel and anti parallel in-register protein fibrils of the K3 (β_2m20-41) and NFGAIL peptide respectively, which are identified using ssNMR (Iwata et al. 2006; Nielsen et al. 2009). (F) Structure model of Aβ42 fibrils obtained using hydrogen exchange, pairwise mutagenesis, and solution NMR (Luhrs et al. 2005). (G and H) High-resolution structural model of Aβ40 fibrils formed under agitation or quiescent conditions, respectively, obtained using ssNMR (Paravastu et al. 2008; Petkova et al. 2006). (I) High-resolution structural model of Het-s (218-289) prion fibrils determined using ssNMR (Wasmer et al. 2008). (J) Low-resolution three-dimensional structural model of amyloid fibrils formed from full-length β_2m obtained by cryo-EM (White et al. 2009). (K) Low-resolution three-dimensional structures of fibrils assembled from the polypeptide hormone insulin consisting of 2, 4, or 6 protofilaments based on cryo-EM (Jimenez et al. 2002). (L) Low-resolution three-dimensional structures of Aβ40 fibrils polymorphism revealed by cryo-EM (Meinhardt et al. 2009). Reused with permission from (Eichner and Radford 2011).

ssNMR has been used to analyse amyloid fibrils formed from various peptides corresponding to different regions of Aβ, and shown to have parallel and antiparallel β-sheet structures depending on the properties of the precursor polypeptide and assembly conditions (Balbach et al. 2002; Lu et al. 2013; Petkova et al. 2004; Petkova et al. 2005). A full length Aβ40 has been found to form fibrils that have an in-register β-structure (Luhrs et al. 2005; Petkova et al. 2002), in which the peptide molecules fold into a β-bend structure and then associate together to form parallel β-sheets (Figure 1-6, C).

The XRFD patterns from many different synthetic amyloid fibrils showed a cross-β structure (Figure 1-6, B). The cross-β diffraction pattern was first identified for silk from the egg stalk of the lacewing (Geddes et al. 1968). The typical cross-β diffraction patterns consist of "two major reflections at 4.7 Å and 10 Å found on orthogonal axes and arising from the hydrogen bonding distances between β-strands and side chain packing between the sheets respectively" (Makin et al. 2006; Rambaran and Serpell 2008; Sunde et al. 1997).

As some short amyloidogenic peptide can form crystals, their atomic structure has been elucidated by X-ray crystallography. In turn, considerable structural information has been gained, revealing the role of side chain interactions in the association of β-sheet ribbons. Atomic structure of Aβ(35–40) segment with amino acid sequence of MVGGVV obtained using X-ray microcrystallography (Figure 1-5, A) revealed a steric zipper conformation (Sawaya et al. 2007). The amyloidogenic peptide GNNQQNY, a fragment of the yeast prion, Sup35, has been characterised structurally by X-ray crystallography and recently, aromatic side chain packing of tyrosine residues have been reported to play a curial role in the fibre-crystal switching (Gazit 2002; Marshall et al. 2010; Nelson et al. 2005).

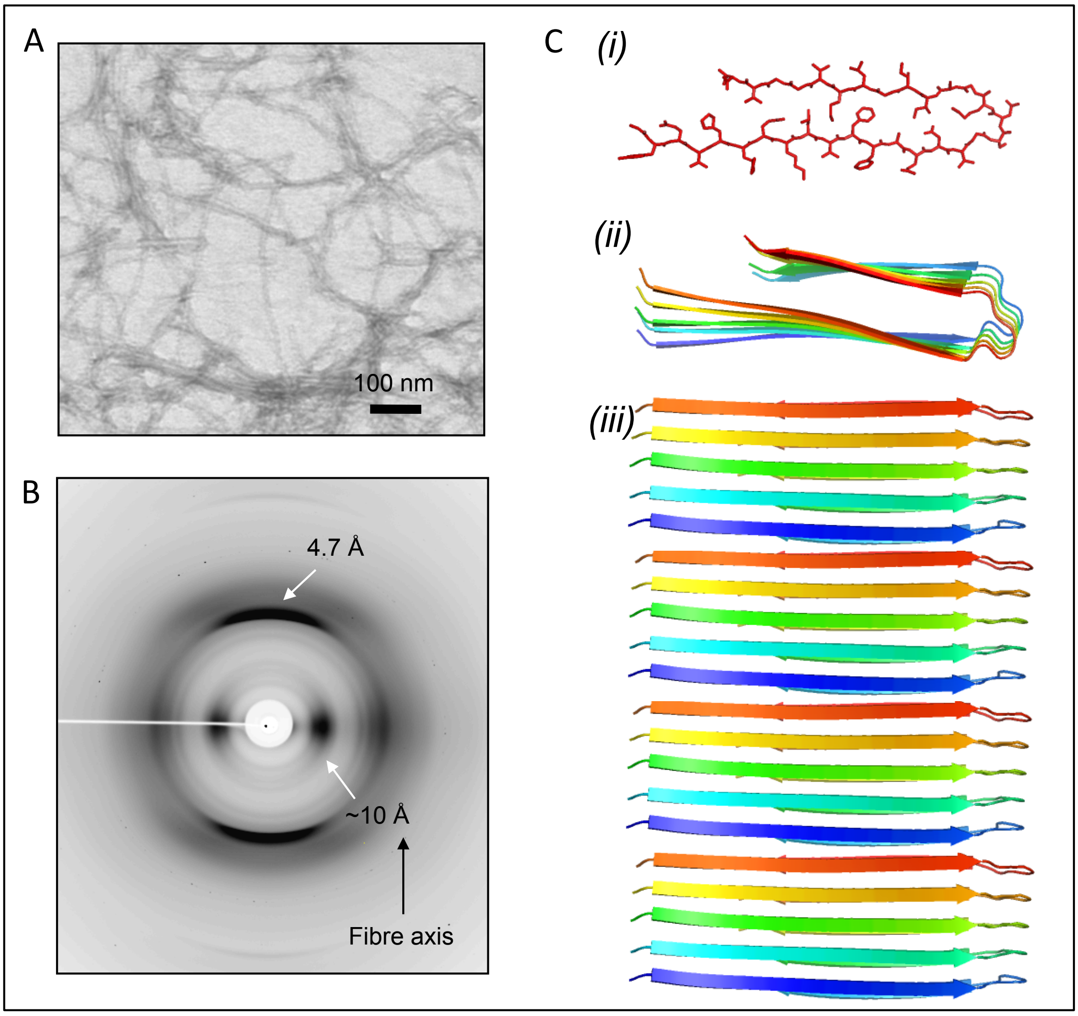

Figure 1-6: Synthetic Aβ fibrils structure based on XRFD, ssNMR and TEM. (A) Aβ fibrils are long, straight, unbranching fibrils under TEM. (B) X-ray fibre diffraction pattern from Aβ fibrils showing a typical cross-β diffraction, characteristic feature of amyloid fibrils. (C) The structural model of amyloid fibrils assembled from Aβ40 based on ssNMR data, (i and ii) the top view of the fiber with side chains and as a cartoon respectively, revealing the importance of side chain packing with in the fiber. The side view (iii) showing the β-strands running perpendicular to the fiber axis. Adapted from (Rambaran and Serpell 2008).

1.4 **Mechanism of amyloid assembly**

Many proteins and peptides with very different sequences have the ability to assemble into amyloid fibrils that share a cross-β core. Thus, it is very important to study and understand the mechanism underlying amyloid assembly, as this will contribute significantly to therapeutic approaches to halting and avoiding many amyloidoses. It is accepted that amyloid assembly mechanism involves formation of partially folded intermediates (Jahn et al. 2006; McParland et al. 2000). Ferrone *et al*. revealed a nucleation dependant mechanism of amyloid assembly (Ferrone 1999). Generally, the mechanism shows the conversion of unfolded monomeric species into partially folded intermediates that then undergo nucleation to form protofibrils that then lengthen into mature fibrils (Figure 1-7) (Harper et al. 1997; Serpell 2000). This mechanism has been shown for α-synuclein (α-syn)(Conway et al. 2000).

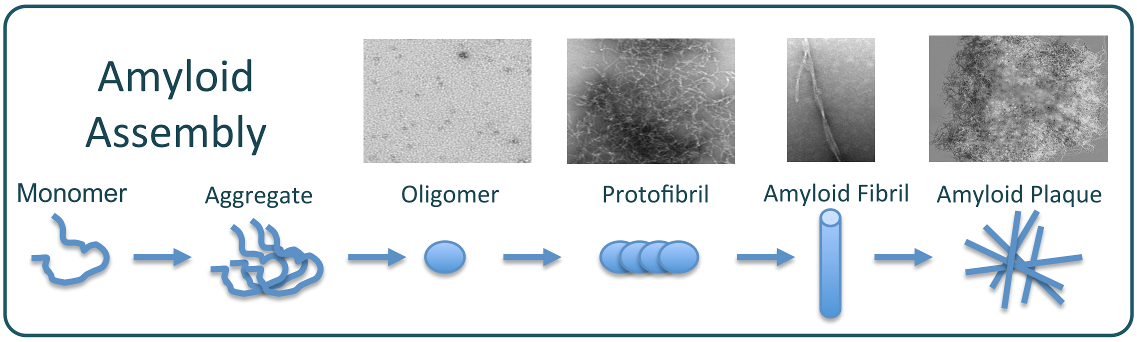

Figure 1-7: Schematic diagram showing amyloid assembly mechanism. The amyloidogenic protein/peptide undergo a multi step misfolding process in which the monomeric species aggregate into oligomeric species, which then form protofibrils which come together to form fibrils, which have very ordered cross β -structure. Provided by Prof. Louise Serpell.

Many biophysical and biochemical techniques, such as light scattering, size exclusion chromatography, fluorimetry and ultracentrifugation, have been used to study the kinetics of amyloid assembly *in vitro*. Thioflavin T fluorescence is often used to monitor amyloid fibril formation (see section 1.11.2.3), and the conventional ThT graphs reveal three phases; lag, growth and plateau phase (Figure 1-8).

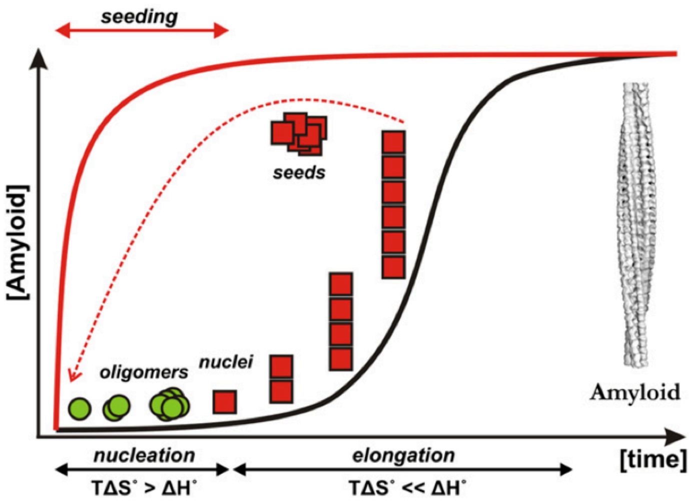

Figure 1-8: ThT graph showing amyloid fibril formation kinetics. Two distinct stages are observed in the amyloid fibril formation: a lag phase corresponds to the formation of thermodynamically disfavored nucleation events, and secondly, an elongation phase which is rapid and thermodynamically favored (black line). The lag phase can be significantly shortened using preformed fibrils as seeds (red line). Adapted with permission from (Eichner and Radford 2011).

Generally, the different species that are involved in amyloid assembly are classified as fibrillar and non-fibrillar species (Murphy 2007). The non-fibrillar species may be intermediates, i.e. monomers and oligomers, on-pathway to fibrillar species. Monomers can be folded or unfolded. When amyloid precursors proteins are natively folded, such as Transthyretin (TTR) and Prion protein (PrP), the folded monomers undergo a conformational switch to form amyloid fibrils (Colon and Kelly 1992; Kelly 1996). For example, some natively folded precursors proteins have α-helical structure that is converted into β-sheet rich fibrils, whereas, others have β-sheet structure that becomes rearranged into an amyloid architecture. On the other hand, monomers may be natively unfolded such as Aβ and α-syn (Uversky et al. 2006a), which undergo a structural transition from an unfolded state into β-sheet rich fibrils.

Oligomers, a second type of non-fibrillar species, are multimeric states and do not have a well-defined structure. For example, *in vitro* some Aβ oligomers display a spherical structure with diameters of 5 – 15 nm. Oligomers can serve as nuclei that are needed to initiate the nucleation of protein to form amyloid fibrils (Lee et al. 2011b). However, fibril fragmentation represents an alternative pathway for nucleation of fibril formation (Xue et al. 2008).

There are three types of fibrillar states; protofibrils, protofilaments and mature fibrils (Morris and Serpell 2013). Protofibrils, also called “bead-like structures” represent early intermediates in amyloid fibril formation. Generally, protofibrils are < 200 nm in length with diameter of up to 11 nm (Murphy 2007). They appear to have a repeating monomer structure that makes them more structurally defined than non-fibrillar species (Harper et al. 1999). Whereas, protofilaments are well defined filamentous species that laterally associated to form a mature amyloid fibril. Cryo-EM studies showed that protofilaments have a β-sheet rich core (Serpell and Smith 2000; Serpell et al. 2000b; Tattum et al. 2006). Mature fibrils are structurally defined using TEM and shown to be long and unbranched fibrils with a diameter of 7-12 nm and an indeterminate length (Makin and Serpell 2005; Morris and Serpell 2013). They are composed of a number of protofilaments with β-sheet structure (Eichner and Radford 2011).

1.5 Amyloid in diseases (amyloidosis)

Amyloid fibril formation is associated with protein misfolding (Dobson 2003, 2013). The natively folded or unfolded polypeptide chain undergoes conformational change resulting in the formation of amyloid structure. However, exactly how amyloid fibrils form *in vivo* is yet unknown. Amyloid fibrils may deposit at one or several sites in the body. Thus, amyloidosis can be classified very broadly into either localised or systemtic amyloidosis, based on the location of the amyloid deposits (Westermark et al. 2007). Generally, amyloid appearing at one site or in one type of tissue is called “localised” such as Alzheimer’s disease, which is characterised by deposition of Aβ into amyloid plaques in the brain. By contrast, deposition of amyloid in peripheral organs is called systemic amyloidosis such as AL-amyloidosis that affects many organs including heart, liver and kidneys and associated with deposition of fibrils that are derived from monoclonal immunoglobulin light chains. Apparently, this classification seems to be an easy and logical definition. However, one essential criterion to define systemic amyloidosis correctly is that the precursor protein has to be expressed in at least one site, and then released to plasma and eventually deposited from the blood stream at another site (Westermark et al. 2007). Thus, according to the definition systemic amyloids are derived from a plasma protein. On the other hand, the typical localised amyloid is formed in close proximity to the site of deposition, in other words it is derived from protein expressed by cells at the deposition site (Westermark et al. 2007). Some examples of amyloidoeses and their corresponding aggregated protein or peptide are summarised in Table 1-1.

*Table 1-1: Some human diseases associated with protein misfolding and the formation of extracellular amyloid deposits or intracellular inclusions that are showing amyloid-like characteristics. Adapted from (Dobson 2013). Diseases may be predominantly sporadic such as Alzheimer's disease, or hereditary such as Huntington's disease. * Intracellular misfolding diseases.*

Disease	**Aggregated peptide or protein (no. of residues)**	**Structure of precursor peptide or protein**
Neurodegenerative diseases		
Alzheimer's disease	Amyloid β peptide (40 or 42)	Natively unfolded
Spongiform encephalopathies	Prion protein or fragments thereof (253)	Natively unfolded (1-120) and α-helical (121-230)
Parkinson's disease*	α-synuclein (140)	Natively unfolded
Amyotrophic lateral sclerosis	Superoxide dismutase 1 (153)	All β
Huntington's disease*	Huntingtin with long polyQ stretches (3144)	Largely natively unfolded or unknown
Familial amyloidotic polyneuropathy	Mutants of transthyretin (127)	Mostly β
Non-neuropathic systemic amyloidoses		
AL amyloidosis	Immunoglobulin light chains or fragments thereof (~ 90)	All β
AA amyloidosis	Fragments of serum amyloid A protein (76-104)	All α
Senile systematic amyloidosis	Wild type transthyretin (127)	Mostly β
Hemodialysis-related amyloidosis	β-Microglobulin (99)	All β
Finnish hereditary amyloidosis	Fragments of gelsolin mutants (71)	Natively unfolded
Lysozyme amyloidosis	Mutants of lysozyme (130)	α and β
Non-neuropathic localized amyloidosis		
ApoAI amyloidosis	Fragments of apolipoprotein AI (80-93)	Natively unfolded/ α-helical
Type II diabetes	Amylin (37)	Natively unfolded
Medullary carcinoma of the thyroid	Calcitonin (32)	Natively unfolded
Hereditary cerebral hemorrhage with amyloidosis	Mutants of amyloid β peptide (40 or 42)	Natively unfolded
Injection-localised amyloidosis	Insulin chains A (21) and B (30)	All α

1.5.1 Alzheimer's disease and Aβ

Alzheimer's disease (AD) is a neurodegenerative disease that results from neuronal dysfunction and represents the most common cause of dementia (Selkoe 2000), affecting around 496,000 people in the UK (http://www.alzheimers.org.uk). Currently, over 35 million people worldwide are affected with dementia and this number is expected to double by 2030 and more than triple by 2050 to 115 million (http://www.alz.co.uk/research/world-report-2013). In 1904, AD was identified for the first time by the German neurologist Alois Alzheimer, describing it as a physical disease affecting the brain (Alzheimer 1904). Alzheimer carried out a postmortem examination of brain tissue from a 55-year old woman who had suffered from a progressive behavioral and cognitive disorder. The results revealed the presence of two distinctive pathological features: neurofibrillary tangles and neuritic plaques (Alzheimer et al. 1995) (Figure 1-9). In 1984, Glenner and Wang were able to isolate and purify these neuritic plaques and showed that they were consistent with a peptide that is primarily 40 or 42 amino acid in length with molecular weight of 4.2 kDa, assuming it was derived from cleavage of a large precursor protein (Glenner and Wong 1984).

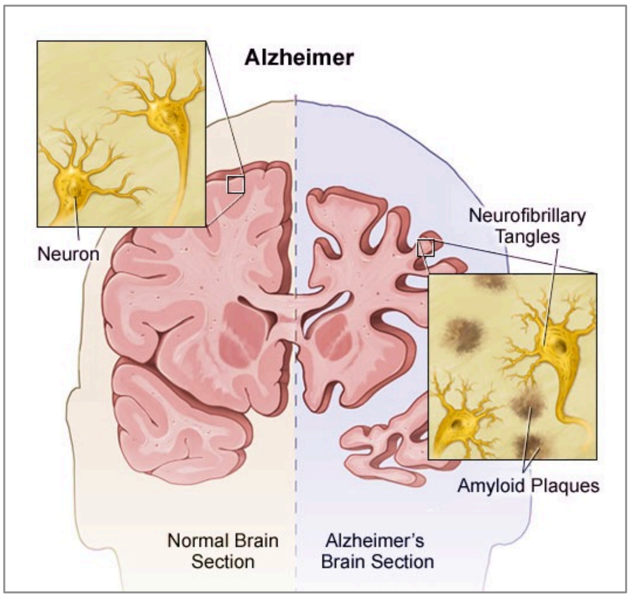

Figure 1-9: Healthy brain verses Alzheimer's affected brain. The cell death in AD brain leads to severe changes in the whole brain including shriveling of the cortex, tissue shrinkage especially in the hippocampus and increased ventricles. As a consequence, many fundamental living activities involving thinking, planning and remembering are excessively affected. AD is associated with deposition of extracellular amyloid plaques and intracellular neurofibrillary tangles of hyper-phosphorylated tau protein. Reproduced from (http://www.hopkinsmedicine.org/).

AD is clinically characterised by global cognitive decline, associated with brain pathology involving deposition of extracellular Aβ fibrils as senile plaques and intracellular neurofibrillary tangles of hyper-phosphorylated tau protein (Bothwell and Giniger 2000). Aβ plaque formation is accompanied by astrogliosis and microgliosis (Gupta and Pansari 2003). The neocortex and hippocampus are the most affected brain areas (Figure 1-9) (Sisodia and Gallagher 1998).

The Aβ is an amyloidogenic peptide and cleaved from the large, transmembrane amyloid precursor protein (APP) (Selkoe 1991). APP is proteolytically hydrolysed through two distinct amyloidogenic and non-amyloidogenic pathways (Figure 1-10). The non-amyloidogenic pathway refers to the sequential enzymatic cleavage of APP by α- and γ-secretases (Figure 1-10, B) and leads to production of transcriptional regulator APP intracellular domain (AICD) and p3 fragment whose functions are not well known (Hicks et al. 2012; O'Brien and Wong 2011). By contrast, amyloidogenic processing refers to the sequential cleavage of APP by the action of membrane-bounded β- and γ-secretases (Figure 1-10, C) (Zhang et al. 2012). In this process, APP is first cleaved by β-secretase and released as a soluble ectodomain (sAPPβ) and the C-terminal fragment CTF99. The latter is then cleaved by γ-secretase, releasing the 39 – 42 amino acid Aβ peptide, and also producing the AICD (Zhang et al. 2012). Soluble ectodomains, sAPPβ and sAPPα that are released from both amyloidogenic and non-amyloidogenic pathways respectively, have been reported to have neuroprotective properties (Turner et al. 2003; Zhang et al. 2012).

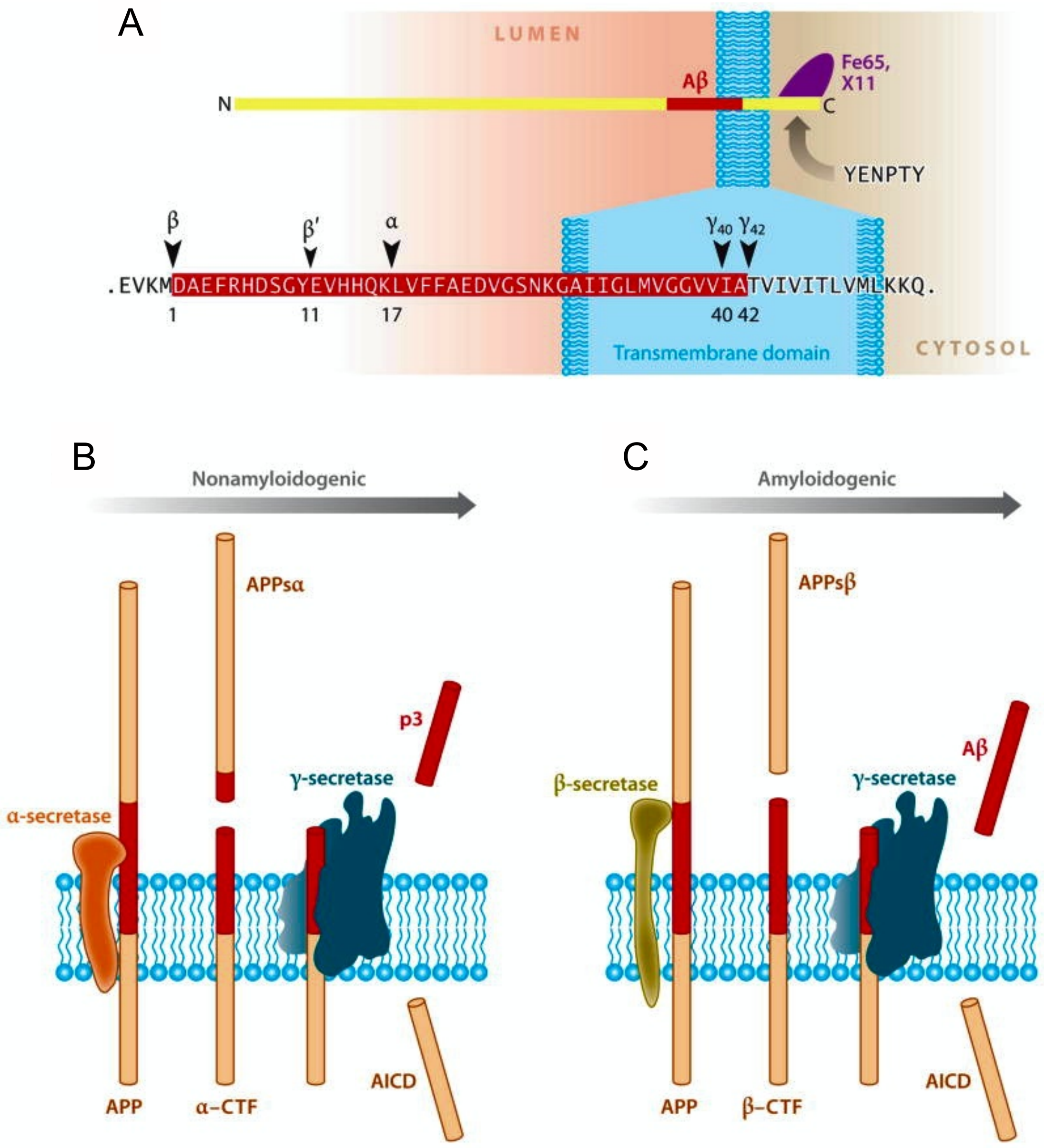

Figure 1-10: Schematic presentation showing proteolytic processing of amyloid precursor protein (APP). (A) The Aβ peptide, which is shaded in red color, starts within the ectodomain and continues into the transmembrane region. The major sites of cleavage by α-, β-, and γ-secretases are indicated with black arrows. Sequential cleavage of the APP occurs by two distinct pathways: nonamyloidogenic and amyloidogenic processing (B and C respectively). Nonamyloidogenic processing of APP is carried out by the action of α-secretase followed by γ-secretase, whereas amyloidogenic processing of APP refers to sequential action of membrane-bound β- and followed by γ-secretase. Both processes produce soluble ectodomains (sAPPα and sAPPβ) and identical intracellular C-terminal fragments (AICD). Reused with permission from (O'Brien and Wong 2011).

It is hypothesised that accumulation of Aβ peptide into amyloid plaques is the cause of AD. This accumulation is attributed to an imbalance between Aβ production and clearance which triggers a sequence of pathogenic events leading to AD (Selkoe 2000). This is known as the "amyloid cascade hypothesis of AD " which is assumed based on a large body of evidence showing that Aβ production is strongly correlated with AD

(Hardy and Selkoe 2002; Karran et al. 2011; Selkoe 2000). However, it is important to mention that Aβ fibrils are not necessarily the toxic species. The main evidence for amyloid hypothesis is the accumulation of amyloid fibrils, which are formed from Aβ peptide, into amyloid plaques in the brain, the characteristic pathological feature of AD. The presence of intracellular neurofibrillary tangles that consist of tau protein is also correlated with Aβ. It has been suggested that these neurofibrillary tangles are formed after and likely as a consequence of APP processing to release Aβ (Hardy and Selkoe 2002; Lewis et al. 2001). Moreover, genetic evidence has been reported to strongly support that Aβ is responsible for AD. It has been demonstrated that the epsilon4 allele of apolipoprotein E (APOE) represents the major genetic risk factor for AD, and can affect Aβ metabolism (Kim et al. 2009). Support for the amyloid hypothesis has been provided by the identification of APP mutants that leads to either over production of Aβ or increase Aβ inherent propensity to aggregate (Kim and Hecht 2008). In addition, mutations in the presenilin proteins PS1 and PS2, part of the γ-secretase complex that cleaves APP in a typical site to form Aβ, can also cause AD (Cruts and Van Broeckhoven 1998; De Strooper 2007; Xia et al. 2000). The majority of AD cases are sporadic with onset of symptoms correlating with increasing age (Chiti and Dobson 2006). However, in early-onset cases, AD can be hereditary and is due to mutations that lead to either over production of Aβ by APP or produce a higher ratio of Aβ42 to Aβ40 (Walsh and Selkoe 2007), where Aβ42 found to be much more fibrillogenic (Jarrett et al. 1993).

The Aβ peptide is normally formed in all individuals although it is found to be responsible in large part for the pathogenesis of AD due to its ability to aggregate and form oligomeric species, i.e. dimers, trimers and higher level oligomers, which are neurotoxic and cause neuronal death (Lesné et al. 2013; Roher et al. 1996; Walsh et al. 2002; Zhang et al. 2012). The oligomeric Aβ is further aggregated into amyloid plaques, the common pathogenic hallmark of AD, and this process is considered as a scavenging process (Zhang et al. 2012).

According to the amyloid cascade hypothesis, Aβ is principally responsible for many of the pathological characteristic of the disease (Hardy and Higgins 1992; Sakono and Zako 2010). Over recent years it has become widely accepted that oligomeric Aβ species are neurotoxic rather than Aβ fibrils (Hayden and Teplow 2013; Kayed and Lasagna-Reeves 2013; Klein 2006; Lesné et al. 2013). The classic amyloid cascade hypothesis for AD (Hardy and Selkoe 2002) was updated to a new "oligomer-driven" amyloid hypothesis (Figure 1-11) (Klein 2006). This hypothesis is strongly supported by many observations. Many Aβ oligomers have been extracted and isolated from brain tissue of both human AD and animal AD models (Shankar et al. 2008; Walsh et al. 2002; Walsh and Selkoe 2007). Also, it has been shown that Aβ oligomers that are prepared *in vitro* are neurotoxic (Atwood et al. 2004). However, the identity and structural composition of these *in vivo* oligomeric species and what is making them stable has not yet determined. One hypotheses is that Aβ monomers may interact by covalent cross-linkage or strong ionic interactions to form these oligomers (Atwood et al. 2004; Drew et al. 2013; Naylor et al. 2008), and this is central to the work in this thesis.

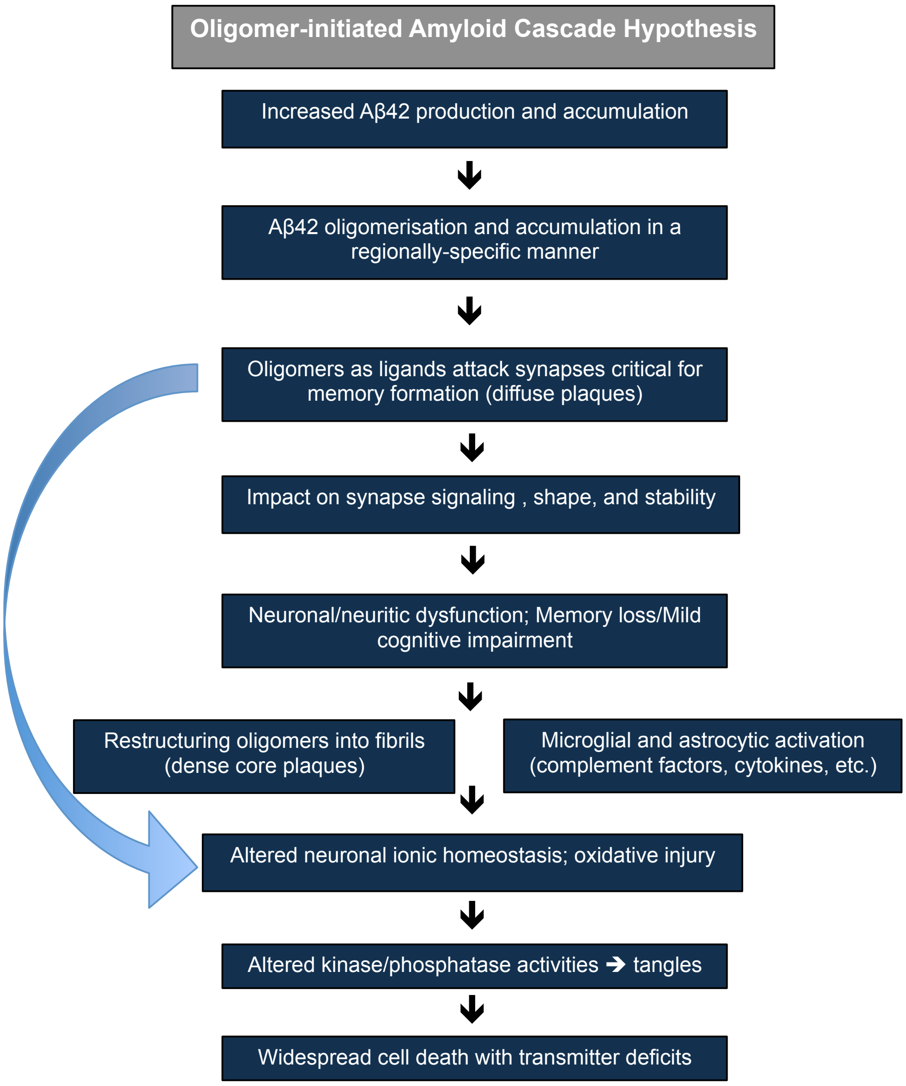

Figure 1-11: A new oligomer-driven amyloid cascade hypothesis for AD. Adapted from (Klein 2006).

1.5.2 **Parkinson's disease and α-syn**

Parkinson's disease (PD) is the most common neurodegenerative motor disorder, and the second most common progressive neurodegenerative brain disorder of humans, after AD. Clinically, PD is characterised by severe movement symptoms including uncontrollable resting tremor, muscular rigidity, impaired postural reflexes, and bradykinesia, which vary from patient to patient (Recchia et al. 2004). The pathological hallmark of PD is degeneration of dopaminergic neurons in the substantia nigra and this is accompanied by intracellular accumulation of filamentous α-syn protein into Lewy bodies in the surviving dopaminergic neurons and other affected regions of the central nervous system as shown in Figure 1-12 (Davie 2008; Recchia et al. 2004). However, the mechanism underlying the deposition of α-syn fibrils into Lewy bodies is not fully defined. It has been revealed that familiar or inherited forms of PD are linked to the mutation of genes coding α-syn, i.e. SNCA (Hardy et al. 2009; Stefanis 2012).

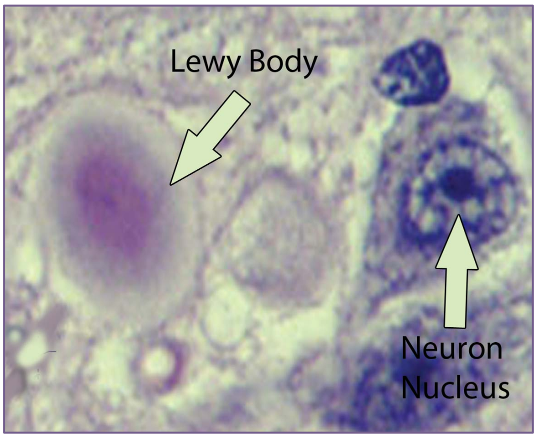

Figure 1-12: Immunohistochemical image showing neuron containing a Lewy body found within the substantia nigra, the pathological hallmark of PD. Reproduced from (http://www.virtualmedstudent.com/links/neurological/parkinsons.html).

α-syn is a soluble and predominantly neuronal protein that is abundantly expressed at presynaptic terminals in the central nervous system (Stefanis 2012). α-syn consists of 140 amino acids with molecular weight of 14.5 kDa and has three distinct regions (Figure 1-13): the highly conserved N-terminal domain of α-syn (1–65), the central hydrophobic domain of α-syn (61–95) is known as the non-Aβ component of plaques (NAC) and the acidic negatively charged C-terminal domain (96–140) (Recchia et al. 2004; Stefanis 2012).

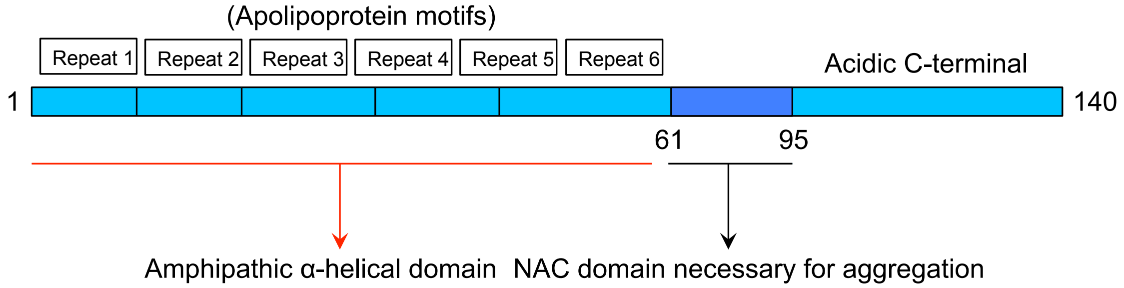

Figure 1-13: Schematic showing structure of α-syn showing the three distinct domains.

The N-terminal domain of α-syn contains six apolipoprotein motifs that may bind lipids to form amphipathic α-helices (Stefanis 2012). It has been demonstrated that lipid environments enhance the ability of α-syn to form an α-helical conformation by the interaction with negatively charged phospholipids, indicating that α-syn may normally be membrane associated (Davidson et al. 1998; Eliezer et al. 2001). It has been demonstrated that mutations in the N-terminal domain at position 53 (A53T) and 30 (A30P) are associated with early-onset, familial PD. Mutant α-syn has been shown to adopt a random coil state that facilitates self-assembly (Clayton and George 1999; Kruger et al. 1998). Moreover, these mutations have been found to increase the rate of α-syn oligomerisation and make it more prone to aggregation and fibril formation (Rochet et al. 2000).

The hydrophobic NAC domain, which is the second main component of amyloid plaques in AD, represents the amyloidogenic region of α-syn that is responsible for amyloid fibril formation (Giasson et al. 2001). It has been shown that deletion or disruption of this domain blocks the ability of α-syn to form amyloid fibrils (Giasson et al. 2001).

The acidic C-terminal domain consists primarily of acidic amino acids and exhibits a strong negative charge and does not show any distinct structural conformation (George 2002). Unlike N-terminal and NAC domains, C-terminal domain is highly variable in size and in sequence (Lavedan 1998). Several phosphorylation sites have been identified in the C-terminal domain including Tyr125, -133, and -136, and on Ser129 (Negro et al. 2002). It has been reported that Tyr125 residue can undergo phosphorylation by two Src family protein tyrosine kinases, c-Src and Fyn (Ellis et al. 2001; Nakamura et al. 2001), although it has been shown that phosphorylation by Src family of kinases does not suppress or promote the propensity of α-syn to aggregate.

A cascade of events involving misfolding or α-syn dysfunction can be triggered by various environmental and genetic factors, and this in turn may lead to dopaminergic cell loss and PD. It is believed that the α-syn toxic species are responsible for neuronal dysfunction and death and ultimately PD. Many studies have been carried out to identify these species. However, the mechanism by which α-syn induces neuronal cell toxicity is not well understood. Like AD, soluble oligomeric α-syn species are suggested to be the toxic species rather than fibrillar α-syn. Moreover, it has been suggested that amyloid aggregates may serve as a reservoir for these oligomeric forms (Marques and Outeiro 2012). The neurotoxicity of oligomeric α-syn species has been assessed *in vivo* using animal models of PD (Karpinar et al. 2009; Winner et al. 2011). Variants of α-syn that enhance oligomer formation were designed and tested for their toxicity *in vivo*. For example, it has been shown that over-expression of α-syn mutants that are less fibrillogenic leads to increased toxicity in *Caenorhabditis elegans* and *Drosophila* models (Karpinar et al. 2009).

1.6 Metal ions and neurodegenerative diseases

1.6.1 Introduction

An enormous number of biochemical reactions in the brain utilise metal ions, such as copper, zinc and iron. Similarly, redox-active metal ions are essential for antioxidant defences such as cytochrome *c* oxidase and superoxide dismutase 1 (Cu), haemoglobin (Fe), and superoxide dismutase 2 (Mn) (Kozlowski et al. 2012; Strozyk and Bush 2006). However, abnormal interactions of proteins with metal ions mediate different neurodegenerative diseases such as AD and PD. Two basic mechanisms have been described to explain abnormalities in metal ion biochemistry in the brain (Strozyk and Bush 2006). First, "protein aggregation mediated by metal ions", and second, "oxidative reactions catalysed by redox-active metals" (Strozyk and Bush 2006). Inappropriate electron transfer from redox-active metals, such as copper and iron to a protein can lead to generation of reactive oxygen species (ROS), free radicals and nitrogen species (Strozyk and Bush 2006). The metallobiology of neurodegenerative diseases have been extensively studied and reviewed (Bush 2003b; Kozlowski et al. 2006; Kozlowski et al. 2012; Roberts et al. 2012; Viles 2012). The transfer of metal ions through the blood-brain barrier is tightly regulated. Many transporters, enzymes and chaperones strictly control metal uptake and delivery to its correct site in the brain, regulating the metal content and preventing a passive metal fluctuation from the environment to the brain (Outten and O'Halloran 2001). Thus, the homeostatic failures of the endogenous content of metals in the brain are associated with many neurodegenerative diseases. It is well known that the brain has the highest metabolic rate of any tissue and requires oxygen for aerobic metabolism (Strozyk and Bush 2006). Several proteins are involved in the maintenance of copper homeostasis, including copper transporters and metal chaperones (Cerpa et al. 2005). If metal chaperones do not work effectively, the concentrations of free redox-active metal ions will increase in the brain, and this may increase the vulnerability of brain tissue to radical attack. ROS generation by redox-active metals and its consequences are shown in Figure 1-14.

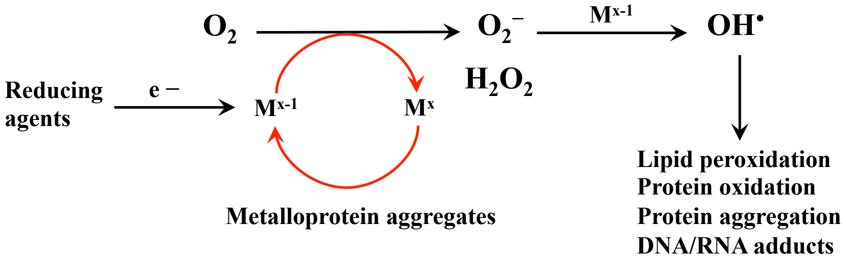

Figure 1-14: Simplified diagram showing ROS generation by redox-active metals. Redox-active metal ions such as Cu and Fe ions in their reduced state (M^{x-1}) can reduce dissolved molecular oxygen (O_2) to superoxide O_2^-, which is then enzymatically converted to H_2O_2. H_2O_2 is freely permeable across lipid membranes and can react with encountered M^{x-1} to generate the highly reactive hydroxyl radical ($OH^{\bullet}$), which reacts with the adjacent substrates and generates a variety of oxidative damage species that has been observed in neurodegenerative disorders such as AD and PD. Adapted from (Strozyk and Bush 2006).

ROS and free radicals can be generated through sequential processes that involve reduction of molecular oxygen (O_2) by redox-active metals in their reducing state (M^{x-1}) to form superoxide (O^-_2), which is then converted to H_2O_2 (Figure 1-14). The metal catalysed generation of H_2O_2 has been considered to play a role in neurodegenerative diseases characterised by protein aggregation such as AD and PD (Strozyk and Bush 2006). The protein oxidation and oxidative stress in neurodegenerative diseases has been studied and reviewed extensively (Eskici and Axelsen 2012; Jomova et al. 2010; Mariani et al. 2005; Moreira et al. 2007; Pennathur et al. 1999b; Smith et al. 1996; Souza et al. 2000), highlighting that oxidative protein modification is implicated in the pathogenesis of AD and PD.

1.6.2 Alzheimer’s disease

Transition metal ions have been frequently reported to be involved in the pathogenesis of AD, PD and prion diseases (Bush 2003b; Huang et al. 2004a; Kozlowski et al. 2006; Strozyk and Bush 2006; Viles 2012). High concentrations of zinc, copper and iron have been observed in amyloid plaques from AD brains (1 mM, 400 μM and 1 mM, respectively) (Lovell et al. 1998). Also, it has been found that levels of copper and zinc in the cerebrospinal fluid (CSF) of patients affected by both AD and PD are two or three fold higher than control levels (Hozumi et al. 2010). Accumulation of iron is also reported in the brain of both AD and PD (Barnham and Bush 2008; Stankiewicz et al. 2007). It has been revealed that Aβ is a metalloprotein and appears to have both low and high affinity for copper and zinc (Atwood et al. 1998; Atwood et al. 2000; Bush et al. 1994a).

Induction of Aβ accumulation by zinc in AD has been reported by Bush *et al*. (Bush et al. 1994b). AD studies using Tg2576 transgenic mice as a model for AD showed that genetic ablation of zinc transporter 3 (ZnT3), the protein required for transporting and concentrating zinc into synaptic vesicles, leads to significant reduction in Aβ deposition (Friedlich et al. 2004; Lee et al. 2002). Recently, it has been found that zinc transport capacity is modulated by the dimeric state of ZnT3 (Salazar et al. 2009), explaining that dityrosine cross-linked ZnT3 dimeric species, which are formed in response to H_2O_2, are the likely ZnT3 functional states, indicating the important role of oxidative stress in the pathogenesis of AD.

Bush suggested a sequence of biochemical processes leading to AD as shown in Figure 1-15: (1) Copper and iron cellular levels increase with increasing age in the brain cortex (Maynard et al. 2002), and this will result in overproduction of APP and Aβ in order to suppress the cellular elevation of metal ion levels (Rogers et al. 2002). Under slightly acidic conditions Aβ becomes hypermetalled (Bush 2003b), copper and iron bind Aβ and Aβ-chelated zinc is totally displaced by copper and iron (Atwood et al. 1998; Atwood et al. 2000; Nair et al. 2010). (2) Some hypermetallated Aβ species can catalytically generate H_2O_2 from O_2 in the presence of biological reducing agents that help to recycle metal ions (Opazo et al. 2002). (3) The resulting H_2O_2 can oxidise Aβ-copper complexes and form oxidised and cross-linked Aβ species that are liberated from the membrane and also exhibit protease resistance (Atwood et al. 2004). (4) These oxidised Aβ species represent the major components of amyloid plaque deposits (Al-Hilaly et al. 2013; Head et al. 2001). The soluble Aβ can be precipitated in the presence of high concentration of zinc, which is released close to the synapses. Thus, plaques contain a mixture of Aβ complexes with zinc, copper and iron. (5) Microglial activation can be initiated by oxidised Aβ. It has been revealed that high concentration of H_2O_2 and myeloperoxidase can be produced by activated microglial cells (Giulian et al. 1998; Reynolds et al. 1999), and this in turn supplies further H_2O_2 outside the cortical cells. (6) H_2O_2 can easily cross the cellular membrane into cellular compartments and react with redox-active metal ions, causing oxidative damage to nucleic acids, proteins and lipids that are observed in AD-affected brain tissue (Sayre et al. 2000).

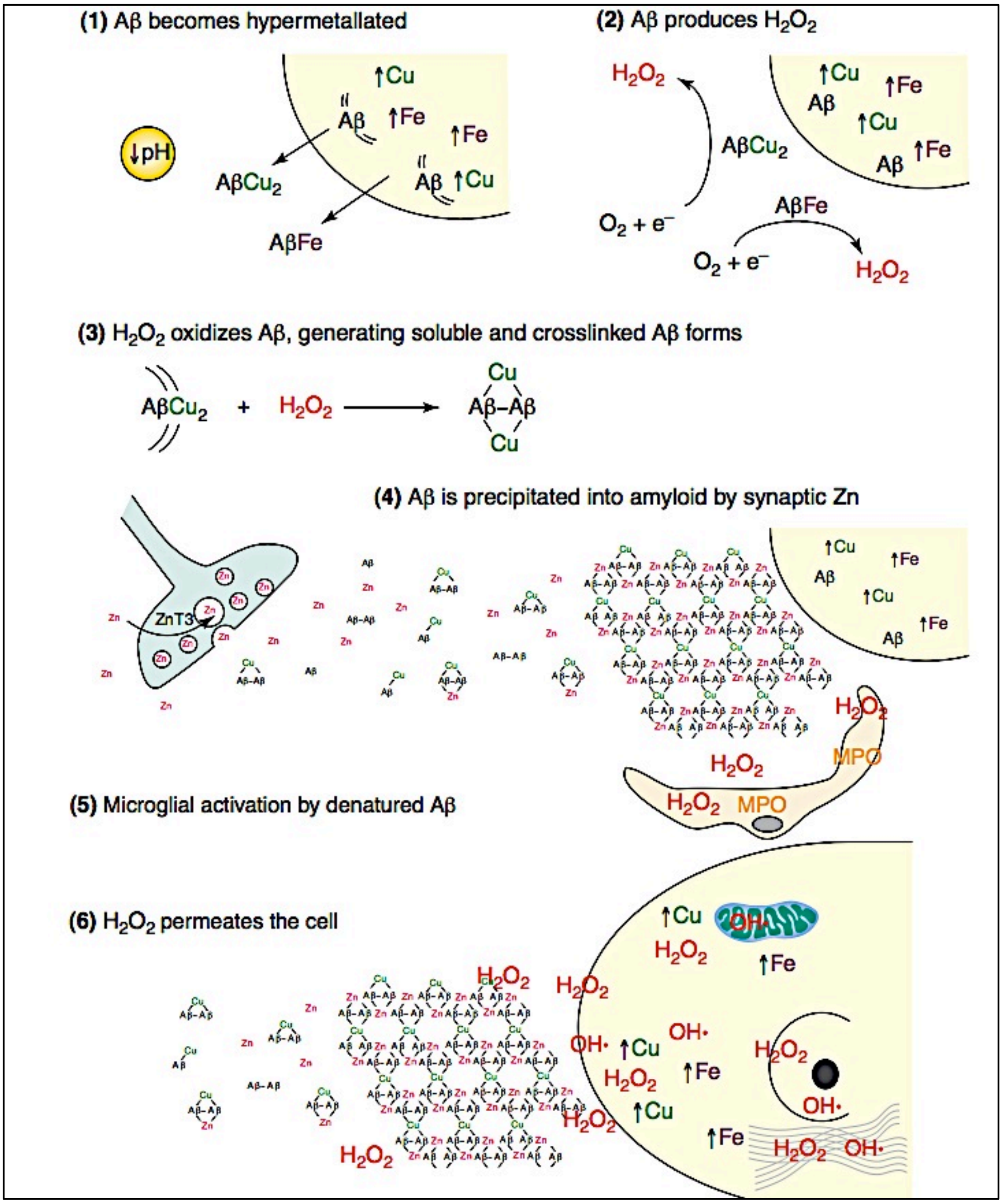

Figure 1-15: Summarised model for the metallobiology of Aβ in AD revealing the suggested sequence of biochemical processes leading to AD. Reproduced from (Bush 2003b).

In 1934, Haber and Weiss proposed that the highly reactive hydroxyl radical could be generated from an interaction between superoxide and hydrogen peroxide, which has known then as the Haber-Weiss reaction (Haber and Weiss 1934). Thermodynamically, Haber-Weiss reaction is unfavourable in biological systems, and has a second order rate constant of zero in aqueous solution as reported by Kehrer (Kehrer 2000). However, Haber and Weiss discussed the ability of iron salts to serve as catalysts in this reaction, and they illustrated that two chemical steps can be involved to give the net reaction of hydroxyl radical formation (Reaction 3).

$$Fe^{3+} + O_2^{\bullet -} \longrightarrow Fe^{2+} + O_2 \qquad [1]$$

$$Fe^{2+} + H_2O_2 \longrightarrow Fe^{3+} + OH^{-} + OH^{\bullet} \qquad [2] \quad \text{Fenton reaction}$$

$$O_2^{\bullet -} + H_2O_2 \longrightarrow O_2 + OH^{-} + OH^{\bullet} \qquad [3] \quad \text{Haber-Weiss reaction}$$

Many oxidative markers have been found in AD and reported that they can be formed according to Fenton reaction (Reaction 2) that includes the reaction of Fe or Cu in their reduced forms with H_2O_2 to form hydroxyl radicals that show high chemical activity and can attack many macromolecules, such as proteins, lipids and nucleic acids, and generate lipid peroxidation products, protein carbonyl modifications and nucleic acid adducts. All these oxidative modification products are characteristic of AD neuropathology (Smith et al. 1996; Smith et al. 1997). It has been elucidated that biological reducing substances, such as cholesterol and long-chain fatty acids, are required to recycle the redox-metal ions (Barnham et al. 2004; Smith et al. 2006a). Moreover, it has been reported that lipid oxidation products, such as oxysterols and 4-hydroxynonenal, are increased in AD brain tissue and mouse models of the disease (Haeffner et al. 2005; Opazo et al. 2002; Smith et al. 2006a).

Many amino acids in Aβ can be copper-induced oxidised by H_2O_2 to form different oxidative products. Copper can catalyse the oxidation of methionine at position 35 to form methionine sulfoxide and methionine sulfone (Ali et al. 2005; Ciccotosto et al. 2004). Intermolecular histidine bridges have been formed in the presence of copper (Smith et al. 2006a). The tyrosine residue at position 10 has been oxidised using an copper/H_2O_2 oxidation system to many different oxidised products including nitrotyrosine and dityrosine, and many of them have been assessed in AD brain tissue and also in the CSF (Abdelrahim et al. 1997; Atwood et al. 2004; Barnham et al. 2004; Hensley et al. 1998; Smith et al. 2007; Yoburn et al. 2003). Different Aβ isoforms have been found to have different redox activity, and shown the following order $A\beta42_{human} > A\beta40_{human} >> A\beta40_{mouse} \sim 0$ (Huang et al. 1999b). Similarly, different Aβ forms exhibit different neurotoxicity in neuronal cultures which could be attributed to the variation in the redox activity behaviors of these Aβ forms that bind copper differently (Huang et al. 1999b; Opazo et al. 2002). It has been observed that chelators such as clioquinol can significantly reduce the neurotoxicity of Aβ in cell culture by extraction of metal ions (Puglielli et al. 2005).

1.6.3 **Parkinson's disease**

The involvement of metal ions in the pathogenesis of PD has been investigated and reviewed extensively (Barnham and Bush 2008; Kienzl et al. 1995; Kozlowski et al. 2012; Sian-Hulsmann et al. 2011). Zinc and iron accumulation in the substantia nigra has been observed, whereas copper has been found to decrease (Barnham and Bush 2008). It has been revealed that the elevation of iron may play a role in the oxidative stress and loss of dopaminergic neurons and also may contribute to the deposition of Lewy bodies (Barnham and Bush 2008; Kaur et al. 2003). This was essentially supported by *in vivo* observations in PD animal models showing that using iron chelators protect against and/or prevent PD (Kaur et al. 2003; Youdim et al. 2004; Zhu et al. 2007). Similarly, the overexpression of iron-sequestering ferritin is able to protect and/or prevent the death of dopaminergic neurons in PD animal models (Kaur et al. 2003).

It is well established that α-syn is a metalloprotein and *in vitro* is found to interact with zinc, copper and iron with different affinities (Barnham and Bush 2008; Brown 2009; Valiente-Gabioud et al. 2012). The interaction of α-syn with these metal ions leads to protein aggregation and covalent cross-linking (Cole et al. 2005; Paik et al. 1999; Paik et al. 2000). A number of *in vitro* studies have shown that α-syn fibrillisation accelerated in the presence of some metal ions such as Cu^{2+} (Binolfi et al. 2010; Paik et al. 1999; Uversky et al. 2001; Yamin et al. 2003). However, it is important to know that most of these studies have used high concentrations, i.e. millimolar, of both α-syn and metal ions, and this would not reflect the physiological relevance of these ions. Interestingly, Rasia *et al.* have found that *in vitro* incubation of α-syn with Cu^{2+} at 1:1 molar ratio using a physiologically relevant concentration (100 μM) significantly enhanced α-syn fibrillisation by reducing the lag-time of α-syn fibrillisation (Rasia et al. 2005). By contrast, the other metal ions, such as Fe^{2+}, Mn^{2+}, Co^{2+} and Ni^{2+}, hardly effect the α-syn fibrillisation using (1:1) metal: α-syn ratios (Binolfi et al. 2006). The enhancement of α-syn fibrillisation by Cu^{2+} was attributed to the formation of a α-syn-Cu^{2+} complex (Binolfi et al. 2010). The coordination of copper ions to α-syn has been investigated and the results revealed that α-syn has three binding sites. Two strong anchoring sites are located in N-terminal domain and corresponding to Met1 and His50, while the third anchoring site, which is weak and nonspecific, is located in C-terminal domain (Ahmad et al. 2012; Rasia et al. 2005).

Recently, the neurotoxicity of oligomeric α-syn species has been tightly correlated with the interaction of copper with α-syn (Wang et al. 2010; Wright et al. 2009). The toxicity of α-syn was assessed in the presence of copper using cell culture, and the results revealed that only the oligomeric α-syn species is neurotoxic and requires the presence of copper but not iron (Wright et al. 2009). Using a cell culture, another study showed that copper has a critical role in both α-syn aggregation and localisation, compared to iron, which did not show any significant role in the aggregation formation and localisation (Wang et al. 2010). Reduction in copper levels was found to highly decrease the oligomer formation in the cells and also α-syn became more localised to the plasma membrane. Interestingly, these changes were reversed when copper was restored to the cell, indicating that copper ions palys a vital role in the toxicity of α-syn oligomers (Wang et al. 2010).

1.7 Lipofuscin and AD pathogenesis

In 1912 the term "lipofuscin" was used for the first time (Hueck 1912), which originates from Greek *lipo* (for fat) and Latin *fuscus* (for dark). It is a complex matrix of oxidised proteins and lipid peroxidation products, along with lesser amounts of carbohydrates and metals (Porta 2002; Terman and Brunk 1998b, 2004). Iron is the major component of the metal content in lipofuscin (Brunk 1989), also copper and zinc have been found in lipofuscin (Elleder 1981; Gutteridge 1984). Chemical analysis of isolated lipofuscin pigments reveals that protein content represents 30 – 70% of the lipofuscin, while lipid represents 20 – 50% as reviewed in many studies (Brunk and Terman 2002; Terman and Brunk 1998b). It has been reported that carbohydrates represent only 4 – 7% of lipofuscin composition (Terman and Brunk 1998b). Proteomic and ultrastructural analysis of human lipofuscin had identified over 160 proteins and revealed a heterogeneous core structure composed of lipofuscin granules which are surrounded by substantial extra-granular material (Gugiu et al. 2005).

Lipofuscin is hydrophobic and insoluble yellow-brown pigment that accumulates in the nervous system of animals and it is more abundant in aged individuals than in young ones, therefore it is called "aging pigment" (Szweda et al. 2003; Terman and Brunk 1998a; Terman and Brunk 1998b). Lipofuscin is considered to be a biomarker of aging and the age-dependent accumulation of lipofuscin in the nervous system of individuals has made reliable estimation of absolute age possible. Currently, lipofuscin is defined operationally rather than structurally due to its complex chemical composition. Morphologically, lipofuscin inclusions appear yellow-brown under light microscopy, with variation in the amounts, intensity, and shade. Under light microscopy, lipofuscin is observed as a homogeneously dark mass with irregular shape and surrounded by a 100 nm thick lysosomal membrane (Double et al. 2008).

Auto-fluorescence is the most characteristic property of lipofuscin pigment, with an excitation wavelength around 400 nm and a broad range of emission maxima between 530 and 650 nm (Porta 2002). The wide range of the emission is due to the differences in the sources of lipofuscin. However, although the nature of the auto-fluorescence substances that are responsible for the auto-fluorescence feature of lipofuscin is not yet completely known, evidence suggests that various fluorophores can be formed as a result of reactions between carbonyls (mainly aldehyde, produced by lipid peroxidation) and amino compounds (Brunk and Terman 2002).

Two mechanisms have been suggested to explain cellular lipofuscin formation (Brunk and Terman 2002; Terman and Brunk 1998b):

1- Age-dependent (unrelated) mechanism: In postmitotic cells, when the autophagocytosed material cannot be completely eliminated through lysosomal degradation or by exocytosis, this will result in lipofuscin formation by conversion of these indigestible material into lipofuscin, and the rate of the lipofuscin formation will be higher than its elimination rate. According to this mechanism, lipofuscin will accumulate more or less linearly with time.

2- Age-dependent (related) mechanism: Lipofuscin can be accumulated as a result of age-related changes in lysosomal function, such as inhibition of lysosomal enzymes, enhanced autophagocytosis, and/or decreased exocytosis. Formation of lipofuscin would be likely to be exponential.

As described in section 1.6.2, oxidative stress is widely implicated in AD pathogenesis and also represents one of the biological pathways by which Aβ can be accumulated in the lysosomes. There is a great body of evidence that confirms the involvement of oxidative stress in lipofuscin pigment accumulation over age progression. It seems that the autophagocytosis of mitochondria is the major contributor to lipofuscin formation (Figure 1-16) (Collins et al. 1980). Although ROS, such as hydrogen peroxide, superoxide anion, and hydroxyl radical, can be formed from different *in vivo* sources (e.g. auto-oxidation, photochemical, and enzymatic reactions), mitochondria represent the main *in vivo* source of ROS formation (Chance et al. 1979; Loschen et al. 1971). At the same time, the mitochondrion is the main target of ROS attack (Harman 2002), resulting in the formation of peroxidised, undegradable macromolecules. Recently, Murakami and Shimizu have clarified the role of cytoplasmic superoxide radical as a possible contributing factor to intracellular Aβ oligomerisation in AD (Murakami and Shimizu 2012). It also has been suggested that intraneuronal Aβ oligomers cause neuronal death by activating endoplasmic reticulum stress, endosomal/lysosomal leakage and mitochondrial dysfunction (Umeda et al. 2011).

In the same manner to iron ions, many transition metals, such as copper, can catalyse the hydroxyl radical generation. Hydrogen peroxide, an example of ROS, can easily diffuse into lysosomes and react with iron ions released from the degradation of different metalloproteins during their intralysosomal degradation. The interaction of hydrogen peroxide with iron ions results in the formation of the highly reactive hydroxyl radicals. The latter would attack intralysosomal macromolecules, such as Aβ, causing cross-linking of these materials and leading to lipofuscin formation (Figure 1-16). The oxidative modification specially cross-linking of autophagocytosed material, is the most probable cause of non-degradability of these materials.

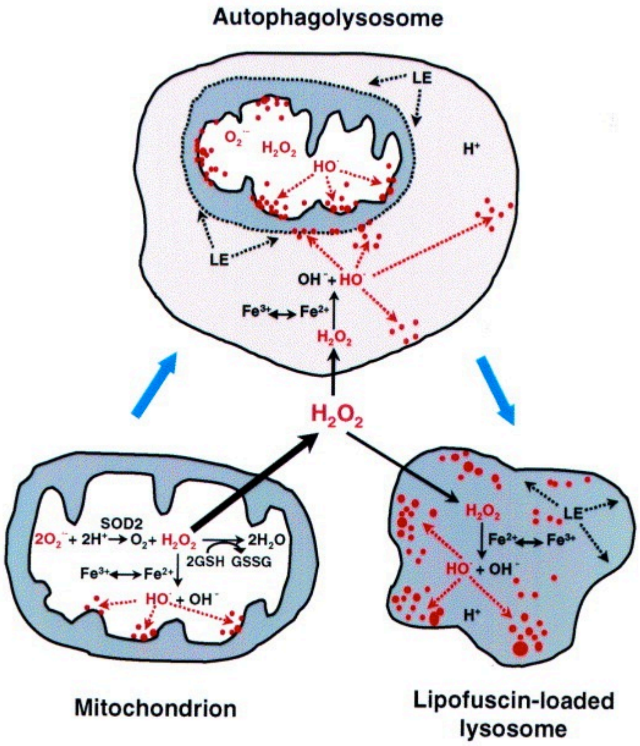

Figure 1-16: Schematic mechanism of lipofuscin formation in the lysosome. In mitochondria, hydrogen peroxide is generated from superoxide anions, a byproduct of mitochondria respiration. In the presence of ferrous ion, hydrogen peroxide can be converted into hydroxyl radical that attacks surrounding macromolecules and leads to oxidative modification. Red dots represent the oxidatively damaged undegradable macromolecules. LE is lysosome enzymes. Reproduced from (Brunk and Terman 2002).

The excessive accumulation of these non-digested materials could result in endosomal/lysosomal leakage and, as a consequence, acid hydrolases will be released causing cell death. In support of this hypothesis, it has been shown that the inhibition of lysosomal proteases would dramatically enhance the effect of oxidative stress on lipofuscin formation, leading to delay in the degradation of autophagocytosed substances and allowing more time for its oxidation (Terman and Brunk 1998a). On the other hand, lipofuscin accumulation has been shown to be retarded by the iron chelator desferrioxamine, and many antioxidants including vitamin E, selenium, and glutathione (Terman and Brunk 1998b). Vitamin E deficiency is associated with increased lipofuscin accumulation (Moore and Wang 1947).

1.8 **Dityrosine cross-linkage**

Dityrosine is a tyrosine dimer that results from the ortho-ortho coupling of two tyrosyl radicals (Figure 1-17). It has a strong fluorescence emission maximum at 410 nm upon excitation at 285 – 325 nm depending on the pH of the solution (Abdelrahim et al. 1997). Dityrosine was initially recognised in 1955 by Gross and Sizer (Gross and Sizer 1955), who described the *in vitro* formation of dityrosine by peroxidase oxidation of tyrosine in the presence of H_2O_2. Previous work had established that peroxidase enzymes can catalyse the oxidation of phenols and aromatic amines by hydrogen peroxide (Elliott 1932). Later, it was revealed that mechanism of diphenyl compound production involved free radical formation as intermediates (Waters 1952). Based on these observations, Gross and Sizer suggested that dityrosine formation was achieved through generation of tyrosyl radical as an intermediate (Gross and Sizer 1959). The subsequent studies mainly focused on the native role of dityrosine in many elastic natural materials and also in invertebrate tissues. Dityrosine was found in resilin, the rubber-like protein found in arthropods (Andersen 1964), and this represents the first documentation of the natural occurrence of this cross-linker in proteins, explaining that its function was to stabilis resilin through formation of a stable three dimensional of network (Andersen 1964). It has been reported that dityrosine cross-links occur naturally in several elastic and structural proteins including elastin, fibroin, keratin, cuticlin, and collagen (Fujimoto 1975; Labella et al. 1967; Raven et al. 1971; Waykole and Heidemann 1976). In these proteins, dityrosine cross-links can contribute to increasing the mechanical strength and subsequently their insolubility (Skaff et al. 2005).

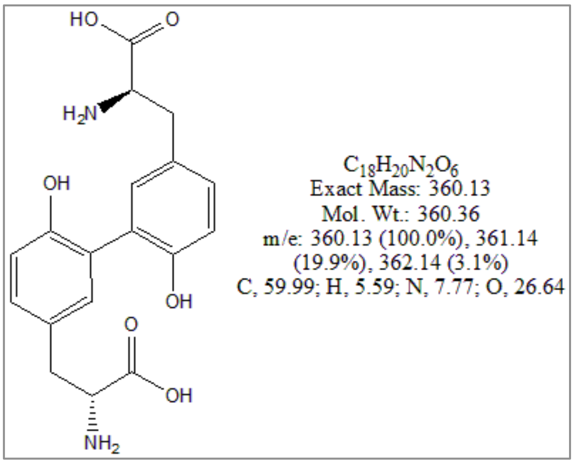

Figure 1-17: Chemical structure and molecular formula of dityrosine produced using Chemdraw ultra 8.

Moreover, it is believed to play a protective role in proteins (Bailey 1991; Kanwar and Balasubramanian 1999). Dityrosine cross-linking has also been implicated in the biosynthesis of thyroxine and melanin (Bayse et al. 1972). Additionally, dityrosine has been found in fungal cell wall proteins (Smail et al. 1995), the fertilization envelope of the sea urchin egg (Foerder and Shapiro 1977), Ascaris suum (Fetterer et al. 1993), and insect eggs (Li et al. 1996). Recently, many publications have demonstrated the dityrosine native role in many elastic and structural proteins (Dalsgaard et al. 2011; Fenaille et al. 2004; Hanft and Koehler 2005). Chakraborty *et al.* (Chakraborty et al. 2010) have recently investigated the formation of dityrosine in the DNA binding domain of the regulatory factor X5.

1.9 Physiological mechanisms of dityrosine formation in oxidatively damaged proteins

DiMarco and Giulivi (DiMarco and Giulivi 2007) reported that the mechanisms of dityrosine formation in oxidatively damaged proteins begin with the generation of a tyrosyl radical and this is consistent with reports from Atwood *et al.* (Atwood et al. 2004). The production of dityrosine involves the ortho-ortho cross-linkage of two tyrosyl radicals (Figure 1-18). Consequently, protein dimers are formed and can be detected as protein dimers by Sodium Dodecyl Sulphate-Polyacrylamide Gel Electrophoresis (SDS-PAGE) under reducing conditions (Giulivi and Davies 2001; Giulivi et al. 2003).

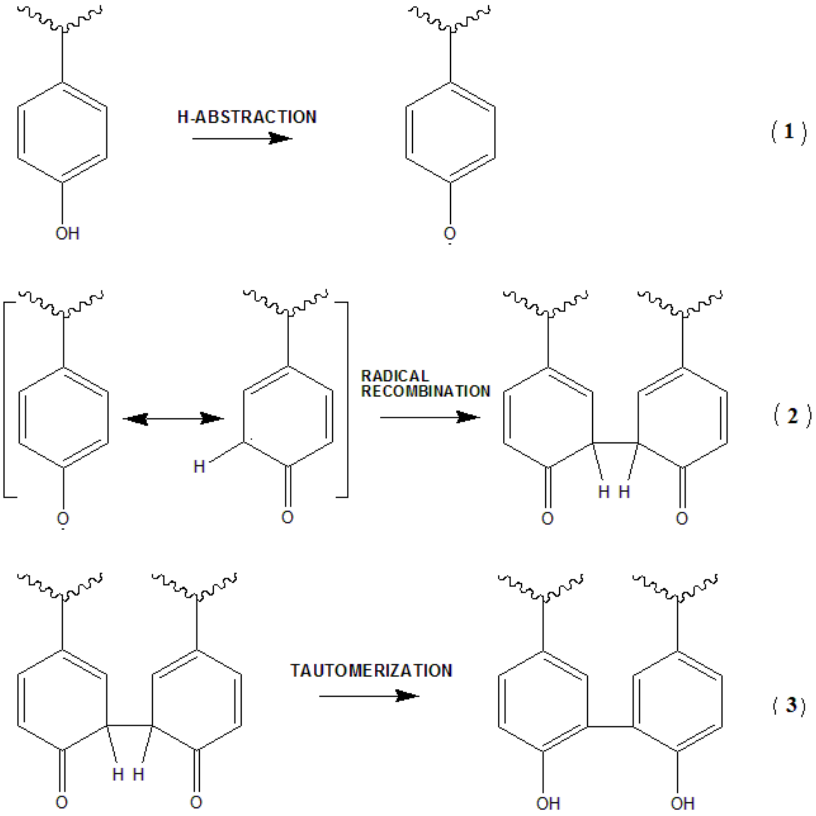

Figure 1-18: The mechanism of dityrosine formation in oxidatively damaged proteins begins with the generation of a tyrosyl radical, which then undergo radical isomerisation followed by diradical coupling, and finally tautomerisation.

Tyrosyl radicals can be generated by different mechanisms. Atwood *et al*. (Atwood et al. 2004) demonstrated two biochemical mechanisms for the generation of tyrosyl radicals and subsequently dityrosine cross-links: metal-catalysed oxidative and peroxidase-mediated tyrosyl radical formation.

Pre-existing Cu^{2+}-tyrosinate complexes react with H_2O_2 to produce species that have phenoxy radical like character, which subsequently undergo bimolecular coupling. Alternatively, Barnham *et al*. (Barnham et al. 2004) revealed that the Aβ peptide coordinates Cu^{2+} to form an Aβ-Cu^{2+} complex. In turn, the Aβ-Cu^{2+} complex is able to produce H_2O_2 catalytically in the presence of a reducing substrate such as ascorbate and underling this process, tyrosine radicals are generated, which are later coupled and result in Aβ aggregation. Another oxidative mechanism of proteins involves peroxidase-mediated tyrosyl radical formation (Atwood et al. 2004; Leeuwenburgh et al. 1997b; Marquez and Dunford 1995; Takasaki et al. 2005). Dityrosine can be generated by coupling of two tyrosyl radicals, which are generated by peroxidase.

1.10 Dityrosine as a biomarker of oxidative stress and its pathological role in diseases

Although dityrosine cross-links are formed naturally in many proteins for strength and protective purposes, the formation of dityrosine cross-links in proteins has also been implicated in many diseases, including AD and PD (Atwood et al. 2004; Souza et al. 2000), cystic fibrosis (Van Der Vliet et al. 2000), atherosclerosis (Leeuwenburgh et al. 1996), and cataracts in the eye lens (Bodaness and Zigler 1983; Wells-Knecht et al. 1993). It has been reported that dityrosine cross-links in γb-crystallin, calmodulin, ribonuclease A, and bovine serum albumin (BSA) resulted in protein denaturation and enhanced precipitation (Kanwar and Balasubramanian 1999, 2000; Yoburn et al. 2003).

It is also noteworthy that dityrosine can be formed in several proteins as a result of exposure to ROS, UV and γ–irradiation, aging, nitrogen dioxide, and lipid hydroperoxides (Giulivi and Davies 1993, 1994; Kato et al. 1994), and this may cause changes in the solubility, elasticity, and conformation of the cross-linked proteins (Souza et al. 2000). DiMarco and Giulivi (DiMarco and Giulivi 2007) reported that tyrosine was oxidised to dityrosine in response to oxidative stress by a peroxidase-catalysed mechanism in chymotrypsin, myoglobin, haemoglobin, and calmodulin. In this regard, dityrosine has been used as an important biomarker for the identification of oxidative protein damage as well as aging diseases (DiMarco and Giulivi 2007; Giulivi and Davies 1994). Suitability of dityrosine as a biomarker for oxidative stress of proteins is attributed to its chemical stability. It remains unchanged by exposure to oxygen and high pH (DiMarco and Giulivi 2007). Furthermore, it is highly resistant to acid hydrolysis and proteases (Amado et al. 1984; Giulivi and Davies 1994).

There has been a focus to investigate the possibility of using dityrosine as a marker of oxidative stress in many different diseases. Many analytical methods have been developed to enhance the sensitivity and selectivity to measure dityrosine levels with low concentration in real biological samples, and they are reviewed by (DiMarco and Giulivi 2007). In 1993, dityrosine was considered as an index of organismal oxidative stress in urine and red blood cells (Giulivi and Davies 1993). In 1996, Malencik *et al.* applied isocratic HPLC assay with fluorescence detection to measure underivatised dityrosine *in vitro* (Malencik et al. 1996). Fluorescence HPLC was also used to measure dityrosine in spiked samples of human CSF with detection limit of 60 picogrammes (Abdelrahim et al. 1997). Quantitative stable isotope dilution GC-MS assay was used to measure dityrosine levels in low density lipoprotein (LDL) that had been isolated from atherosclerosis plaques, and revealed a significant elevation of dityrosine levels compared to those in free-circulating LDL (Leeuwenburgh et al. 1997a). It has been found that dityrosine cross-linked proteins of mouse cardiac and skeletal muscle increased with age, and this increase is prevented by caloric restriction (Leeuwenburgh et al. 1997b). Isotope dilution GC-MS method, which is modified by Leeuwenburgh *et al*. (Leeuwenburgh et al. 1997a), has been used to quantify urinary dityrosine and *o*-tyrosine in children suffering from kwashiorkor (Manary et al. 2000), and the results revealed a very significant elevation of dityrosine levels in the affected children compared to normal children. Moreover, they suggested that this increase in urinary dityrosine levels reflects an increase in oxidative stress rather than an alteration in renal excretion of its precursor amino acid, i.e. tyrosine (Manary et al. 2000).

HPLC- electrochemical detection was used to measure dityrosine and nitrotyrosine in four specific sections of post-mortem brain tissue from both AD and control subjects (Hensley et al. 1998). Also, dityrosine was measured in CSF of AD and control subjects. The results revealed that dityrosine levels were elevated markedly in the hippocampus and neocortical regions of the AD brain and in ventricular cerebrospinal fluid (VF), suggesting that AD pathogenesis may involve the activation of oxidant producing inflammatory enzyme systems, including nitric oxide synthase (Hensley et al. 1998).

Enzyme-linked immunosorbent assay (ELISA) was used to investigate dityrosine in lipofuscin pigments from aged human brains (Kato et al. 1998). In this assay, polyclonal antibodies raised in rabbits were used to detect dityrosine. The results showed a significant elevation of dityrosine cross-links with age and the immunosorbent assay suggested “protein oxidation by free radicals and/or peroxidases may play an important role in lipofuscin accumulation” (Kato et al. 1998). Subsequently, Kato *et al*. has succeeded in preparing a monoclonal dityrosine antibody (1C3) used to investigate dityrosine in atherosclerotic lesions in Apo E deficient mice using immunohistochemical techniques, explaining that immunohistochemical techniques represent a simple method that provides details about dityrosine prevalence in cells and tissues, preventing the complex sample pretreatment required for GC-MS and HPLC-electrochemical detection (Kato et al. 2000).

Dityrosine cross-linked Aβ42 dimer was formed and purified *in vitro* using H_2O_2/peroxidase (Galeazzi et al. 1999). The Aβ dimers were detected by high resolution SDS-PAGE electrophoresis, and the identity of dityrosine cross-links was confirmed using HPLC with fluorescence detection, suggesting that dityrosine may be involved in the formation of the amyloid plaques in AD (Galeazzi et al. 1999).

Electrospray mass spectrometry and a dityrosine specific antibody (1C3) was used to investigate the dityrosine role in the Aβ aggregation mechanism *in vitro* and eventually in AD pathogenesis (Atwood et al. 2004). They found that incubation of Aβ with Cu^{2+} at a concentration lower than that in amyloid plaques leads to formation of Aβ oligomers that showed SDS-resistance, a characteristic feature of the neurotoxic Aβ extracted from Alzheimer's brain (Walsh and Selkoe 2007). These Aβ oligomers were found to give a dityrosine fluorescence signal. Furthermore, they revealed that addition of H_2O_2 significantly promoted dityrosine formation compared to incubation with Cu^{2+} only (Atwood et al. 2004).

Pennathur *et al.* investigated the use of dityrosine, *o*-tyrosine and nitrotyrosine as markers of oxidative stress in PD using a mouse model (Pennathur et al. 1999a). The PD mouse model was produced by injection of 1-methyl-4-phenyl-1,2,3,6-tetrahydropyridine (MPTP) 1 day before sacrifice. Dityrosine, *o*-tyrosine and nitrotyrosine in several brain regions were measured and the results revealed dityrosine and nitrotyrosine were increased in the striatum and midbrain, but not in brain regions resistant to MPTP. Pennathur *et al.* suggested that oxidative species including hydroxyl radicals, tyrosyl radicals or peroxynitrite might mediate the damage caused by MPTP to dopaminergic neurons (Pennathur et al. 1999a). Souza *et al.* have investigated the role of dityrosine in intracellular α–syn deposition in the Lewy bodies in PD, (Souza et al. 2000). Human recombinant α-syn was incubated with nitrating agents and resulted in dityrosine cross-linked α-syn oligomers, which showed high stability. HPLC-UV and HPLC-fluorescence analysis following acid hydrolysis of resulting oligomers revealed the formation of dityrosine cross-links, suggesting the mediation of oxidative and nitrative stress in the pathogenesis of PD (Souza et al. 2000).

1.11 Techniques by which to determine the oxidative and structural modification of peptide/protein.

1.11.1 Liquid chromatography-mass spectrometry (LC/MS)

1.11.1.1 Introduction

Coupling of MS to chromatographic techniques, such as LC and GC, has always been desirable due to high sensitivity and specificity of MS compared to other chromatographic detectors such as UV detection. Although the coupling of MS with LC is a powerful analytical technique that is used for many analysis applications, progress in this area was limited for a long period, and this is because of the relative incompatibility of existing MS ion sources with a continuous liquid stream. In 1989, Fenn developed the electrospray ion source (Fenn et al. 1989), and this made good progress and had an important impact in the application of LC-MS. One of the most important applications of LC-ESIMS peptide and protein analysis (Fenn et al. 1989).

1.11.1.2 The principle of mass spectrometry

The mass spectrometric analysis in general includes three essential steps, ionisation, fragmentation, and finally ion analysis (Figure 1-19). The first step in the mass spectrometric analysis, i.e. ionisation, is a process of converting the molecule of interest to a positively charged ion, which in turn undergoes many fragmentations to form many charged fragments. Finally, these ions and fragments are analysed on the basis of their mass to charge ratio (*m/z*) and eventually the resolved ions are detected according to their relative abundance.

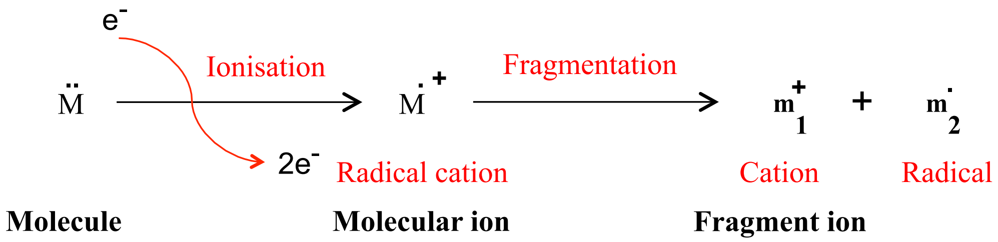

Figure 1-19: Schematic diagram showing mass spectrometric analysis of a molecule. Firstly the analyte molecule undergoes ionisation to produce gas phase ion of the molecule, and then this molecular ion undergoes fragmentation to form many charged fragment ions.

The mass spectrometry instrument consists of three major components (Figure 1-20): an ion source for producing gas phase ions of the compound under investigation, an analyser for separating the gaseous charged ions into their characteristic mass components based on their mass to charge ratio (*m/z*), and finally a detector for detecting the resolved ions and recording their relative abundance. All of these processes are operated under vacuum.

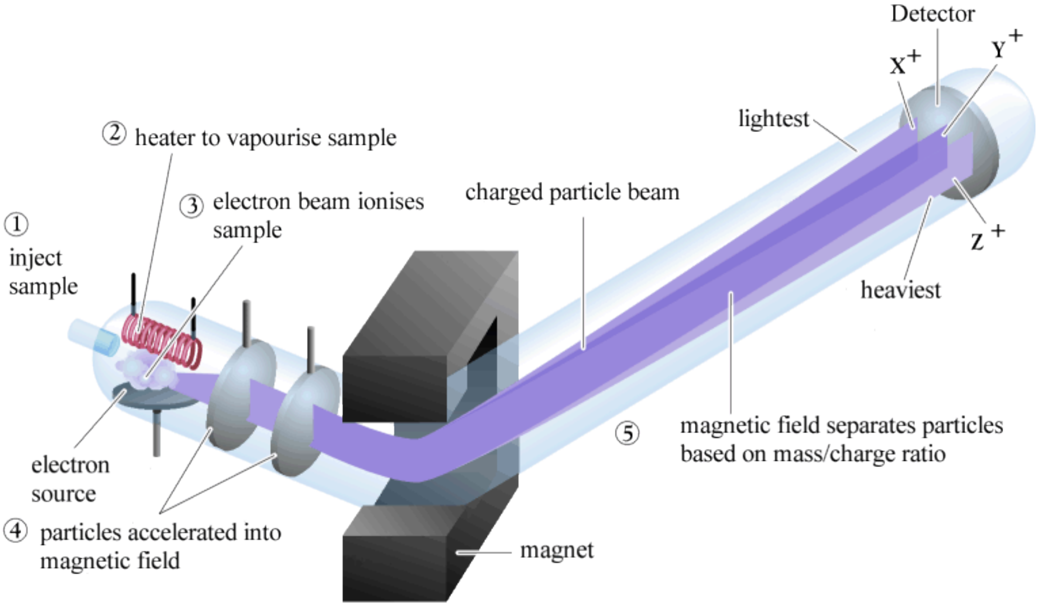

Figure 1-20: An example of mass spectrometry instrument. An electron beam fragments gaseous analyte molecule into cations (positively charged ions), and then these ions are accelerated and subsequently deflected along a circular path by a magnet. The heaviest particles are deflected less than lightest particle and eventually detected based on their relative abundance. Adapted from (http://www.mhhe.com/physsci/chemistry/carey/student/olc/ch13ms.html).

1.11.1.3 **Electrospray ionisation mass spectrometry**

Both the ionisation and ion analysis processes can be performed using many different technologies. Different combinations of these two processes result in various types of mass spectrometers. There are many types of ion source such as electrospray ionisation source (ESI), atmospheric pressure chemical ionisation source, and atmospheric pressure photo ionisation source. However, this description will focus on electrospray ionisation because it is used widely in many different areas in chemical, biochemical, pharmacological, and environmental studies. In addition, all of the mass spectra in this thesis were collected using an ESI.

In ESI, electrical energy is applied to assist the conversion of ions from solution into the gaseous phase before they are subjected to ion analyser. Thus the ESI enhances the sensitivity of the MS to detect ions in solution. In addition to the ionic species, neutral molecules can be also analysed using ESI-MS. The ionic form of the neutral molecules can be produced in solution or in gaseous phase by either protonation or cationisation such as metal cationisation.

Typically, the ESI process involves three steps to transfer the molecular ionic forms from solution into the gas phase as described in Figure 1-21. The first step is dispersal of a fine spray of charged droplets, followed by rapid solvent evaporation by application of heating and dry nitrogen, and finally, the residual electrical charge on the droplets transfer to the analyte molecule (Gross and Roepstorff 2011; Ho et al. 2003).

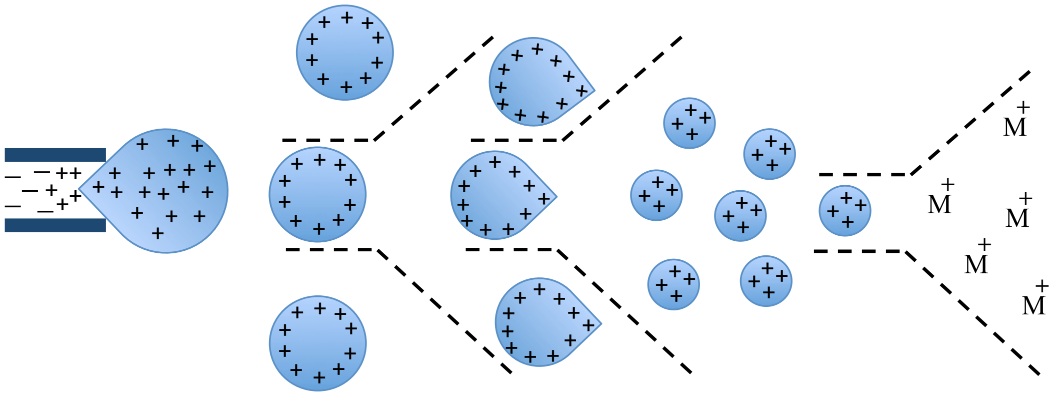

Figure 1-21: Schematic diagram of electrospray ionisation mechanism. The ionic species of the analyte compound can be transferred from the solution into gaseous phase through three main steps. The solution contained ionic species is pumped through a metal capillary tube, which is maintained at 2.5-6.0 kV, and then a fine spray of charged droplets is generated at the tip of the tube, followed by solvent evaporation and finally charge transferring from the charged droplets to the molecules.

Within an ESI source, a continuous flow of liquid samples is pumped through a metal capillary tube, which is maintained at 2.5 to 6.0 kV, and then a mist of charged droplets produced at the tip of the capillary tube, and followed by solvent evaporation under heat and nitrogen dry gas. As a result, the charged droplets are continuously reduced in size, and finally the charges transfer from the charged droplets to the molecules (Ho et al. 2003; Pitt 2009). The emitted charged molecules are then accelerated into the mass analyser for subsequent analysis of molecular mass and measurement of relative ion abundance.

1.11.1.4 **Tandem quadrupole mass spectrometry (MS/MS)**

Tandem quadrupole mass spectrometry has been frequently used as a standard analytical tool for both GC-MS/MS and LC-MS/MS applications, especially for cases where accurate quantitation is desired. Continuous developments have been made for tandem quadrupole mass spectrometry to improve its resolution, sensitivity, and the covered mass range. A Quadrupole is a mass analyser in which ions are separated using an electric field, and typically it consists of four parallel hyperbolical or cylindrical metal rods. Each opposing rod pairs are held at the same potential that is composed of a DC and an AC component (Gross and Roepstorff 2011; Watson and Sparkman 2007).

Tandem quadrupole also called triple quadrupole simply consists of three quadrupoles that are set up linearly as shown in Figure 1-22, in which the first (Q1) and third (Q3) quadrupoles are mass-selective, whereas the second quadrupole (Q2) serves as a collision cell. The targeted analyte ion, often called the precursor ion, is mass-selected by the Q1 and then collided with a collision gas (usually argon) in a Q2, which is always operated in the radio frequency (RF) mode. In Q2, the precursor ion undergoes further fragmentation and this process is known as collision-induced dissociation (CID). The resulting fragmented ions, usually called daughter ions, are related to the molecular structure of the precursor ions and can be analysed by a Q3 providing structural information of the precursor ions (Banerjee and Mazumdar 2012; Burlingame et al. 1996; Ho et al. 2003). When a mixture of molecular ions, which have different *m/z* ratios are introduced into Q1, only mass-selected precursor ions are allowed to pass through the Q1 into Q2, while the other molecular ions are filtered out. Therefore there is no need to purify the sample prior to MS/MS analysis, and this advantage eliminates complicated and time-consuming sample purification procedures prior to MS analysis.

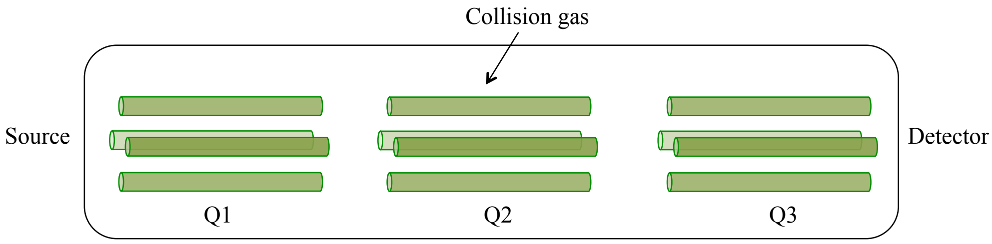

Figure 1-22: Schematic diagram showing a triple quadrupole MS/MS system. The first quadrupole (Q1) and third quadrupole (Q3) are mass spectrometers and the centre quadrupole (Q2) is a collision cell.

Tandem quadrupole mass spectrometry MS/MS can be operated in four different modes (Gross and Roepstorff 2011; Ho et al. 2003) based on Q1 and Q3 operation mode:

1- Product scan (also known as daughter scan): Q1 is static, allowing only the mass-selected ions of specific *m/z* ratio to pass through to fragmented in Q2, and then the resulting product ions are scanned in Q3 scans.

2- Precursor scan (also known as parent scan): In this mode, a wide range of precursor ions is allowed to pass through Q1 to be fragmented in Q2. Whereas, Q3 is static and set up to select one unique product ion resulting from CID of a class of precursor ions.

3- Neutral loss: Both Q1 and Q3 are scanned together at a constant difference in *m/z* ratio. This is used to monitor the loss of a neutral fragment for structurally related molecules from CID.

4- Multiple reaction monitoring (MRM): Both Q1 and Q3 are static and focus on a distinct pair of precursor and product ions. This significantly induces both specificity and sensitivity of the MS/MS system and is often used in ESIMS/MS quantification analyses.

1.11.1.5 **Biochemical applications of LC-ESIMS**

LC-ESIMS is a powerful analytical tool that has been used widely and extensively in a wide range of biochemical application. Biochemical genetics was one of the first areas that benefitted from LC-ESIMS. Metabolic profiling of amino acids and acylcarnitines from blood spots for a range of inborn errors of metabolism have been assessed by electrospray tandem mass spectrometry and this was one of the early applications of

LC-ESIMS (Rashed et al. 1997). Many books and reviews have reported the biochemical application of LC-ESIMS (Gross and Roepstorff 2011; High 2003; Ho et al. 2003). Quantification of proteins and peptides can be accurately assessed by LC-ESIMS, and also post-translational modification and metabolites can be detected and quantified using LC-ESIMS (Cutillas and Timms 2010; Johnson and Eyers 2010; Lipton and Paša-Tolic 2009), and this can significantly enhance understanding the biochemical pathways of many biological systems. In addition to biochemical applications, LC-ESIMS has been frequently used in pharmacological, forensic and environmental studies to identify and quantify small molecules such as drugs, natural metabolites and pesticides (Gross et al. 2012; Jungblut 2012). Applying MS/MS, such as MRM, can significantly enhance the specificity of the LC-ESIMS/MS quantification. MRM has been frequently used in proteomics identification and quantification (Cutillas and Timms 2010; Kiyonami and Domon 2010). The use of MRM for quantitative biomarker analysis in proteomics and metabolomics was reviewed in many articles (Issaq and Blonder 2009; Kitteringham et al. 2009).

1.11.2 **Fluorescence**

1.11.2.1 **Introduction to fluorescence**

Fluorescence is a process of absorbing and re-emitting light by a fluorescent molecule, i.e. fluorophore, on a timescale of about 10^{-8} seconds (Lakowicz 1999, 2007). The Jablonski diagram is usually used to demonstrate the processes that occur between the absorption and emission of light. As shown in the simplified Jablonski diagram (Figure 1-23), after light absorption, the fluorophore is usually excited to some higher vibrational level of either S1 or S2, and then returns to the lower energy level, S0 and consequently light is emitted (Figure 1-23). An internal conversion process occurs when a fluorophore rapidly relaxes to the lowest vibrational level of S1. This process is generally complete prior to emission as it occurs within 10^{-12} seconds or less (Lakowicz 2007).

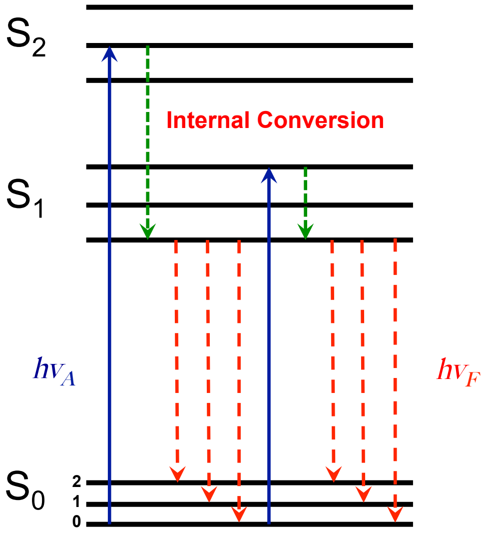

Figure 1-23:A Simplified Jablonski diagram showing that photons are absorbed ($h\nu_A$) and re-emitted ($h\nu_F$) at different wavelengths. S_0, S_1, and S_2 represent the singlet ground, first, and second electronic energy levels respectively. At each of these electronic energy levels the fluorophores can exist in a number of vibrational energy levels, labelled by 0, 1, 2. The transitions between states are labelled as vertical lines. hv represent the photon energy, and v represents its frequency (Lakowicz 2007).

Fluorescence usually emits from aromatic molecules, such as perylene and quinine. Each fluorophore has characteristic excitation and emission wavelengths. Fluorescence generally occurs at lower energies, i.e. longer wavelengths, and this is because the energy of the emission is less than that of absorption. The difference between the excitation and emission wavelengths is called the Stokes Shift (Figure 1-24). The Stokes Shift represents a key aspect in the detection of the emitted fluorescence in biological applications, as each fluorophore has a distinct characteristic Stokes shift. It is important to have a fluorophore with large Stokes shift as using fluorophores with very small Stokes will lead to overlap between the excitation and emission wavelengths, making the detection much more difficult.

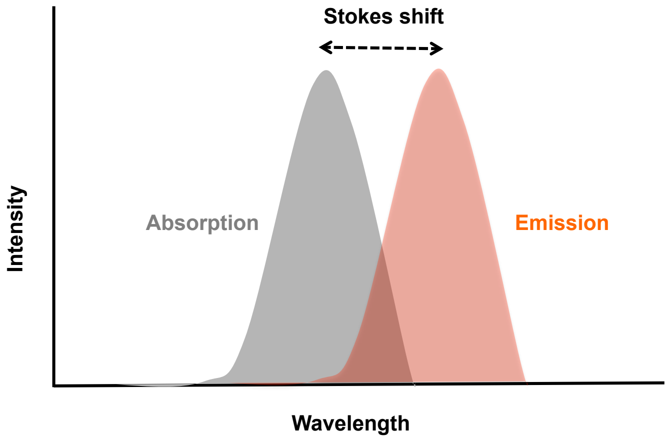

Figure 1-24: General excitation and emission spectra of a fluorophore. The difference between the excitation and emission wavelengths is called the Stokes Shift. As much as difference is large, the distinction would be easer.

1.11.2.2 **Fluorophores**

Generally, fluorophores can be divided into two main classes, intrinsic and extrinsic, based on their natural occurrence. Intrinsic fluorophores are molecules that naturally fluoresce, such as aromatic amino acids, NADH, flavins, derivatives of pyridoxyl, and chlorophyll. Extrinsic fluorophores are synthetic/external molecules that are added to a specimen to produce fluorescence when none exists, or to change the spectral properties of the specimen. Extrinsic fluorophores include dansyl, fluorescein, rhodamine, ThT and numerous other substances (Lakowicz 1999, 2007).

Intrinsic protein fluorescence results from the presence of aromatic amino acids, tryptophan, tyrosine, and phenylalanine. They have distinct absorption and emission wavelengths as shown in Table 1-2. As shown in the table, the three residues differ greatly in their quantum yields and lifetimes. The fluorescence spectra of the proteins containing these three residues are usually dominated by fluorescence from tryptophan. This is due to the indole groups in tryptophan that show higher UV absorbance and emission compared to the other amino acids (Lakowicz 2007). Phenylalanine emission can be observed only when a protein does contain neither tyrosine nor tryptophan residues.

Table 1-2: The table summarises the fluorescence characteristics of aromatic amino acids recorded in water at neutral pH. (Lakowicz 2007).

Amino acid	**λ_{ex} (nm)**	**λ_{ex} (nm)**	**Bandwidth (nm)**	**Quantum yield**	**Lifetime (ns)**
Phenylalanine	260	282	_	0.02	6.3
Tyrosine	275	304	34	0.14	3.6
Tryptophan	295	353	60	0.13	3.1 (mean)

The three aromatic amino acids can serve as intrinsic fluorescent probes for protein conformational changes. Tryptophan fluorescence is extremely sensitive to its local environment, thus conformational changes of many proteins can be investigated through tryptophan fluorescence. Many phenomena such as protein–protein interactions and binding of ligands cause in spectral shifts of protein fluorescence emission. A blue shift and an increase in intensity of tryptophan emission has been reported upon decreasing the solvent polarity (Seidel et al. 1993). This can be interpreted by burial in the hydrophobic core of the protein (Giancotti et al. 1980). Predominantly, tyrosine emission is quenched in native proteins as a result of its interaction with the peptide chain or energy transfer to tryptophan. By contrast, enhanced tyrosine emission is observed upon denaturation of proteins (Lakowicz 2007). It has been showed that the intrinsic fluorescence of the tyrosine increased by about 400% as the Histone H1 protein folds from a random coil to a globular structure (Giancotti et al. 1977). Measurements of external quenching by a wide range of quenchers shows higher reduced quenching in the folded state as compared to the disordered state, indicate that the tyrosine is a buried residue (Giancotti et al. 1977; Giancotti et al. 1980). Tyrosine intrinsic fluorescence of Aβ has been widely used to investigate the metal association (Maiti et al. 2008; Syme et al. 2004; Tougu et al. 2008).

Tryptophan, tyrosine, and phenylalanine fluorescence has been widely used to probe amyloid assembly. The aggregation of a Y39W α-syn variant was investigated using intrinsic tryptophan fluorescence as a probe and identified two classes of oligomeric intermediates, one formed during the lag period of fibril formation and the other present at the end of the process (Dusa et al. 2006). Similar studies of substituted tryptophan residue proteins, such as Aβ and β_2-microglobulin have been also carried out (Kihara et al. 2006; Touchette et al. 2010). Tyrosine intrinsic fluorescence of Aβ has been found to decrease at an early stage of Aβ aggregation, suggesting the possibility to use it as an indicator of Aβ aggregation (Rolinski et al. 2010). Recently, intrinsic and quenched tyrosine fluorescence has been used to investigate the structural switch from fiber to crystal structural of Sup35 yeast prion fragment, GNNQQNY (Marshall et al. 2010). Intrinsic phenylalanine fluorescence has been used to probe the fibrillisation of Aβ (16-20), i.e., KLVFF.

1.11.2.3 **Thioflavin T fluorescence**

Thioflavin T, a benzothiazole dye, is widely used to determine the presence of amyloid fibrils. Upon binding to amyloid, ThT undergoes a red shift in its emission fluorescence maximum from 445 nm to ~ 482 nm (Khurana et al. 2005; LeVine 1993; Vassar and Culling 1959). Based on the chemical structure, the ThT dye has a hydrophobic group with a dimethylamino group attached to a phenyl group, which is then linked to a more polar benzothiazole group containing the polar nitrogen and sulfur (Figure 1-25). The presence of polar and hydrophobic groups raises the possibility for ThT molecules to form micelles in aqueous solution, in which the positively charged nitrogen pointing toward the solvent and with hydrophobic interior.

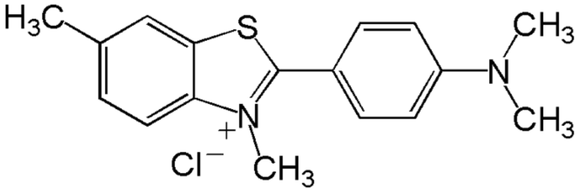

Figure 1-25: Chemical structure of thioflavin T dye. ThT has two different groups in its chemical structure, polar and hydrophobic group.

Although many mechanisms have been suggested to explain the binding of ThT to amyloid fibrils, the exact molecular mechanism of the ThT binding to amyloids remains elusive. It has been suggested that the mechanism underlies the enhancement fluorescence ThT involves hydrogen bond formation between charged nitrogen in the thiazole group to amyloid fibrils (Kelenyi 1967). Another explanation of the observed ThT fluorescence upon binding to amyloid was due to the formation of ThT micelles (Khurana et al. 2005), explaining that changes in the excitation spectra and enhanced emission fluorescence result upon binding of ThT micelles to amyloid fibrils. ThT micelles bound to the surface of amyloid fibrils were observed by atomic force microscopy (Khurana et al. 2005). Recently, it has been suggested that ThT fluorescence enhanced upon binding with amyloids may arise from the formation of an ThT excimer (dimer or oligomer) localised at the surface of the mature fiber (Sabate et al. 2013). Structurally, ThT molecule has a pair of rings, i.e. benzothiazole and benzamine that freely rotating around a shared C–C bond (Figure 1-26). The photo-physical properties of ThT were studied in various solvents and the results indicate that the quantum yield of ThT increases with viscosity of the solvent because of the impediment of the internal rotation of the two rings (Amdursky et al. 2012; Stsiapura et al. 2008). A hindrance of ThT rotational intrinsic movement upon binding to amyloid surfaces can result in ThT fluorescence enhancement through stabilisation of the fluorescent species (Sabate et al. 2013).

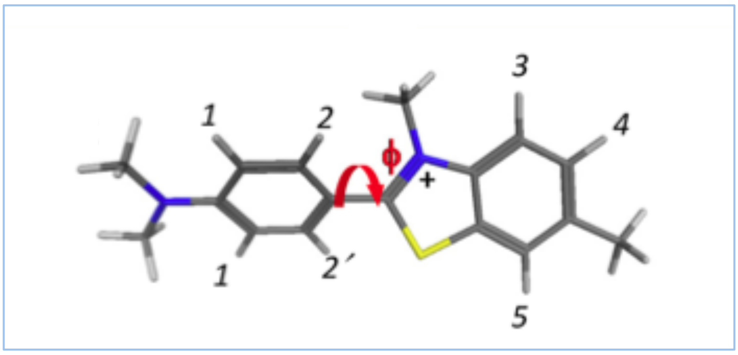

Figure 1-26: Structural model showing the ThT rotational intrinsic movement. Adapted from (Robbins et al. 2012). Benzothiazole and benzamine rings are freely rotating around a shared C – C bond.

ThT dye has been extensively used to follow amyloid formation due to its selectivity to bind amyloid fibrils and not amorphous aggregates (LeVine 1993), and it has been considered essential in defining a substance as amyloid (Nilsson 2004). Commonly, ThT fluorescence is used to follow kinetics of amyloid formation. However, induced ThT fluorescence varies greatly depending on the amyloid precursor of interest and can be very low for certain amyloidogenic short peptides (Sabate and Saupe 2007). The pH at which ThT is performed strongly affects the affinity of ThT to amyloid fibrils, and it has been revealed using pH 8 would greatly increase the affinity of the dye to the fibrils (LeVine 1999), thus maximum enhancement will gained. However, basic pH would not be always effective to produce amyloid fibrils since many proteins and peptides can not form fibrils at basic pH, therefore experiments must be carried out rapidly to avoid fibril dissociation (LeVine 1999). Furthermore, ThT dye exhibits great sequence specificity.

Sequences that contain aromatic residues, such as tyrosine and phenylalanine, seem to induce binding and that is probably due to hydrophobic interactions and $\pi - \pi$ stacking (Wu et al. 2009). By contrast, the high content of positively charged residues inhibits the dye binding (Wu et al. 2009).

1.11.3 **Circular dichroism**

1.11.3.1 **Theoretical principles and instrumentation**

Circular dichroism (CD) spectroscopy is a biophysical technique that is usually used to probe and investigate the secondary structure of peptides, proteins and nucleic acids by measuring the difference in the absorption of left and right circularly polarised light (Schellman 1975). In peptides and proteins, the asymmetry of the attached chemical groups surrounding the α-carbon atom of the amino acid can give rise to chirality, thus differential absorption of left and right circularly polarised light will be produced and consequently a CD spectrum obtained. Interaction of non-chiral molecules with chiral molecules will induce the chirality of the former and lead to CD signal production (Rodger 2010; Wallace and Janes 2009). CD can be expressed by the following equation:

$$\text{CD signal} = A_L - A_R$$

Where A_L and A_R are the absorption of the left and right circularly polarised light by the chiral substance respectively. The CD signal is wavelength dependent and at some wavelength the chiral molecules will absorb the left and right handed polarised light to different extents and the resulting CD signal could be either positive or negative depending on the relative intensity of the absorbance (Wallace and Janes 2009).

In a CD spectrometer, the linear polarised light that is emitted from a UV source, i.e. xenon arc lamp, is passed into a Photo elastic modulator (PEM) and converted into alternating left and right circularly polarised light (Kelly and Price 2000). Then, an optically active molecule absorbs the two circular polarised components to different extents, and the difference in absorption is detected with a Photo multiplier tube (PMT) as shown in Figure 1-27. Circularly polarised light, when passed through a chiral molecule, results in a beam that is elliptically polarised and this is because the chiral molecule absorbs the circular polarised components with different magnitudes. Thus, the CD signal can also be expressed in terms of ellipticity (Wallace and Janes 2009).

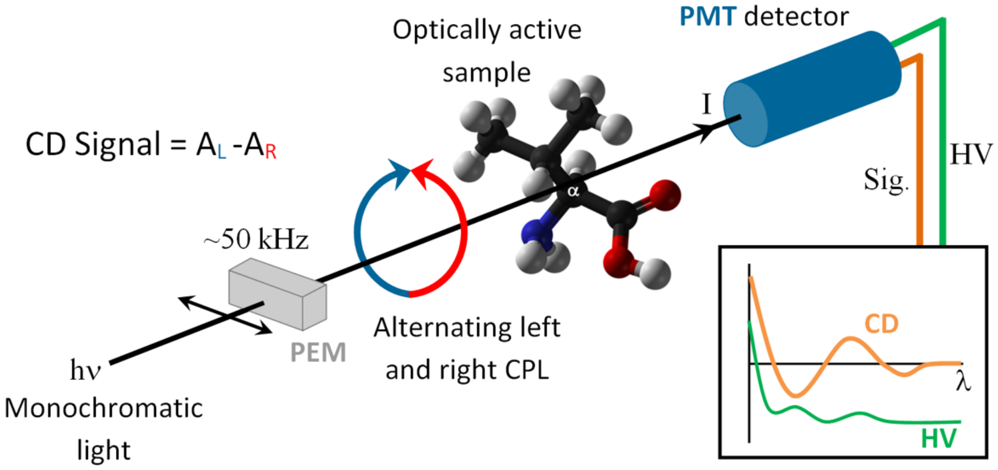

Figure 1-27: Schematic diagram describing the principle of CD spectroscopy. The linear polarised light that is emitted from UV source is passed into a Photo Elastic Modulator (PEM) and converted into alternating left and right circularly polarised light. An optically active molecule differently absorbs the two polarisations, and the difference in absorption is detected with a Photo Multiplier Tube (PMT). Reproduced from (http://www.isa.au.dk/facilities/astrid/beamlines/cd1/cd1_3.asp).

The CD spectrum has three prominent regions, near UV, far UV and vacuum UV which correspond to ~360 – 260 nm, 260 – 190 nm, and 190 – 120 nm respectively (Wallace and Janes 2009). Furthermore, CD signals can be obtained in the visible wavelength region by coloured chiral molecules such as myoglobin. However, most CD measurements of biomolecules are carried out in the UV region. CD signals of amide groups in peptides and proteins dominate the far UV region, whereas distinct CD peaks in the near UV region are produced from the contribution of the aromatic side chains of proteins, e.g. tyrosine residues. Nucleic acids usually have CD signals over the entire UV range (Wallace 2009). Carbohydrates tend to produce peaks in the vacuum UV region, which can be obtained using synchrotron radiation CD (SRCD) (Wallace and Janes 2009).

1.11.3.2 **Far-UV CD: electronic transitions of peptide bond in the protein**

Typically, CD signals of amide groups in peptides and proteins dominate the far UV region, and they are produced by electronic transitions from a ground state orbital to excited state orbital. Mainly, the peptide bond exhibits two electronic transitions, i.e. n to π* (nπ*) and π to π* (ππ*), which contribute significantly in the far UV CD of the proteins and peptides, and reflect their conformational structure (Greenfield 1996; Kelly et al. 2005). A CD band at ~ 220 nm is produced as a result of nπ* transition, whilst the ππ* transition induces a CD signal at ~190 nm as shown in Figure 1-28 (Norden et al. 2010; Wallace and Janes 2009).

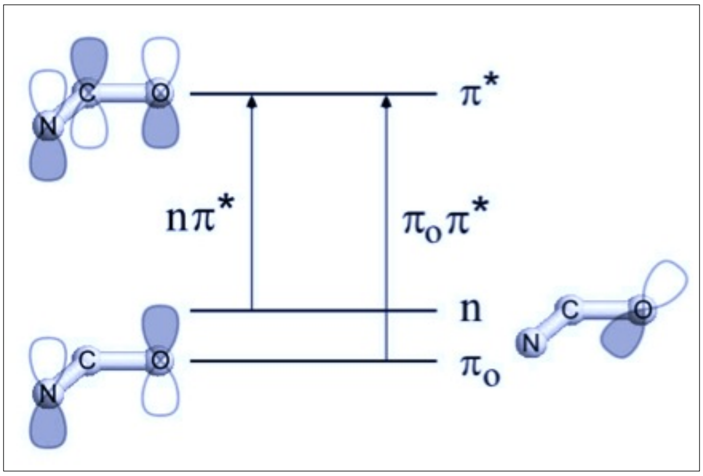

Figure 1-28: Schematic diagram of the electronic transitions of the amide bond generating CD signals in the far-UV region. The 'n' is associated with the lone pair orbitals while the π_0 and π are non-bonding delocalised π -orbitals and anti-bonding orbitals respectively. Adapted from (Wallace and Janes 2009).*

The three dimensional secondary structure that is adopted by peptides and proteins modifies the electronic transitions of the peptide bond and this is due to the additional chirality features that is induced by interaction of the peptide chains and also by contributions of the side chain groups of the amino acids (Norden et al. 2010). In turn, different and characteristic CD spectra can be obtained in each case. The CD spectral features associated with different protein secondary structures are illustrated in Figure 1-29. There are three main classes of secondary structure: α-helix, β-sheet, and random coil, each structure has a distinct CD spectrum. The α-helix conformation shows two negative CD bands at ~ 222 nm and ~ 208 nm and a positive band ~ 190 nm (Figure 1-29), which corresponds to nπ*, ππ*parallel ($\pi\pi^*_{\parallel}$), and ππ* perpendicular ($\pi\pi^*\perp$) respectively (Wallace and Janes 2009). The ππ* parallel and perpendicular transitions produced as result of excition coupling that splits the ππ* transition into two components defined relative to the helix axis (Juban et al. 1997; Wallace and Janes 2009). The CD spectrum of β-sheet conformation has two characteristic bands at ~ 215 nm for nπ* and ~ 195 nm corresponds to ππ*, however, different types of β-sheet structure show some wavelength shifting and spectrum shape variation (Wallace and Janes 2009). The random coil structure has a small positive band at ~ 217 nm for the nπ* transition, and a strong negative band ~ 197 nm for the $\pi\pi$* transition (Bulheller et al. 2007; Juban et al. 1997).

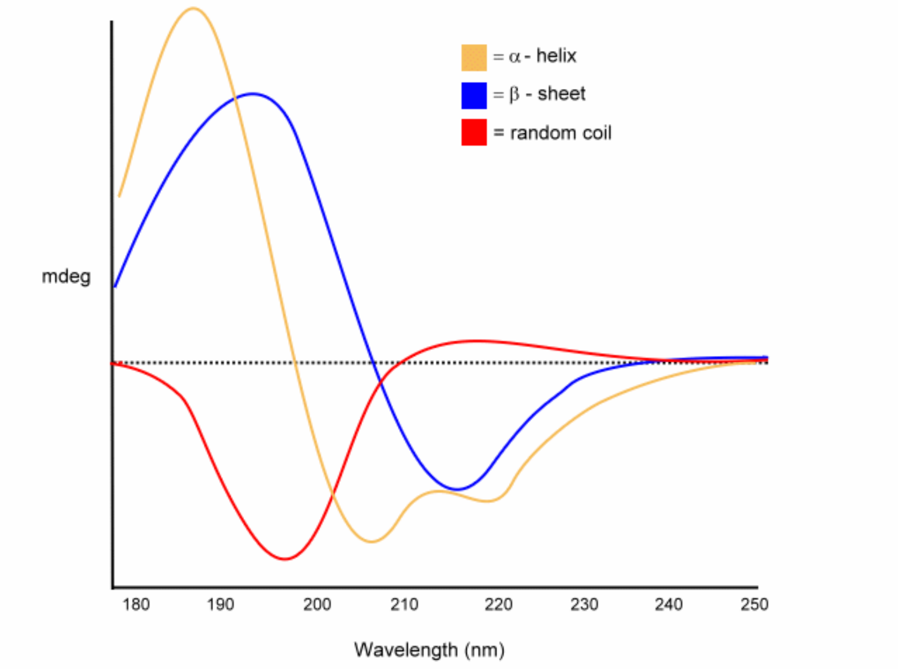

Figure 1-29: Schematic graph showing typical CD spectra for α-helical, β-sheet, and random coil structures. Reproduced from (http://www.proteinchemist.com/cd/cdspec.html).

Aromatic residues, such as tyrosine and tryptophan, can contribute to the far-UV CD spectra of protein. The contribution of aromatic residues has been studied extensively (Woody 1978, 1994). However, the contribution of the aromatic residues to the far-UV CD is less detectable than that in near-UV CD, and this is because peptide bond transitions dominate in the far-UV region.

CD is an important technique that is used to determine and investigate the protein structure. However, the resolution of structural details is more limited than the information produced by other techniques such as X-ray crystallography or NMR spectroscopy, and this is because CD can determine only the total secondary structure content and cannot attribute secondary structures to specific regions of the molecule (Wallace and Janes 2009). Unlike X-ray crystallography, CD is really useful for determining secondary structure elements in solution. Additionally, CD is a powerful method to examine protein structure under more physiological conditions compared to those required for NMR data collection such as low pH and high concentrations (Wallace and Janes 2009).

1.11.3.3 **Near-UV CD: Aromatic contributions to CD spectra of proteins**

Aromatic residues, such as tyrosine and tryptophan, have been found to have a considerable contribution to the CD spectra of proteins and peptides in the near-UV region through the aromatic transitions (Sreerama et al. 1999; Strickland 1974). The near-UV CD spectrum provides information about protein tertiary structure and reflects the conformational changes of these residues that are associated with different processes. The transitions of tyrosine and tryptophan residues in the near-UV region are shown in Figure 1-30, as well as the far-UV transitions of both α-helix and β-sheet. The tyrosine residue has one transition at ~ 275 nm in the near-UV, whereas tryptophan has two at ~ 295 nm and 267 nm (Hicks et al. 2010).

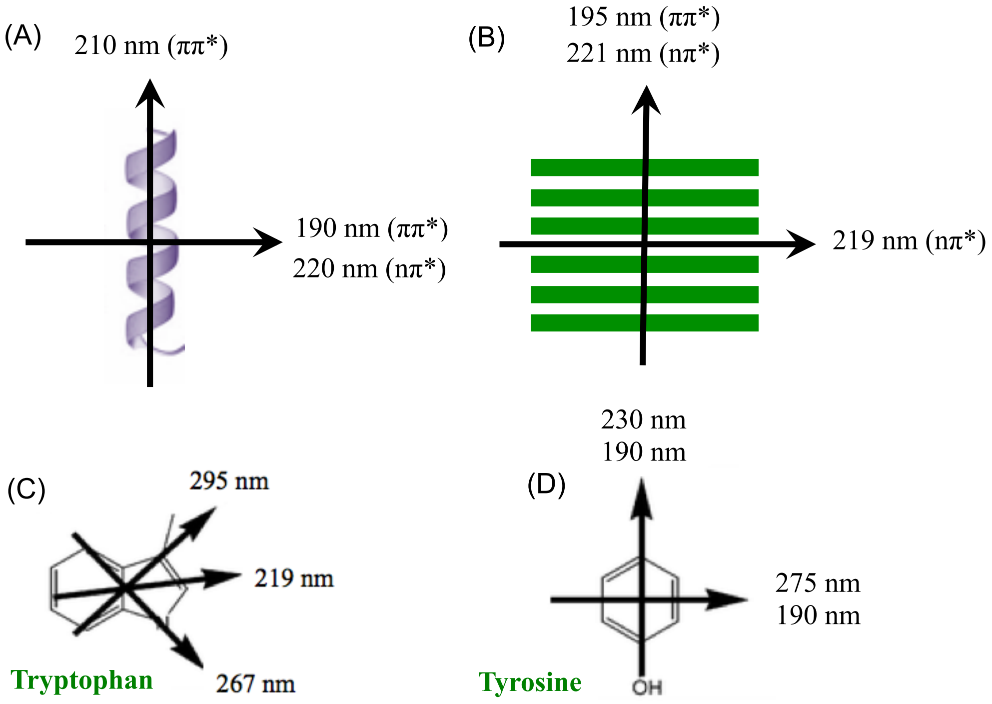

Figure 1-30: Orientations of electronic transition polarisations for (A) α-helix, (B) β-sheet, (C) tryptophan and (D) tyrosine. Adapted from (Hicks et al. 2010; Rodger et al. 2006).

A red shift observed in the CD band (~ 275 nm) of tyrosine compared to phenylalanine (~ 263 nm) is due to the presence of the hydroxyl group (Fasman 1996). Moreover, the intensity of the tyrosine CD signal is much higher, thus the detection is much easier. Although protein structural studies are commonly performed in the far-UV, the theoretical basis and interpretation of the CD spectra in the near-UV region has been extensively studied (Horwitz et al. 1970; Strickland 1974). The near-UV CD spectral changes accompanied with folding processes can reflect the exposure and burial environment around the aromatic residues within protein structure. For example, a change in absorption of the tyrosine CD band has been used to investigate the extent of burial of the tyrosine residues in bovine pancreatic ribonuclease (Horwitz et al. 1970). The near-UV CD of aromatic residues containing proteins can be affected by the presence of metal ions and this could reflect the possibility of coordination of these ions with the protein via the aromatic residues. The presence of a zinc ion can affect the formation of insulin oligomers and this effect was studied by monitoring the near-UV CD spectrum development (Wood et al. 1975).

1.11.3.4 **Structural determination of amyloidogenic peptides and proteins by CD**

CD has been frequently used to investigate the conformational development that accompanies amyloid assembly and aggregation (Abe and Nakanishi 2003; Barrow et al. 1992; Marshall and Serpell 2009). The conformational changes during the conversion of monomeric species into β-sheet rich fibres were studied widely using both far and near-UV CD (Jean et al. 2008; Lee et al. 2007b). CD is a useful technique that can provide valuable details about the secondary structure of the early unfolded or partially folded oligomeric species and their subsequent role in amyloid assembly (Uversky and Fink 2004). A CD signal in the near-UV region at 285 nm has been attributed to amyloid formation by a non-amyloid-β component EQVTNVGGAVVTG (NAC1-13), as it does not contain any aromatic residues in the polypeptide backbone (Abe and Nakanishi 2003). Many near-UV CD studies have been carried out to follow amyloid fibril formation and the accompanied structural changes from different proteins, such as TTR (Colon and Kelly 1992), α-syn (Ulrih et al. 2008) and β-microglobulin (Eakin et al. 2004). Also, CD was used to investigate the effects of Cu^{2+} on the secondary structure of PrP (Younan et al. 2011).

Similar to proteins, many short peptides exhibit the ability to form amyloid-like fibrils and macro-biostructures such as nanotubes, and their structure has been investigated using CD. However, short peptides that contain aromatic residues in their sequences significantly showed CD spectra that differ from the observed regular CD. Nanotubes that formed from diphenylalanine peptide showed a CD spectrum with two positive bands at 197 nm and 220 nm, and a broad negative band at ~ 280 (Gupta M 2007), suggesting that this red shift to 280 nm generated as a result of the phenylalanine residues stacking in the nanotube structure. Two tyrosine-containing peptides, APYG and LPYG, were designed to adopt β-turn conformation and were characterised using CD. The CD spectra exhibited two minima bands around 205 nm and 225 nm and a weak maximum around 193−195 nm (Tinker et al. 1988), and it was proposed that the CD minimum near 225 nm is characteristic of the β-turn. Similarly, AAKLVFF peptide was found to give β-turn structure in solution interpreted from the observed negative maximum CD band at 228 nm and a weaker positive signal at 209 nm (Krysmann et al. 2008), and was interpreted to arise from nπ* aromatic stacking interactions between phenylalanine residues. Interestingly, Aβ16-20 pentapeptide (KLVFF) with methylated K and V that inhibits Aβ fibrillogenesis has CD spectrum consistent with a β-sheet conformation with a red shift of 217 to 226 nm (Gordon et al. 2002) and this was attributed to a twist (Cerpa et al. 1996; Manning et al. 1988; Orpiszewski and Benson 1999).

Caution should take into account regarding interpretation of CD spectra of amyloid. Many factors can significantly complicate the CD data analysis and interpretation. Firstly, artificial linear dichroism (LD) signals that are generated from ordered systems can greatly mask the CD signal, as they have a much higher magnitude than CD (Davidsson et al. 1980). CD measurements are usually carried out on samples that show no direction dependence, i.e. isotropic samples. However, amyloid fibrils may show directional dependence, thus their collected CD spectra cannot be directly interpreted. Therefore, some sample pretreatment such as sonication is necessary to abolish the LD artifacts. Two other factors that can particularly affect the CD spectra are light scattering and absorption flattening (Ji and Urry 1969; Mao and Wallace 1984; Starck and Sutherland-Smith 2010). Light scattering is produced due to the presence of non-dissolved particles that can lead to loss of light intensity and subsequently production of false high measured absorbance. In amyloid samples the presence of aggregates will lead to light scattering. Absorption flattening leads to decrease of absorbance due to a decrease in the effective concentration of absorbers, i.e. particles able to absorb light. Amyloidogenic peptides and proteins usually aggregate to form oligomeric species that are may be suspended in solution, thus over time the effective concentration of the species that are able to absorb the light will decrease and result in false low measured ellipticity (Calloni et al. 2008; Starck and Sutherland-Smith 2010).

1.11.3.5 **Good practical considerations in data collection**

Many factors can affect the obtained CD spectrum leading to a poorly collected CD spectrum. Therefore, it is essential to optimise the data collection conditions ensuring careful sample preparation and applied instrument parameters. Sample preparation has an enormous influence on the quality of the obtained CD data. Good CD strategy should consider sample preparation in terms of purity, concentration and buffers used for dissolution. Many buffers and solvents have to be avoided in CD data collection, due to their ability to absorb the light in both far and near UV regions, and this consequently results in poor CD spectra (Kelly and Price 2000; Kelly et al. 2005). Also, it is important to choose a buffer/solvent that has ability to maintain protein integrity. The pathlength of the cuvette that is used to collect the data is another factor that should be taken into account. It has been revealed that pathlength of many cuvettes, especially the shortest ones, have an error in their cited length and need to re-determined before use (Wallace and Janes 2009).

1.11.4 **Transmission electron microscope**

1.11.4.1 **Introduction**

The basic principle of electron microscopy is generally similar to light microscopy except that electron microscopes use an electron beam to illuminate the specimen instead of visible light as in light microscopy. As the electrons have much shorter wavelengths compared to visible light, electron microscopies have greater resolution. A high resolution of 0.1 – 0.2 nm can be gained by electron microscopes, whereas light microscopy can only provide a resolution of about few hundreds nm (Williams and Carter 2008). There are different types of electron microscopy such as transmission electron microscope (TEM), scanning electron microscope (SEM), and scanning tunneling electron microscope (STM).

Transmission electron microscope mainly consists of four parts; electron source, electromagnetic lens system, a sample holder, and an imaging system (Figure 1-31). A tungsten filament at the top of a cylindrical column of about 2 m high is used as an electron source. A voltage in the anode accelerates the emitted electrons and applying higher anode voltage will enhance the electron speed, as a result a high-resolution image will be produced (Reimer and Kohl 2008). The collision of the electrons with air would lead to electron scattering, therefore, it is very important to evacuate the air from the whole optical system. A condenser, which consists of electromagnets called magnetic lenses, is used to focus the electronic beam on the specimen. The imaging system consists of two parts; electromagnetic lens system and a screen, which has a phosphorescent or fluorescent plate. The plate glows when hit by the transmitted electrons through a thin section of the sample. Black and white images with high resolution are produced by interaction of energetic electrons and the sample under vacuum (Reimer and Kohl 2008).

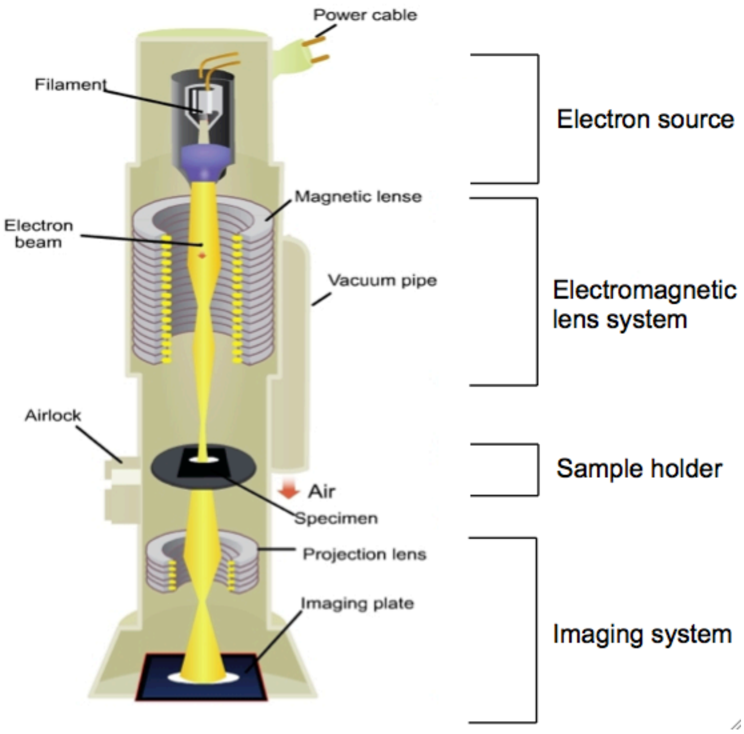

Figure 1-31: Schematic diagram showing the TEM. Adapted from (http://www.hk-phy.org/atomic_world/tem/tem02_e.html).

Many morphological and compositional details can be provided by TEM. Two-dimensional information with high-resolution images can be collected by TEM, thus TEM can be used in a wide range of science and industry applications.

TEM has made a high impact in the study of AD, amyloid plaques and Aβ fibrillogenesis and has been reviewed in many publications (Harris 2005; Walsh et al. 1997; Wegiel et al. 2001; Williams and Carter 2008). TEM was used widely to investigate the existence and structure of amyloid plaques in post-mortem brain sections from AD patient and transgenic (Tg) mouse animal AD models (Richardson et al. 2003; Sasaki et al. 2002; Wegiel et al. 2002; Wegiel et al. 2003). A wealth structural detail of extracellular diffuse and compact amyloid plaques has been provided by TEM. Moreover, an enormous number of AD studies using cultured neurons, microglia, astrocytes and other cells were performed using TEM (Sasaki et al. 2002; Wegiel et al. 2001). Previously, TEM studies of brain and cell culture were performed using conventional thin sectioning of resin-embedded samples. Recently, pre- and post-embedding antibody labelling protocols, also called TEM immunolabelling, have been modified and used to study amyloid plaques in brain sections from AD patients and a Tg mouse AD model (Al-Hilaly et al. 2013; Wang et al. 2012). Similarly, TEM immunolabelling has been used to study AD using various cell cultures *in vitro* (Al-Hilaly et al. 2013; Romano et al. 2003; Soura et al. 2012).

TEM has contributed extensively to knowledge regarding the structure and morphology of Aβ fibrils and other amyloid systems *in vitro*. TEM has been frequently used to monitor the fibrillogenesis process of many amyloid fibre-forming systems such as Aβ and α-syn, providing extensive morphological details of each characteristic species, i.e. oligomers, protofibrils, and fibrils (Bitan et al. 2003; Fitzpatrick et al. 2013; Soto et al. 1995; Walsh et al. 1997). TEM runs parallel with a wide range of available biophysical, biochemical and biological techniques, such as XRFD, ESIMS, CD, NMR and ssNMR spectroscopy, to get insight into molecular and supramolecular amyloid structures and to study the fibrillogenesis (Marshall and Serpell 2010; Morris and Serpell 2012, 2013; Williams et al. 2010). Negative staining TEM analysis of oligomerisation of Aβ40 and Aβ42 by Bitan *et al.* revealed the presence of ~ 5 to 20 nm spherical particles (termed "paranuclei"), which in turn aggregated to form larger elongated oligomers and clusters

(Bitan et al. 2003). Nybo *et al*. previously showed this for Aβ42 using TEM. A combination of biophysical techniques and TEM were used to identify Aβ protofilament intermediates involved in fibrillogenesis (Lashuel et al. 2000; Malinchik et al. 1998; Walsh et al. 1997). Aβ protofilament with ~ 5 nm width was identified. In a series of publications, fibrils morphologies formed from different Aβ peptides have been defined using negative stain TEM and generally found to be long, straight, unbranched fibrils with twisting as shown in Figure 1-32 (Fandrich et al. 2009; Meinhardt et al. 2009; Serpell 2000).

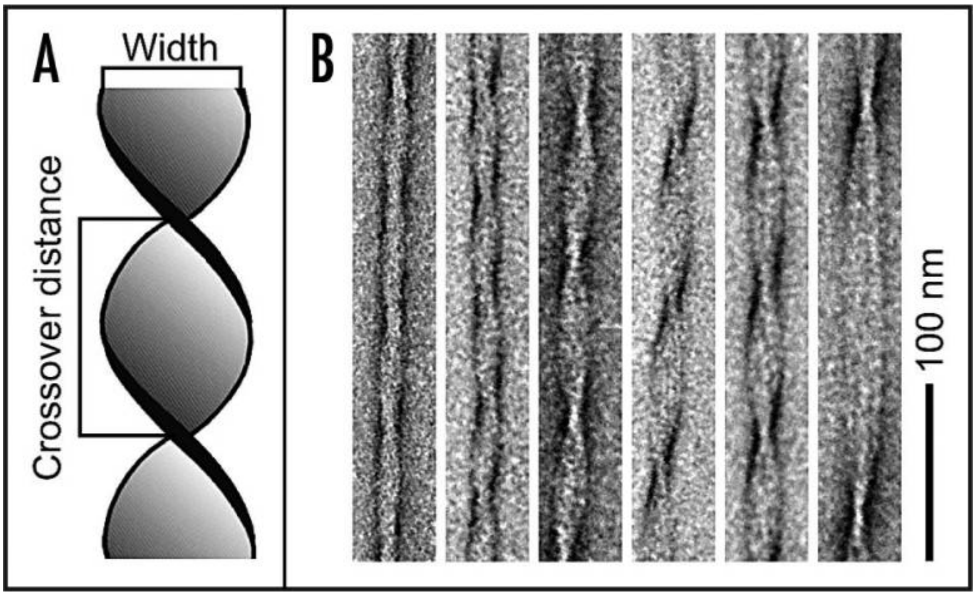

Figure 1-32: Structural polymorphism of Aβ40 fibrils. (A) Schematic representation of an amyloid fibril showing the definitions of fibril width and crossover distance. (B) TEM images of negatively stained Aβ40 amyloid fibrils produced from the same sample, revealing different structural types of amyloid fibril polymorphism. Reproduced from (Fandrich et al. 2009).

1.11.4.2 **TEM immunogold labelling**

Immunogold labelling is a technique that has been used for more than seven decades to identify biomolecules particularly proteins in tissue and cell sections (Amiry-Moghaddam and Ottersen 2013). The principle of immunogold labelling techniques is that antibodies can be labelled directly or indirectly using colloidal gold particles so that they can be visualised in the electron microscope (Figure 1-33) (Griffiths et al. 1993; Griffiths 1993). Thus, the target protein or epitope can be located and identified precisely within the section due to the selective binding properties of the applied antibody (Amiry-Moghaddam and Ottersen 2013).

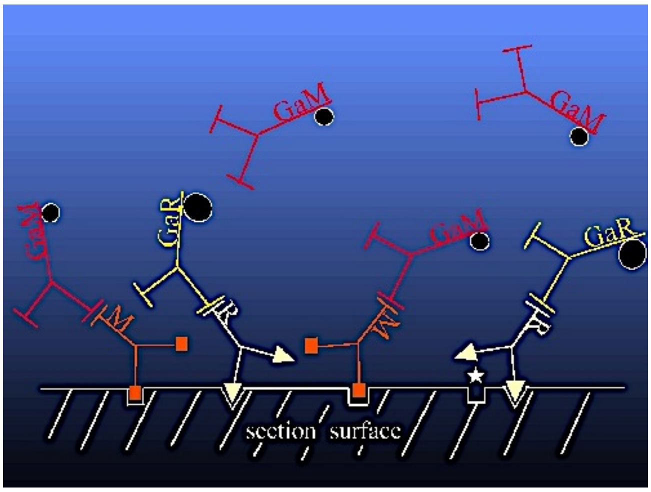

Figure 1-33: Schematic representation showing the principle of immunogold labelling. Adapted from (http://www.lifesci.sussex.ac.uk/home/Julian_Thorpe/immuno4.htm). GaM and GaR, goat anti-mouse and anti-rabbit, are secondary antibodies that labelled with two different sized gold particles. M and R are primary antibodies that are raised against specific antigens in mouse and rabbit respectively.

Using negative stain immunogold labelling TEM, the structure of both synthetic and neuronally secreted Aβ fibrils was assessed by Romano *et al*. (Romano et al. 2003). Monoclonal antibodies against Aβ peptide epitopes 1−17 and 17−24 were used, and the results showed that only the neuronally secreted Aβ fibrils interfere with long-term memory loss in an invertebrate, i.e. crab, learning model (Romano et al. 2003). In a recent study, a combination of immunogold labelling TEM and X−ray fluorescence microscopy has used to assess and follow the developments of Cu^{2+} and Zn^{2+} levels and their interaction with Aβ42 in the brain tissue of Tg mouse as AD model (Wang et al. 2012). The results showed that Cu^{2+} and Zn^{2+} ions are associated with Aβ42 during plaque deposition (Wang et al. 2012). This observation provides strong evidence of the involvement of metal ions in the aggregation and toxicity of Aβ42.

1.11.5 **Research hypothesis and aims**

AD and PD are neurodegenerative diseases and pathologically characterised by deposition of Aβ and α-syn into plaques or Lewy bodies respectively. Metal ion dyshomeostasis and oxidative stress have also been reported to be associated with AD and PD (Kenche and Barnham 2011; Lovell et al. 1998; Viles 2012). High levels of oxidative stress can be produced as a consequence of metal-protein interactions leading to protein misfolding and cross-link formation. One of the possible oxidative modifications of proteins is dityrosine cross-links which are suggested to play an important role in oligomer production. Increasing evidence points to the pivotal role of the Cu^{2+} ion in Aβ and α-syn misfolding and aggregation. However, no previous comprehensive *in vitro* and *in vivo* study has been carried out to establish the role played by dityrosine cross-links in amyloid fibril formation and to explain the link between dityrosine cross-links and misfolding of amyloidogenic proteins, such as Aβ and α-syn, leading to amyloid assembly. The aim of this study is to understand the role for oxidative stress and subsequent dityosine crosslinks in self-assembling peptides and neurodegenerative disease processes.

The research aims here were firstly, synthesis of dityrosine as a standard for comparison, as it is not available commercially. Secondly, a system of oxidation using Cu^{2+}/H_2O_2 was tested using two short peptides as a model system to provide more information about the nature of oxidative modification on tyrosine containing peptides. Two previously characterised short tyrosine-containing peptides, HYFNIF and VIYKI, were used to determine and optimise the oxidative conditions required to form dityrosine cross-links and analyse any possible structural changes. The oxidative conditions used Cu^{2+}/H_2O_2 that are believed to enhance oxidative modifications *in vivo.*

In chapter five, *in vitro* and *in vivo* investigation of dityrosine cross-links in Aβ examined the effects on fibril stability and morphology providing more details to enhance our understanding of the putative role played by dityrosine cross-links in Aβ and subsequently in the pathogenesis of AD. The relevance of dityrosine cross-linked Aβ was investigated by examining the existence of dityrosine in plaques in AD brains and in CSF. These aims were to define the role of dityrosine cross-links in the pathogenesis of AD.

Finally, in parallel, chapter six aims to investigate the role of dityrosine cross-links in α-syn aggregation and to identify the tyrosine involved. Studying the influence of dityrosine cross-links in the α-syn conformation and solubility during fibrillogenesis provides insights into the importance of oxidative modification of tyrosine residues in the pathogenesis of PD.

2 Materials and Methods

2.1 General

Milli-Q filtered water with a resistivity of 18.2 MΩ was used in all preparations. A microbalance (Denver Instruments SI-234) with a tolerance of ± 0.1 mg was used in all balance measurements. All pH measurements were made using a FiveEasy^{TM} pH meter connected to LE409 pH electrode (Mettler-Toledo AG, Switzerland). In order to minimise sample loss and binding of fibrillar substances, low-binding plastic wares, including Eppendorf low-bind sterile (Eppendorf, Hamburg, Germany) and AvantGuard low-bind sterile filter barrier tips, were used. To remove any cross contaminated material, routine cleaning of cuvette was achieved using water, followed by 2% Hellmanex, water, ethanol, and finally drying with nitrogen gas. Also, 2 M nitric acid was used to clean the cuvette surfaces from sticky contaminated material.

2.2 Methods relevant to chapter 4

2.2.1 Preparation of Waltz peptide fibrils

The lyophilised Waltz peptides (See 4.1), HYFNIF and VIYKI (JPT peptide technologies, Germany), were dissolved in 0.22 μm filtered Milli-Q water and incubated at a concentration of 2 mg/ml for one week at room temperature in order to generate fibrillar HYFNIF and VIYKI. Fibril formation was confirmed by negative stain TEM as described in section 2.2.11. The stock solutions of the fibrils were stored in the dark at room temperature until required.

2.2.2 Monitoring oxidation of HYFNIF and VIYKI fibrils

A stock solution of both HYFNIF and VIYKI fibrils was diluted in (a) water and (b) 50 mM phosphate buffer pH 7.4, to a final concentration of 0.1 mM. The diluted fibrils were incubated with Cu^{2+} (0.1 mM) and H_2O_2 (2.5 mM) at 37 °C with agitation of 300 rpm for three days. To monitor dityrosine formation, the fluorescence spectra were recorded every 24 h as described in fluorescence methods (section 2.2.4). Controls were obtained either in water or in 50 mM phosphate buffer pH 7.4 as illustrated in Table 2-1.

Table 2-1: Details of control preparation for waltz peptides comparison.

Substrate	Control 1	Control 2	Control 3
HYFNIF or VIYKI fibrils	X	X	X
Cu^{2+}	X	-	-
H_2O_2	-	X	-
Phosphate buffer	X	X	X
Water	X	X	X

2.2.3 Oxidation of HYFNIF and VIYKI fibrils for CD studies

(a) A stock solution of HYFNIF and VIYKI fibrils was diluted in water to a final concentration of 1.135 and 1.480 mM respectively and incubated in the presence of Cu^{2+} at a molar ratio of 1:1 (Cu^{2+}/peptide) and H_2O_2 (28.3 mM) and (37.0 mM) respectively. The oxidation reactions were performed at 37 °C with agitation of 300 rpm for three days. CD spectra were recorded as explained in CD measurement using a 0.1 mm path length cuvette (section 2.2.6).

(b) 0.25 mM of VIYKI fibrils was oxidised using Cu^{2+} (250 µM) and H_2O_2 (6.25 mM) in phosphate buffer (12.5 mM) at 37 °C with agitation at 300 rpm for three days. CD spectra were recorded every 24 h as explained in CD measurement using a 1 mm cuvette.

2.2.4 Tyrosine and dityrosine fluorescence

Fluorescence measurements were made using a Varian Cary Eclipse fluorimeter (Varian Ltd., Oxford, UK) with a single cell peltier accessory set at 21 °C. Fluorescence spectra were collected using 1 cm path length quartz cuvette (Starna, Essex, UK). Dityrosine fluorescence was monitored using an excitation wavelength of 320 nm and the emission wavelength was monitored between 340 and 500 nm, with maximum fluorescence intensity at around 410 – 420 nm. Tyrosine fluorescence signal was monitored using an excitation wavelength of 280 nm and emission wavelength of 305 nm. Excitation and emission slits were both set to 10 nm, and the scan rate was set to 300 nm/min with 2.5

nm data intervals and an averaging time of 0.5 s. The photomultiplier tube detector voltage was set at 500 V.

2.2.5 **Standard curve of dityrosine**

To estimate the dityrosine content of HYFNIF and VIYKI peptides, we generated a dityrosine standard curve. A set of dityrosine standard concentrations (0.1, 0.5, 1, 2, 3, and 5 μM) was made up in Milli-Q water. Each concentration was prepared in triplicate and dityrosine fluorescence was recorded for each concentration using an excitation wavelength of 280 nm and an emission wavelength of 410 nm. The mean values of dityrosine fluorescence intensity for each concentration were plotted against dityrosine concentration and a line as function was fitted by linear regression analysis using Microsoft Excel 2011 software. This equation was then used to quantify the dityrosine content of HYFNIF and VIYKI peptides.

2.2.6 **Circular dichroism spectroscopy**

Far and near UV CD spectra were collected using a Jasco J-715 spectropolarimeter (Jasco UK, Great Dunmow, UK) connected to a peltier temperature control system. All spectra were recorded at 21°C with a continuous scan at a pitch of 0.1 nm and a scan rate of 50 nm/min (response time 4 sec, slit width 1 nm). The spectra were recorded between 180 – 320 nm by averaging triplicate scans and corrected by subtracting the averaged triplicate scans of blank buffer spectra. Quartz demountable cells (Starna Scientific Ltd) were used to measure the CD intensity, and generally the path lengths were between 1– 0.1 mm to obtain better spectra with a high tension voltage (HT [V]) of > 600.

Raw data was processed and converted into molar ellipticity ($\text{degree.cm}^2.\ \text{dmol}^{-1}$) using the following equation:

$$\boldsymbol{\theta\ (\text{deg.cm}^2.\text{dmol}^{-1}) = 100.\ \theta\ (\text{mdeg})\ /\ c\ (\text{M}).\ l\ (\text{cm})}$$

Where l is path length in cm, c is molar concentration of the sample in mole/L, and *θ is* ellipticity reading in mdeg.

CD spectra of the non-oxidised and oxidised HYFNIF and VIYKI fibrils were recorded either in water or in 12.5 mM phosphate buffer at pH 7.4, and the secondary structures at different concentrations were explored.

2.2.7 Linear dichroism artifact identification

Linear dichroism artefacts, which arise from the orientation effects of fibrils, was determined by placing the cuvette close to the detector and rotate it around the optical axis as shown in Figure 2-1.

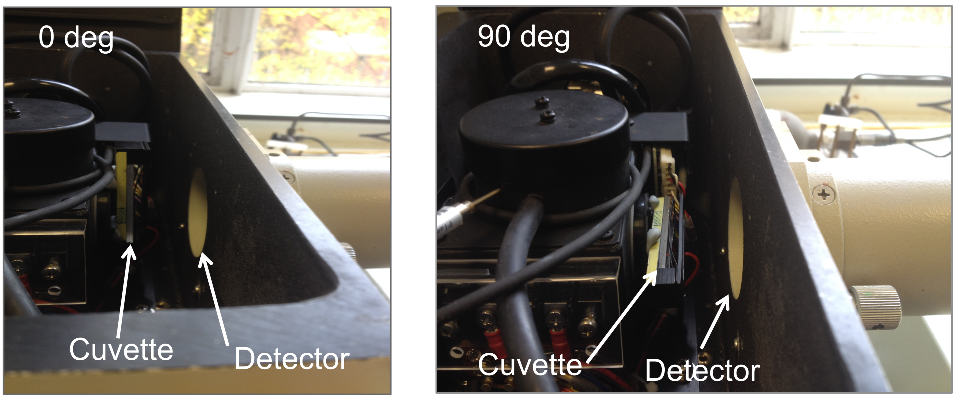

Figure 2-1:Linear dichroism artefact identification by placing the cuvette at 0 and 90 deg to the detector.

2.2.8 Sample preparation for LC-ESIMS/MS analysis

Oxidised (100 µM) HYFNIF and (50 µM) VIYKI fibrils prepared in water were lyophilised using a Modulyo 4K Freeze Dryer (Edwards, Crawley, England), and then hydrolysed using evacuated sealed tubes under acidic conditions of (6 M) HCl, 10% TFA, and 1% phenol at 110 °C for 48 h. The resulting hydrolysates were then dried under nitrogen gas, dissolved in 100 µl of 0.1% formic acid in water and then filtered using a Millipore 0.22 µm filter into a 0.2 ml tube.

2.2.9 Detection of dityrosine by LC-ESIMS/MS

20 µl of oxidised fibril hydrolysate was injected on to a Phenomenex Gemini 3u C_6–phenyl 110 (150 mm x 4.6 mm, 3 micron) column using an HPLC system (Waters Alliance 2695, Ireland) coupled to the mass spectrometer (MicroMass Quattro Premier, Waters, Ireland) operated in the MRM mode with positive ESI. The solvents for the

mobile phase were A: 0.1% formic acid in water; and solvent B: 0.1% formic acid in acetonitrile. The gradients were as follows: t = 0 min, 0% B; t = 1 min, 0% B; t = 15 min, 100% B; t = 20 min, 100% B; t = 25 min, 0% B; t = 30 min, 0% B, and the flow rate was 200 μl/min. Mass spectrometric detection was performed by positive ESI tandem mass spectrometry on a triple quadrupole mass spectrometer (MicroMass Quttro Premier, Waters, Ireland). The conditions for the mass spectrometer were as follows; electrospray ionisation spray voltage 3.5 kV, the cone voltage 35 V, the source temperature at 100 °C, whereas the desolvation temperature was 400 °C. Argon was used as the collision gas at 5.95×10^{-3} mbar at 26 ev collision energy.

2.2.10 **Exploring the effect of buffer type on dityrosine cross-link formation**

In order to investigate the effect of buffer type on dityrosine cross-link formation in both HYFNIF and VIYKI fibrils, 0.1 mM HYFNIF and 0.1 mM VIYKI fibrils were incubated respectively with Cu^{2+} using 1:1 molar ratio and 2.5 mM H_2O_2 in; a) 50 mM phosphate buffer pH 7.4 and b) 50 mM HEPES buffer pH 7.4 and the oxidation reactions were performed at 37 °C with agitation of 300 rpm for 26 h. The dityrosine formation was monitored by fluorescence and the spectra were recorded over 26 h.

2.2.11 **Negative stain TEM**

Four microliter aliquots of fibril samples were placed onto Formvar/carbon coated 400-mesh copper grids (Agar Scientific, Essex, UK) for 1 min, and the excess was removed using filter paper. Subsequently the grid was washed using 4 μl of Milli-Q water filtered with 0.22 μm filter and blotted dry, then negatively stained twice with 4 μl of filtered 2% (w/v) uranyl acetate for 1 min and blotted dry. The grid was allowed to air-dry before examination on a Hitachi 7100 transmission electron microscope (Hitachi, Germany) fitted with a Gatan Ultrascan 1000 CCD camera (Gatan, Abingdon, UK) at an operating voltage of 100 kV.

2.2.12 **Immunogold labelling negative stain TEM**

A modified phosphate-buffered saline, pH 8.2, containing 1% BSA, 500 μl/l Tween-20, 10 mM NaEDTA, and 0.2 g/l NaN_3 (henceforward termed PBS+), was used throughout all the following procedures for all dilutions of antibodies and secondary gold probes.

HYFNIF and VIYKI fibrils were oxidised in phosphate buffer for 3 h as described previously in section 2.2.2, and immunogold labelled 'on grid' for dityrosine (Thorpe et al. 2004). In general, 4 μl aliquots of the oxidised fibrils were pipetted onto Formvar/ carbon coated 400 mesh copper TEM support grids (Agar Scientific, Essex, UK), left for 1 min, the excess was removed by filter paper, and then blocked in normal goat serum (1:10 in PBS+) for 15 min. Grids were then incubated with (10 μg/ml IgG) mouse dityrosine monoclonal antibody (Japan Institute for the Control of Aging JaICA, Shizuoka, Japan) for 2 h at room temperature, rinsed in 3x2 min PBS+, and then immunolabelled in a 10 nm gold particle-conjugated goat anti-mouse IgG secondary probe (GaM10 British BioCell International, Cardiff, UK; 1:10 dilution) for 1 h at room temperature. After 5x2 min PBS+ and 5x2 min distilled water rinses, the grids were negatively stained as described in negative stain TEM.

2.3 Methods relevant to chapter 5

2.3.1 Preparation of fibrillar and oligomeric Aβ42

1,1,1,3,3,3-hexafluoro-2-propanol (HFIP) Aβ42 was purchased from rPeptide (Bogart, GA, USA). To remove preformed aggregates in the rPeptide purchased Aβ42, lyophilised Aβ42 (0.2 mg) was dissolved in 200 µl of HFIP >99.0% (Williams et al. 2010; Williams et al. 2011), and the mixture was vortexed for 60 s and sonicated in a 50/60 Hz bath sonicator for 60 s. The HFIP was removed using nitrogen gas current, and the peptidic films were vacuum desiccated for 30 min. Then Aβ42 film was resolubilised in 200 µl of dimethyl sulfoxide (DMSO) >99.7%, extra dry (Acros organics, Belgium), and the mixture was vortexed for 60 s and then sonicated for 60 s. In turn, the mixture was added to a 2 ml Zeba buffer exchange spin column (Thermo Scientific, USA) equilibrated with 0.22 µm filtered Milli-Q water. A 40 µl of 0.22 µm filtered Milli-Q water was added to the column immediately after mixture absorbed into the column resin. The column was spun in a 4 °C controlled Mikro 22R centrifuge (Hettich UK, Manchester, UK) at 1000 g for 2 min. The eluted peptide was centrifuged in at 4 °C with 16,000 g for 30 min to remove contaminants and preformed fibrillar material. The supernatant was placed in a clean nonstick microcentrifuge tube and kept at 4 °C until use to minimise fibrillisation. The concentration was determined using a molar extinction coefficient of 1490 $M^{-1}cm^{-1}$ and the absorbance was measured at a wavelength of 280 nm using an Eppendorf Biophotometer (Eppendorf UKLtd., Cambridge, UK). The resulting stock peptide concentrations of 90-130 µM were used immediately for early oligomeric Aβ42 experiments, or incubated for at least two weeks at room temperature (22 °C) in order to generate Aβ42 fibrils (confirmed using TEM).

2.3.2 Oxidation of fibrillar and early oligomeric Aβ42

Stock solutions of soluble or fibrillar Aβ42 were diluted in (a) water or (b) 50 mM phosphate buffer pH 7.4 to obtain 20 µM Aβ42 as a final concentration and incubated with or without (20 µM) Cu^{2+} and (0.5 mM) H_2O_2 at 37 °C with agitation in a shaking incubator for three days. The oxidation reaction was quenched using a final concentration of 250 µM EDTA.

2.3.3 Dityrosine cross-linked Aβ42 fibril stability

Aβ42 was assembled under oxidising and non-oxidising conditions and stored at - 80 °C for more than one year and the dityrosine content was assessed using fluorescence with an excitation wavelength of 320 nm as described in section 2.2.4. Both oxidised and non-oxidised Aβ42 fibrils were centrifuged for 30 min at 16,000 g at 4 °C, and then the soluble Aβ42 concentration in the supernatant was measured using absorbance at 280 nm (as described for peptide preparation in section 2.3.1). TEM grids were prepared to examine the Aβ42 fibrils in the pellet. The oxidised and non-oxidised fibrils were then dissolved in 80% (v/v) formic acid with agitation. The resulting solution was centrifuged using the same conditions above, and again the dissolved Aβ42 concentration was determined. TEM grids for the pellet were prepared to examine the morphology of the dissolved fibrils and to compare their density.

2.3.4 Fluorescence spectroscopy

Fluorescence spectra of dityrosine were recorded every 24 h. Fluorescence measurements were made as described previously in section 2.2.4.

2.3.5 Sample preparation for LC-ESIMS/MS analysis

Oxidised Aβ42 fibrils prepared in water, were lyophilised using a Modulyo 4K Freeze Dryer (Edwards, Crawley, England), and then hydrolysed using evacuated sealed tubes under acidic conditions of (6 M) HCl, 10% TFA, and 1% phenol at 110 °C for 48 h. The resulting hydrolysate was then dried under nitrogen gas, dissolved in 100 μl of 0.1% formic acid in water and then filtered using a Millipore 0.22 μm filter into a 0.2 ml tube.

2.3.6 Detection of dityrosine by LC-ESIMS/MS

Dityrosine formation in oxidised Aβ42 hydrolysate was detected using LC-ESIMS/MS as described previously in section 2.2.9.

2.3.7 Thioflavin T fluorescence assay

The fibril formation of Aβ42 was monitored using ThT fluorescence. A 0.2 μm filtered (3.14 mM) aqueous ThT stock solution was prepared and stored frozen at − 20 °C in 1−10 μl aliquots until required. ThT was added to 10 μM Aβ42 sample (50 mM phosphate buffer pH 7.4) to a final concentration of 20 μM, gently vortexed, and allowed to bind for 3 min before readings were taken. Using a microvolume cuvette (Starna, Essex, UK) of 1 cm path length, ThT fluorescence was measured using a Varian Cary Eclipse fluorimeter (Varian, Oxford, UK) with excitation wavelength of 450 nm. The emission spectrum was recorded between 460 − 600 nm at 21°C. Phosphate buffer baselines were subtracted from the data. Excitation and emission slits were set to 5 nm and 10 nm respectively. The scan rate was 600 nm/min with 1 nm data intervals and an averaging time of 0.1 s. The voltage on the photomultiplier tube was set to high (800 v) and experiments were carried out in triplicate to confirm trends.

2.3.8 Negative stain TEM

Negative stain TEM of Aβ42 fibrils were performed as in section 2.2.11.

2.3.9 SH-SY5Y neuroblastoma cell treatment with Aβ42

Undifferentiated human neuroblastoma SH-SY5Y cells were provided by Mrs. Maris Stewart-Parker. The cells were incubated with final concentration of 10 μM Aβ42 or buffer only at 37 °C for 24 h.

2.3.10 Immunogold labelling TEM of sections

AD and aged matched control brain from middle frontal gyrus tissues (Table 2-2) were obtained from London Neurodegenerative Diseases Brain Bank. Tissue was removed according to Local Ethics Committee guidelines, and informed consent for brain donation was obtained from the next of kin and stored at –80 °C until required. SH-SY5Y cells were incubated for 24 h with a final concentration of freshly prepared 10 μM Aβ42 and control cells were administered with buffer only (Soura et al. 2012). SH-SY5Y cells and brain tissues were prepared for immunogold labelling TEM by minimal, cold fixation and embedding protocols that were performed by Dr. Julian

Thorpe (Thorpe et al. 2001). Immunogold labelling was performed using an established methodology (Thorpe 1999), with PBS+ buffer being used for all dilutions of immuno reagents and for rinsing. Thin sections were collected upon TEM support grids, then incubated with normal goat serum (1:10 dilution) for 30 min at room temperature to block non-specific secondary antibody binding. In turn, grids were labelled with (10µg/ml IgG) anti-dityrosine mouse monoclonal antibody (Japan Institute for the Control of Aging JaICA, Shizuoka, Japan) or double-labelled using a mixture of (10µg/ml IgG) anti-Aβ42 rabbit polyclonal antibody AB5078P (Chemicon, Temecula, CA, USA) and (10µg/ml IgG) anti-dityrosine mouse monoclonal antibody and incubated overnight at 4°C. After 3x2 min PBS+ rinses, sections were then immunolabelled with GaM10 or a mixture of GaR5 and GaM10 secondary probes (both 1:10 dilution), respectively, for 1 h at room temperature. After 3x10 min PBS+ and 4x5min distilled water rinses, the grids were post-stained in 0.22 µm-filtered 0.5% (w/v) aqueous uranyl acetate for 1 h. The grids were examined on a Hitachi 7100 TEM (Hitachi, Germany) fitted with a Gatan Ultrascan 1000 CCD camera (Gatan, Abingdon, UK), and operating with a voltage of 100 kV.

Table 2-2: Demographic details of cases from which middle frontal gyrus tissues were obtained.

Case	**Age**	**Sex**	**Pathological diagnosis**
Normal 1	89	F	Control case but with Hypoxic-type changes and amyloid angiopathy
Normal 3	80	F	Control-minimal ageing changes
AD 1	68	M	Alzheimer's disease HP-tau stage 6 with mild to moderate amyloid angiopathy
AD 2	93	F	Alzheimer's disease HP-tau stage 6 with moderate amyloid angiopathy
AD 3	91	M	Alzheimer's disease HP-tau stage 6 with moderate amyloid angiopathy
AD 4	86	F	Alzheimer's disease HP-tau stage 6 with mild amyloid angiopathy
AD 5	77	F	Alzheimer's disease -modified Braak BNE stage 5

2.3.11 **Analysis of immunogold labelled sections**

Counting and size analyses of immunogold particle were performed using in house software written by Dr. Kyle Morris in Matlab. Briefly, raw digital electron micrograph images files were uploaded and circular particles detected using inbuilt Matlab circular Hough transforms functions. The detection range diameter was calculated from user input and conversion to pixel size values read from the image header. 15 or 10 nm gold particles were distinguished from 5 nm particles based on a user-selected threshold of 7 nm.

2.3.12 **Immunogold labelling, negative stain TEM (for fibrils and cerebrospinal fluid)**

A PBS+ buffer was used throughout all the following procedures for all dilutions of antibodies and secondary gold probes. Aβ42 fibrils were oxidised and assembled as described in oxidation of fibrillar and early oligomeric Aβ42 (section 2.3.2) and immunogold-labelled ‘on grid’ for dityrosine as described in section 2.2.12.

CSF samples from AD patients and control age matched subjects (Table 2-3) were obtained from the London Neurodegenerative Diseases Brain Bank. CSF was removed according to Local Ethics Committee guidelines, and informed consent for brain donation was obtained from the next of kin. The samples were stored at –80 °C in a locked freezer until needed. When required, they were diluted with Milli-Q water (1:3). Diluted CSF samples were double-immunogold-labelled for dityrosine and Aβ42 as described in section 2.2.12, except grids were incubated in a mixture of (10 µg/ml IgG) anti Aβ42 rabbit polyclonal antibody AB5078P (Chemicon, Temecula, CA, USA) and (10 µg/ml IgG) mouse monoclonal dityrosine antibody (Japan Institute for the Control of Aging JaICA, Shizuoka, Japan). A mixture of 5 nm gold particle-conjugated goat anti-rabbit IgG (GaR5 British BioCell International, Cardiff, UK) and 15 nm gold particle-conjugated GaM (British BioCell International, Cardiff, UK; 1:10 dilution) was used for the secondary gold probe.

Table 2-3: Demographic details of cases from which cerebrospinal fluid were obtained.

Case	Age	Sex	Pathological diagnosis
AD 1	68	M	Alzheimer's disease HP-tau stage 6 with mild to moderate amyloid angiopathy
AD 2	93	F	Alzheimer's disease HP-tau stage 6 with moderate amyloid angiopathy
AD 3	91	M	Alzheimer's disease HP-tau stage 6 with moderate amyloid angiopathy
Normal 1	89	F	Control case but with hypoxic-type changes and amyloid angiopathy
Normal 2	92	F	Control-some amyloid angiopathy

2.4 **Methods relevant to chapter 6**

2.4.1 **Preparation of α-syn**

The lyophilised full-length human recombinant α-syn (1 mg) in final buffer of 10 mM Tris-HCl (pH 7.4) was purchased from rPeptide (Bogart, GA, USA) or provided by Dr. Shahin Zibaee (Molecular Biology Lab., MRC Centre, Cambridge). The provided α-syn was of high purity and does not show any Cysteine misincorporation to Tyrosine at position 136, which has been observed for about 20% of human α-syn expressed in *Escherichia coli* (Masuda et al. 2006). The peptide was resuspended in Milli-Q filtered water at concentration of 2 mg/ml, and then the Tris-HCl buffer was removed using Vivaspin-500 concentrator tube, 3000 MWCO PES (Sartorius stedim biotech, Germany). Briefly, the resuspended α-syn was centrifuged at 14,000 g for 30 min, subsequently the obtained concentrated α-syn was again diluted with Milli-Q filtered water at a concentration of 2 mg/ml and the concentrating process was repeated. The resulting α-syn solution in water was collected and filtered using 0.22 μm syringe filter to remove any preformed aggregates. Finally, the concentration was determined using a molar extinction coefficient of 5120 $M^{-1}cm^{-1}$ and the absorbance was measured at a wavelength of 280 nm using an Eppendorf Biophotometer (Eppendorf UKLtd., Cambridge, UK) (Lucas et al. 2010).

2.4.2 **Cu^{2+}- catalysed oxidation of α-syn**

Prior to oxidation, α-syn stock solution was prepared as described in section 2.4.1, to remove any preformed aggregates and fibrils. Soluble α-syn monomer was incubated with Cu^{2+} using molar ratio of 1:1 and concentration of 50 μM and to initiate the oxidation reaction, H_2O_2 (1.25 mM) was added. The oxidation reaction was performed in 20 mM HEPES (pH 7.4) at 37 °C with agitation of 400 rpm. After 24 h, the oxidation reaction was stopped using EDTA at a final concentration of 1.25 mM. The dityrosine formation was monitored by fluorescence spectrophotometer as described in section 2.2.4. Controls were obtained by incubation of 50 μM α-syn with and without Cu^{2+} in 20 mM HEPES buffer pH 7.4 at 37 °C with agitation of 400 rpm.

2.4.3 Exploring the effect of Cu^{2+} on the α-syn fibrillogenesis and structure

To examine the effect of Cu^{2+} on the α-syn fibrillogenesis, a concentration range of Cu^{2+} (50, 100, 400 μM) was used at molar ratio of 1:1 with α-syn. Then the fibril growth and morphology were examined using ThT fluorescence and TEM respectively. Also, CD was used to measure the secondary structure of the formed fibrils. Moreover, XRFD was used to further examine the structure.

2.4.4 Tyrosine and dityrosine fluorescence

Fluorescence measurements were made using a Varian Cary Eclipse fluorimeter (Varian Ltd., Oxford, UK) with a single cell peltier accessory set on 21 °C. Tyrosine and dityrosine fluorescence was measured using excitation wavelengths at 280 and 320 nm respectively as described in section 2.2.4.

2.4.5 ThT fluorescence assay

The α-syn fibril growth was monitored using ThT fluorescence performed as in section 2.3.7.

2.4.6 Circular dichroism spectroscopy

CD was used to measure the α-syn conformational changes associated with fibril formation. CD experiments were carried out at 21 °C in a JASCO J-720 spectropolarimeter as described previously in section 2.2.6.

2.4.7 Negative stain TEM

The α-syn fibril growth and morphology was visualised by negative stain TEM, the detailed protocol and preparation were the same as in section 2.2.11.

2.4.8 Dityrosine detection using LC-ESIMS/MS

For LC-ESIMS/MS analysis, 24 h oxidised α-syn (50 μM) was first desalted to remove the HEPES buffer that could affect the mass spectrum. The desalting was performed using Amicon ultra-4 centrifugal filter units, 10k NMWL (M Millipore, USA) and centrifuged at 6000 RPM and a temperature of 4 °C. The resulting α-syn was then hydrolysed using evacuated sealed tubes under acidic conditions of (6 M) HCl, 10% TFA, and 1% phenol at 110 °C for 48 h. In turn, the α-syn hydrolysate was dried using nitrogen gas then resuspended in 0.1% formic acid in water and filtered using 0.22 µm syringe filter unit and finally analysed by LC- ESIMS/MS that operated on MRM mode as described in section 2.2.9.

2.4.9 **HPLC analysis of oxidised α-syn**

The HPLC analysis was performed using an Agilent 1100 Series HPLC system (Cambridge, UK). Reversed-phase gradient chromatography was performed using a binary solvent system composed of TFA 0.085% (v/v) in acetonitrile (solvent B) and TFA 0.1% (v/v) in water (solvent A). The solvents were mixed using an G1312A binary pump at 1 ml/min as follows: From 0 to 1 min the composition of A–B was held at 95% A, from 1 to 20 min the composition of the solvent was changed, via a linear gradient to 95% B and then from 20 to 27 min the solvent was changed to 95 % A to rinse the column. The solvent was then held at 95%A for 3 min for column re-equilibration prior to the next injection. Oxidised and non-oxidised α-syn samples were injected into C– 4 Phenomenex (150 X 4.6 mm) column and α-syn monitored using UV detector at wavelength of 226 nm.

2.4.10 **SDS-PAGE electrophoresis**

SDS-PAGE electrophoresis analysis was performed as described previously (Bollag and Edelstein 1991). The separation gel consisted of 12% (w/v) acrylamide, 0.32% (w/v) bis-acrylamide, 0.1% SDS, and 0.38 M Tris-HCl (pH 8.8). The polymerisation was initiated by addition of 5 µl TEMED and 50 µl freshly prepared ammonium persulfate (APS) solution per 10 ml of the gel solution. The stacking gel consisted of 5% (w/v) acrylamide, 0.13% (w/v) bis-acrylamide, 0.1% (w/v) SDS, and 0.38 M Tris-HCl (pH 6.8) and polymerisation was initiated by addition of 5 µl TEMED and 20 µl freshly prepared ammonium persulfate (10% w/v) per 4 ml of the gel solution. Electrophoresis buffer consisted of 25 mM Tris-HCl (pH 8.3), 19 mM glycine, and 0.1% (w/v) SDS. Laemmli sample buffer (Sigma-Aldrich, UK), which consisted of 4% SDS, 20% glycerol, 10% 2-mercaptoethanol, 0.004% bromophenol blue and 0.125 M Tris- HCl (pH 6.8), was used in preparation of the protein samples using 1:1 volume ratio, then the resulting mixture was boiled for 5 min at 100 °C and centrifuged for 1 min. The SDS electrophoresis analysis was performed using Bio- Rad chamber (Bio-Rad, Hercules) under constant voltage (200 V). A protein marker standard (Sigma-Aldrich, UK) with range of 6,500 – 200,000 Da was run along side with the samples.

The separated protein bands were visualised using Coomassie Brilliant Blue R-250 and Silver staining. The Coomassie Brilliant Blue R-250 staining was performed as described previously (Bollag and Edelstein 1991). Generally, the gel was incubated in the Coomassie stain solution for ~ 1 h with gentle shaking, and then rinsed with deionised distilled water several times. For de-staining, the gel was incubated with ~ 50 ml of Coomassie gel destain solution with overnight agitation.

The silver staining was performed according to the manufacture's instructions (Bio-Rad, U.S.). In brief, the gel was placed in the fixative enhancer solution with gentle agitation for 20 min, then rinsed with deionised distilled water for 10 min, this step was repeated once more and then the rinsed water was decanted. For staining, the gel was placed in the staining solution for ~15 – 20 min until the desired staining was reached, then 5 % (v/v) acetic acid was added and left for 15 min to stop the reaction. Finally, the gel was rinsed for 5 min with Milli-Q water, and then the gels were photographed.

2.4.11 **In gel digestion protocol**

The α-syn oxidation mixture (after 5 h of oxidation) were separated by SDS-PAGE and stained using Coomassie Blue as described above, then the separated bands (monomer and dimer) were excised and divided into 3 – 4 pieces and de-stained with 30% acetonitrile for 15 min with agitation followed by 50% acetonitrile / 25 mM ammonium bicarbonate for 15 min with agitation. This step was repeated until the gel pieces were completely de-stained. The de-stained gel pieces were then dehydrated using vacuum centrifugation for 5 min without heating. 12.5 ng/ml of trypsin solution in 25 mM ammonium bicarbonate was added and the gel pieces were allowed to rehydrate for 5 min, then the excess trypsin solution was removed and the gel pieces covered by 25 mM ammonium bicarbonate and incubated at 37 °C for 6 h. Formic acid was added to ~5% (v/v) and the resulted mixture was vortexed and centrifuged at 1000 g for 1 min and the supernatant was removed, the remaining peptides were extracted from the gel pieces using 50% acetonitrile with agitation and brief sonication. This step was repeated and all supernatants were pooled and the volume was reduced by vacuum centrifugation. The resultant sample solution was stored at –80 °C until analysed by nanoLC-LTQ-OrbitrapXL mass spectrometry.

2.4.12 **α-syn fibril preparation for XRFD**

α-syn fibrils were formed in 20 mM HEPES buffer (pH 7.4) by incubation with and without Cu^{2+} at molar ratio of 1:1 and concentration of 400 μM for 5 days at 37 ºC and with agitation of 450 rpm. To remove HEPES buffer, which can affect the quality of X-ray diffraction, the resulting fibrils were centrifuged for 30 min at 20,000 g and 4 ºC, then the obtained pellet was re-suspended in 10 μl Milli-Q water and aligned as described below.

2.4.13 **X-ray fibre diffraction**

Fibre diffraction specimens were prepared by suspending a 10 μl droplet of α-syn fibril solution, which is prepared as described above, between two wax-tipped 1.2 mm O.D, 0.94 mm I.D borosilicate capillaries (Harvard apparatus), then left at room temperature in a parafilm sealed petri dish until dry. X-ray diffraction patterns were collected using a Rigaku 007HF Cu Kα (λ 1.5419 Å) rotating anode generator with a Saturn 944+ CCD detector with exposure times of 10 – 120 seconds and specimen to detector distances of 50 or 100 mm. The images were displayed and examined using Mosflm (Leslie 1992).

3 Dityrosine synthesis and characterisation

3.1 Introduction

Dityrosine is a tyrosine dimer that results from the ortho-ortho coupling of two tyrosyl radicals (Figure 1-18). It has a strong fluorescence emission maximum at 410 nm upon excitation at 285-325 nm depending on the pH of the solution (Abdelrahim et al. 1997). The formation of cross-linked tyrosine is one of oxidative modifications that may mediate the toxicity of Aβ oligomers (Atwood et al. 2004). The aim of this chapter is the synthesis of a dityrosine standard, which is not commercially available, and its use as a reference in the rest of the study.

3.2 Protocols of dityrosine synthesis

Several methods have been described for the synthesis of dityrosine (Hutton and Skaff 2003; Lee et al. 2008; Tilley et al. 2004), here we present the most efficient two methods that were used to prepare dityrosine.

3.2.1 Enzymatic oxidative coupling of tyrosine derivative

A wide variety of tyrosine derivatives have been oxidised by peroxidase-hydrogen peroxide system to produce dityrosine. This oxidation includes phenolic coupling through carbon-carbon construction. Jacob *et al.* prepared dityrosine through the oxidative phenolic coupling of L-tyrosine converted to the tyrosyl radical by myeloperoxidase, and they revealed that the major reaction of tyrosyl radicals under these conditions is dimerisation to form dityrosine (Jacob et al. 1996). Alternatively, Malencik *et al.* employed horseradish peroxidase (HRP) to catalyse the oxidative coupling of tyrosine (Malencik and Anderson 1996). Consequently, dihalogenated tyrosine derivatives have been used to synthesise dityrosine using HRP as a catalyst (Guo et al. 1997). The amino group of dihalogenated tyrosine was acylated to prevent possible side reactions (Figure 3-1). Recently, Lee *et al.* have used *N*-Boc-L-tyrosine as the substrate of HRP and synthesised dityrosine on a large scale (Lee et al. 2011a).

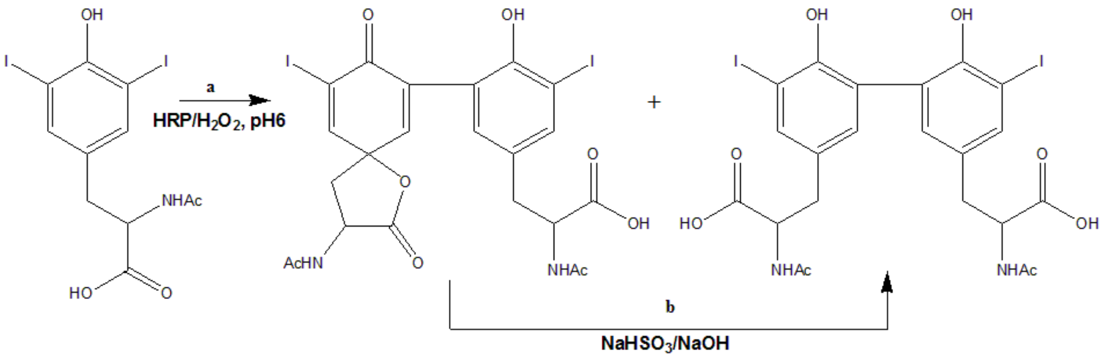

Figure 3-1: Dityrosine synthesis using horseradish peroxidase and hydrogen peroxide system.

1.1.1 Dityrosine synthesis by Suzuki-Miyaura coupling reaction

The palladium-catalysed Suzuki-Miyaura cross coupling is one of the most efficient strategies for carbon-carbon bond formation. It is widely used in organic synthesis to build more complex molecules from simple precursors. The Suzuki-Miyaura coupling reaction is based on the coupling of an aryl or vinyl halide with a boronic acid derivative, in the presence of a palladium catalyst and base (Hutton and Skaff 2003).

Doan *et al*. reported that the Suzuki-Miyaura cross-coupling reaction has been used in many applications (Doan et al. 2008). For example, the synthesis of Losartan, an angiotensin II receptor antagonist, is one of the Suzuki-Miyaura coupling reactions applied in the pharmaceutical industry.

Dityrosine was prepared through a tandem Miyaura borylation-Suzuki coupling of 3-iodotyrosine derivative (Skaff et al. 2005). It involves protection of 3-iodo-L-tyrosine under standard conditions, followed by Miyaura borylation with bis(pinacolatodiboron) to give the tyrosine-3-boronate derivative. In turn, the tyrosine-3-boronate derivative was coupled with 3-iodo-L-tyrosine derivative by Suzuki coupling to give protected dityrosine (Figure 3-2).

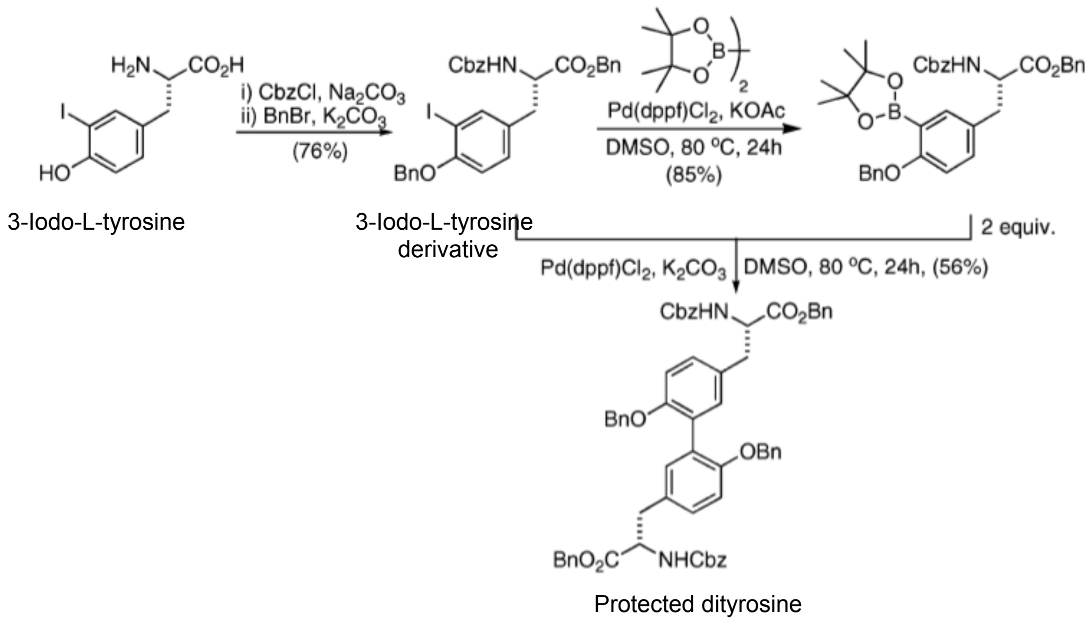

Figure 3-2: Two-step Suzuki-Miyaura coupling reaction. Adapted from Skaff et al., 2005.

This procedure was developed to prepare the protected dityrosine through a one-pot, tandem Miyaura borylation-Suzuki coupling from the 3-iodo-L-tyrosine derivative (Figure 3-3).

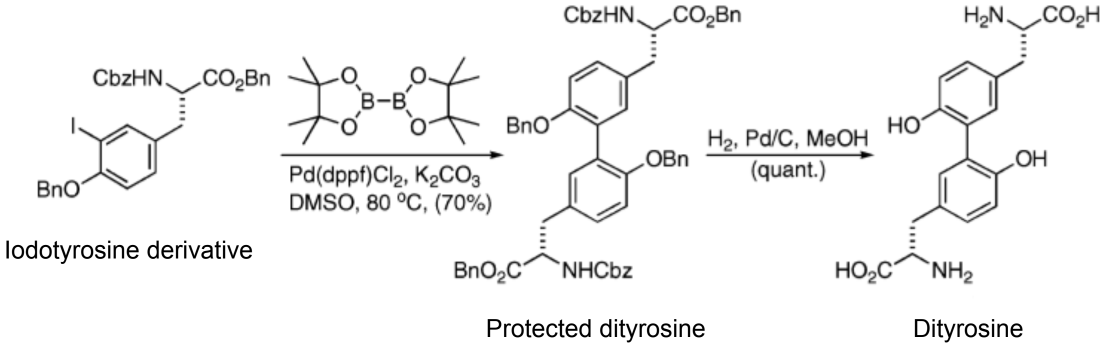

Figure 3-3: One-pot tandem Suzuki-Myiaura coupling reaction. Adapted from Skaff et al., 2005.

3.3 Experimental

3.3.1 Dityrosine synthesis

In order to explore the most effective strategy of dityrosine synthesis, four protocols were tested as described below:

3.3.1.1 Suzuki-Miyaura coupling reaction

Dityrosine was prepared in three steps based on the procedure of Skaff *et al.* (Skaff et al. 2005) with some modifications.

Step 1: Synthesis of N-Cbz-4-O-benzyl-3-iodo-L-tyrosine ester (3-iodo-L-tyrosine derivative).

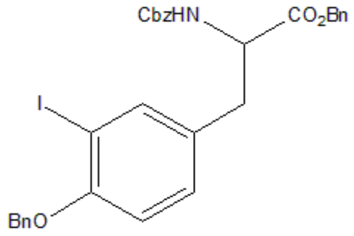

$C_{31}H_{28}INO_5$
Exact Mass: 621.1
Mol. Wt.: 621.46
m/e: 621.10 (100.0%), 622.10 (33.9%), 623.11 (6.6%)
C, 59.91; H, 4.54; I, 20.42; N, 2.25; O, 12.87

Figure 3-4: Chemical structure of N-Cbz-4-O-benzyl-3-iodo-L-tyrosine.

3-Iodo-L-tyrosine (2.5 g, 8.14 mmole) was added to an ice-cold solution of potassium carbonate (3.38 g, 24.4 mmole) in 30 ml water, then 4.2 ml of 50% (v/v) benzyl chloroformate in toluene solution was added over 30 min at 0 °C. The mixture was stirred at 25 °C for 21 h. In turn, the resulting mixture was acidified to pH 4.0 with 3 M HCl and extracted with EtOAc (4x50 ml). In order to obtain Cbz-3-iodo-L-tryrosine, the combined organic extracts were washed with saturated sodium chloride solution (2x50 ml), dried using $MgSO_4$, and concentrated in vacuo to give white powder. Subsequently, the crude Cbz-3-iodi-L-tyrosine was added to a solution of potassium carbonate (3.4 g, 24.6 mmole) and tetrabutylammonium iodide (40 mg) in 100 ml of dry acetone. Later, a nitrogen gas was bubbled through the mixture for 15 min, then 2.15 ml of benzyl bromide was added and the resulting mixture was heated under reflux in the dark for 20 h. The resulting mixture was cooled and concentrated in vacuo and 50 ml of water was added to the residue and the resulting mixture was extracted with DCM

(3x50 ml). The combined organic extracts were dried using $MgSO_4$ and concentrated in vacuo to give pale yellow oil. Flash chromatography was carried out on silica using EtOAc/hexane (1:3-1:1 gradient) to give the desired compound (3.45 g, 68%) as a colourless solid: ^1H NMR (500 MHz, Chloroform-*d*) δ 7.55 (d, 1H), 7.40 – 7.30 (m, 15H), 6.92 (dd, *J* = 1.9, 8.0 Hz, 1H), 6.67 (d, *J* = 8 Hz, 1H), 5.26 (br d, *J* = 7.0 Hz, 1H), 5.17 – 5.08 (m, 6H), 4.70 – 4.60 (m, 1H), 3.07 – 2.96 (m, 2H); ^{13}C NMR (126 MHz, cdcl$_3$) δ 171.1 (C), 156.4 (C), 155.5 (C), 140.1 (CH), 136.4 (C), 134.9(C), 130.2(CH), 130.1 (C), 128.7 (CH), 128.7 (CH), 128.6 (C), 128.5 (CH), 128.5 (CH), 128.2 (CH), 128.1 (CH), 128.1 (CH), 127.9 (CH), 127.0 (CH), 112.5 (CH), 86.8 (C), 70.9 (CH_2), 67.4 (CH_2), 67.0 (CH_2), 54.9 (CH), 36.9 (CH_2); HR-MS (ESI +ve) *m/z* calculated for $[M+Na]^+$ 644.0904, found 644.0893. See appendix i and ii for ^1H and ^{13}C NMR specta of 3-iodo-L-tyrosine derivative respectively.

Step 2: Synthesis of protected dityrosine

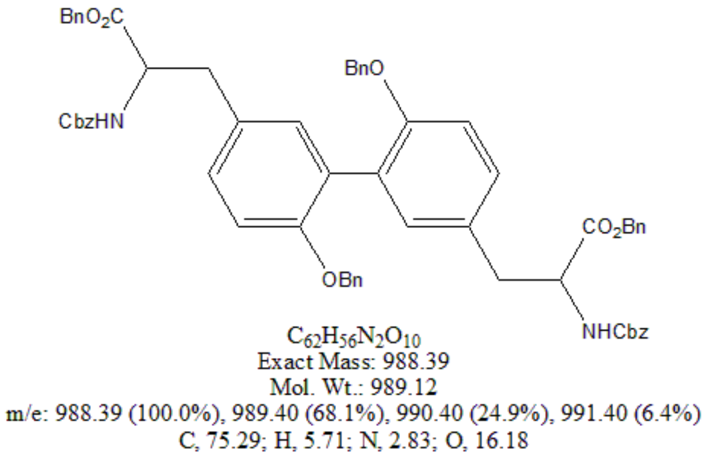

Figure 3-5: Chemical structure of protected dityrosine.

Bis(pinacolato)diboron (20.5 mg, 0.086 mmole) was added to a solution of iodotyrosine derivative (52.9 mg, 0.09 mmole), Pd(dppf)C_{l2}.NH_2-C_{l2} (2.0 mg), and potassium carbonate (44.7 mg, 0.36 mmole) in 1.5 ml of dry DMSO. The resulting mixture was stirred under nitrogen at 80 °C for 48 h. In turn, it was extracted with EtOAc (3x30 ml) and the combined organic extracts were washed with 50% saturated sodium chloride solution (2x30 ml), dried using $MgSO_4$, and concentrated in vacuo to give crude protected dityrosine as a dark brown oil. Subsequently, the oil was chromatographed on silica eluting with ether/DCM/hexane (1:2:3-1:2:2 gradient) to give pure protected dityrosine (16.7 mg, 40%) as a pale yellow oil: ^{1}H NMR (600 MHz, Chloroform-*d*) δ 7.28 – 7.08 (m, 30H), 6.98 – 6.96 (m, 2H), 6.91 (dd, *J* = 1.9, 8.4 Hz, 2H), 6.77 (d, *J* = 8.4 Hz, 2H), 5.22 (br d, *J* = 7.8 Hz, 2H), 5.10 – 4.98 (m, 8H), 4.89 (s, 4H), 4.66 – 4.62 (m, 2H), 3.10 – 2.97 (m, 4H); ^{13}C NMR (151 MHz, cdcl$_3$) δ 171.41 (C), 155.63 (C), 155.30 (C), 137.35 (C), 136.22 (C), 135.12 (C), 132.57 (CH), 129.19 (CH), 128.50 (CH), 128.43 (CH), 128.36 (CH), 128.34 (CH), 128.26 (CH), 128.05 (CH), 127.99 (CH), 127.48 (C), 127.33 (CH), 126.53(CH), 113.12 (CH), 70.26 (CH$_2$), 67.09 (CH$_2$), 66.87 (CH$_2$), 54.92 (CH), 37.33 (CH$_2$) (one quaternary carbon not observed); HR-MS (ESI, +ve) *m/z* calculated for $[M+Na]^+$ 1011.3827, found 1011.3833. See appendix iii and iv for ^{1}H and ^{13}C NMR specta of protected dityrosine respectively.

Step 3: Hydrogenation of protected dityrosine

30 mg of 10% palladium on charcoal was added to a solution of 290 mg of protected dityrosine in 12 ml of dry MeOH. The resulting mixture was stirred under hydrogen using 1 bar pressure at 25 °C for 48 h. The resulting mixture was filtered through Celite and refluxed with 30 ml of 6 M HCl for 10 h, then concentrated in vacuo to give crude dityrosine. RP-HPLC was carried out in order to obtain pure dityrosine, which was then dried using a Freeze dryer (Edwards, England).

3.3.1.2 Dityrosine synthesis using KBrO$_3$

10 mg of L-tyrosine was dissolved in 2 ml deionised water with addition of 100 µl (1.6 M) HCl. The resulting mixture was divided into six glass (13x100 mm) tubes. Then 2 ml aqueous potassium bromate (2.4 mM) was added to each tube, which were covered with aluminium foil and heated at 150 °C for 25 min in a convection oven. The resulting mixture was cooled, concentrated in vacuo and dissolved in 3 ml of deionised water. The resulting mixture was centrifuged through 0.22 µm nylon centrifuge tube filters at 2700 g, and analysed by mass spectrometry as described in section 3.3.2.2 (Tilley et al. 2004).

3.3.1.3 Dityrosine synthesis via Mn(III)-mediated oxidation of tyrosine

Mn(III) acetate (25 ml, 5 mM) was added to 25 ml of (5 mM) tyrosine solution in 0.2 M phosphate pH 2.1. After 1 min the resulting mixture was filtered to remove any undissolved Mn(III) acetate and the filtrate was dried under vacuum at 80 °C. Ammonia water was added in excess to remove the phosphate, which was in turn filtered and the remaining ammonia water was removed in vacuo. Unreacted tyrosine remaining in the dry material was removed by washing with cold acidic water (4 °C, pH 2) and filtration. The resulting product was analysed by mass spectrometry as described in section 3.3.2.2 (Lee et al. 2008).

3.3.1.4 **Enzymatic-catalysed synthesis of dityrosine**

Dityrosine synthesis was achieved here according to modifications of established procedures (Atwood et al. 2004; Guo et al. 1997), which is involved two steps:

Step 1: Synthesis of diiodo diacetyl dityrosine.

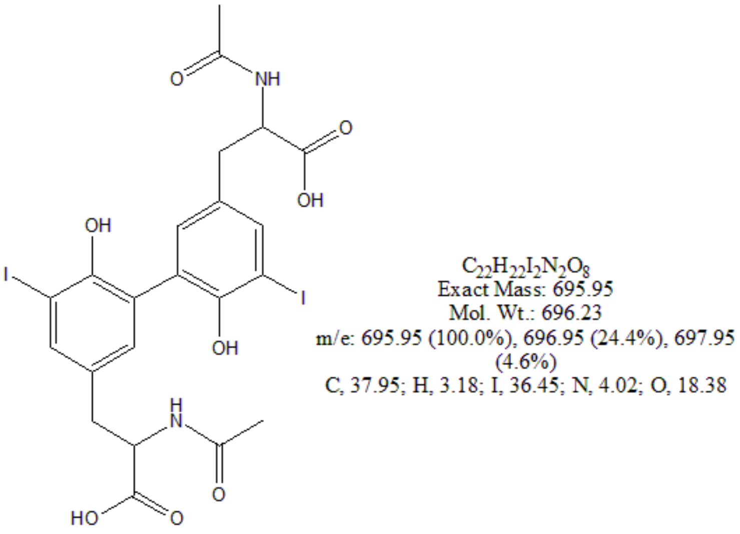

Figure 3-6: Chemical structure of diiodo diacetyl dityrosine.

20 units of HRP were added to a clear solution of *N*-acetyl-3,5-diiodo-L-tyrosine (190 mg, 0.4 mmole) in 40 ml of 0.1 M phosphate buffer pH 6.0 containing 10% of acetonitrile then mixed gently. Immediately, H_2O_2 (0.48 ml, 1 M) was added then the reaction mixture was stirred gently for 60 min at 24 °C, quenched with 1.2 ml of 1 M $NaHSO_3$ and the pH of the mixture was adjusted to 7.5 with 1 M NaOH. After stirring for 10 min the mixture was acidified to pH 3.0 with 2 M $KHSO_4$ and then extracted with ethyl acetate (3x30 ml). The combined organic residues were concentrated in vacuo to give a tan residue, which was purified by flash chromatography using

EtOAc/acetone/acetic acid (100: 10: 2 gradient) to give (41 mg, 29.1%) 3,3`-diiodo-*N,N*`-diacetyldi-L-tyrosine. ^{1}H NMR (500 MHz, Acetone-d_6) δ 7.64 (s, 2H), 7.33 (d, J = 8.0 Hz, 2H), 7.14 (s, 2H), 4.82 – 4.76 (m, 2H), 3.16 (dd, J = 13.9, 5.3 Hz, 2H), 2.93 (dd, J = 13.9, 7.9 Hz, 2H), 1.91 (s, 3H);^{13}C NMR (126 MHz, acetone) δ 172.80 (C), 171.85 (C), 170.54 (C), 153.19 (C), 140.89 (CH), 133.63 (CH), 131.82 (C), 86.19 (C), 53.91 (CH), 37.02 (CH_2), 22.56 (Me); HR-MS (ESI, +ve) *m/z* calculated for $[M+H]^+$ 696.9538, found 696.9531. See appendix v and vi for ^{1}H and ^{13}C NMR spectra of diiodo diacetyl dityrosine respectively.

Step 2: De-protection of protected dityrosine

The resulting 3,3`-diiodo-*N,N*`-diacetyldi-L-tyrosine was hydrogenated in 50% methanol acetic acid to give *N,N*`-diacetyldi-L-tyrosine, which was heated at reflux in a 1:1 mixture of tetrahydrofuran and concentrated HCl for 6 h to give dityrosine. Gel filtration on sephadex G-10 was carried out in order to remove the salt and further purification achieved using RP-HPLC. Finally, the purified dityrosine was dried by Freeze dryer (Edwards, England), and then analysed by mass spectrometry, fluorescence photometer, and NMR as described below.

3.3.2 **Detection and characterisation of synthesised dityrosine**

3.3.2.1 **HPLC analysis**

The HPLC analysis was performed using an Agilent 1100 Series HPLC system fitted with an ultraviolet absorbance detector at 280 nm. Purified dityrosine (10 µl) was injected onto a C_{18} SunFire reversed–phase column (5 µm particle size, 4.6x250 mm, Waters, Ireland) using a stepwise gradient (3, 20, 100, 3) of acetonitrile containing 0.1% Trifluoroacetic acid (TFA) at 0, 10, 20, 30 min respectively, with a flow rate of 1 ml/min and a column temperature of 25 °C. Dityrosine eluted at 11.6 min and collected, in turn it was dried using nitrogen gas for further analyses.

3.3.2.2 **Mass spectrometric detection**

High resolution mass spectrum (HRMS) of synthesised dityrosine was acquired using Bruker Daltonios Apex III 4.7 Tesla Fourier Transform ion cyclotron resonance mass spectrometer (FT-ICR-MS) with ESI. The synthesised dityrosine was dissolved in a solution of 1:1 methanol and water with 0.1% formic acid.

3.3.2.3 **Fluorimetric detection**

The purified dityrosine was detected by measuring the fluorescence intensity on Varian Cary Eclipse fluorimeter (Varian, UK), using excitation wavelength 280 nm and emission wavelength 410 nm in acidic solution (0.02 N HCl).

3.3.2.4 **NMR analysis**

The identity and purity of synthesised dityrosine were confirmed by ^1H and ^{13}C NMR spectra, which were recorded in D_2O on Varian VNMRS 500 MHz spectrometer using residual protic solvent as an internal reference.

3.3.2.5 **Development of LC-ESIMS/MS method for analysis of dityrosine**

A- Mobile phase optimisation

A primary goal of the present work was to optimise the LC-ESIMS/MS condition including, mobile phase composition and choosing an effective column, that enables efficient analysis of dityrosine. A preliminary optimisation of the mobile phase was first performed using tyrosine standard instead of dityrosine due to the limitation of the dityrosine amount that I have prepared and also because of the similarity in chromatographic behavior of tyrosine and dityrosine, which was previously seen in optimising the HPLC condition. Standard tyrosine was analysed in ESI ve+ with two different mobile phase eluents, and the mass spectra were acquired using full scan mode and Phenomenex Synergi 4u Hydro-RP 80 Å (150 mm x 2 mm, 4 micron) column. For the first experiment the mobile phase eluent was: (A) 0.1% formic acid in water and (B) methanol. For the second experiment the mobile phase eluent was: (A) 10 mM ammonium acetate adjusted to pH 5.8 using acetic acid, and (B) methanol. The LC conditions in both experiments were as described in Table 3-1 using a flow rate of 0.2 ml/min. Mass spectrometric detection was performed by ESI ve+ tandem mass spectrometry on a triple quadrupole mass spectrometer (MicroMass Quttro Premier, Waters, Ireland). The conditions for the mass spectrometer were as follows; electrospray ionisation spray voltage 3.5 kV, the cone voltage 35 V, the source temperature at 100 °C, whereas the desolvation temperature was 400 °C. Argon was used as the collision gas at 5.95 x 10^{-3} mbar at 26 eV collision energy.

Table 3-1: Liquid chromatography conditions that were used in tyrosine detection using LC-ESIMS/MS.

Time (min)	A%	B%	Curve
0	100	0	1
15	0	100	6
20	100	0	6
30	100	0	1

B- Column performance

Two different columns were tested to gain better mass spectrometry detection of dityrosine, Phenomenex Synergi 4u Hydro-RP 80 Å (150 mm x 2 mm, 4 micron) and Phenomenex Gemini 3u C_6-phenyl 110 Å (150 mm x 4.6 mm, 3 micron) column. For the detection using Gemini 3u C_6-phenyl column, 0.1% formic acid was used as a modifier with an acetonitrile and water mobile phase using a flow rate of 0.2 ml/min. The mass spectrum was acquired on MRM mode using LC condition as described in (Table 3-2).

Table 3-2: Liquid chromatography conditions which were used in dityrosine detection by LC-ESIMS/MS, using Phenomenex Gemini 3u C_6-phenyl 110 A° (150mm x 4.6mm, 3 micron) column.

Time (min)	A%	B%	Curve
0	100	0	1
1	100	0	1
15	0	100	6
20	0	100	1
25	100	0	6
30	100	0	1

Mass spectrometric detection was performed by ESI ve+ tandem mass spectrometry on a triple quadrupole mass spectrometer (MicroMass Quttro Premier, Waters, Ireland). The conditions for the mass spectrometer were as follows; ESI voltage 3.5 kV, the cone voltage 35 V, the source temperature at 100 °C, whereas the desolvation temperature was 400 °C. Argon was used as the collision gas at 5.95 x 10^{-3} mbar at 26 eV collision energy.

Dityrosine detection using Phenomenex Synergi 4u Hydro-RP 80 Å was performed as described above in tyrosine detection using formic acid as a modifier and solvent B was acetonitrile instead of methanol, and following the same LC and mass conditions.

3.4 **Results and discussion**

3.4.1 **Dityrosine synthesis**

Dityrosine is an unusual amino acid that results from a carbon-carbon bond formation between two tyrosine residues. Although many protocols have been developed to synthesise dityrosine, just a few strategies have succeeded in preparing dityrosine to sufficient yield. To compare the relative efficiency of dityrosine synthesis strategies, four alternative enzymatic and chemical oxidative coupling methods were evaluated as follows: enzymatic oxidative phenolic coupling (Guo et al. 1997), the Suzuki-Miyaura coupling reaction (Skaff et al. 2005), Mn(III)-mediated oxidation of tyrosine (Lee et al. 2008), and chemical oxidative coupling of tyrosine by $KBrO_3$ (Tilley et al. 2004).

Dityrosine formation by enzymatic oxidative phenolic coupling was achieved according to the method described by Guo *et al.* (Guo et al. 1997) with some modifications. *N*-acetyl-3,5-diiodo-L-tyrosine was oxidatively dimerised under enzymatic conditions using horseradish peroxidase and hydrogen peroxide in phosphate buffer pH 6. The modification of the original procedure included the reduction of phosphate buffer concentration from 0.2 to 0.1 M, which resulted in a significantly higher yield of dityrosine. Further modifications were included increasing the incubation period to 60 min instead of 10 min and mixing the reaction mixture very gently. The latter change strongly affected the product yield and that due to enzyme inactivation by prolonged agitation (Malencik et al. 1996). Finally, 3,3'-diiodo-*N,N'*-diacetyl di-L-tyrosine (DADT) was hydrogenated in 50% methanolic acetic acid (Atwood et al. 2004) which gave higher yield than the aqueous methanolic HCl (Nishiyama et al. 1994).

Alternatively, dityrosine can be prepared by chemical oxidative coupling using different oxidative agents. Authentic dityrosine was synthesised in three steps from 3-iodo-L-tyrosine using the one pot Miyaura borylation-Suzuki coupling strategy, which is the most efficient method among the chemical oxidative coupling methods. The amino, carboxyl, and hydroxyl groups were blocked under standard conditions to prevent any side reactions such as decarboxylation. In addition, the use of benzyl carbamate, ester, and ether protective groups was employed to allow a one-step global deprotection of the protected dityrosine derivative. Subsequently, the protected 3-iodo-L-tyrosine underwent Miyaura borylation with bis(pinacolatodiboron) to give tyrosine-3-boronate derivative. In turn, the tyrosine-3-boronate derivative coupled with 3-iodo-L-tyrosine derivative through Suzuki coupling to give the protected dityrosine. Then the conversion of protected dityrosine was achieved by treatment with palladium-on-charcoal under an atmosphere of hydrogen and 6 bar pressure.

Published data have established that the Suzuki-Miyaura coupling reaction is the most effective among the chemical and enzymatic oxidative coupling strategies in preparation of dityrosine. On the other hand, high level skills and experience of organic synthesis are required to perform the Suzuki-Miyaura coupling procedure and furthermore it takes longer than other procedures as shown in Table 3-3.

Table 3-3: Comparison of dityrsoine synthesis protocols. It is revealed that Susuki-Miyaura coupling procedure (protocol 2) has higher yield.

Number	Reference	Starting material	Number of steps	Reported Yield %	Experimental Yield %
1	Lee et al., 2008	L-tyrosine	One	15.8	-
2	Skaff et al., 2005	3-Iodo-L-tyrosine	Three	53	15
3	Tilly et al., 2004	L-tyrosine	One	31	-
4	Guo et al., 1997	*N*-acetyl-3,5-diiodo-L-tyrosine	Two	-	10

Finally, both Lee *et al.* (Lee et al. 2008) and Tilley *et al.* (Tilley et al. 2004) described a simple procedures to rapidly prepare dityrosine from L-tyrosine in good yield using Mn(III) acetate and $KBrO_3$ respectively as oxidising agents. Unfortunately, although I repeated these protocols several times, these methods did not give me the desired product. In the Tilley *et al.* method the formation of dityrosine requires the proximity of two tyrosyl radicals, thus the bromonation would be favoured because of steric hindrance requirements.

3.4.2 Detection and Characterisation of Synthesised Dityrosine

Detection and characterisation of synthesised dityrosine were performed by RP-HPLC followed by mass spectrometric and fluorimetric detection. In addition, ^{1}H NMR and ^{13}C NMR were obtained to confirm that the oxidation product of tyrosine derivatives, which were prepared using different procedures, was dityrosine.

The purified dityrosine was loaded onto a C_{18} SunFire column and monitored using a UV absorbance detector at absorbance 280 nm. The RP-HPLC pattern of the purified dityrosine (Figure 3-7) showed a major single peak with retention time (Rt =11.6 min) and maximum absorbance at 280 nm. Consequently, the major peak was collected and dried in N_2 flow, then redissolved in methanol and water 50:50 in 0.1% formic acid in order to obtain the mass spectrum.

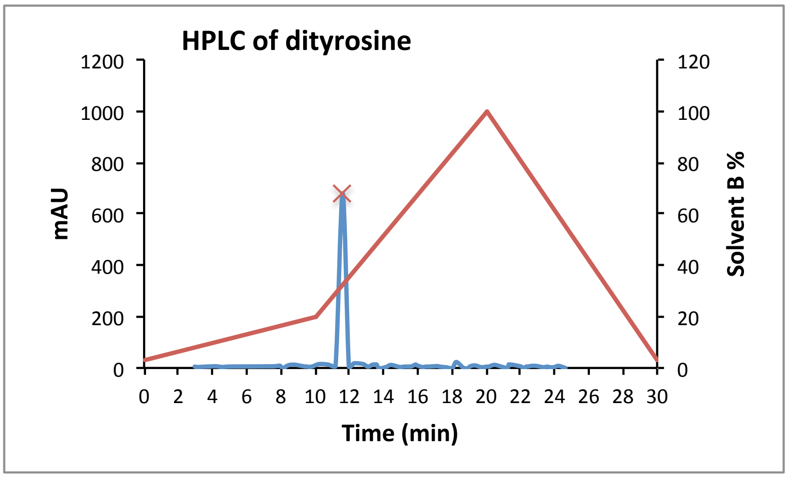

Figure 3-7: RP-HPLC chromatogram of synthesised dityrosine with retention time 11.6 min at absorbance 280 nm.

Synthesised ditryrosine was analysed by Bruker Daltonics APEX III 4.7 Tesla Fourier Transform ion cyclotron resonance mass spectrometer (FT-ICR-MS) with ESI +ve and found to be *m/z* $[M + H]^{+}$ 361.1404 compare with calculated *m/z* 361.1394 (Figure 3-8), and that was consistent with published results (Guo et al. 1997; Lee et al. 2008; Skaff et al. 2005).

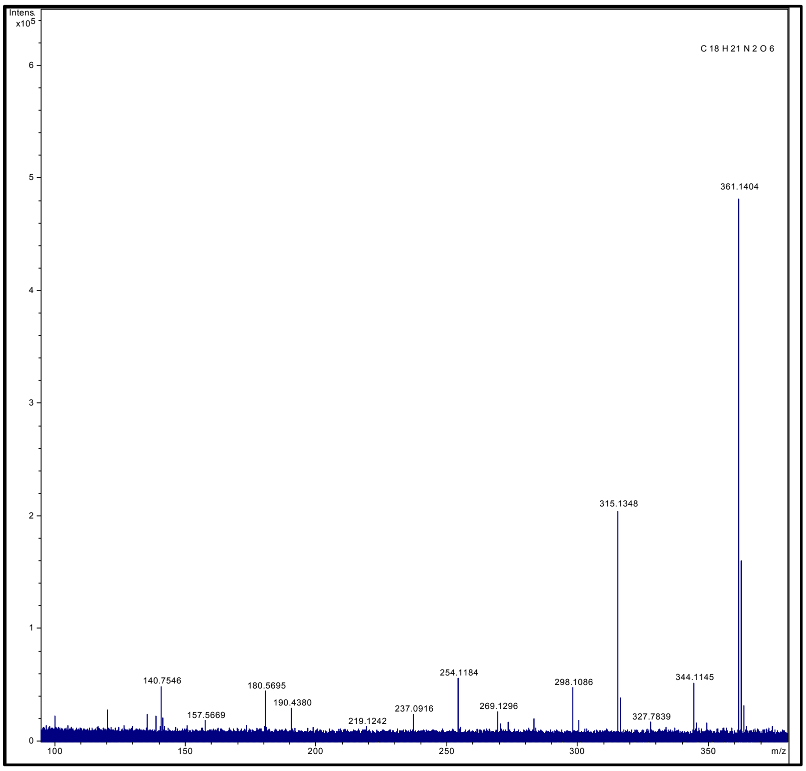

Figure 3-8: Mass spectrum of synthesised dityrosine. HRMS of dityrosine is calculated m/z 361.1394 and found to be 361.1404. The mass spectrum reveals the most intense fragmentation ion 315.1348, which is used later on detection of dityrosine by LC-MS/MS using MRM mode.

Dityrosine is a fluorescent molecule, thus fluorescence intensity measurements were carried out on a Cary Eclipse fluorescence spectrophotometer. The results showed a fluorescence signal at emission wavelength 405 – 410 nm and excitation at 280 nm in (0.02 N) HCl (Figure 3-9) and this agrees with data reported by (Jacob et al. 1996). In contrast, tyrosine exhibits fluorescence signal at emission 305 nm and excitation 280 nm (Lakowicz 2007).

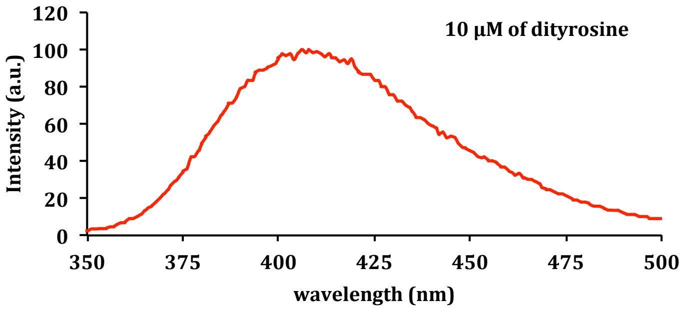

Figure 3-9: Fluorescence spectrum of synthesised dityrosine showing characteristic dityrosine fluorescence signal at 410 nm. The excitation wavelength was set at 280 nm.

The ^1H NMR spectrum of synthesised dityrosine and its chemical structure are shown in Figure 3-10. This spectrum is very similar to those published elsewhere (Jacob et al. 1996; Lee et al. 2008; Skaff et al. 2005). The ^1H NMR spectrum contained six proton signals with chemical shifts of: 7.30 ppm (H, d), 7.21 ppm (H, s), 7.07 ppm (H, d), 4.26 ppm (H, m), 3.35 ppm (H, dd), and 3.26 ppm (H, dd) (Figure 3-10).

The ^1H NMR spectrum of tyrosine shows two equivalents sets of aromatic shifts at δ 6.9 and 7.2 ppm (Sharma and Jain 1998). On the other hand, the synthesised dityrosine appeared to have three different sets of aromatic protons at δ 7.30, 7.21, and 7.07 ppm (Figure 3-10), and that were consistent with the ^1H NMR spectrum of dityrosine reported elsewhere (Lee et al. 2008; Sharma and Jain 1998; Skaff et al. 2005).

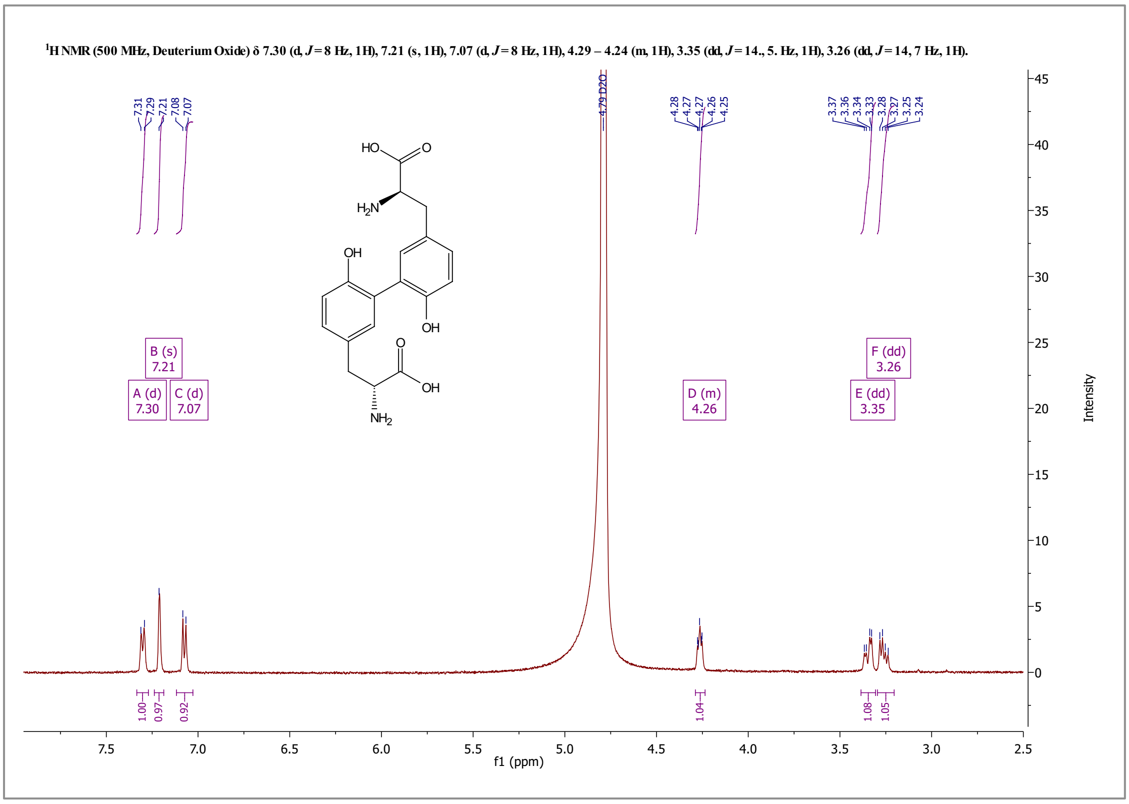

Figure 3-10: (A) ^{1}H NMR spectrum of synthesised dityrosine. The spectrum was recorded in D_2O on Varian VNMRS 500 MHz using residual protic solvent as an internal reference. The ^{1}H NMR spectrum of dityrosine shows six proton signals. Dityrosine appeared to have three different sets of aromatic protons at δ 7.30, 7.21, and 7.07 ppm.

The ^{13}C NMR spectrum of synthesised dityrosine reveals nine carbon signals with chemical shift of: 173.93, 153.09, 132.00, 130.20, 126.78, 125.93, 116.70, 56.05, and 35.41, as shown in Figure 3-11. The chemical structure of dityrosine shows nine different carbon atoms: 3 aromatic (CH), 3 aromatic (C), 1 aliphatic (CH_2), and 1 (C) from carboxylic group. The carbon atom types and their corresponding chemical shift are described in Table 3-4, and they literature values match well.

Table 3-4: ^{13}C NMR chemical shifts of authentic dityrosine and their corresponding carbon atom.

Number of carbon atom	**Type of Carbon (CH_n)**	**Chemical shift (δ) ppm**
3	CH (aromatic)	130.20, 126.78, 116.70
3	C (aromatic)	153.09, 132.00, 125.93
1	CH (aliphatic)	56.05
1	CH_2 (aliphatic)	35.41
1	C (from carboxylic group)	173.93

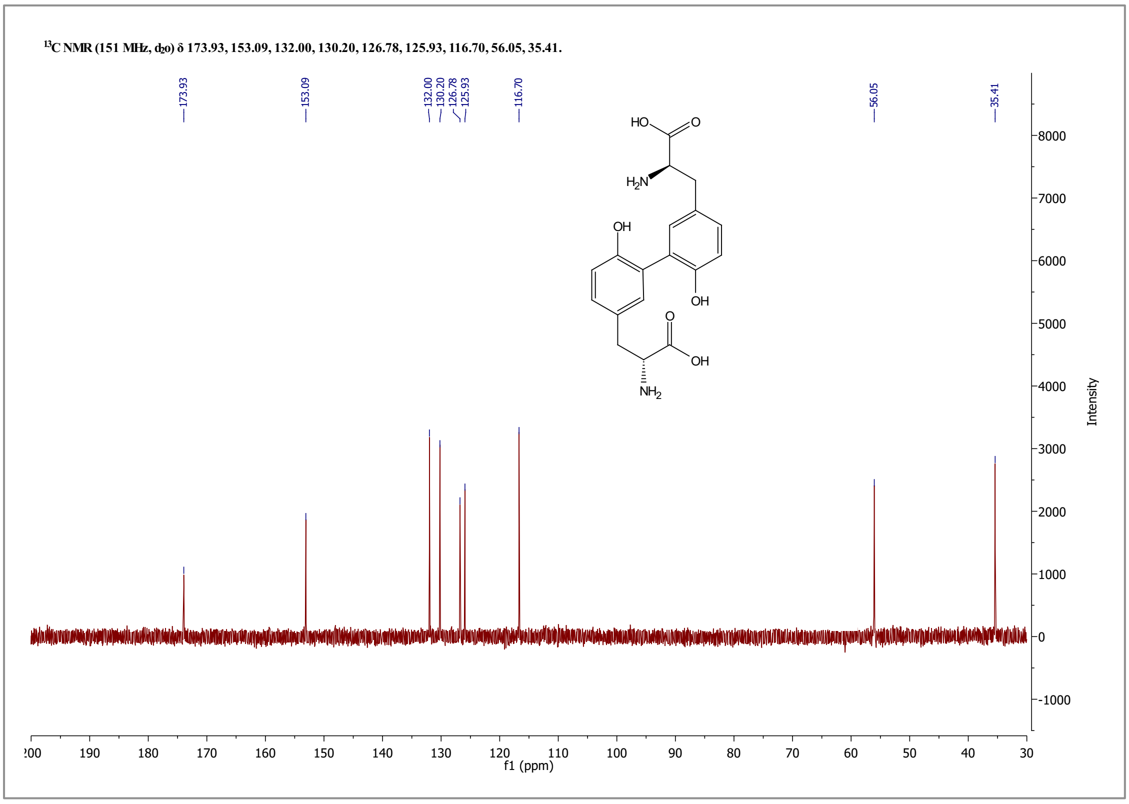

Figure 3-11: ^{13}C NMR spectrum of authentic dityrosine recorded in D_2O on Varian VNMRS 500 MHz using residual protic solvent as an internal reference. The ^{13}C NMR spectrum revealed nine carbon signals which corresponding to the carbon atoms of dityrosine.

3.4.3 **Development of LC-ESIMS/MS methodology to detect dityrosine**

A range of experimental conditions was examined in order to facilitate the detection of dityrosine using LC-ESIMS/MS, include mobile phase optimisation and column performance.

3.4.3.1 **Mobile phase optimisation**

Mass spectrometry is a powerful tool for detection and monitoring the posttranslational modifications of proteins (Cox et al. 2005). However, mobile phase composition and its pH seem important to obtain better chromatographic separation and mass detection. A preliminary optimisation of the mobile phases was first performed using tyrosine standard instead of dityrosine due to the limitation of dityrosine amount that was prepared and also because of the similarity in chromatographic behavior of tyrosine and dityrosine, which was previously seen in optimising HPLC seperetion condition. Standard tyrosine was analysed using LC-ESIMS/MS.

Two different mobile phase systems were tested, and the mass spectra were acquired using full scan mode and Phenomenex Synergi 4u Hydro-RP 80 Å (150 mm x 2 mm, 4 micron) column. For the first experiment the mobile phase eluent was: (A) 0.1% formic acid in water (pH 2.7), and (B) methanol. For the second experiment the mobile phase eluent was: (A) 10 mM ammonium acetate adjusted to pH 5.8 using acetic acid, and (B) methanol. The results indicate that using ammonium acetate as a modifier improves the retention time from 2.2 min, in the case of formic acid as a modifier, to 5.8 min (Figure 3-12). In turn, this would improve the resolution.

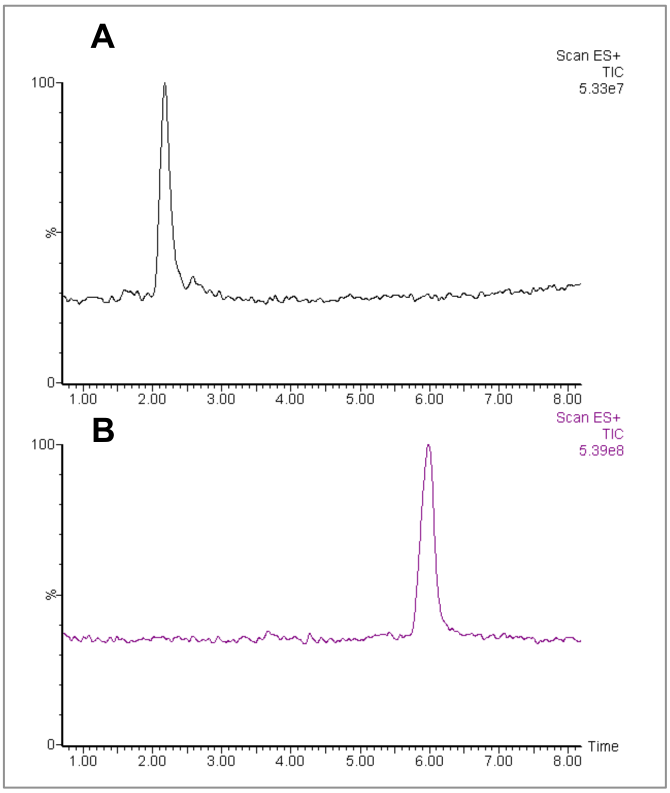

Figure 3-12: LC-ESIMS/MS chromatograms of tyrosine standard acquired on full-scan mode using Phenomenex Synergi 4u Hydro-RP 80 A° (150 mm x 2 mm, 4 micron) column. A) LC-MS chromatogram obtained using formic acid as a modifier with retention time of 2.2 min. B) LC-MS chromatogram obtained using ammonium acetate as a modifier with retention time of 5.8 min. Using ammonium acetate as a modifier result in better retention time.

LC-ESIMS/MS of the dityrosine standard was accomplished using 10 mM ammonium acetate (pH 5.8) as a modifier, the mass spectra were acquired on both full-scan and single ion reaction (SIR) mode. Further mass analyses show a peak with retention time of 7.5 min that corresponds to the dityrosine standard (Figure 3-13, B), compared to tyrosine, which has retention time 5.7 min (Figure 3-13, A), indicating good chromatographic separation.

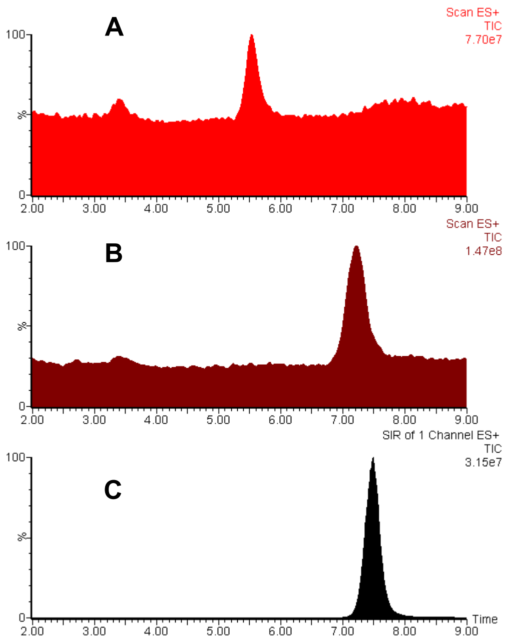

Figure 3-13: LC-ESIMS/MS chromatograms showing tyrosine standard in panel A, dityrosine standard in panel B and C. The LC-MS chromatograms were acquired using 10 mM ammonium acetate (pH5.8) as a modifier and Phenomenex Synergi 4u Hydro-RP 80 A° (150 mm x 2 mm, 4 micron) column.

In order to improve the mass sensitivity and specificity of dityrosine, the SIR technique was carried out using 10 mM ammonium acetate to monitor protonated ion $[M+H]^+$ 361.1 (Figure 3-13, C). Using the SIR technique, a much higher sensitivity of dityrosine detection and also better peak shape was obtained (Figure 3-13, C).

3.4.3.2 **Column performance**

Although adding ammonium acetate to the mobile phase improved the retention time, detecting dityrosine at low concentrations is still challenging due to signal suppression by ammonium ions. As a result, a new chromatographic strategy was followed using a different column, and formic acid as a modifier instead of ammonium acetate. Formic acid helped to avoid ion suppression and also to obtain good peak shape and retention time.

Two different types of columns were tested in terms of column performance in dityrosine retention: Phenomenex Synergi 4u Hydro-RP 80 A° (150 mm x 2 mm, 4 micron) and a Phenomenex Gemini 3u C_6-phenyl 110 Å (150 mm x 4.6 mm, 3 micron) column. The latter shows higher efficiency in dityrosine retention using formic acid as a modifier instead of ammonium acetate and that resolves the signal suppression problem. Moreover the MRM technique was used (Figure 3-14, A) instead of a full-scan (Figure 3-14, B), resulting in much higher sensitivity and specificity.

Elimination of carbon chain length from C18, in Phenomenex Synergi 4u Hydro-RP 80 Å column, to C6 in Phenomenex Gemini 3u C_6-phenyl 110 Å, resulted in reduction of the hydrophobic character of the stationary phase and improved the retention of dityrosine, which is hydrophilic. Also, adding a phenyl group to the end of the carbon chain leads to an aromatic-aromatic interaction, which in turn modulates dityrosine retention in the stationary phase.

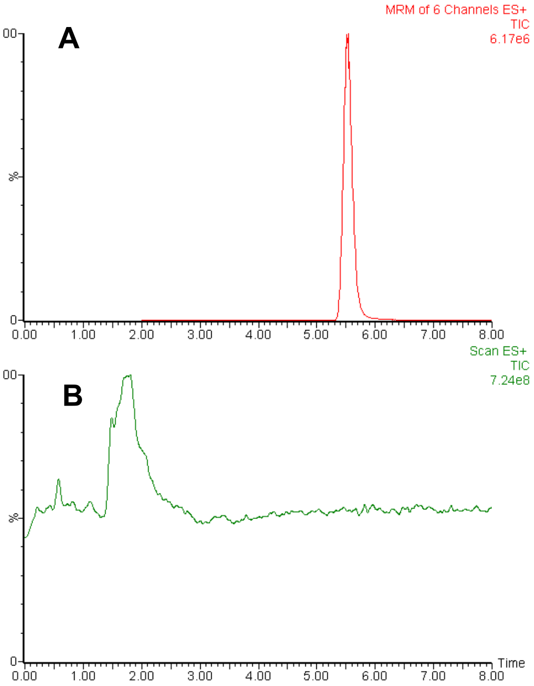

Figure 3-14: LC-ESIMS/MS chromatograms of dityrosine. A) LC-ESIMS/MS chromatograms of dityrosine standard acquired on MRM mode using Phenomenex Gemini 3u C_6-phenyl 110 A° (150 mm x 4.6 mm, 3 micron) column and formic acid as a modifier with retention time of 5.5 min. B) LC-ESIMS/MS chromatograms of dityrosine standard acquired on full-scan mode using Phenomenex Synergi 4u Hydro-RP 80 A° (150 mm x 2 mm, 4 micron) column and formic acid as a modifier with retention time of 1.8 min.

Characterisation of authentic dityrosine was achieved using Phenomenex Gemini 3u C_6-phenyl 110 Å (150 mm x 4.6 mm, 3 micron) column, the mass spectrometry was operated in the MRM mode with ESI ve+. The solvent of the mobile phase were A: 0.1% formic acid in water; and solvent B: 0.1% formic acid in acetonitrile, and the flow rate was 200 μl/min. Dityrosine has been reported to show a fragmentation pattern

(Figure 3-15) to give the following protonated product ions at *m/z*; 315, 283, 269, 254, and 237 (Fenaille et al. 2004; Takasaki et al. 2005).

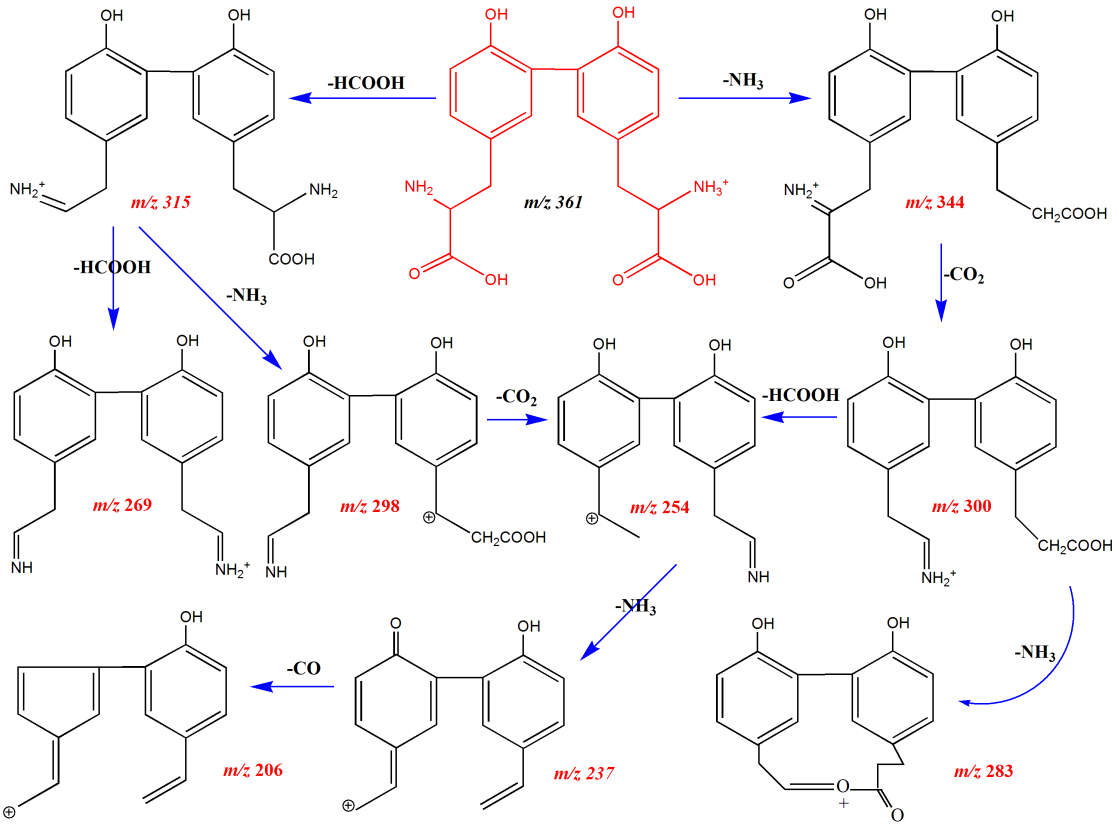

Figure 3-15: Dityrosine fragmentation pattern as proposed by (Takasaki et al. 2005) and (Fenaille et al. 2004).

Dityrosine identification was achieved by monitoring the transition reactions; 361.1→315, 361.1→283, 361.1→269, 361.1→254, and 361.1→237 as shown in (Figure 3-16, A). The mass spectrum shows that 361.1→315 transition is the most intense (Figure 3-16, B), thus it will be used to detect dityrosine in the rest of the study.

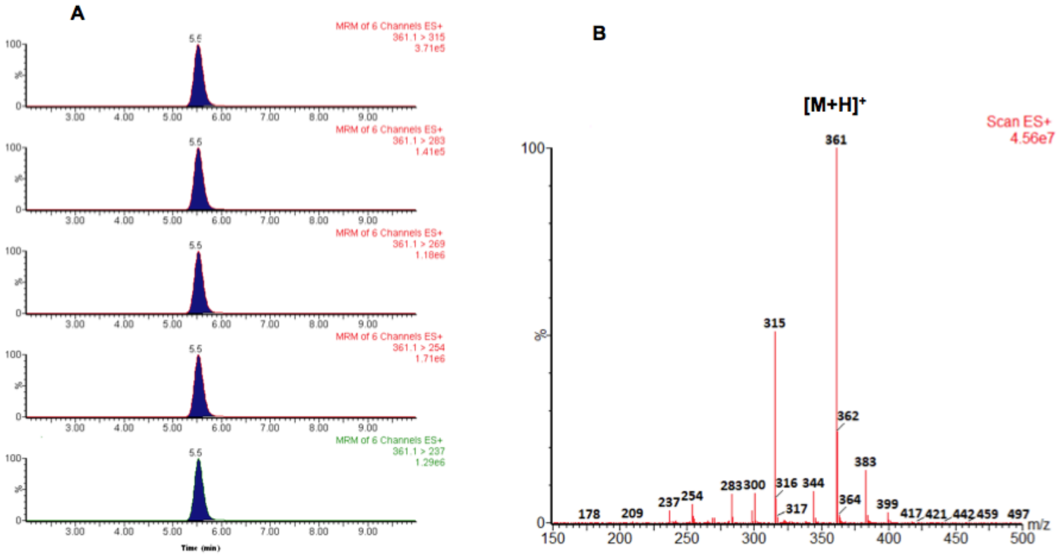

Figure 3-16: A) LC-ESIMS/MS chromatograms of authentic dityrosine were recorded using MRM mode, showing the characteristic dityrosine product ions. B) The total ion chromatogram of authentic dityrosine with m/z 361 $[M+H]^+$ (the protonated ion of dityrosine).

In LC-MS, certain modifiers are often added to the mobile phase to obtain better resolution and retention. Formic and acetic acid are commonly used as modifiers due to their ability to improve retention and/or peak shape. Moreover, many mass spectrometric analyses are accomplished in positive mode, which is achieved by the addition of a proton to form the molecular ion $[M+H]^+$. However, polar and ionic compounds are poorly retained on the column that used in RP-HPLC and usually elute near the solvent front. Volatile salt, such as ammonium acetate and formate, are mobile phase modifiers for LC-MS detection that achieved under neutral conditions. However, compared to their corresponding organic acid, i.e. acetic and formic acid respectively, their use in mass analyses is more complex. They have limited solubility in organic solvents and also the pH value of mobile phase is changed during a gradient. Using ammonium salts could result in mass signal suppression due to affinity of ammonium ion toward proton, in turn affects the amount of protonated ion in the gas phase that ultimately reaches the mass detector (Watson and Sparkman 2008).

Ion pairing reagents, e.g. TFA, are commonly used to enhance the retention of ionic and hydrophilic compounds by ion pair formation. TFA is commonly added to mobile phase for RP-HPLC of proteins and peptides, resulting in a neutral species formation, increasing the hydrophobic character, and enhancing the retention. In addition, TFA improves peak shape and resolution by reducing silanol interaction (Watson and Sparkman 2007). Whereas TFA is often cited as a good modifier for PR-HPLC due to its ability to improve retention and peak resolution, the presence of TFA in the mobile phase adversely affects the mass signal (Watson and Sparkman 2008).

3.5 **Conclusion**

Dityrosine is a tyrosine dimer that results from the ortho-ortho coupling of two tyrosine residues. However, as dityrosine was not commercially available it was very important to synthesise authentic dityrosine and use it in the rest of our study as a standard. In this chapter, dityrosine synthesis was explored using several protocols and milligram quantities were prepared. Synthesised dityrosine was characterised using different analytical techniques including RP-HPLC, mass spectrometry, fluorescence spectrophotometry, and NMR. Our results revealed that Suzuki-Miyaura coupling reaction is the most effective among the chemical and enzymatic oxidative coupling strategies in preparation of dityrosine. In order to detect dityrosine in our samples, LC-ESIMS/MS method was developed and optimum conditions were obtained. The data shows that using formic acid as a modifier in the mobile phase results in acquiring better mass spectra, moreover Phenomenex Gemini 3u C_6-phenyl 110 Å showed better performance in dityrosine retaining using formic acid as a modifier.

4 Results and Discussion

Cu^{2+}/H_2O_2 oxidation system leads to dityrosine generation in two short amyloidogenic peptides

4.1 Introduction

Amyloid fibrils are associated with a large number of diseases in which proteins and peptides abnormally assemble to form insoluble amyloid deposits in tissues. It has been well established that amyloid fibrils share a core cross-β structure (Jahn et al. 2010; Serpell et al. 1999) and many different proteins and peptides can form amyloid-like fibrils, which all share an amyloid-like conformation (Dobson 2003; Jahn et al. 2010; Sunde et al. 1997). The recent focus on the importance of sequence on amyloid forming propensity has lead to a number of algorithms designed to identify short amyloidogenic peptides (Maurer-Stroh et al. 2010; Pawar et al. 2005). Waltz is an algorithm aimed at identifying amyloidogenic peptides with a particular emphasis on the position of particular amino acid residues and this has identified a number of peptides that form highly ordered amyloid-like fibrils that share amyloid properties (Maurer-Stroh et al. 2010). Several of these peptides identified contain aromatic residues including tyrosine, which is often favoured at position five within a hexapeptide but is also allowed at positions two and four (Maurer-Stroh et al. 2010). The hexa- and pentapeptides HYFNIF and VIYKI were of particular interest due to their highly organised fibrillar structure and the positions of the tyrosine residues allowing for potential dityrosine formation. The current study explored the oxidative modification of two short peptides, HYFNIF and VIYKI, using the Cu^{2+}/H_2O_2 oxidation system, and studied the morphological and conformational changes of these amyloid fibrils over the oxidation process. This chapter describes the investigation into the influence of dityrosine cross-linking (Figure 1-17) on the assembly and structure of the HYFNIF and VIYKI peptides. These peptides were selected as simple amyloid model systems that have been previously structurally characterised (Morris et al. 2013b) to better understand the dityrosine formation at a structural level and to optimise the oxidation conditions. In turn, these oxidation conditions can be used to enhance the dityrosine cross-link formation in both Aβ and α-syn as shown in chapter 5 and 6 respectively.

4.2 Results and discussion

4.2.1 Oxidation of tyrosine containing synthetic amyloid-like fibrils

The Waltz identified peptides, HYFNIF and VIYKI, form well characterised amyloid fibrils in water. These have been extensively studied by TEM, CD, LD, and XRFD (Morris et al. 2013b). HYFNIF and VIYKI peptides were dissolved in water at a concentration of 1.14 and 1.48 mM respectively and allowed to assemble to form fibrils at room temperature for 7 days. They were examined using negative stain TEM, which showed the expected long straight unbranching amyloid-like fibrils. Some showed lateral association and twisted morphologies as shown in insets (Figure 4-1). Fluorescence spectroscopy of the preformed amyloid fibrils at a concentration of 100 µM revealed a strong peak at 305 nm, characteristic of the fluorescence arising from tyrosine residues (Figure 4-1).

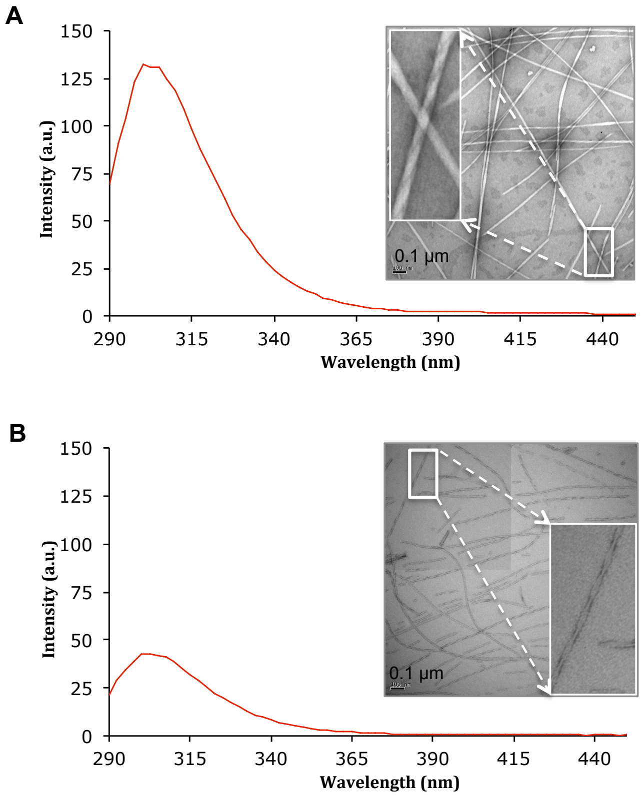

Figure 4-1: (A) Fluorescence spectrum of (100 µM) VIYKI amyloid-like fibrils in water, and transmission electron microscopy image obtained from VIYKI fibrils. B) Fluorescence spectrum of HYFNIF amyloid-like fibrils in water at concentration of 100 µM, and transmission electron microscopy image obtained from HYFNIF fibrils. Upon excitation at 280 nm the tyrosine residue results in a peak at 305 nm.

Comparison of the signal intensity arising from the two peptides revealed a significantly stronger signal (a.u. ~ 125) for fibrils formed by VIYKI compared to HYFNIF (a.u. ~ 40). This may reflect differences in the arrangements of the peptides within the fibrils and the exposure/burial of the tyrosine residues as discussed later.

To shed light on the relative susceptibility of HYFNIF and VIYKI fibrils to oxidative dityrosine cross-linking, the effect of oxidation on the assemblies was examined, using Cu^{2+}/ H_2O_2. Preformed amyloid-like fibrils of HYFNIF and VIYKI were incubated for 72 h in the presence of Cu^{2+} (100 µM) and H_2O_2 (2.5 mM) in water (pH of 5.0 and 6.1 respectively) at 37 ºC with agitation by shaking at 300 rpm. Fluorescence spectroscopy was used to monitor the extent of amyloid-like fibril oxidation and the results showed a new signal at 410 nm (Figure 4-2) corresponding to dityrosine cross-linking formation and consistent with the fluorescence signal exhibited by the dityrosine standard (Figure 3-9). This was accompanied by a corresponding decrease in the signal intensity at 305 nm arising from tyrosine (Figure 4-2). Again, differences in signal intensity were observed, whereby oxidised fibrils formed by HYFNIF gave a much lower signal than VIYKI. It might be that tyrosine residues in HYFNIF are more buried compared to that in VIYKI, thus they have less propensity to cross-link.

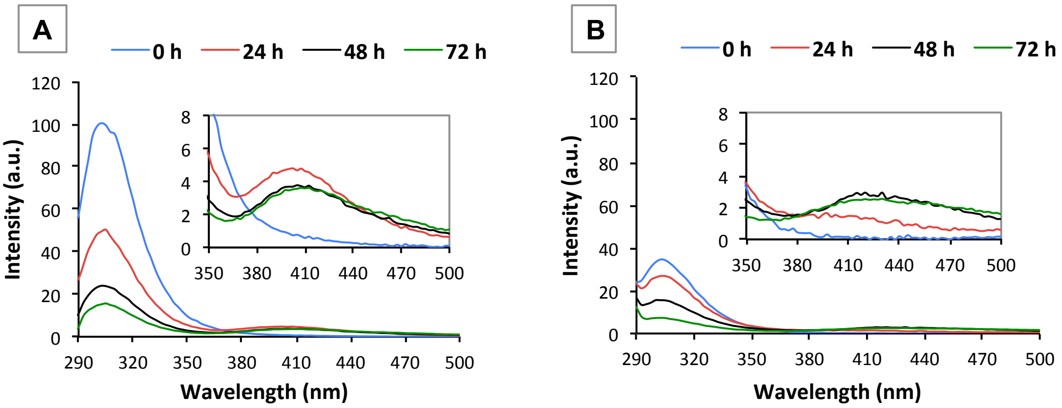

Figure 4-2: Time course monitoring of HYFNIF and VIYKI fibril oxidation in water. 100 µM of (A) VIYKI and (B) HYFNIF fibrils were incubated in presence of Cu^{2+}/ H_2O_2 in water for three days at 37°C with agitation of 300 rpm. The insets showing dityrosine fluorescence signal arising at 410 nm, indicating of tyrosine oxidative modification under Cu^{2+}-catalysed stress.

The presence of dityrosine in oxidised fibrils was confirmed using LC-ESIMS/MS following acidic hydrolysis of the oxidised VIYKI and HYFNIF fibrils. The dityrosine formation was identified using transition reactions ions 361.1→315, the most intense transition reaction ion as shown in chapter three, and has a retention time 5.5 min (Figure 4-3), consistent with that of authentic dityrosine.

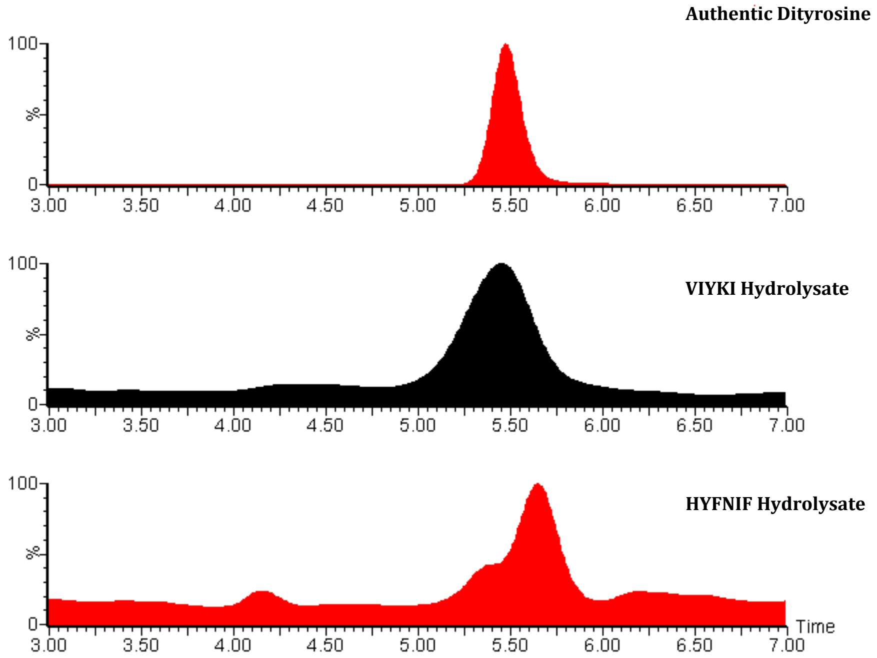

Figure 4-3: LC-ESIMS/MS chromatograms recorded in the MRM mode for dityrosine from authentic dityrosine, VIYKI and HYFNIF fibrils hydrolysate. Oxidised VIYKI and HYFNIF fibrils were obtained from incubation of 50 µM VIYKI and 100 µM HYFNIF fibrils with Cu^{2+}/H_2O_2 *in water at 37 ºC with agitation of 300 rpm. In HYFNIF hydrolysate, there is a slight shift in the retention time due to experimental error of the LC-MS.*

LC-ESIMS/MS (MRM) technique is characterised by high sensitivity and specificity (Cox et al. 2005; Orhan et al. 2005), which enables us to follow and detect oxidative modifications of peptides and proteins at low concentration. Although the dityrosine that resulted from oxidation of 50 µM HYFNIF fibrils can be detected using LC-ESIMS/MS (MRM), hydrolysis of 100 µM oxidised HYFNIF fibrils resulted in a better-shaped (higher intensity and sharper) peak as shown in Figure 4-3, and this is because more dityrosine was released. Also, this could reflect the resulting dityrosine content in HYFNIF fibrils.

To estimate the dityrosine content in oxidised HYFNIF and VIYKI peptides, a dityrosine standard curve was generated. A set of dityrosine standard concentrations (0.1, 0.5, 1, 2, 3, and 5 μM) was made up in Milli-Q water using the synthetic dityrosine. Each concentration was prepared in triplicate and dityrosine fluorescence was recorded for each concentration using an excitation wavelength of 280 nm and emission wavelength 410 nm. The mean values of dityrosine fluorescence intensity for each concentration were plotted against dityrosine concentration and a standard curve was constructed by linear regression analysis using Microsoft Excel 2011 software (Figure 4-4). The equation of this line was used to quantify the dityrosine content of HYFNIF and VIYKI peptides, taking into account any differences in the environment of the dityrosine residues.

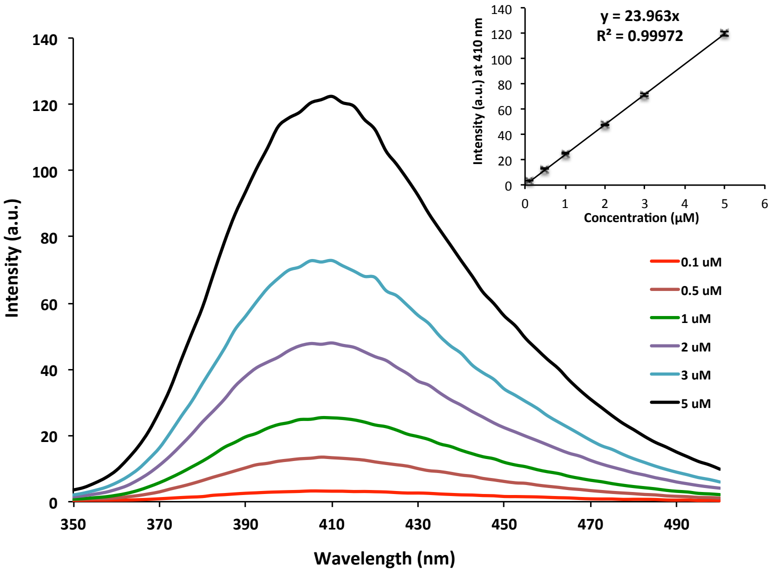

Figure 4-4: Standard calibration curve for dityrosine standard (error bars indicate ± standard deviation of three experimental repeats). Linear standard curve of dityrosine was obtained over a concentration range (0.1-5 μM), dityrosine fluorescence signal was line when plot against concentration (inset panel).

Although LC-ESIMS/MS (MRM) has a high sensitivity and selectivity and can be used to quantify dityrosine content with high accuracy, dityrosine content was assessed using fluorescence spectroscopy due to possible incomplete release of dityrosine using acid hydrolysis. In addition, fluorescence spectroscopy shows high sensitivity and no need to hydrolyse the peptide, making it a good technique to quantify dityrosine. After 24 h of oxidation, 0.06 and 0.2 μM of dityrosine was obtained from the oxidation of (100 μM)

HYFNIF and (100 μM) VIYKI fibrils respectively (Figure 4-2), indicating that more dityrosine was formed in VIYKI fibrils compared with HYFNIF.

By contrast, 0.15 and 0.1 μM of dityrosine was formed in HYFNIF and VIYKI fibrils respectively after 72 h of oxidation, suggesting that further oxidation took place in VIYKI fibrils, whilst HYFNIF fibrils exhibited more resistance to the oxidative modification. There are many factors that need to be taken into account regarding the fluorescence data analysis. Firstly, HYFNIF and VIYKI have different molecular proportions of tyrosine residue. While HYFNIF consist of six amino acids, VIYKI has just five and that could result in more intense tyrosine fluorescence signal compared with HYFNIF. Secondly, both HYFNIF and VIYKI have different amino acid sequences and that could affect the oxidation process. Finally, the arrangement of the tyrosine residue within fibrils is completely different, as described later, consequently the tyrosine environment (buried/exposure) may play an important role in the resultant fluorescence signal.

4.2.2 **Dityrosine cross-link formation at physiological pH**

To maximise the oxidation conditions and to examine the pH effect on the extent of oxidation, 100 μM of both HYFNIF and VIYKI fibrils were oxidised in phosphate buffer pH 7.4 under Cu^{2+}/ H_2O_2 condition. The fluorescence results indicate that the dityrosine formation increased significantly over oxidation time in phosphate buffer pH 7.4 (Figure 4-5, A and Figure 4-6, A) compared to that in water (~ pH 6.1 for VIYKI and 5.0 for HYFNIF) (Figure 4-2). The oxidation of VIYKI fibrils over time revealed that dityrosine signal reaches the maximum amount after 24 h of incubation, while no significant increase was observed between 24 and 48 h of incubation. Prolonged oxidation was observed after 72 h of incubation, which appeared to result in a decline in dityrosine yield. Dityrosine can undergo further oxidative modification to form trityrosine, another tyrosine oxidative modification product (Jacob et al. 1996; Skaff et al. 2005). By contrast, HYFNIF fibrils exhibited more resistance to the oxidation, 72 h of incubation with Cu^{2+}/H_2O_2 was required to yield maximum amount of dityrosine as shown in Figure 4-6, A.

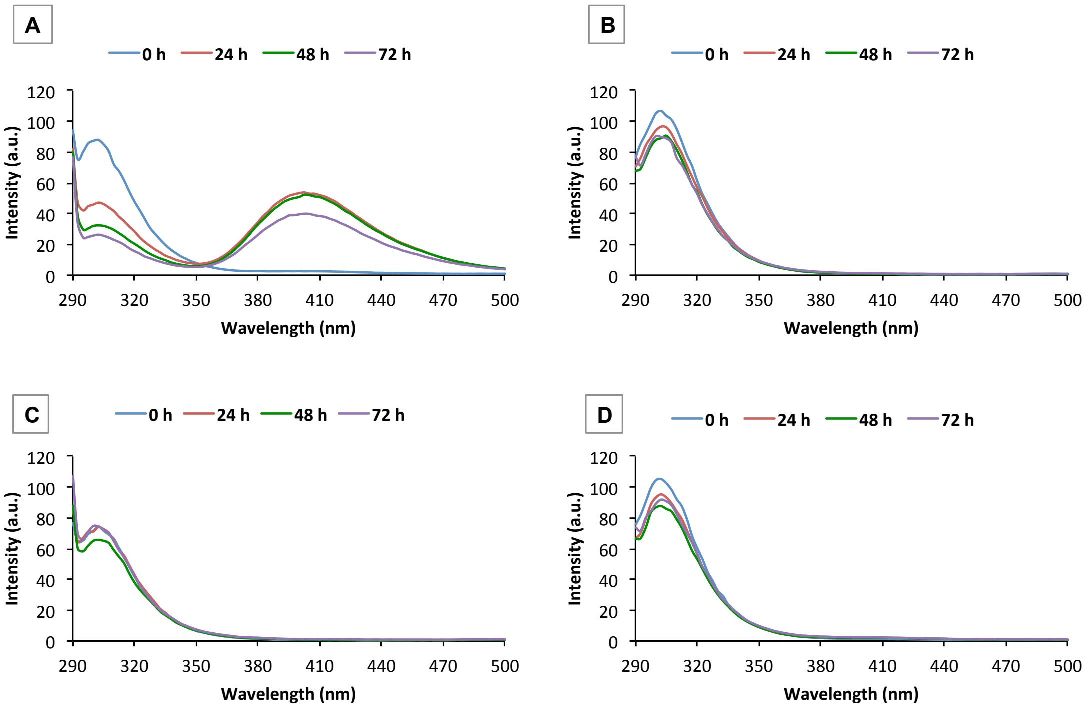

Figure 4-5: Time course monitoring the VIYKI fibril oxidation in phosphate buffer pH 7.4. 100 µM of VIYKI fibrils were incubated in presence (A) and absence (B) of Cu^{2+}/ H_2O_2 respectively, and the data revealed dityrosine fluorescence signal arising at 410 nm upon incubation with Cu^{2+}/ H_2O_2. In addition, VIYKI fibrils were incubated with (C) Cu^{2+} only, and (D) H_2O_2 only showing no indication of a dityrosine signal at 410 nm.

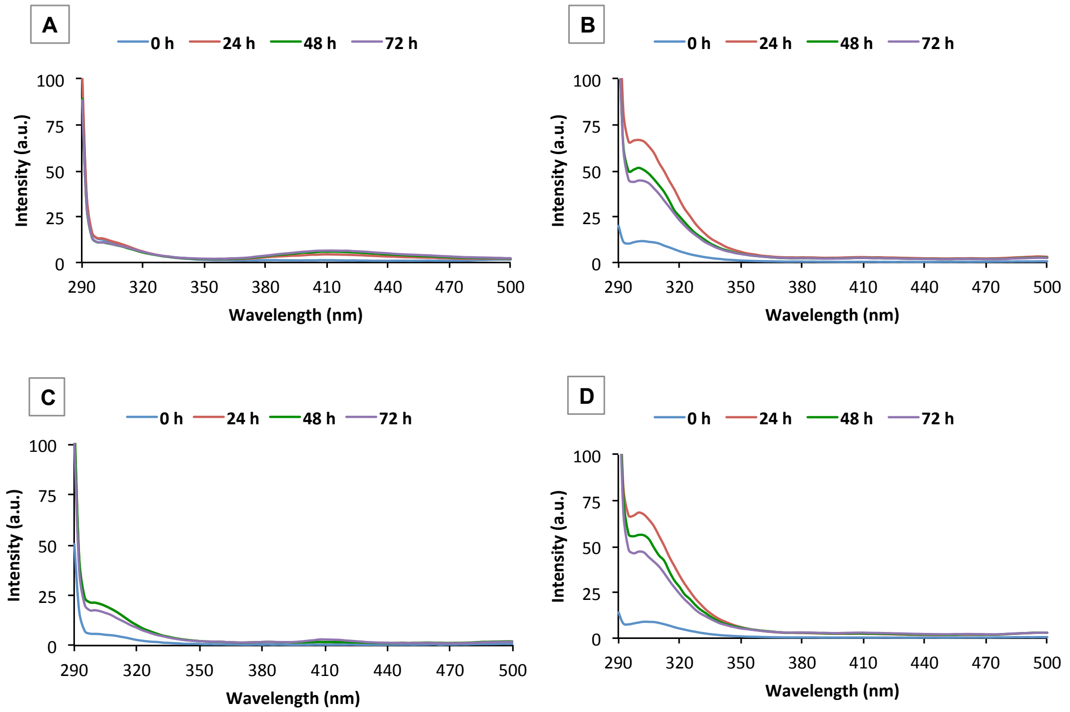

Figure 4-6: Time course study showing oxidation of HYFNIF fibrils in phosphate buffer pH 7.4. 100 µM of HYFNIF fibrils were incubated in presence (A) and absence (B) of Cu^{2+}/ H_2O_2 respectively. In addition, HYFNIF fibrils were incubated with (C) Cu^{2+}, and (D) H_2O_2 only.

It is obvious that HYFNIF fibrils oxidised to give dityrosine linkages in a different manner than for VIYKI fibrils, which showed a higher propensity to form dityrosine linkages. The result of oxidation over time of HYFNIF and VIYKI amyloid-like fibrils revealed that dityrosine cross-link formation in VIYKI fibrils is more rapid than for HYFNIF fibrils (Figure 4-7), and also more dityrosine was yielded in VIYKI fibrils. This conclusion is supported by the TEM micrograms of oxidised HYFNIF and VIYKI fibrils, which revealed an extensive morphological change in oxidised VIYKI fibrils compared with HYFNIF (Figure 4-8).

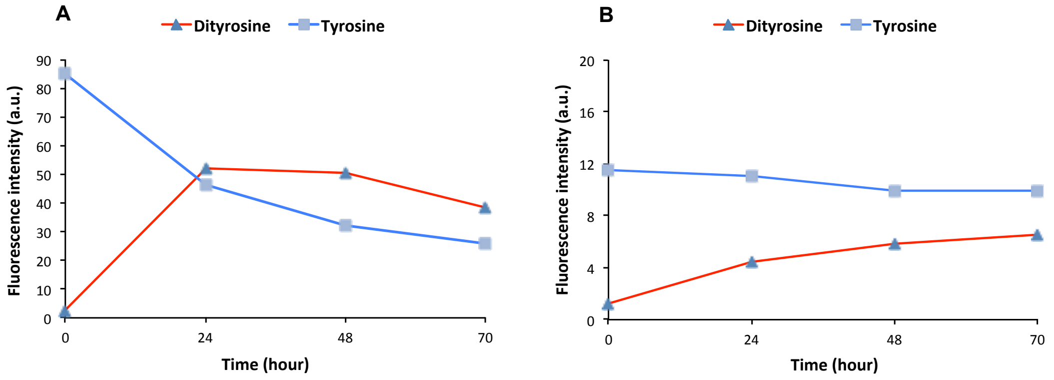

Figure 4-7: Dityrosine formation extent in both (A) VIYKI and (B) HYFNIF fibrils using phosphate buffer pH 7.4. The data show that VIYKI fibrils form dityrosine linkage rapidly and more efficiently than HYFNIF.

Addition of H_2O_2 alone to the amyloid-like fibrils did not result in any dityrosine cross-links formation as shown in (Figure 4-5, D) and (Figure 4-6, D), indicating the importance of catalytic role played by Cu^{2+} ions in the oxidative coupling of tyrosine residues. The addition of Cu^{2+} ions to the oxidation solution induced dityrosine cross-link formation and this is consistent with the results reported for Aβ (Atwood et al. 2004; Huggins et al. 1993; Smith et al. 2007). Furthermore addition of Cu^{2+} ions only showed no dityrosine signal and also quenched the tyrosine fluorescence signal at 305 nm as shown in (Figure 4-5, C) and (Figure 4-6, C), and that may be due the coordination of Cu^{2+} ion with tyrosine residue or that tyrosine residue located close to the binding site of the Cu^{2+} as shown for Aβ (Maiti et al. 2008; Tougu et al. 2008).

Quenching of tyrosine signals were also observed after 24 h of incubation of VIYKI fibrils with and without H_2O_2 as shown in (Figure 4-5, D, and B) respectively, and this could be attributed to maturation of the fibril structure leading to further quenching of tyrosine by solvent or precipitation of the fibrils at pH 7.4.

On the other hand, the tyrosine signal was enhanced after 24 h of incubation of HYFNIF fibrils with and without H_2O_2 as shown in (Figure 4-6, D and B) respectively, which could be due to increased solubility of HYFNIF fibrils in phosphate buffer over the agitation, in turn that will result in more tyrosine residues to be solution accessible. Also, HYFNIF fibrils could be undergoing a structural change as they mature that enhances the tyrosine signal.

Studies of autoxidation and oxidation by H_2O_2 of phenols catalysed by Cu^{2+}-ethylenediamine complexes (Kushioka 1983; Kushioka et al. 1989) showed that Cu^{2+}-ethylenediamine complexes have the ability to catalyse the oxidation of phenols and produce biphenol compounds. It was demonstrated that the mechanism of the oxidation of phenols involved Cu^{2+} ion coordination to nitrogen and oxygen of the phenols and explained that the coordination of oxygen to Cu^{2+} is weaker than that of nitrogen. These results support the notion of formation of carbon-carbon covalent bond in the proteins and peptides that contain tyrosine residues (which has a phenyl group in it's side chain) in their backbone. In our study, Cu^{2+}-peptide complexes can be formed by coordination of Cu^{2+} with HYFNIF via His and Tyr residues, and VIYKI via Lys and Tyr residue. These complexes can catalyse the oxidation of tyrosine residue and produce dityrosine via a C-C bond. As explained above, Cu^{2+}-ethlenediamine complexes can catalyse the formation of C-C bond to produce biphenol compounds, however the ability of these complexes to catalyse the oxidation of phenols is different. The most catalytically active complexes are those that are less stable (Kushioka 1983). It has been shown that imidazole moiety of the His residue exhibits high affinity toward Cu^{2+} ion, forming a stable complex (Patel et al. 2002). In general, amino acid sequence has an important influence on the Cu^{2+} ions coordination, while the side chains of some amino acid, e.g. histidine and glutamine, show high affinity toward binding to metal ions, other exhibit less affinity (Glusker 1999). HYFNIF and VIYKI peptides have different amino acid sequences and this in turn will affect the coordination with Cu^{2+} ions, and as a result different amounts of dityrosine will result. Another factor that could affect the dityrosine formation is the steric hindrance provided from the neighbouring amino acid side chains within the fibril architecture.

The pH value has a profound influence on the electrostatic nature of the peptide via changing the net peptide charge. However, Cu^{2+} ions coordination to peptides and proteins can also be affected by the pH value. For example, it has been shown that binding of Cu^{2+} to Aβ is highly pH-dependent (Atwood et al. 1998), explaining that there is a transition between two complex forms as the pH is raised (Syme et al. 2004). Cu^{2+} ions are acting as electrophiles and sharing electron pairs with other atoms to form ionic bond or charge-charge interactions. At a neutral pH value, Cu^{2+} ion concentrations can be high (Glusker 1999), and as a consequence more Cu^{2+} ions are available to form complexes with the ligands. It is important to generate a neutral or negatively charged peptide to facilitate the coordination with Cu^{2+} ions. At pH 7.4, HYFNIF and VIYKI peptide have a more neutral net charge (0.1 and 0.8 respectively) than that in water (1.2 for HYFNIF and 1.1 for VIYKI), where the pH is more acidic (the pI of HYFNIF and VIYKI fibrils are 8.0 and 10.3 respectively). As a result, Cu^{2+}-peptide complexes can be easily generated at pH 7.4, subsequently these complexes can catalyse the tyrosine cross-linking, and that may explain why less dityrosine yield was obtained at acidic pH in water compared to more efficient dityrosine formation at pH 7.4.

4.2.3 **Morphological changes of amyloid-like fibrils over oxidation**

The appearance of the oxidised amyloid-like fibrils were visualised by electron microscopy and displayed a remarkable diversity. The image of oxidised fibrils in phosphate buffer showed evidence of shortening of the fibrils (49.0 – 863.0 nm for VIYKI, and 104.0 – 2435.0 nm for HYFNIF), compared to those non-oxidised (1762.0 – 1855.0 nm for VIYKI), and also clumping of short fibrils (Figure 4-8).

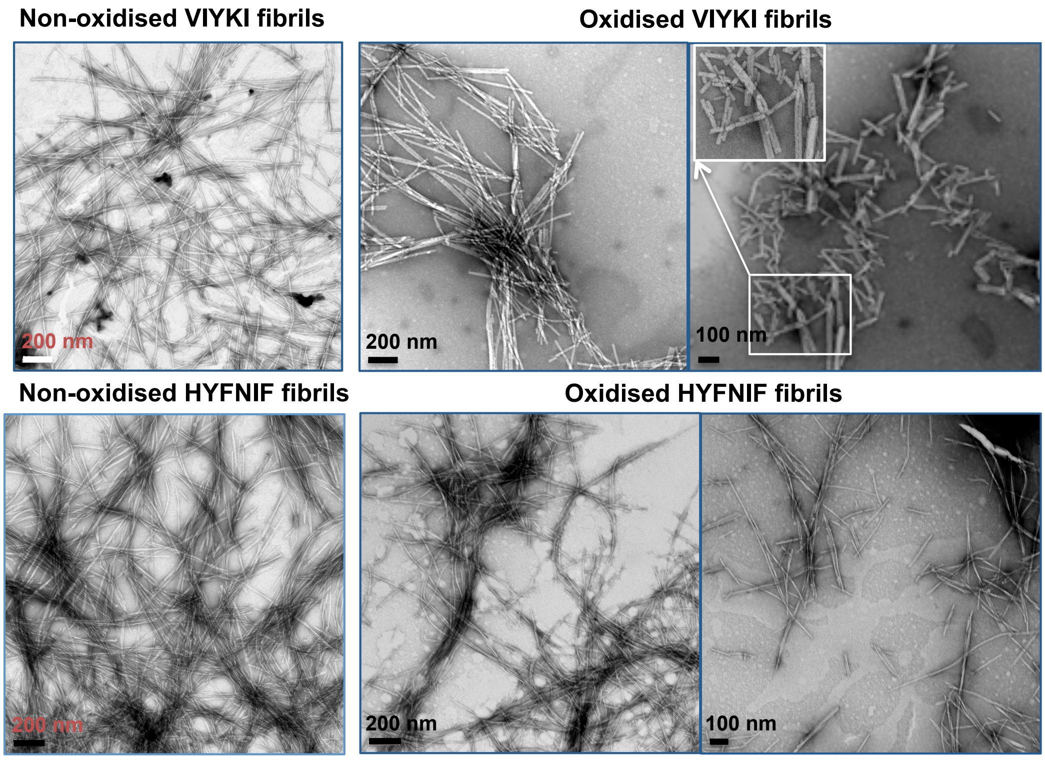

Non-oxidised VIYKI fibrils

Oxidised VIYKI fibrils

Non-oxidised HYFNIF fibrils

Oxidised HYFNIF fibrils

Figure 4-8: Morphological changes over oxidation in phosphate buffer pH 7.4. Transmission electron micrographs of non-oxidised HYFNIF and VIYKI after 24 h of incubation in (50 mM) phosphate buffer pH 7.4 with agitation of 300 rpm reveal they have amyloid-like fibrillar morphologies. Upon oxidation using Cu^{2+}/H_2O_2*, amyloid-like fibrils showed evidence of shortening (VIYKI 49.0 - 863.0 nm, HYFNIF 104.0 - 2435.0 nm) of the fibrils compared to the non-oxidised fibrils (VIYKI 1762.0 - 1855.0 nm).*

A previous study (Morris et al. 2013b), showed that HYFNIF and VIYKI peptide are found to spontaneously form a fibrillar structure upon incubation in water. It is clear that upon oxidation and dityrosine cross-link production, morphological changes were observed, in particular for VIYKI fibrils (Figure 4-8). The latter undergoes extensive fragmentation due to oxidative modification, resulting in the formation of shorter fibrils, which in some cases become noticeably thicker (40 nm). In contrast, HYFNIF fibrils showed less morphological changes upon oxidation and this is consistent with the HYFNIF peptide’s apparent lesser ability to form dityrosine cross-links. However, it is not clear if the dityrosine cross-linking process may affect the self-assembly ability of HYFNIF and VIYKI peptide. Incubation of 100 µM of preformed amyloid-like fibrils in (50 mM) phosphate buffer pH 7.4 for 24 with agitation of 300 rpm did not result in a significant morphological change, and the TEM micrographs revealed that both HYFNIF and VIYKI fibrils morphologies are maintained over incubation period as seen in Figure 4-8 (non-oxidised fibrils). Non-oxidised HYFNIF and VIYKI fibrils are heterogeneous, long, straight, and unbranched fibrils (Figure 4-8).

In order to examine the morphologies of fibrils that assembled under oxidative stress conditions, attempts to generate the monomeric species of both HYFNIF and VIYKI peptide were carried out using HFIP or NaOH. Unfortunately, both HYFNIF and VIYKI peptides exhibited high resistance to monomerision.

4.2.4 Negative stain immunogold labelling TEM

To further identify the dityrosine cross-link, and to show the dityrosine distribution in the oxidised fibrils, TEM immunogold labelling using a dityrosine specific monoclonal antibody (1C3) was performed. Figure 4-9 and Figure 4-10 show labelling using an anti-dityrosine, gold-conjugated antibody on HYFNIF and VIYKI amyloid-like fibrils revealing gold distributed close to the fibrils that were grown in an oxidising environment. Non-oxidised HYFNIF and VIYKI fibrils did not label with the dityrosine antibody. Very strong evidence of dityrosine identity was provided using these specific monoclonal dityrosine antibodies, and also it represents an initial examination of the possibility of using these antibodies to detect the presence of dityrosine in both plaques and CSF samples from AD patient as described further in chapter five.

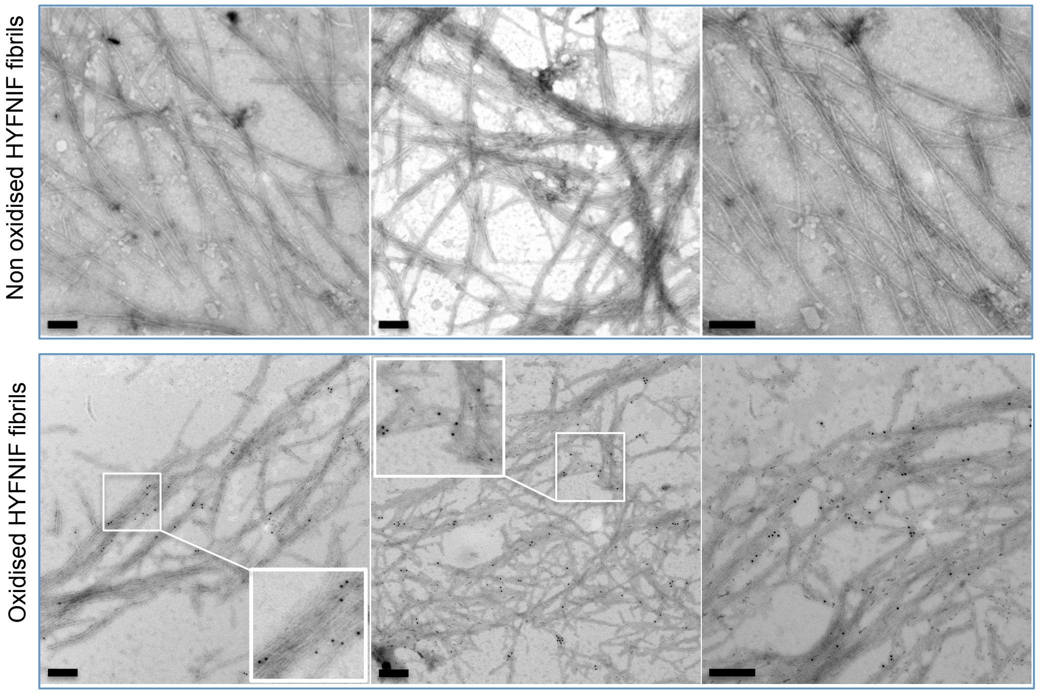

Figure 4-9: TEM immunogold labelling. Non-oxidised and oxidised HYFNIF fibrils were gold labelled using a dityrosine.antibody. (100 µM) HYFNIF fibrils were oxidised for three hs using (100 µM) Cu^{2+} and (2.5) mM H_2O_2 in (50 mM) phosphate buffer pH 7.4. The oxidation process was undertaken at 37 º C, and agitation 300 rpm. The scale bars represent 0.2 µm. The immunogold labelling micrographs shows positive labelling for dityrosine in oxidised fibrils compared with non-oxidised fibrils that did not label with dityrosine antibody.

High magnification TEM micrographs of oxidised VIYKI fibrils, which had been labelled with the gold-conjugated dityrosine antibody, revealed that dityrosine cross-links are distributed along the fibrils (Figure 4-10). It appears that dityrosine coupling is undertaken within the fibrils. Although fluorescence data showed that much higher dityrosine fluorescence intensity was generated in oxidised VIYKI fibrils, it is obvious that less gold labelling was observed in oxidised VIYKI fibrils (Figure 4-10) compared to oxidised HYFNIF fibrils (Figure 4-9), and this may support the view that dityrosine cross-link is formed internally within fibrils. Consequently, the dityrosine cross-link epitope is less accessible to bind the antibody.

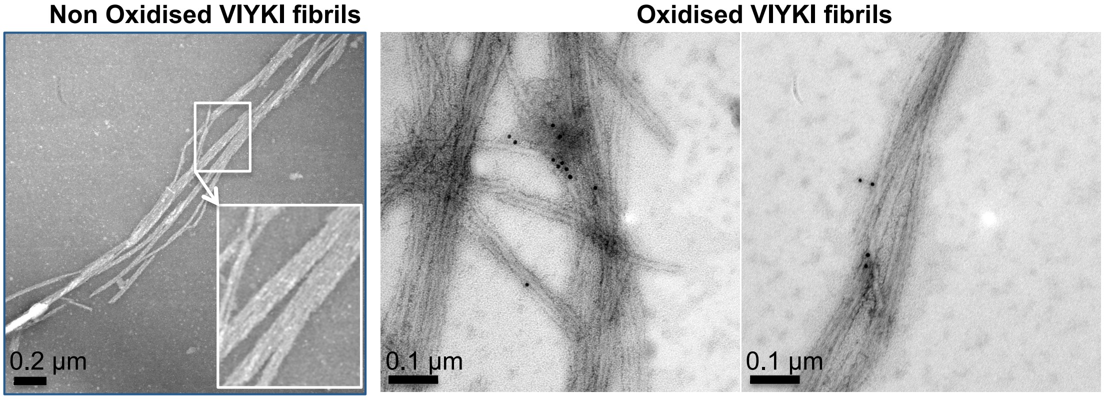

Figure 4-10: TEM immunogold labelling. Non-oxidised and oxidised VIYKI fibrils were gold labelled for dityrosine. 100 µM VIYKI fibrils were oxidised for three hs using (100 µM) Cu^{2+} and 2.5 mM H_2O_2 in phosphate buffer 50 mM, pH 7.4. The oxidation process was undertaken at 37 º C, and agitation 300 rpm.

The immunogold labelling TEM micrographs of dityrosine in both non-oxidised HYFNIF and VIYKI fibrils provide a strong evidence of dityrosine antibody specificity toward dityrosine verses tyrosine, and shows that tyrosine residues in non-oxidised fibrils did not cross bind with the dityrosine antibody.

4.2.5 Exploring the effect of buffer type on dityrosine formation

It has been shown that the Cu^{2+} coordination is varying in different buffer conditions (Tougu et al. 2008). To examine the efficiency of dityrosine formation in amyloid-like fibrils under oxidative conditions, and to explore the performance of the metal-catalysed oxidation system using different types of buffers, phosphate and HEPES buffers were used. HYFNIF and VIYKI fibrils with a concentration of 100 µM were incubated with Cu^{2+}/H_2O_2 in 50 mM HEPES buffer pH 7.4, and in 50 mM phosphate buffer pH 7.4.

The oxidation process was undertaken for 26 h at 37 ºC, and dityrosine formation was monitored using an excitation wavelength of 320 nm instead of 280 nm, which was used previously (Figure 4-11). It has been demonstrated that using an excitation wavelength of 320 nm produced much stronger dityrosine emission signal (Malencik and Anderson 1991; Malencik et al. 1996; Smith et al. 2007). Initially, the results revealed that VIYKI fibrils exhibited more susceptibility to form dityrosine linkages than HYFNIF fibrils in both HEPES and phosphate buffer. Moreover, using phosphate buffer in the oxidation process of VIYKI fibrils leads to higher yield of dityrosine formation compared to that using HEPES buffer as shown in Figure 4-11, B and A respectively. Fluorescence data show that after 26 h of oxidation of VIYKI fibrils in phosphate buffer, high dityrosine intensity at around 410 – 420 nm was obtained compared to that in HEPES buffer (Figure 4-11, A).

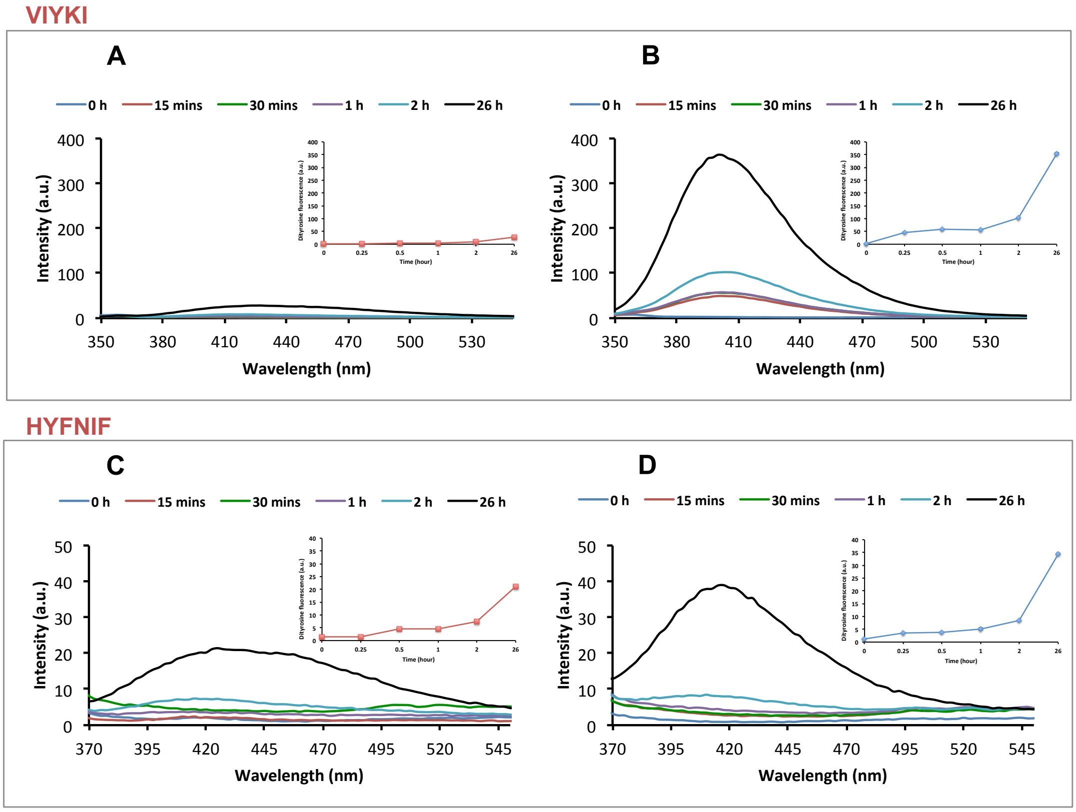

Figure 4-11: Dityrosine cross-link formation efficiency using two different types of buffers, HEPES and phosphate buffer. (A) & (B) Oxidation of VIYKI fibrils in HEPES and phosphate buffer respectively. (C) & (D) Oxidation of HYFNIF fibrils in HEPES and phosphate buffer respectively. Dityrosine formation was monitored using excitation wavelength of 320 nm. The emission spectra were recorded over 340-600 nm. Inserts showing dityrosine fluorescecne increase with time.

Alternatively, HYFNIF fibrils show less ability to form dityrosine cross-links in both buffers compared with VIYKI fibrils (Figure 4-11, C and D), indicating that the differences in the amino acid sequences of the amyloidoegenic peptide and their structural architecture affect their ability to produce dityrosine cross-links. The intensity of the dityrosine signal at 410 – 420 nm obtained from HYFNIF fibrils after 26 h of oxidation was much less than the signal from VIYKI fibrils. Also, it took just 15 min to give a significant dityrosine signal in VIYKI fibrils (Figure 4-11, B), compared to the 2 h required to yield dityrosine in HYFNIF fibrils (Figure 4-11, D). Our results show that using phosphate buffer to perform the Cu^{2+}-catalysed oxidation process produces increased dityrosine formation Figure 4-12.

It has been revealed that HEPES buffer is the most suitable buffer to perform copper coordination experiment, since it does not form ternary complexes with copper ions, (Tougu et al. 2008), thus HEPES would not compete with peptide and proteins to bind copper ions. However, it seems from our data that HEPES buffer is less efficient at producing dityrosine. This might be due to the formation of stable Cu^{2+}/peptide complexes in HEPES buffer, which in turn may have less catalytic activity.

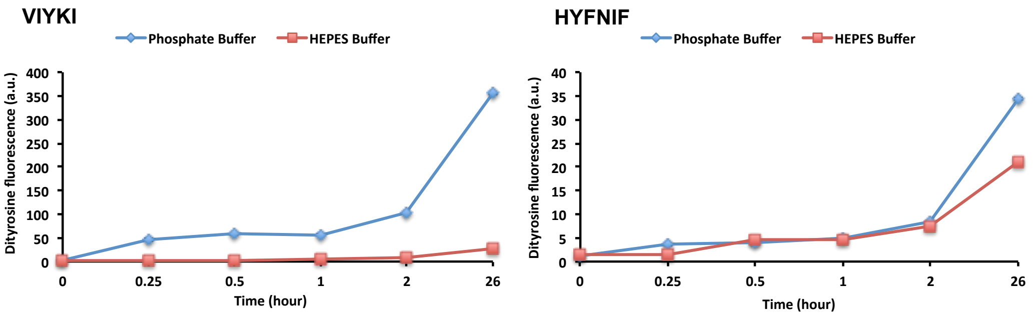

Figure 4-12: Using different types of buffer significantly affects the performance of copper-catalysed oxidation process, and in turn the amount of resulting dityrosine. A) Oxidation of VIYKI fibrils in phosphate buffer gives much higher signal of dityrosine compared to that in HEPES buffer. B) No significant differences of dityrosine formation in HYFNIF fibrils using HEPES and phosphate buffer upon early points of oxidation compared to that in VIYKI, but at 26 h it is clear that using phosphate buffer yields more dityrosine in HYFNIF fibrils.

Morphological changes of HYFNIF and VIYKI fibrils upon oxidation were examined by TEM, and the TEM images revealed significant morphological changes upon oxidation of HYFNIF and VIYKI especially in phosphate buffer as shown in Figure 4-13. Electron micrographs of oxidised VIYKI fibrils revealed significant changes upon oxidation, it is clear that VIYKI fibrils underwent fragmentation as a result of oxidation. Shorter VIYKI fibrils with larger diameters were observed after 26 h of oxidation in phosphate buffer, while less fragmentation was observed after 26 h of oxidation in HEPES buffer (Figure 4-13), and that may reflect the extent of oxidation using different types of buffers.

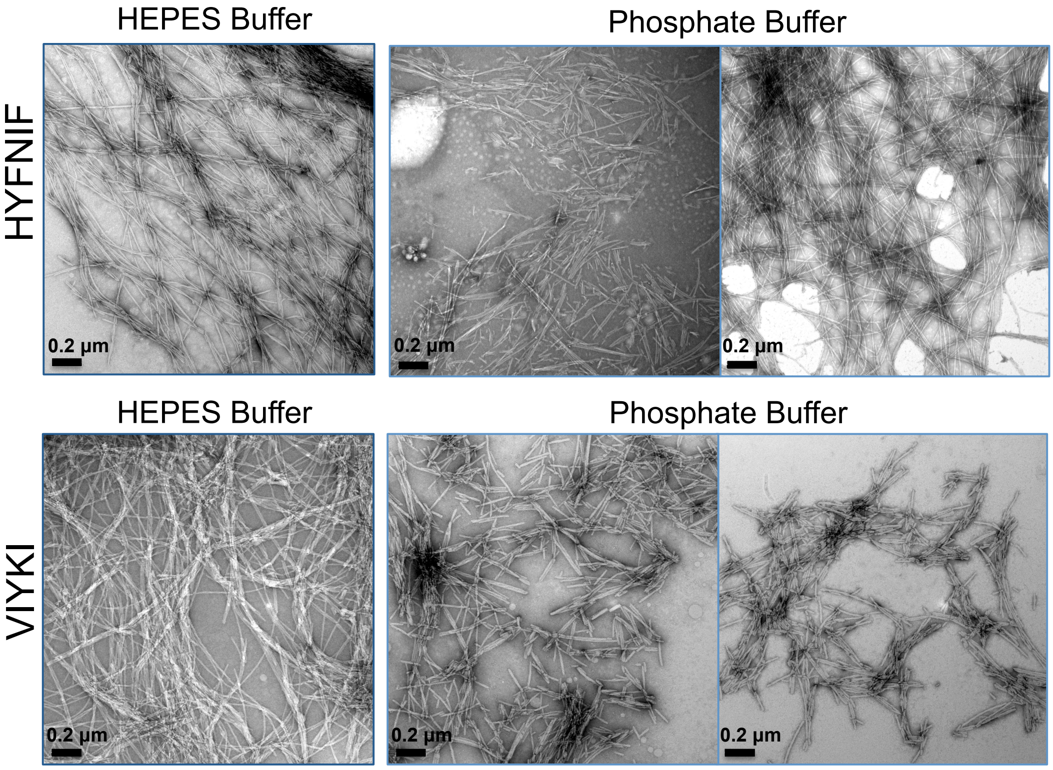

Figure 4-13: TEM micrographs of oxidised HYFNIF and VYIKI fibrils formed in both HEPES and phosphate buffer pH 7.4. While VIYKI fibrils underwent noticeable morphological changes upon oxidation in both HEPES and phosphate buffer, HYFNIF fibrils showed less changes especially in HEPES buffer.

Similar to VIYKI fibrils, HYFNIF fibrils underwent fragmentation upon oxidation in phosphate buffer, but TEM images showed that after 26 h of oxidation in phosphate buffer both long and short HYFNIF fibrils were observed (Figure 4-13). The fluorescence results (Figure 4-11) revealed that HYFNIF fibrils have less ability to form dityrosine cross-links and that may suggest that this leads to the less affected morphology of oxidised HYFNIF fibrils. It is clear from the TEM micrographs of both oxidised HYFNIF and VIYKI fibrils in HEPES buffer that they underwent less fragmentation, and the main morphological change is that the fibrils became thicker and clumped together along the fibril length (Figure 4-13).

4.2.6 Structural development of HYFNIF and VIYKI fibrils upon oxidation

The structures of HYFNIF and VIYKI fibrils have been extensively studied using a wide variety of techniques including XRFD, CD, LD, and FTIR (Morris et al. 2013b). The data showed that both HYFNIF and VIYKI fibrils have a cross-β conformation, and also indicated an important role played by aromatic side chains in peptide packing and in the stability within the fibrils.

CD spectra of HYFNIF and VIYKI fibrils showed features that were unlike commonly observed spectra shown for cross-β rich amyloid fibrils (Figure 4-14). Although a classic β-sheet conformation shows a typical signal at ~ 195 (positive) and ~ 216 nm (negative), HYFNIF and VIYKI fibrils exhibited slightly shifted signals (Figure 4-14). VIYKI fibrils exhibited a negative signal maximum at 218 – 220 nm (Figure 4-14, B) that corresponds to the negative β-sheet signal. On the other hand a positive maximum signal at 200 nm was observed in CD spectra of both HYFNIF and VIYKI fibrils, which could be attributed to an artefactual LD signal (explained below). Additionally, two signals arising from tyrosine were observed at 275 and 235 nm were observed (Figure 4-14). The signal at 275 nm underwent splitting into two peaks at 276 and 282 nm and was taken to arise from electron coupling of the tyrosine residues indicating proximity of tyrosines within the amyloid-like fibril structure (Marshall et al. 2011; Morris et al. 2013b).

To test if the signal at 200 nm is arising from the artefactual LD signal, CD spectrum was recorded by positioning the cuvette at 90 deg, and showing the inversion the signal at 200 nm which in turn indicates the orientation dependent of this signal (Figure 4-15). The artefactual LD signal results from the alignment of the amyloid-like fibrils within the cuvette due to sample loading (Davidsson et al. 1980).

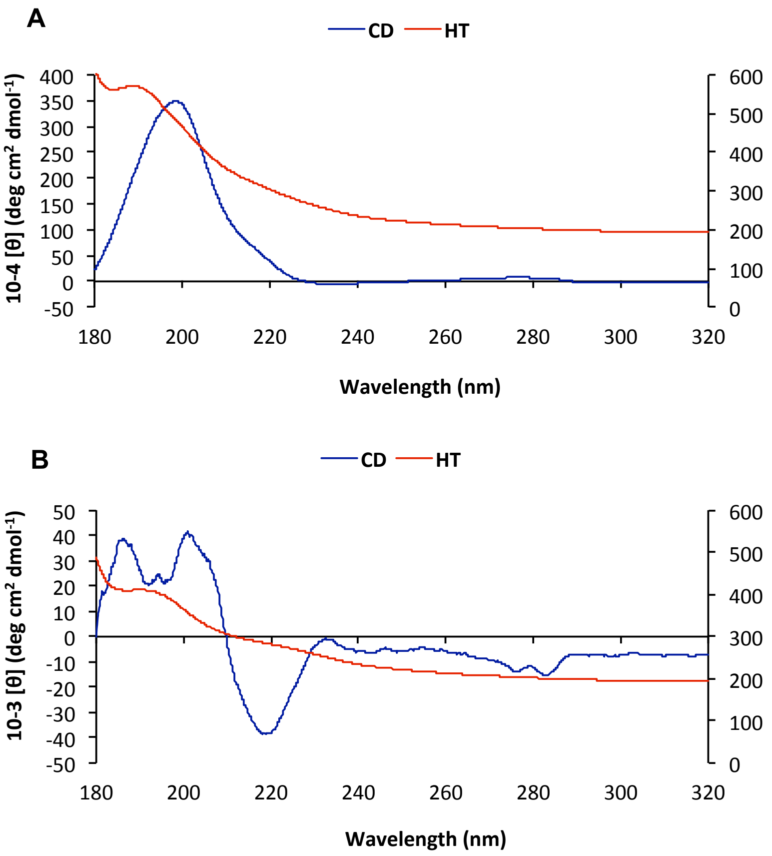

Figure 4-14: Near and far UV CD spectra of non-oxidised (A) (1.135 mM) HYNIF and (B) (1.480 mM) VIYKI fibrils. The region from 200-250 nm (far UV) shows the secondary structure, and the near UV region 250-310 nm shows the tertiary structure. Both, HYFNIF and VIYKI fibrils show unusual CD spectrum with a positive maximum signal at 200 nm that attributed to LD effect.

Linear dichroism is the difference in the absorbance of light linearly polarised parallel and perpendicular to the orientation axis (Norden et al. 2010), and can be only obtained from the sample that is intrinsically orientated or can be aligned by external force during the measurement. This LD effect is more pronounced than CD effects (Norden et al. 2010), therefore this can dominate a spectrum. Some linearly polarised light will exit along with the circularly polarised light due to inefficiencies in the photoelastic modulator (Norden et al. 2010). Because LD signal is orientation dependent, rotating the cuvette by 90 deg should invert the spectrum, by contrast the CD signals are not orientation dependent and rotation will not affect the signal. LD signals could dominate the CD spectrum because LD effects are stronger than CD (Davidsson et al. 1980; Norden et al. 2010).

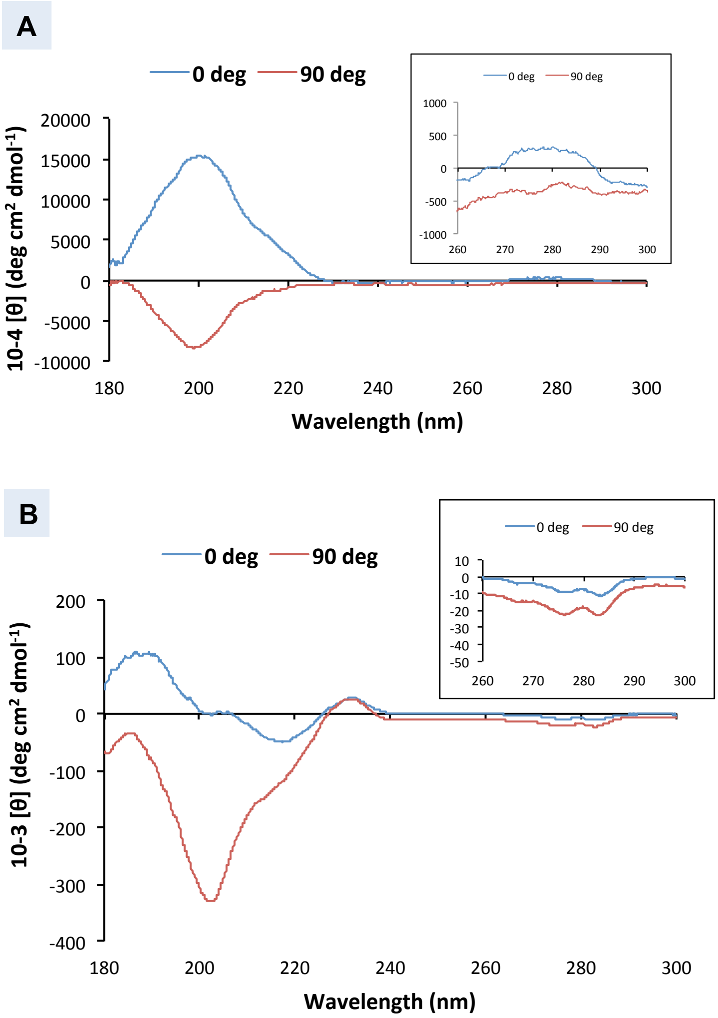

Figure 4-15: CD spectra of non-oxidised A) HYFNIF and B) VIYKI fibrils recorded by positioning the cuvette at 0 and 90 deg, and showing the inversion the signal at 200 nm which is attributed to the artefactual LD signal. The upper panel inset shows that the signal arising from contribution of tyrosine residues does not invert by positioning the cuvette at 90 deg.

CD showed interesting development in both near and far UV CD spectra of oxidised amyloid-like fibrils in water. Incubation of HYNIF fibrils with Cu^{2+}/H_2O_2 resulted in the appearance of a positive CD band at 190 nm and a negative band at 220 nm and is accompanied by a loss of signal at 200 nm thought to arise from artefactual LD from the self-aligned fibrils (Figure 4-16). The oxidised VIYKI fibrils showed a decrease in the intensity of tyrosine peaks at 275 nm and 235 nm, and decrease of the peak at 200 nm (Figure 4-16). CD spectra from oxidised fibrils are consistent with more commonly observed signatures for β-sheet structure. Moreover, disappearance of the artefactual LD signal in the resulting CD spectra indicates less alignment of oxidised fibrils.

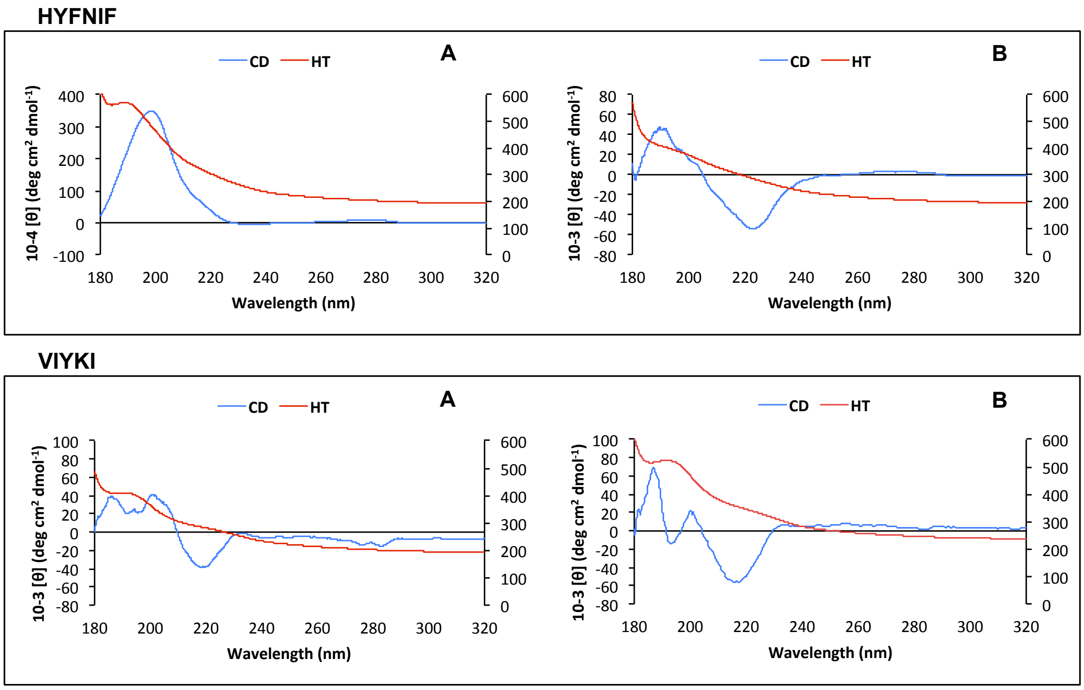

Figure 4-16: Structural development upon oxidation. CD spectra of (1.135 mM) HYNIF and (1.480 mM) VIYKI fibrils (A) before and (B) after incubation with Cu^{2+}/H_2O_2 in water. Incubation of Waltz peptides with Cu^{2+}/H_2O_2 leads to abolish of LD signal at 200 nm, and also appearance of the β-sheet bands. Moreover, a significant decline in tyrosine bands at 276 and 235 nm was obtained which corresponding to loss of tyrosine residue due to the oxidative modification.

CD spectra of oxidised HYFNIF and VIYKI fibrils were measured to gain insight into the effect of dityrosine cross-linking on the secondary and tertiary structures upon the oxidation process. The CD results have indicated that under Cu^{2+}/H_2O_2 condition, both oxidised HYFNIF and VIYKI fibrils have β-sheet structure. Incubation of HYNIF fibrils with Cu^{2+}/H_2O_2 causes an appearance of a positive CD band at 190 nm, which is thought to be masked by the strong LD signal in the CD spectra of non-oxidised fibrils, and a negative signal 220 nm and is accompanied by a loss of positive LD band at 200 nm (Figure 4-16). These results suggest that oxidised fibrils have lost their ability to self-align (resulting in LD contamination of signals) and that may be due to formation of dityrosine cross-linked fibrils, which prevents the lateral alignment that leads to LD artefacts. This is supported by observation of TEM images, which show that oxidised fibrils become shorter and more clumped than that non-oxidised. The near UV CD spectrum of non-oxidised VIYKI fibrils exhibits two prominent negative bands at 276 and 282 nm, which arise from tyrosine residues (Figure 4-14, B). The oxidised VIYKI fibrils exhibit a marked reduction in the intensity of these two signals likely to result in the transition to dityrosine formation.

Further CD experiments were performed to monitor changes in the main chain conformation of VIYKI fibrils over dityrosine cross-linking formation at pH 7.4. As described before that oxidation using phosphate buffer yields more dityrosine (section 4.2.2), thus CD spectra of oxidised VIYKI and HYFNIF using phosphate buffer were recorded. Unfortunately, oxidised HYFNIF fibrils precipitated out of the solution, and no CD signal was recorded. The oxidised VIYKI fibrils exhibit a marked reduction in the intensity of tyrosine two bands, and that could be due to a loss of tyrosine residues as a result of oxidation. Additionally, there was a significant increase in bands at 218 nm (Figure 4-17) suggesting an increase in β-sheet content.

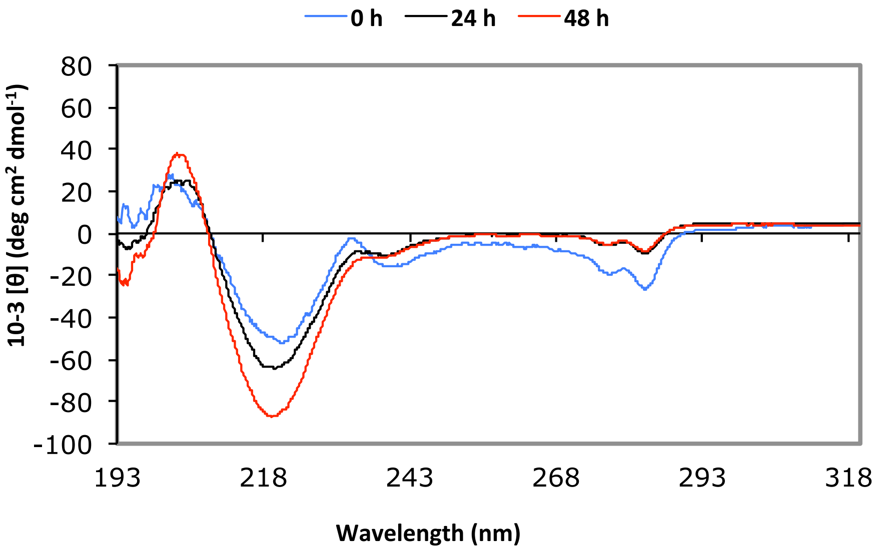

Figure 4-17: CD spectrum development over oxidation of (0.25 mM) VIYKI fibrils at pH 7.4. A significant decline in the intensity of the tyrosine signals at 275 nm and 235 nm was observed, indicating tyrosine losing during the oxidation. Interesting increase in the intensity of the signal at 218 nm observed arising form β-sheet conformation.

In order to test whether LD is contributing to the CD spectrum of oxidised VIYKI fibrils, the CD spectrum was obtained by positioning the sample at both 0 deg and 90 deg to the detector (Figure 4-18), and no inversion in any signal was observed, indicating that none of these bands belong to LD artifacts.

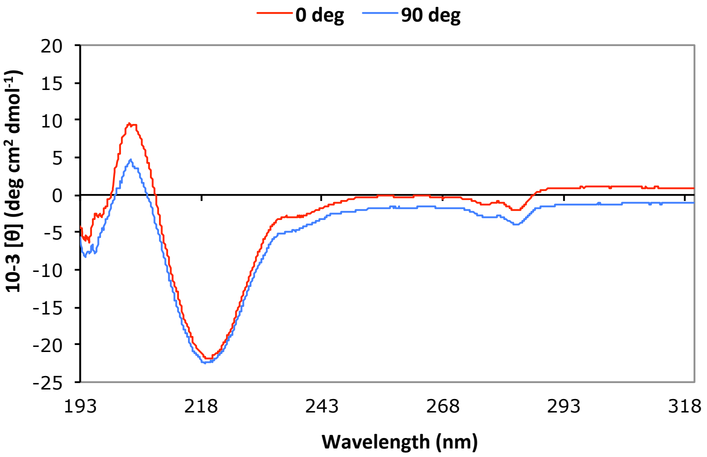

Figure 4-18: CD spectra of (0.1 mM) VIYKI fibrils after 48 h of oxidation in phosphate buffer pH 7.4. The spectra were obtained by positioning the cuvette at 0 and 90 deg to the detector. No LD effect was observed after oxidation, indicating that the fibrils underwent a structural development upon oxidation that prevent fibrils from be aligned and consequently abolished the artefactual LD signal.

To gain more structural details from oxidised HYFNIF and VIYKI fibrils, the fibrils were aligned to test them using XRFD, but unfortunately alignment was unsuccessful for any fibrils probably due to the short length of the resulting fibrils after oxidation.

Many different models of peptides that contain tyrosine residues have been used to investigate the oxidative modification of tyrosine and the formation of dityrosine linkages by applying different oxidation system including the MCO systems and the enzymatic system (Ali et al. 2004; Kato et al. 2001). *N*-acetyl tyrosine was used as a model of tyrosine in proteins to investigate dityrosine formation using four different MCO systems (Kato et al. 2001). Among these MCO systems (Metal-catalysed oxidation), Cu^{2+}/H_2O_2 was the most effective to generate dityrosine and also showed a specificity to produce dityrosine (Ali et al. 2004; Kato et al. 2001). Ali and co-workers were successful in showing the same specificity of Cu^{2+}/H_2O_2 system at pH 7.4 to generate dityrosine using *N*-acetyl tyrosine ethyl ester as a model for tyrosine in proteins (Ali et al. 2004).

In this chapter, two short peptides containing tyrosine residues were used as a model system to investigate the effect of oxidation and their ability to form a dityrosine cross-link. Data presented here, suggest that the phenol groups of tyrosine residues are in close proximity to one another in VIYKI fibrils (Figure 4-19) and this proximity may make the C–C covalent bonding easier than in HYFNIF fibrils in which the phenol groups are ordinated far away from each other (Figure 4-19). Also, from the structural model of the VIYKI fibrils (Figure 4-19, down panel), it appears that a dityrosine crosslink can be formed within and between the fibrils. These results are consistent with other studies conducted on the structural features of HYFNIF and VIYKI fibrils and can be rationalised from structural models which suggest that there is close packing of the aromatic side groups, specifically tyrosine (Morris et al. 2013b). It seems that preorganisation of amyloid-like fibril structure affects the efficiency of dityrosine cross-link formation.

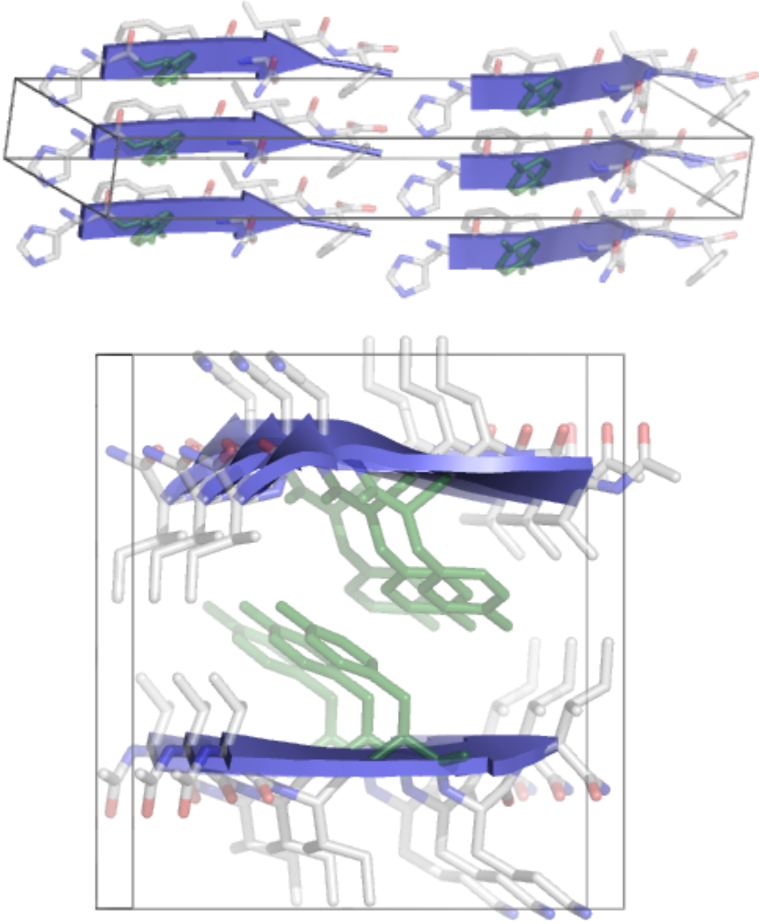

Figure 4-19: Structural models of HYFNIF (Top panel), and VIYKI (Down panel) fibrils determined from XRFD (Morris et al. 2013). In VIYKI fibrils the phenol groups of tyrosine side chain are orientated to be close enough to form dityrosine linkage. While, in HYFNIF fibrils the phenol groups are ordinated far away from each other and this could result in less dityrosine yield. Graphics generated using PyMol (DeLano 2002). Adapted from (Morris et al. 2013b).

Tyrosine fluorescence decreases when the residue goes from a more buried environment to a more solvent-exposed environment (Marshall et al. 2011). Moreover, it has been reported that in aqueous solvents the fluorescence of tyrosine (that is solvent-exposed) is quenched by the carbonyl group in the peptide bond, however the quenching mechanism is unknown (Marshall et al. 2011). From the structural model of VIYKI fibril, it is clear that tyrosine residues are located a way from the fibril surface (Figure 4-19), which could result in less fluorescence quenching, whilst in HYFNIF fibrils, tyrosine residues are located on the fibril surface, and this may explain the tyrosine fluorescence quenching.

Potential contribution of other amino acid groups must be taken into account. As shown in some studies, His residues can form His-bridges in Aβ via coordination with Cu^{2+} (Curtain et al. 2001; Smith et al. 2006a). In the same manner, we hypothesize that the HYFNIF peptide could coordinate with Cu^{2+} to form His-bridges, as a result, this could affect the extent of dityrosine cross-linking. Formation of His-bridged species could leads to more steric hindrance that prevent dityrosine production. Moreover, as explained previously, His residues have high affinity toward Cu^{2+}, forming a stable complex that may have less catalytic activity, yielding less dityrosine.

4.2.7 **Future work**

More structural measurement, e.g. LD, can be applied to find if dityrosine has a unique LD signal and consequently enhance our understanding of the role of dityrosine as a cross-linker in the protein. Synthesis of dityrosine cross-linked peptides with protection against other oxidative modifications on other residues would be more ideal model. Moreover, more precise details could be gained by using a pure dityrosine cross-linked peptide. For future work, it would be better to keep the parallel peptides the same as much as possible, this will rule out many factors that could affect the interpretation of the result. For example, the contribution of the neighbouring residues will be the same, if the same amino acid sequence is used. Also, the difference in the net charge of the peptide should be minimal. As dityrosine is intrinsically fluorescent, more evidence can be gained using confocal microscopy about whether the dityrosine can be intra- or inter fibrils. Many β-sheet peptides have been extensively explored as potentially useful bionanomaterials due to their ability to self assemble to form large complex structures, such as nanotubes, from simple monomers (Morris and Serpell 2010). Applying dityrosine cross-linking to generate synthetic fibrils that are stronger than without dityrosine would have potential technological applications (Figure 4-20), for example in the synthesis of bionanomaterials. Recently, dityrosine cross-linking was used to increase the mechanical stability of a peptide-based hydrogel (Ding et al. 2013), explaining that the mechanical stability was enhanced through the formation of a densely entangled fibrous network of dityrosine cross-linked peptide dimers.

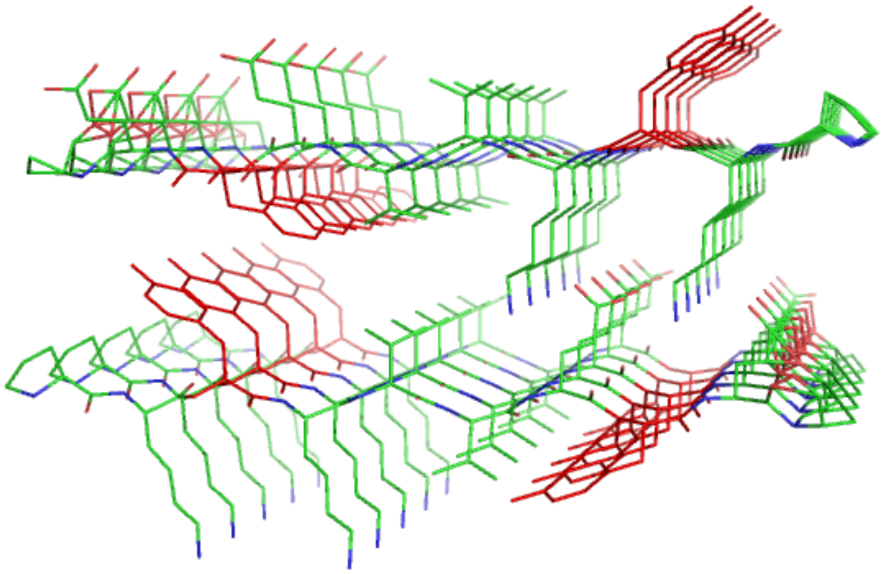

Figure 4-20: Suggested structural model of the suggested PKYKVVEYEP peptide explaining how dityrosine cross-links can stabilise the resulting fibrils. Inter-β-strands and/or inter-β-sheets phenol groups of tyrosine residues can be coupled through C-C to form dityrosine that in turn can stabilise the fibrils. Generated using PyMol (DeLano 2002).

4.3 **Conclusion**

Oxidative stress of Aβ and α-syn has been frequently implicated in the pathogenesis of AD and PD respectively (Butterfield 2002; Eskici and Axelsen 2012; Jomova et al. 2010; Souza et al. 2000). Dityrosine cross-links represent one of the most important modifications resulting from the oxidation of many proteins under oxidative stress conditions, and could affect the folding and the structure of the affected protein. However, studying and investigating dityrosine cross-linking in small peptide models can enhance our understanding of dityrosine's role in the folding and assembly of other physiologically relevant peptides and proteins such as Aβ and α-syn (see chapter 5 and 6). The hexa- and pentapeptides HYFNIF and VIYKI were of particular interest due to their highly organised fibrillar structure and the positions of the tyrosine residues allowing potential dityrosine formation. In the current study, the oxidative modification of the two short peptides, HYFNIF and VIYKI, using Cu^{2+}/H_2O_2 oxidation system was explored, and also the morphological and conformational changes of these amyloid fibrils over the oxidation process were studied. The results showed that VIYKI fibrils have a greater ability than HYFNIF fibrils to oxidise and produce dityrosine cross-links, and also demonstrated that the preorganised fibrils can enhance dityrosine formation by bringing two tyrosine residues close enough to cross-link covalently. The results are in good agreement with structural models of HYFNIF and VIYKI fibrils from a previous study, which revealed that phenolic groups of the tyrosine residues in VIYKI fibrils are packing closely together and become in a close proximity that could make the tyrosine cross-link more favorable (Morris et al. 2013b). In contrast, the structural model of HYFNIF fibrils revealed that side chain of tyrosine residues are organised away from each other, and as a consequence, dityrosine formation was more restricted. The pH of the oxidation environment has a strong influence on the dityrosine production and that is due to the net peptide charge. Although the CD and TEM data of the oxidised fibrils revealed interesting structural and morphological changes upon the oxidation processes, no dityrosine characteristic signal was observed in CD.

5 Results and Discussion

The importance of dityrosine crosslinking in Alzheimer's disease

5.1 Introduction

Previous studies have shown that copper interactions with Aβ could be responsible for causing dityrosine cross-linking and accompanying Aβ aggregation (Atwood et al. 2004; Barnham et al. 2004; Yoburn et al. 2003). High concentrations of copper (0.4 mM), zinc (1 mM), and iron (1 mM) have been found in amyloid plaques and have been implicated in the pathogenesis of AD (Bush 2003a; Lovell et al. 1998; Suh et al. 2000). Smith *et al*. (Smith et al. 2006a) demonstrated that the generation of the Aβ toxic species is modulated by both the Cu^{2+} concentration and the ability to form intermolecular histidine bridges. Many studies have demonstrated that Cu^{2+} ions coordinate to Aβ via the three histidine residues His6, His13, His14 and Tyr10 (Figure 5-1) (Atwood et al. 2004; Curtain et al. 2001; Tickler et al. 2005). However, a recent study showed that Tyr10 is not the fourth bound ligand, but it locates close to the metal centre (Maiti et al. 2008).

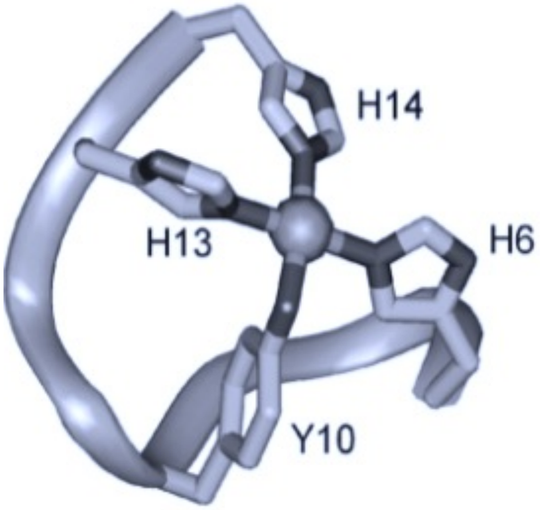

Figure 5-1:Copper ion coordination to Aβ peptide. Cu^{2+} ion coordinates Aβ via the three histidine residues His6, His13, and His14, whilst the fourth ligand could be Tyr 10. Adapted from (Tickler et al. 2005).

Barnham *et al.* revealed that the Aβ peptide coordinates Cu^{2+} to form an Aβ-Cu^{2+} complex. In turn, the Aβ-Cu^{2+} complex is able to produce H_2O_2 catalytically in the presence of a reducing substrate such as ascorbate and underling this process, tyrosine radicals are generated that are later coupled and result in Aβ aggregation (Barnham et al. 2004).

The investigations presented here aim to explore the role of Cu^{2+} in the generation of dityrosine crosslinks in Aβ peptide, thier potential role in AD and subsequently, Aβ aggregation and assembly. The *in vitro* experimental model presented here can help in understanding the early events leading to chemical, structural and conformational modifications before the conversion of soluble Aβ to amyloid fibrils and the eventual formation of senile plaques in AD. In turn, this data could help to design a new inhibitor for an irreversible Aβ deposition process and identify a potential biomarker for early AD. Herein, we have explored the role of Cu^{2+} ions in the formation of dityrosine cross-links in Aβ using many different techniques, including fluorescence spectrophotometry, mass spectrometry and transmission electron microscopy. Immunogold labelling, which has high selectivity and sensitivity, has been used to test the prevalence of dityrosine crosslinks in brain tissue and CSF from AD.

5.2 **Results and Discussion**

5.2.1 ***In vitro* oxidation of Aβ42 resulting in the formation of dityrosine cross-links**

To gain insights into dityrosine crosslink formation process under Cu^{2+}/ H_2O_2 oxidation conditions, formation of dityrosine crosslinks was induced in both preformed fibrils and early soluble species following solubilisation of Aβ42. A wide variety of different techniques were used to establish our understanding of the role of dityrosine in Aβ42 assembly and aggregation.

5.2.1.1 **Dityrosine formation in preformed Aβ42 fibrils**

Initially, we were interested to probe the ability of preformed Aβ42 fibrils to form dityrosine crosslinks and whether induced dityrosine crosslinks can affect the fibril morphology. In order to achieve this, oligomeric Aβ42 species were incubated in water for at least two weeks to form Aβ42 fibrils. The fibril formation was confirmed using TEM (Figure 5-4). Preformed Aβ42 fibrils were incubated with and without Cu^{2+}/ H_2O_2 in phosphate buffer pH 7.4. Oxidation of preformed Aβ42 fibrils was monitored over time and dityrosine crosslinks were monitored using fluorescence spectrometry. The data shows a fluorescence signal arising between 410 – 420 nm corresponding to dityrosine formation (Figure 5-2, A). By contrast, no dityrosine fluorescence signal was observed upon incubation of preformed Aβ42 fibrils in phosphate buffer in the absence of Cu^{2+}/ H_2O_2 (Figure 5-2, B).

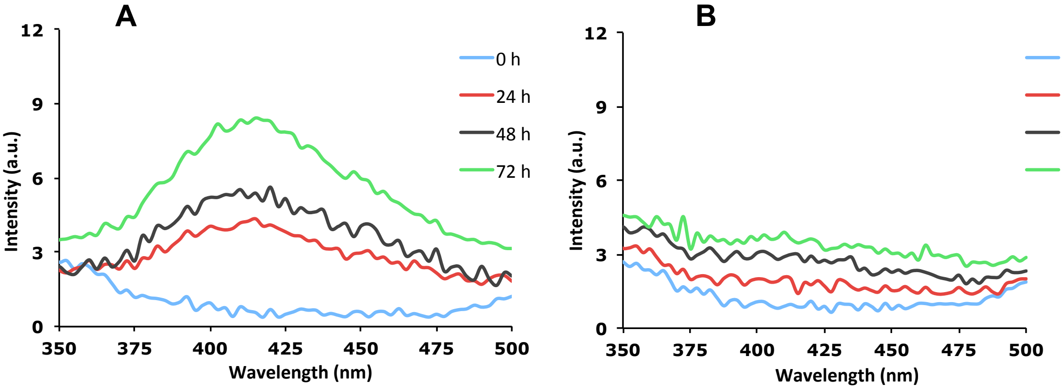

Figure 5-2: Formation of dityrosine crosslinks in Aβ42 fibrils. *Preformed Aβ42 fibrils were incubated in the presence (A) and absence (B) of* Cu^{2+}/H_2O_2 *for 72 hs and the appearance of dityrosine detected using fluorescence ex 320 nm and em 410-420 nm.*

To further confirm the presence of dityrosine within the oxidised Aβ42 fibrils, the fibrils (oxidised in water instead of phosphate buffer) were hydrolysed using 6 M HCl, 10% TFA, and 1% phenol for 48 h and examined using LC-ESIMS/MS (Figure 5-3, B). The dityrosine content was identified by LC-MS/MS using transition reaction ion *m/z* 361.1→315 and a retention time of 5.5 min (Figure 5-3, A), consistent with that of a dityrosine standard (see chapter three). The dityrosine crosslinks showed high resistance to cleavage under acid hydrolysis (6 M HCl at 110 °C), and this highlights the stability of dityrosine. It has been reported that dityrosine shows resistance to cleavage by protease including trypsin, chymotrypsin, and pronase (Smail et al. 1995).

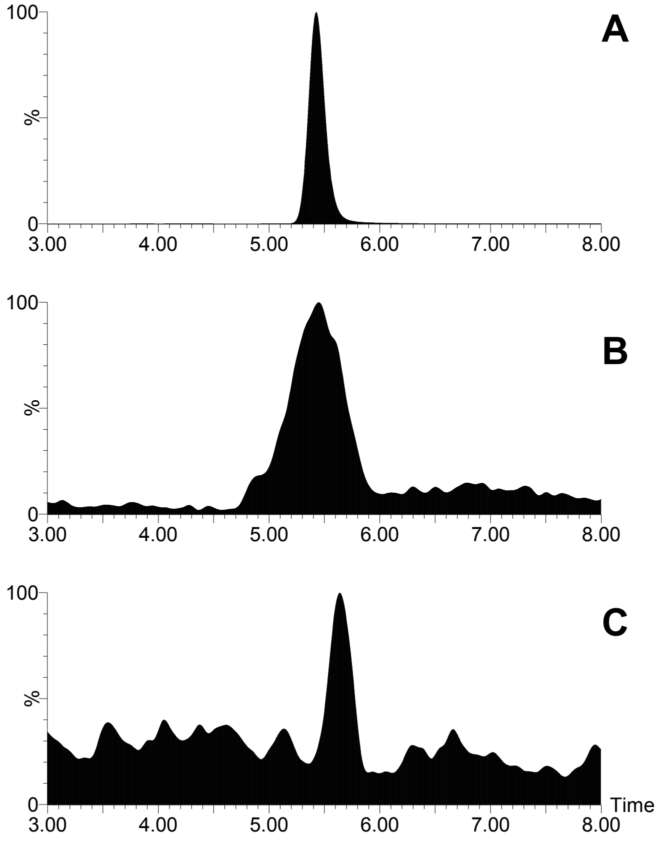

Figure 5-3: The dityrosine content was confirmed using LC-ESIMS/MS that is set on MRM mode. A) LC-ESIMS/MS chromatograms from authentic synthetic dityrosine, B) hydrolysate from oxidised preformed Aβ42 fibrils, C) hydrolysate from Aβ42 fibrils formed under oxidation conditions for three days (the fibrils were obtained from incubation of soluble Aβ42 with Cu^{2+}/H_2O_2 *in water at 37 ºC with agitation.*

Negative stain TEM was used to compare oxidised fibrils with non-oxidised fibrils to evaluate any morphological changes to the sample and revealed short, clumped networks of fibrils in the oxidised sample after 24 h (Figure 5-4) compared to long, straight, and well-dispersed fibrils, common characteristic morphological features of amyloid fibrils, observed in the sample prior to oxidation (0 h). This may suggest that the fibrils are cross-linked laterally to form a network and this is consistent with Tyr10 being exposed on the surface of the fibrils and available for dityrosine crosslinking, between either protofilaments or perhaps individually crossing fibrils.

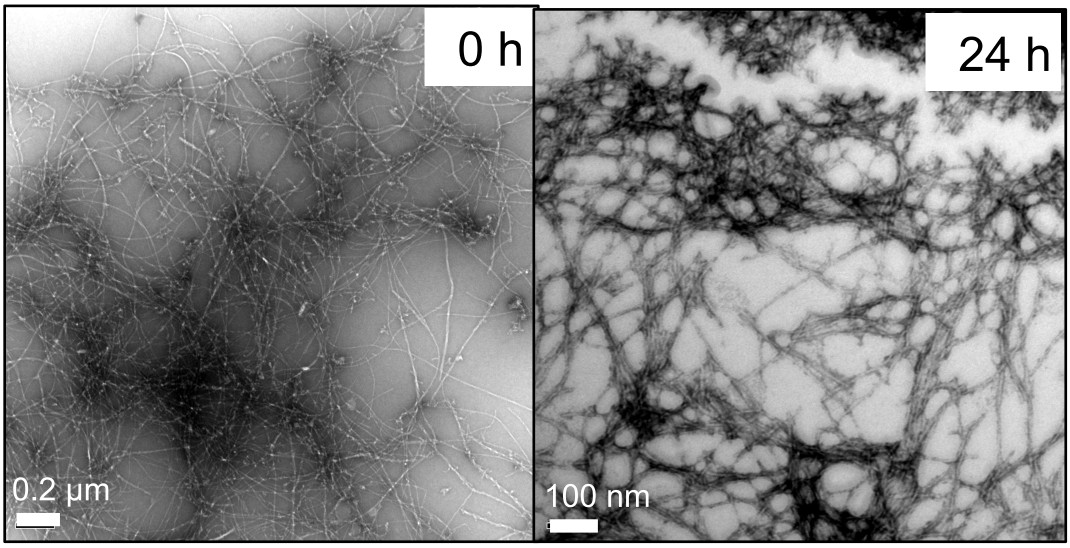

Figure 5-4: Electron micrographs showing the morphology of fibrils prior to oxidation (0 h) and following 24 h oxidation. Aβ42 fibrils exhibited short, clumped networks after 24 h of oxidation compared to well dispersed fibrils at zero h of oxidation.

Structures of Aβ42 and Aβ40 fibrils have tyrosine residues at position 10 at the end of a β-sheet core (Glatzel et al. 2005; Paravastu et al. 2008), showing that they may be surface exposed and available to be involved in lateral association (Figure 5-5). Similarly, structural studies using a combination of X-ray absorption spectroscopy and density functional theory analysis (Streltsov et al. 2008) demonstrated that the structure of the Aβ high-affinity Cu^{2+} binding site is consistent with the hypothesis that the formation of dityrosine-linked dimers found in AD (Naylor et al. 2008) could result from the redox activity of the metal ion bound to Aβ.

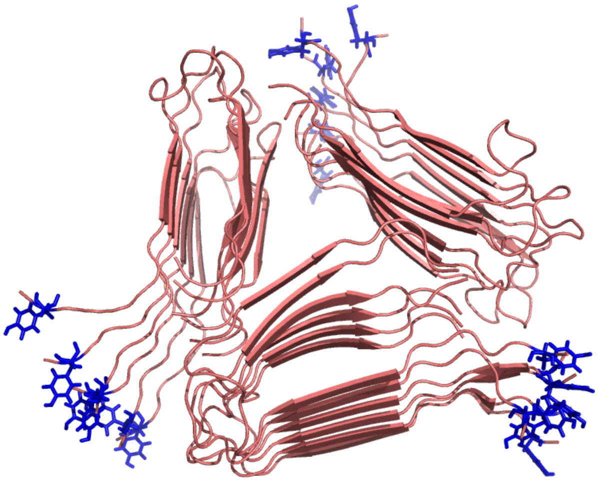

Figure 5-5: Structural model of Aβ40 fibrils that constructed using ssNMR (Paravastu et al. 2008). Tyrosine residues at position 10 are located at the end of β-sheet core and available to form dityrosne links. The model was regenerated using PyMol (DeLano 2002)

The TEM images of oxidised Aβ42 fibrils revealed some shorter fibrils (Figure 5-4) and this could be due to protein fragmentation induced by oxidative modification following oxidation condition of Cu^{2+}/ H_2O_2.

Yoburn *et al*. applied four different oxidative conditions to compare the relative efficiency of dityrosine formation in soluble and fibrillar Aβ40. However, the results showed that both the HRP/H_2O_2 and Cu^{2+}/H_2O_2 conditions led to the production of more dityrosine crosslinks in fibrillar Aβ40 than in soluble Aβ40, explaining that tyrosine residues are orientated within the fibre to favor dityrosine formation. It was suggested that these crosslinks might serve to stabilise the fibrillar state (Yoburn et al. 2003).

5.2.1.2 Aβ42 fibrils formation induced by dityrosine crosslinks formation

Many recent studies have demonstrated that soluble Aβ oligomers, rather than Aβ fibrils, are the most toxic species and that they are disruptive to physiological processes involved in learning and memory in AD (Bruggink et al. 2013; Naylor et al. 2008; Roychaudhuri et al. 2009; Walsh et al. 2002; Williams et al. 2011). Recently, this has been named the oligomeric hypothesis versus the classical amyloid hypothesis (Hardy and Selkoe 2002; Klein 2006), and it has been shown that soluble Aβ oligomers could be generated *in vitro* through covalent crosslinks, i.e. dityrosine (Atwood et al. 2004; Barnham et al. 2004; Naylor et al. 2008), which are stable and irreversible, under MCO. In order to investigate whether dityrosine crosslinks can be formed by soluble Aβ42, freshly solubilised Aβ42 was incubated over three days in the presence or absence of Cu^{2+} and H_2O_2 in phosphate buffer at pH 7.4. Dityrosine formation was monitored using a fluorescence excitation wavelength of 320 nm over three days (Figure 5-6, A and B) and confirmed by LC-ESIMS/MS (Figure 5-3, C).

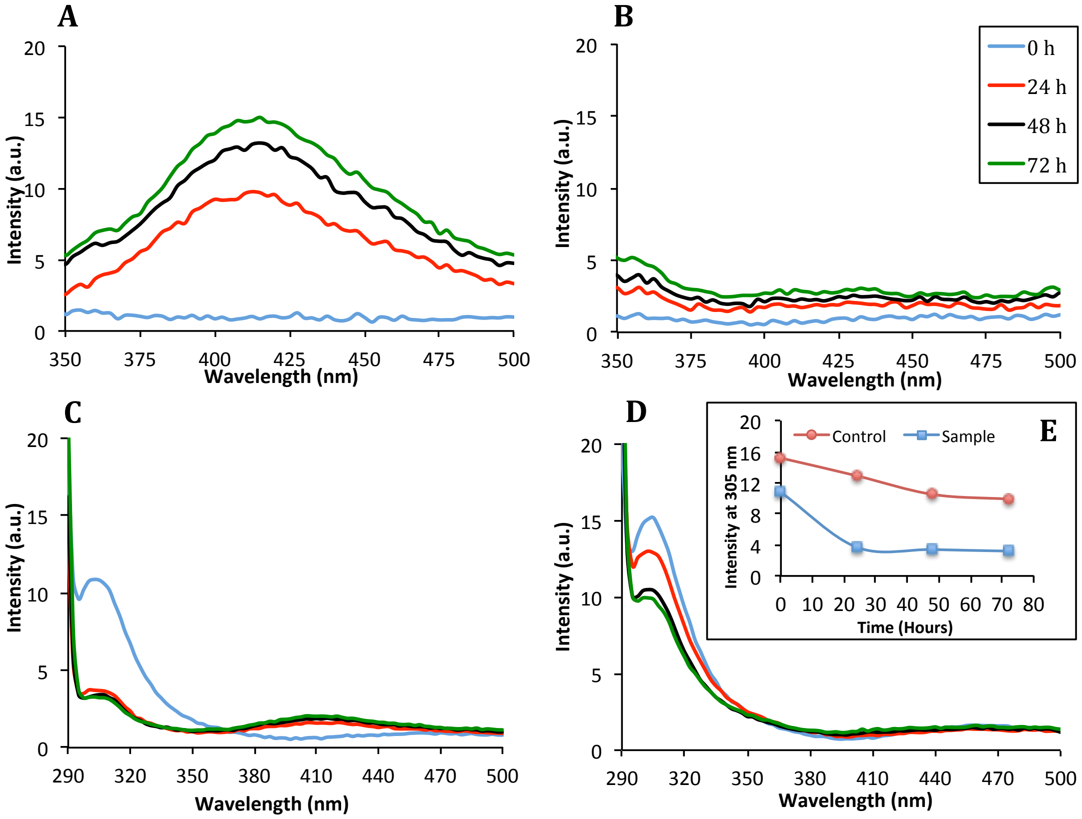

Figure 5-6: Monitoring dityrosine and tyrosine fluorescence during Aβ42 assembly. Freshly prepared Aβ42 was incubated in the presence of Cu^{2+}/H_2O_2 in phosphate buffer and monitored by fluorescence over three days (A, C) and compared to control Aβ42 (B, D). Dityrosine fluoresence is shown in A) and B) and tyrosine fluorescence in C) and D). Dityrosine fluorescence was monitored (Ex.320 nm, Em. 410-420 nm) and A) oxidised Aβ42 shows a strong signal at 24 h incubation compared to no signal in B) control Aβ42 sample. Tyrosine fluorescence (Ex 280 nm, Em 305 nm) was used to follow assembly with time. Both conditions show a decrease in fluorescence signal over time for tyrosine, but C) oxidised Aβ42 shows a significant reduction after 24 h, compared to a slow reduction in tyrosine fluorescence that accompanies assembly for D) control Aβ42. E) The intensity at 305 nm is plotted against time to show the difference between control and oxidised sample.

Fluorescence spectra revealed an increasing dityrosine fluorescence signal with time in the Aβ42 sample incubated in the presence of Cu^{2+} and H_2O_2 (Figure 5-6, A), whilst no such signal was observed in the control sample (Figure 5-6, B). Tyrosine intrinsic fluorescence of Aβ has been frequently used to study the metal coordination site (Maiti et al. 2008; Syme et al. 2004; Tougu et al. 2008). Tyrosine fluorescence excited at 280 nm was also monitored to observe changes to tyrosine with oxidation, the tyrosine fluorescence signal at 305 nm was observed to the decrease over the incubation time of three days (Figure 5-6, C & D). A gradual decrease in tyrosine intensity was observed for control fibrils (Figure 5-6, D) and this decrease is thought to correspond to involvement of tyrosine residues in Aβ42 fibril assembly (Marshall and Serpell 2009), as the tyrosine ring becomes more solvent exposed as assembly and elongation progresses and, as a consequence, tyrosine fluorescence signal is quenched. Tyrosine fluorescence spectra revealed a very significant loss of tyrosine signal concurrent with the increase in dityrosine signal in the oxidised sample following 24 h incubation (Figure 5-6, C) at the same time as a strong dityrosine signal is observed. Comparison of the intensity at 305 nm against time shows the slow decrease in tyrosine fluorescence for the control sample compared to the rapid reduction after 24 h for the oxidised sample. Dityrosine formation appears to occur early in the assembly process consistent with dityrosine coupling being present in early oligomeric species.

At time zero, the intensity at 305 nm is lower for the oxidised sample compared to the control and this is likely to arise from the quenching of the signal due to the binding or involvement of tyrosine in the Cu^{2+} binding site (Maiti et al. 2008; Tickler et al. 2005). Based on absorption spectrscopy data, tyrosine was excluded to be the fourth equatorial ligands bound to Cu^{2+}, explaining that Tyr remains close to the Cu^{2+} centre but not tightly bound to Cu^{2+} (Maiti et al. 2008). Thus, Tyr residue is indirectly involved in the binding Cu^{2+} centre.

Experimental evidence shows that Aβ42 can be soluble and non-amyloidogenic (Dyrks et al. 1992), explaining that the aggregation of Aβ42 does not occur spontaneously. Also, the transformation of soluble monomeric Aβ42 into an aggregating, amyloidogenic state was induced by the addition of metal-catalysed oxidation systems that produce free radicals and the aggregation process induced by the radical initiators can be prevented by addition of radical scavengers such as ascorbic acid. This supports the role of free radicals in the generation of insoluble aggregating Aβ. Similarly, it was showed that noncovalent aggregates of Aβ40 and Aβ42 could be formed by addition of Cu^{2+} (Atwood et al. 1998; Atwood et al. 2000). Dyrks and co-workers demonstrated that metal-catalysed oxidation systems induce amino acid oxidation and protein cross-linking, and these modifications are required to initiate the Aβ42 aggregation process *in vitro* and in AD (Dyrks et al. 1993). Combining our results with others, strongly supports the view that dityrosine cross links occur as early events of the Aβ42 assembly process and preformed Cu^{2+}-induced aggregates facilitate the formation of covalent cross link.

Alternatively, Galeazzi and co-workers demonstrated that *in vitro* soluble Aβ42 undergoes tyrosine oxidative modification under peroxidase oxidation, resulting in stable dityrosine cross-linked Aβ42 dimers (Galeazzi et al. 1999). Moreover, Aβ16-28, which lacks a Tyr10, did not show any detectable peroxidative modifications, indicating the peroxidase oxidation specificity towards tyrosine residue and not other residues such as His and Met residues. Another study has shown the colocalisation of myeloperoxidase with Aβ in senile plaques in AD brain tissue (Reynolds et al. 1999)~~,~~ and revealed that myeloperoxidase is the most efficient enzyme among the peroxidases to catalyse the formation of dityrosine (Marquez and Dunford 1995). These data taken together support the possibility of *in vivo* dityrosine cross-linked Aβ formation in a peroxidase environment as an alternative pathway.

The resulting Aβ42 assemblies were also assessed using TEM (Figure 5-8) and ThT fluorescence (Figure 5-7). ThT fluorescence showed an increase following 72 h incubation of both control and oxidised Aβ42 confirming formation of fibrils in both samples (Figure 5-7).

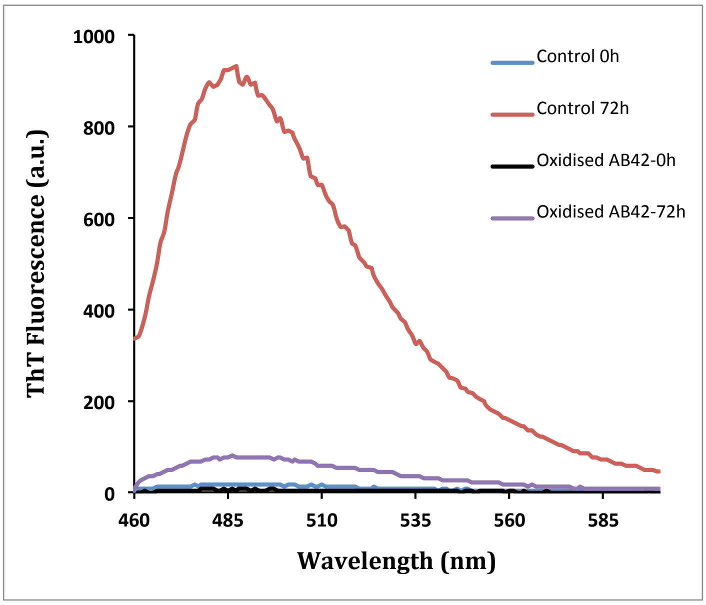

Figure 5-7: Fibril formation was monitored using ThT fluorescence (ex. 450 nm, Em. 485 nm) for freshly prepared Aβ42 in the presence or absence of Cu^{2+}/H_2O_2 *for 72 h.*

The ThT spectrum for oxidised and control samples shows an increase over the incubation time. However, the intensity of the signal from control fibrils is significantly higher than from oxidised fibrils. This may arise from the effect of differences in the buffer conditions on the ThT signal since electron microscopy does not suggest any difference in fibril amounts or morphologies.

To gain further insight into the morphological changes to Aβ42 fibrils induced by oxidation, samples were examined using negative stain TEM (Figure 5-8). Aβ42 immediately following preparation (0 h) showed small globular structures consistent with oligomeric species (5–30 nm) (Figure 5-8). Under oxidation conditions, the freshly dissolved Aβ42 oligomers again appeared to have a spherical appearance (5–25 nm) and these developed into clustered fibrils after 48 h. After incubation for 48 h, control fibrils were observed with both flat, striated ribbons and twisted morphologies. TEM did not reveal any obvious differences in fibril density between Aβ incubated under oxidising and non-oxidising conditions, although the oxidised sample appears to show shorter, more laterally associated fibrils, which may be consistent with some interfibrillar cross-linking. Time course TEM images for incubation of soluble Aβ with and without Cu^{2+}/H_2O_2, or with just Cu^{2+} in phosphate buffer pH 7.4, are shown in Figure 5-8.

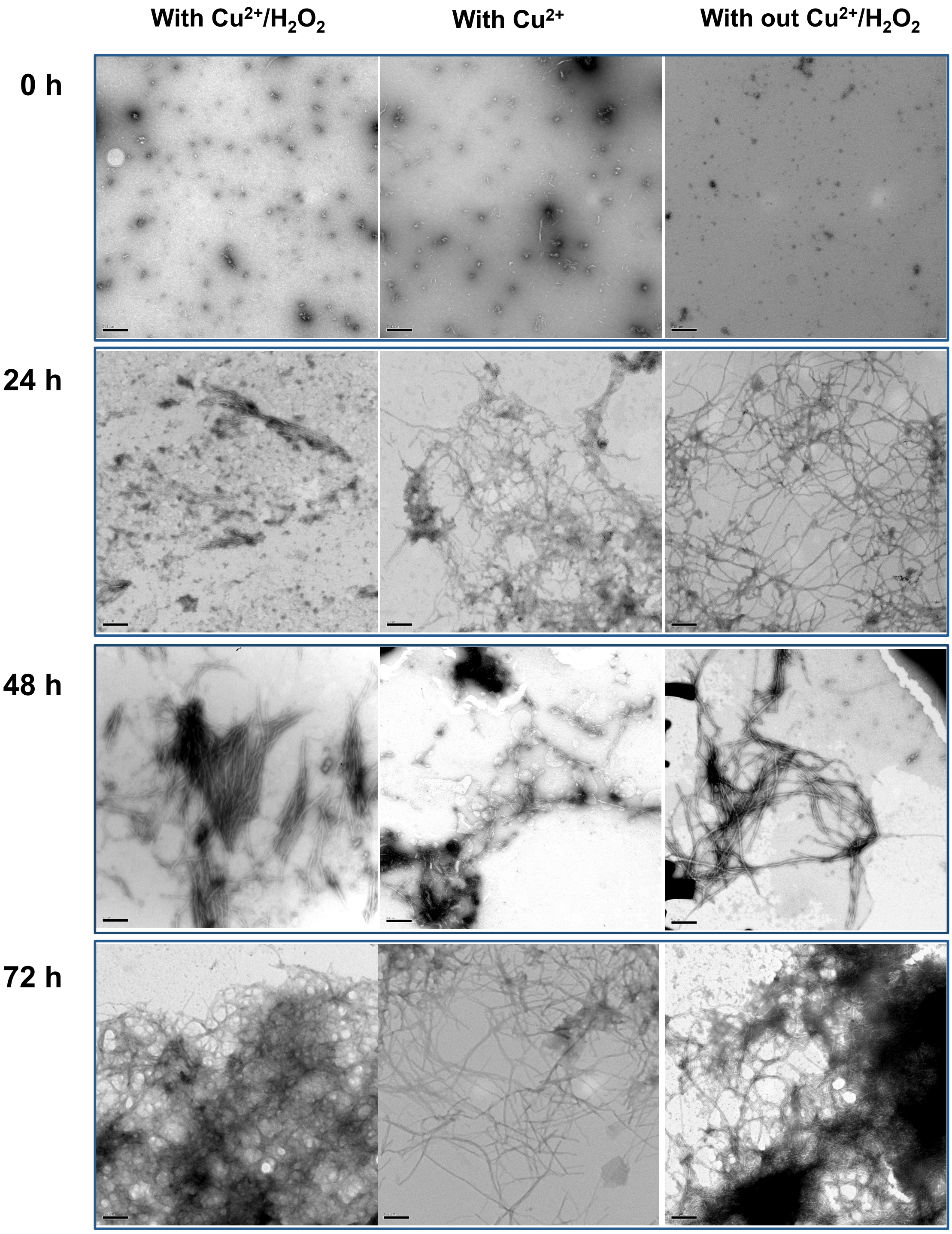

Figure 5-8: Time course TEM images for incubation of soluble $A\beta$ with and with out Cu^{2+}/H_2O_2, and also with just Cu^{2+} in phosphate buffer pH 7.4. Dityrosine was monitored by fluorescence over three days. At zero h, $A\beta42$ shows oligomeric species and fibrils following 24 h incubation with and without Cu^{2+} compared to that resulting from incubation with Cu^{2+}/H_2O_2, which shows no fibril formation. After 48 h of incubation, more matured fibrils were formed in all cases, which are exhibited characteristic morphology features of amyloid fibrils of flat, straight with some twisting fibrils.

Interestingly, no fibrils were observed in the oxidised fibrils at 24 h by TEM despite a very strong signal by dityrosine fluorescence, suggesting presence of dityrosine in oligomeric species.

5.2.1.3 **Probing the stability of Aβ42 - dityrosine cross-linked fibrils**

Dityrosine cross-linking may lend further stability to the already stable amyloid fibrils formed. To investigate this possibility, we compared the stability of oxidised and non-oxidised Aβ42 amyloid fibrils. Fibrils were stored at −80 °C for over one year. Following thawing, dityrosine content was assessed using fluorescence and oxidised fibrils were shown to still contain dityrosine crosslinks after prolonged freezing, whilst no dityrosine fluorescence was detected for non-oxidised, frozen fibrils (Figure 5-9, A). Both sets of fibrils were examined by electron microscopy, and both contained fibrils (Figure 5-9, C and D). Comparison of soluble Aβ42 concentration in the supernatants indicated that there was more soluble Aβ in the oxidised samples (Figure 5-9, B). The fibril pellets were treated with formic acid to dissolve fibrils and the amount of peptide released into the supernatant was compared between the oxidised and non-oxidised samples (Figure 5-9, B). The concentration of Aβ found in the supernatant following formic acid treatment was very significantly lower in oxidised sample compared to the non-oxidised sample (0 versus 14.8 μM), suggesting that the oxidised fibrils were resistant to dissolution with the acid (Figure 5-9, B). Electron microscopy revealed that the oxidised fibrils were shortened, but remained at a broadly similar concentration when compared to amounts prior to oxidation. Those that had not been oxidised were narrower and much more difficult to find on the grid (Figure 5-9, C and D). These results seem to support the view that the dityrosine cross-linking strengthens the fibrils and these fibrils become more resistant to acid dissolution following oxidation.

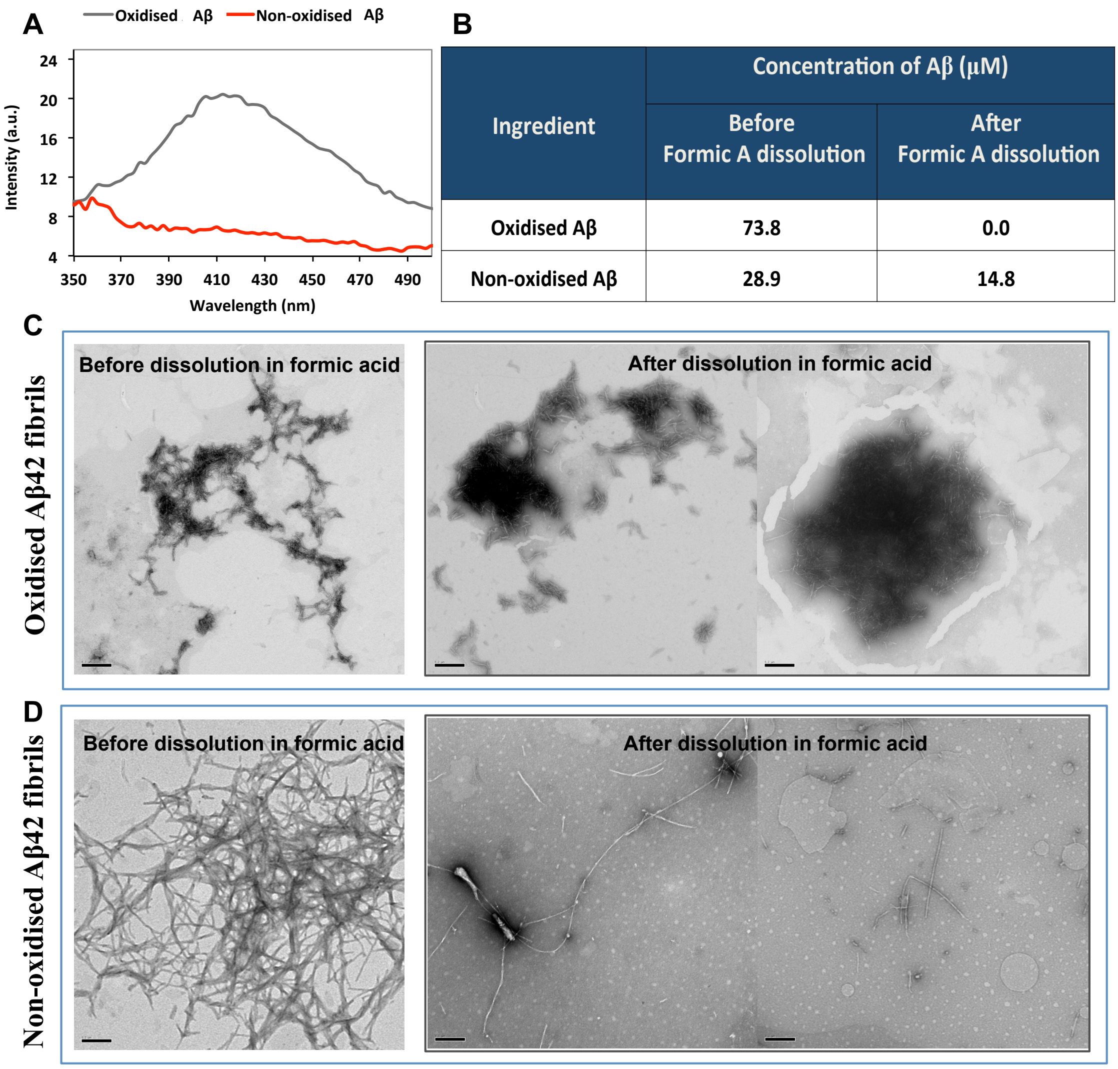

Ingredient	Concentration of Aβ (µM)	
	Before Formic A dissolution	After Formic A dissolution
Oxidised Aβ	73.8	0.0
Non-oxidised Aβ	28.9	14.8

Figure 5-9: Stability of dityrosine cross-linked Aβ42 fibrils that is formed under oxidation condition. A) Oxidised and non-oxidised Aβ42 fibrils were examined using dityrosine fluorescence after prolonged incubation at − 80 °C showing a strong intensity signal at ~ 410 nm for oxidised but not non-oxidised fibrils. B) Formic acid was used to dissolve the fibrils and the concentration of Aβ42 in solution was compared before and after formic acid dissolution for oxidised and non-oxidised fibrils. C) Electron micrographs of oxidised fibrils before and after formic acid treatment showing that the dityrosine crosslinked fibrils are resistant to formic acid. D) Electron micrographs of non-oxidised fibrils before and after formic acid treatment showing the fibrils are susceptible to damage by formic acid. Scale bars represent 0.2 µm.

5.2.1.4 Negative stain TEM immunogold labelling of dityrosine crosslinks

In order to examine whether dityrosine crosslinks can be detected within the amyloid fibrils and to show the dityrosine distribution, TEM immunogold labelling using a dityrosine specific monoclonal antibody was performed. Figure 5-10 shows anti-dityrosine labelling on Aβ42 fibrils revealing gold distributed close to the fibrils grown in an oxidising environment. Control Aβ42 did not label with the dityrosine antibody

(Figure 5-10, B). Very strong evidence of dityrosine identity was provided using these specific monoclonal dityrosine antibodies. These *in vitro* findings suggest that conditions similar to oxidative stress can promote the formation of dityrosine cross-links in self-assembling Aβ42 samples resulting in a high density within the fibrils.

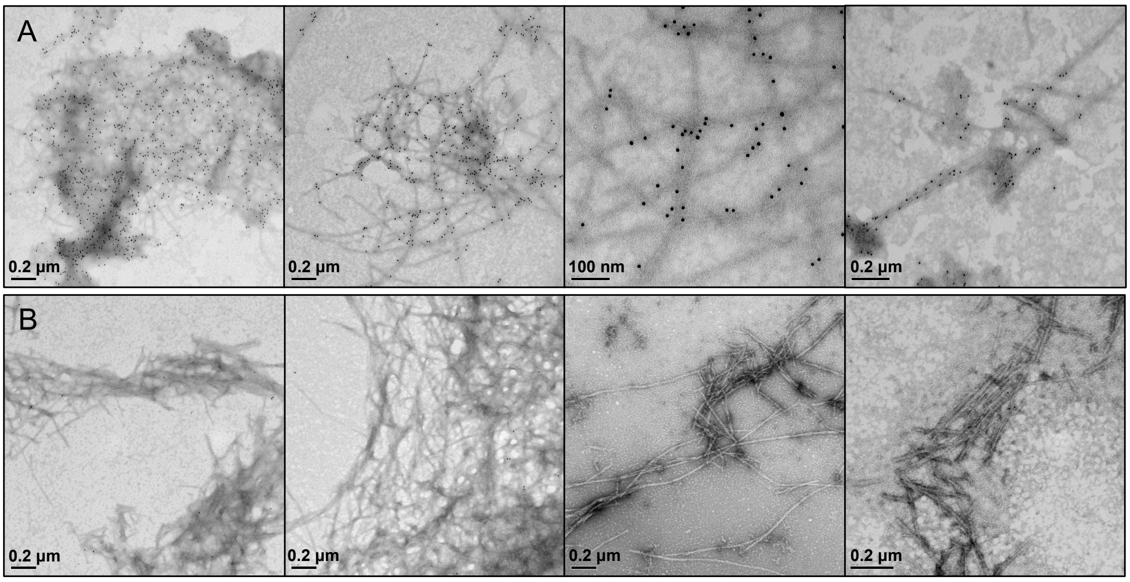

Figure 5-10: TEM immunogold labelling of dityrosine in Aβ42 fibrils. 20 µM of Aβ42 oligomers were oxidised using Cu^{2+} ions and hydrogen peroxide. After 72 h of oxidation, the process was quenched by adding EDTA, and then the assembled fibrils were immunogold labelled with dityrosine antibody as shown in the A, which reveals the high density and localisation of dityrosine cross links (10 nm gold particles) in oxidised Aβ42 fibrils compared to non oxidised fibrils B. For clarity bigger images were provided, see appendix (vii).

5.2.1.5 **Copper ion induces soluble Aβ42 aggregation**

Redox-active metal ions, such as Cu^{2+} and Fe^{3+}, have been suggested to play a role in the pathogenesis of many neurodegenerative disorders, including AD and PD (Bush and Curtain (2008). There is a large body of evidence pointing to the importance of interactions between redox-active metal ions and proteins in the pathogenesis of many diseases (Ali et al. 2003; Huang et al. 2004a; Sarell et al. 2010). Two mechanisms have been suggested to explain the abnormalities of these interactions in neural tissue: (a) the aggregation of protein mediated by redox-active metal ions; and (b) metal-catalysed oxidation reactions (Strozyk and Bush 2006). Metal-protein interactions could result in protein misfolding (Drew et al. 2013; Strozyk and Bush 2006; Viles 2012). In order to examine whether the assembly of soluble Aβ42 was enhanced by dityrosine cross-link formation alone or via the interaction with Cu^{2+} ions, 20 µM of freshly prepared oligomeric Aβ42 was incubated in the presence or absence of 20 µM Cu^{2+} only in phosphate buffer pH 7.4. Dityrosine fluorescence was monitored over three days and showed no significant yield of dityrosine, and the data is supported by the data of other studies that revealed that incubation of Aβ with Cu^{2+} ion does not lead to tyrosine oxidation (Jiang et al. 2007; Tougu et al. 2008). Amyloid fibril content was monitored over 48 h using a ThT assay combined with TEM. The ThT data show that incubation Aβ42 in the presence of Cu^{2+} ion reduces the ThT fluorescence signal (Figure 5-11, B), indicating a less amyloidogenic material, and this is consistent with TEM images that show fewer amyloid fibrils after 72 h of incubation of oligomeric Aβ42 in the presence of Cu^{2+} ions (Figure 5-11, F).

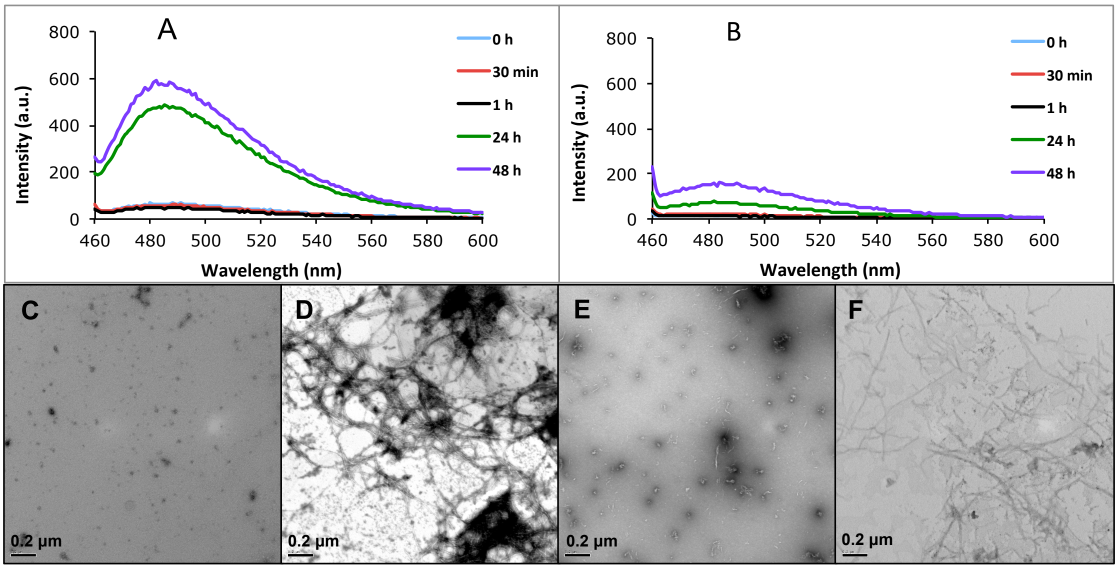

Figure 5-11: Aβ42 fibrils growth monitored using ThT assay combined with TEM. A) ThT fluorescence of Aβ42 fibrils incubated without Cu^{2+} which show higher ThT intensity compared to that incubated in presence of Cu^{2+}(B). TEM images of control Aβ42 oligomers at zero h (C) and after 72 h (D) reveal formation of straight, long, and unbranched fibrils. E) TEM image of Aβ42 oligomers at zero h and after 72 h of incubation with Cu^{2+} (F), showing that less amount of fibrils were formed consistent with ThT fluorescence results.

The data show that incubation of Cu^{2+} ions with Aβ42 at 1:1 molar ratio results in fewer amyloid fibrils (Figure 5-12) and this may be due to the formation of Cu^{2+} induced aggregates, which are unable to convert into amyloid fibrils. These results are in good agreement with a previous study (Smith et al. 2007).

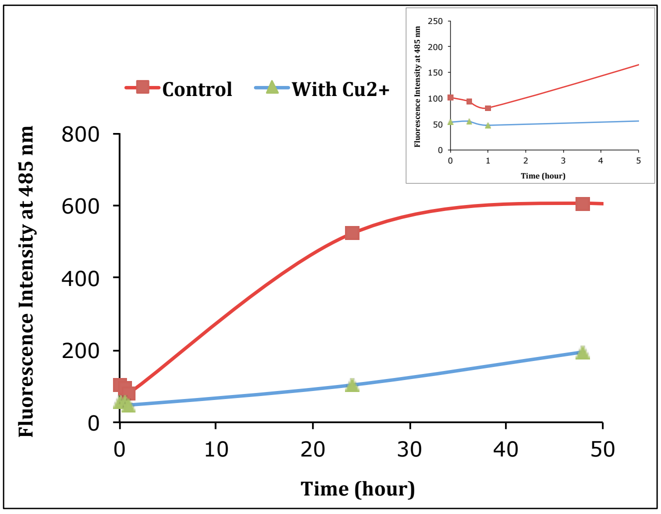

Figure 5-12: ThT assay revealed that incubation of Aβ42 with Cu^{2+} ions results in slowed elongation rates compared to control.

It has been demonstrated that metal ions such as Cu^{2+} at very low concentrations are required for Aβ40 fibril formation, explaining that solutions depleted of metal ions do not form amyloid fibrils and the addition of trace metal ions such as Cu^{2+} and Zn^{2+} accelerate Aβ40 amyloid formation (Huang et al. 2004b). It is suggested that Aβ-metal ion complexes induce amyloid fibril formation through either acting as nuclei or inducing structure within the peptide (Dai et al. 2006). Cu^{2+} ions can also mediate the conversion of Aβ42 peptide from amyloid material to a non-amyloidogenic aggregate (Smith et al. 2007). Smith and co-workers demonstrated that the switch between the two aggregate morphologies is centered at an equimolar Cu^{2+}: peptide ratio, suggesting two mutually exclusive aggregation pathways. In a previous study, it has been suggested that the formation of His-bridge Cu^{2+} dimer at Cu^{2+}: peptide ratio of 0.3:1 and above can mediate the Cu^{2+} induced assembly (Smith et al. 2006a).

5.2.1.6 Aβ42 is internalised into neuroblastoma cells and becomes dityrosine cross-linked

In previous work, the Serpell group have shown that freshly prepared Aβ42 can be internalised into SH-SY5Y neuroblastoma cells and that it accumulates over 24 h in lysosomal compartments (Soura et al. 2012). It was of interest to investigate whether the Aβ42 administered to these cells formed dityrosine cross-links during incubation in contact with neuroblastoma cells. Cells were treated in an identical way to previous experiments (Soura et al. 2012), administered with a final concentration of freshly solubilised 10 μM Aβ42 and incubated for 24 h. Sectioned cells were co-labelled with the mouse monoclonal dityrosine antibodies and rabbit polyclonal Aβ antibodies for Aβ42. Previously, a monoclonal, conformational specific antibody Nu1, which was raised against oligomeric Aβ, was used to detect Aβ (Soura et al. 2012). Alternatively, a rabbit polyclonal antibody AB5078P was raised against C-terminus of Aβ42 (1-6) and used to detect Aβ in the following experiments. This antibody has been shown to not cross react with APP (Agholme et al. 2012) and presumably detect monomeric, oligomeric and fibrillar Aβ. For the purpose of this study, secondary antibodies were 5 nm gold conjugated goat anti-rabbit IgG and 10 nm gold conjugated goat anti-mouse IgG, allowing the identification of both Aβ (5 nm) and dityrosine (10 nm) respectively in the sectioned cells and the opportunity to detect whether they co-localised. TEM of sectioned neuroblastoma cells treated with Aβ42 confirms the appearance of internalised Aβ42 concentrated in lysosomal regions (Figure 5-13, A), as shown previously (Soura et al., 2012).

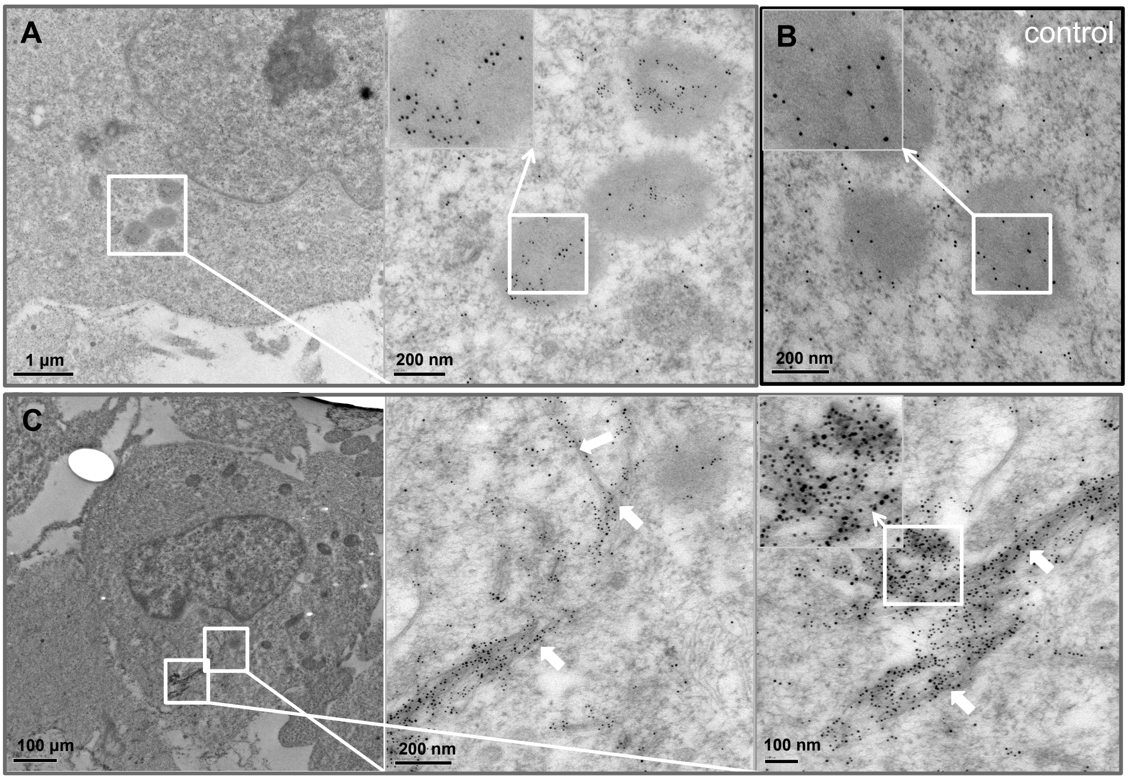

Figure 5-13: Immunogold labelling TEM showing neuroblastoma cells treated with oligomeric Aβ. A) The images reveal dityrosine (10 nm gold particles) and Aβ42 (5 nm gold particles) labelling within the lysosomes of treated cells. B) Low level dityrosine labelling was observed within lysosomes in vehicle treated, control cells, but no Aβ labelling was observed. C) Cells were observed containing fibrillar Aβ labelled for both Aβ (5 nm gold particles) and dityrosine (10 nm gold particles). Inserts show magnified images for further clarity, and also bigger images were provided, see appendix (viii).

Close examination also showed that dityrosine and Aβ42 were co-localised together inside the lysosomes (Figure 5-13, A). Examination of control cells showed some labelling of dityrosine within lyosomes, but no co-localisation with Aβ labelling (Figure 5-13, B). These findings may indicate the importance of dityrosine cross-links in the internalisation of Aβ. Further investigation revealed the presence of fibrillar Aβ42 around (Figure 5-14) and within the cells, where the fibrils exhibited clear co-localisation of dityrosine and Aβ (Figure 5-13, C, Figure 5-14). This suggests that Aβ is crosslinked both inside and outside of the neuroblastoma cells. Occasionally extracellular Aβ was observed to be entering the cells at the plasma membrane (Figure 5-14) and again showed co-localisation of Aβ and dityrosine labelling. Taken together, these results suggest that the externally administered Aβ42 becomes oxidised during incubation in the cellular environment and that dityrosine cross-linked oligomers (and possibly fibrils) can be internalised into lysosomes.

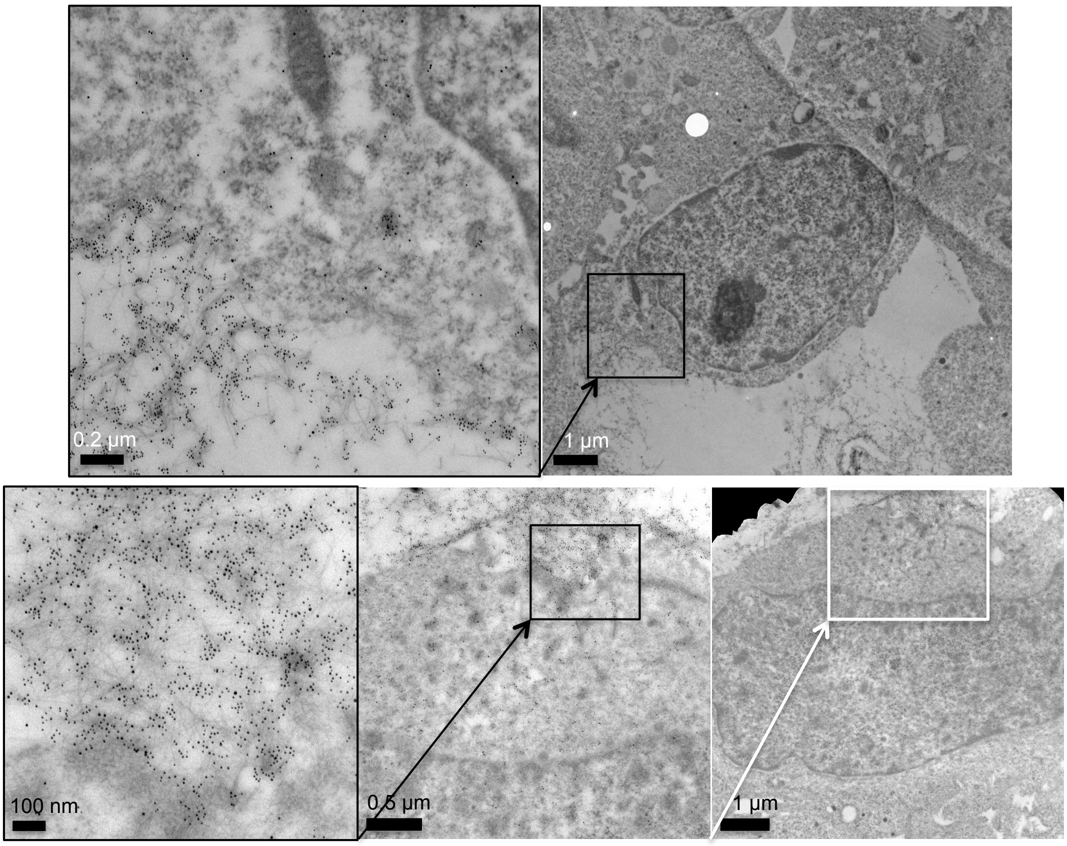

Figure 5-14: Electron micrographs of sections of Aβ42 treated neuroblastoma cells showing immunogold labelling of Aβ (5nm) and dityrosine (10 nm gold particles). The images reveal colabelled fibrils outside and also inside the cells.

5.2.2 The presence of dityrosine within amyloid plaques in AD brain

We have established that Aβ42 is able to undergo oxidation leading to formation of dityrosine cross-links *in vitro* and in a cellular environment. To determine the possible physiological relevance of dityrosine formation in the Aβ accumulation in AD brain, immunogold labelling TEM was carried out to detect any co-localisation of Aβ and dityrosine in AD brain and compared to age matched control brain. Previously, dityrosine has been detected and quantified in AD brain (Hensley et al. 1998). Using HPLC with electrochemical array detector (HPLC-ECD), dityrosine was quantified in four regions of the AD brain (Hensley et al. 1998). It was reported that dityrosine levels were elevated significantly in the hippocampus and neocortical regions of the AD brain. However, no previous study has successfully detected dityrosine in plaques, and no cellular localisation study of dityrosine in human brain has been reported before. Immunogold labelling using anti-dityrosine antibody was performed on brain sections taken from AD and control patients (Table 2-2), which revealed high density of dityrosine within amyloid plaques in AD brain sections (Figure 5-15, A). Double immunogold labelling TEM was also used to confirm that the amyloid plaques labelled with the anti-Aβ antibody as well as anti-dityrosine (Figure 5-15, B). These results show the high density and the cellular localisation of dityrosine within plaques (Figure 5-15), suggesting a potentially important role for dityrosine in amyloid accumulation in amyloid plaques. For clarity and to easily distinguish between the two different gold particles, the image was analysed using in house software written in Matlab as shown in Figure 5-15, C. The immunogold particles analysis revealed two different sizes corresponding to dityrosine (red dot) and Aβ (blue dot). A control was performed using an irrelevant antibody (to hair cell antigen) at identical an IgG concentration and showed virtually no labelling (<<1 gold particles/micron) compared to the serial section showing dityrosine/Aβ labelling of the same plaque in (Appendix ix a and b respectively) (showing 100 gold particles/μm^2).

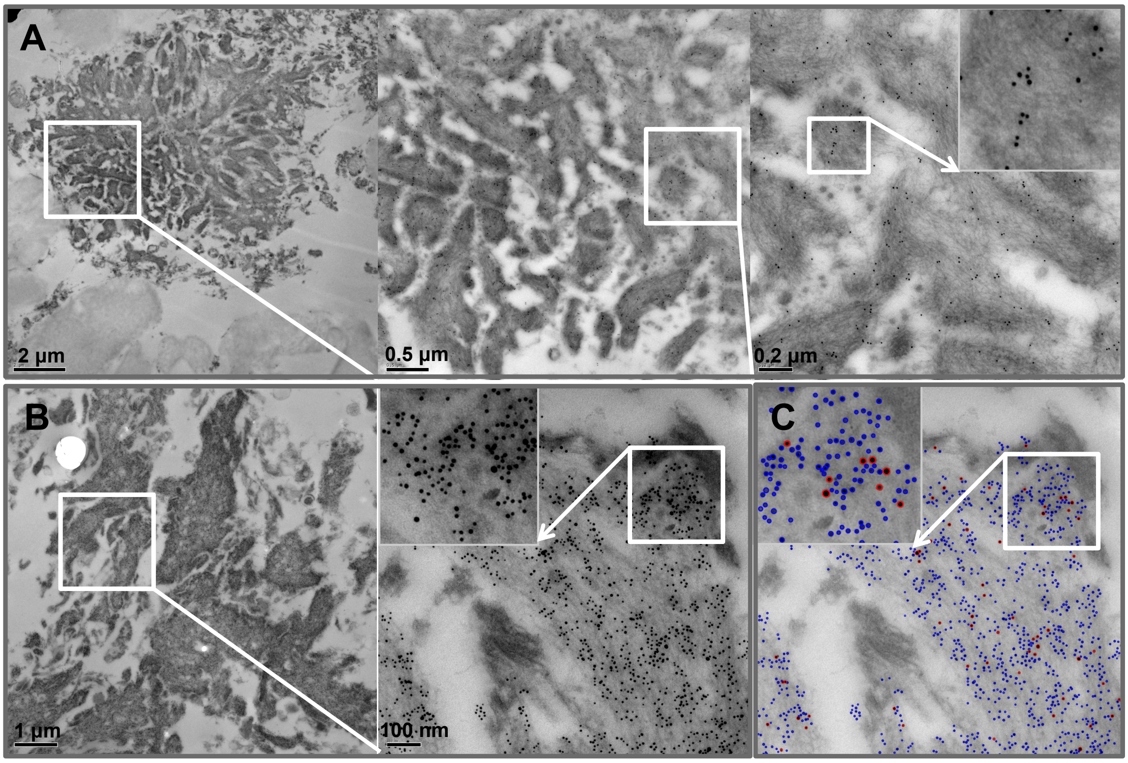

Figure 5-15: Immunogold labelling TEM within amyloid plaques from AD brains. A) Shows single labelling using the dityrosine antibody only and reveals very dense labelling of the amyloid plaques. B) Double labelling with anti-Aβ (5 nm gold particles) and anti-dityrosine (10 nm gold particles) reveals colocalisation within amyloid plaques. C) Shows the 10 nm labelling for dityrosine highlighted in red and 5 nm labelling for Aβ in blue. Immunogold particle counting and size analyses were performed using in house software written in Matlab by Dr Morris. Inserts show magnified images for further clarity.

In brain, tyrosine can be oxidised by peroxidases such as myeloperoxidase (Heinecke et al. 1993; Heinecke 2002; Leeuwenburgh et al. 1997b) and also by free radicals (Huggins et al. 1993; Ischiropoulos and Al-Mehdi 1995). Hydroxyl radicals, which are generated according to Fenton chemistry in both mitochondria and lysosomes, can attack tyrosine residues, leading to tyrosyl radical formation. In turn, a tyrosyl radical could be coupled to give dityrosine or attack the lipids, causing lipid peroxidation (Savenkova et al. 1994). Dityrosine is a covalent, irreversible and stable cross-link, and also showed high resistance to hydrolysis by proteases (Atwood et al. 2004; Giulivi and Davies 1994). Therefore, it represents a good contributor to amyloid plaque formation.

Oxidised and non-oxidised Aβ peptides were separated by SDS-PAGE (Figure 5-16) and analysed by densitometry (data and analysis provided by Dr. Tom Williams). Aβ42 dimer of molecular mass of 9 kDa was observed after ten minutes of oxidation as shown in Figure 5-16, whilst non-oxidised Aβ42 did not exhibit a strong dimer band and shows SDS separation similar to that observed elsewhere (Bitan et al. 2003).

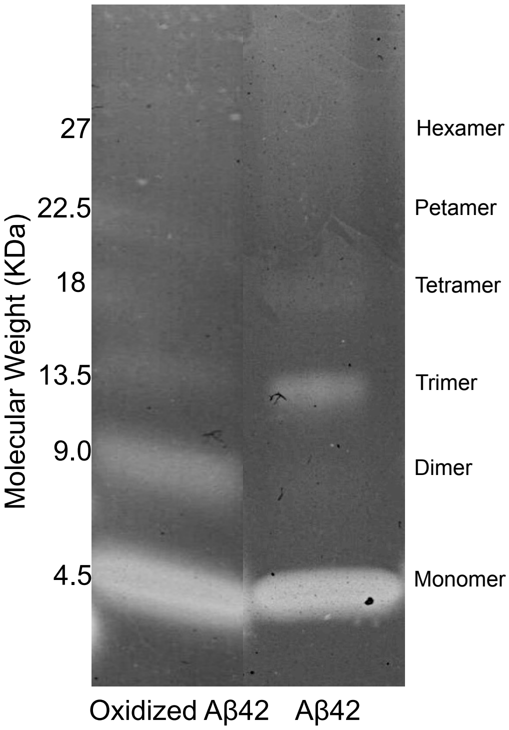

Figure 5-16: Oxidised and non-oxidised Aβ42 were separated and analysed using SDS-PAGE/sliver staining. Dimeric Aβ42 was observed only in oxidised Aβ42 compared with unoxidised Aβ42 that produced monomeric and trimeric isomers.

The Aβ42 dimer of 9 kDa that formed under oxidative condition corresponding to expected dityrosine cross-linked dimeric Aβ42 and strongly support the formation of dityrosine cross-linked oligomers of Aβ in small oligomeric species.

Photo-induced cross-linking of unmodified protein (PICUP) chemistry was used to cross-link Aβ42. As a result, Aβ42 oligomers were formed and detected using SDS-PAGE (Bitan et al. 2003). It has been found that uncross-linked Aβ42 produced predominantly two bands, a monomer band and a broad trimer band (Bitan et al. 2003), explaining that the trimer band was found to be induced by SDS. However, an analogous trimer band was not observed after cross-linking of Aβ42 using PICUP method.

Water-soluble oligomers of Aβ were isolated and quantified in the cerebral cortex of normal and AD brains (Kuo et al. 1996). Interestingly, the levels of these oligomers were markedly elevated in AD brain compared to normal brain. Later on, stable Aβ42 dimer and trimer were purified from neuritic and vascular amyloid deposits and using size exclusion chromatography in the presence of 80% formic acid or 5 M guanidine thiocyanate pH 7.4, the molecular mass of Aβ dimer and trimer were determined and found at 9 and 13.5 kDa respectively (Roher et al. 1996). The toxicity of the purified Aβ42 dimers was tested on rat cultured neurons and exhibited toxicity only in the presence of microglia, which has been shown to release free radicals (Roher et al. 1996).

Consistent with our data, dimeric Aβ42 that has been purified from neuritic amyloid plaques could correspond to dityrosine cross-linked Aβ dimer observed by SDS-PAGE. We suggest that dityrosine cross-linked Aβ plays an essential role in the pathogenesis of AD and may represent the early building blocks that may initiate the formation of insoluble Aβ fibrils.

5.2.3 **Lipofuscin formation could be moderated by dityrosine crosslinks**

Lipofuscin is considered to be a biomarker of aging and the age-dependent accumulation of lipofuscin in the nervous system of individuals has made possible the reliable estimation of absolute age (Gray and Woulfe 2005; Szweda et al. 2003). However, it has been reported that amyloid-containing Alzheimer neurons contain a large amount of lipofuscin and lysosomal protease enzymes (Adamec et al. 2000), suggesting that the accumulation of Aβ may contribute to lipofuscin formation under oxidative stress conditions. Probing the contribution of oxidative stress on the tyrosine residue in Aβ will help to raise our understanding of the mechanism underlying the increased lipofuscin accumulation in AD.

In order to establish whether oxidised Aβ42 is found in lipofuscin pigments in AD brains, immunogold labelling for dityrosine and Aβ42 in lipofuscin of AD and control age matched brains was carried out. Single immunogold labelling of dityrosine was observed in the lipofuscin granules of a control age-matched human brain (Figure 5-17), A & B). TEM micrographs of lipofuscin in age-matched controls show dityrosine labelling, indicating the possibility of dityrosine contribution in lipofuscin formation. Interestingly, TEM immunogold labelling of dityrosine in lipofuscin of AD brain reveals two different labelling areas, low-density dityrosine labelling (Figure 5-17, C) and high density dityrosine labelling (Figure 5-17, D), indicating different levels of oxidative stress may have occurred and leading to a variety of dityrosine content that accumulates in lipofuscin. Additionally, it could be due to a variety of proteins that contribute to lipofuscin accumulation. The quantification and counting analysis of immunogold particles show significantly more dityrosine labelling in AD brain compared to age-matched control (Figure 5-17, E).

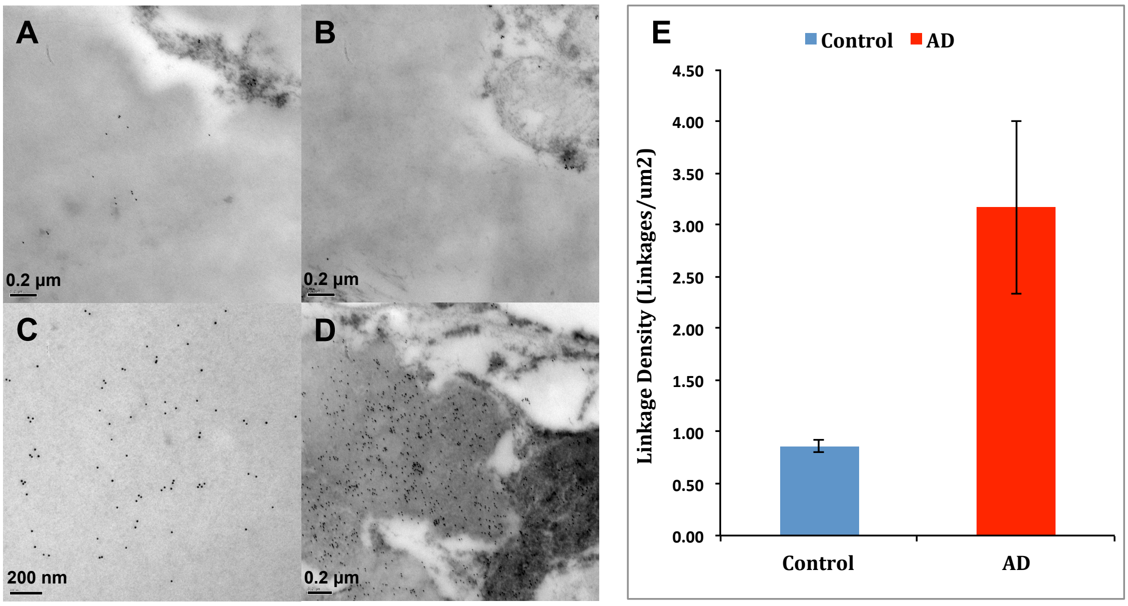

Figure 5-17: Immungold electron microscopy of lipofuscin in AD brain compared to age matched controls. Micrographs reveal single labelling for dityrosine at low levels in lipofuscin in control brains (A, B) and high levels in AD brain (C, D). Quantification shows significantly more dityrosine labelling in AD brain compared to age matched controls (E).

These results are in good agreement with a previous study using immunohistochemical detection (Kato et al. 1998), which showed dityrosine in the lipofuscin granules of the pyramidal neurons in control age-matched brain. However, here we find that comparison of AD and age-matched controls revealed a significant increase in density of dityrosine labelling in lipofuscin in AD brains, compared to that in control (Figure 5-17). These results are in agreement with the capacity of oxidative stress to induce protein modifications resulting in the formation of intralysosomal lipofuscin.

To examine the co-localisation of dityrosine and Aβ within lipofuscin pigments and to determine whether dityrosine resulted from the oxidative modification of Aβ, immunogold co-labelling for dityrosine and Aβ in lipofuscin of AD and control age matched brains was carried out. TEM immunogold co-labelling of dityrosine and Aβ in AD brain reveals some colocalisation within lipofuscin (Figure 5-18), although some areas showed low levels of Aβ labelling. These results may indicate that dityrosine cross-links could be generated from oxidation of various proteins that contain tyrosine residues.

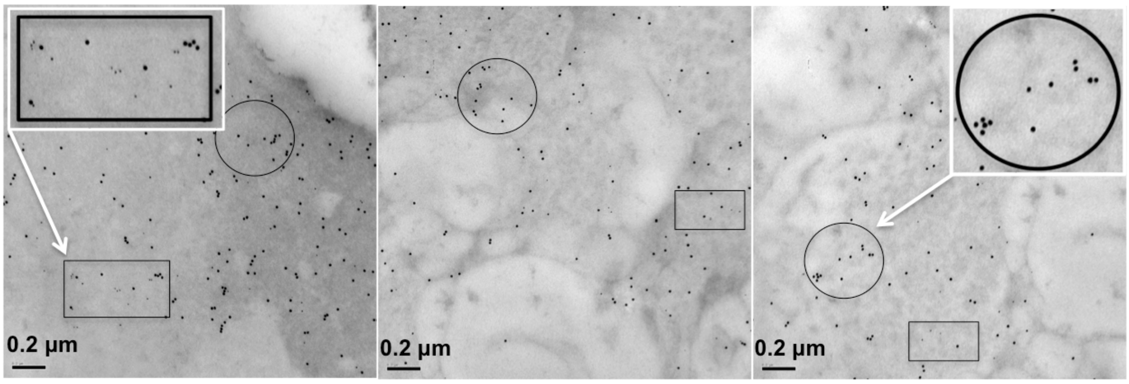

Figure 5-18: Immunogold labelling TEM of lipofuscin in AD brains. Double labelling with anti-Aβ (5 nm) and anti-dityrosine (15 nm) reveals colocalisation within lipofuscin. The images reveal two different areas of labelling, one shows delocalisation of dityrosine and Aβ as marked with circles, and the second area shows colocalisation of dityrosine and Aβ as marked with rectangles, indicating that dityrosine crosslinks can produce from various proteins that accumulate to form lipofuscin.

The protease resistant feature of dityrosine that has been reported in many studies (Amado et al. 1984; Atwood et al. 2004; Giulivi and Davies 1994) supports the view that dityrosine can associate with lipofuscin formation.

It is important to keep in mind that the number of AD brain samples that we have tested is not enough to confirm the elevation of dityrosine levels in lipofuscin in AD brain, as other data collected by a project student did not show a significant increase in the dityrosine level in lipofuscin in the AD brain. Further investigations are needed to gain a better understanding of the role of dityrosine in lipofuscin accumulation and also to verify whether the dityrosine level undergo any elevation upon AD progress or not. On the other hand, dityrosine is markedly increased in lipofuscin in healthy control individuals along with age progress and this is consistent with other results that used immunohistochemical technique to assess dityrosine level in lipofuscin of healthy aged matched individuals (Kato et al. 1998).

Both lipofuscin and plaques could form as a result of oxidative stress effects, these findings point to a relationship between dityrosine and amyloid accumulation in the AD brain and support strongly the hypothesis of dityrosine contribution to AD pathogenesis.

5.2.4 Dityrosine as a biomarker of oxidative stress in AD

Given our results showing that there are dityrosine cross-linked amyloid fibrils deposited in AD brains and that neuroblastoma cells incubated with Aβ42 also show cross-linked Aβ42, we were interested to see if dityrosine cross-linked Aβ could be identified in cerebrospinal fluid and could therefore be a useful biomarker for AD.

Here, TEM immunogold labelling for dityrosine was used to detect dityrosine and gain a general view of protein oxidation represented by dityrosine in CSF of AD and healthy age-matched control subjects. TEM immunogold colabelling-negative staining of CSF reveals a higher density of dityrosine and Aβ labelling in CSF taken from three AD patients (Table 2-3) (Figure 5-19, A) compared to age matched controls (Figure 5-19, B). Overall there was a much higher density of labelling for both Aβ and dityrosine in the AD CSF compared to controls, highlighting the presence of Aβ and also showing the increased level of dityrosine cross-linked proteins in CSF from AD. In the CSF from AD patients, two different areas of labelling were observed: those with low-density co-localisation, and others showing high-density co-localisation of dityrosine and Aβ indicating that the Aβ found in the CSF may contain dityrosine cross-links, but also that other tyrosine containing proteins are cross-linked in the CSF from AD. More TEM images of negatively stained CSF from other AD patients and age-matched control are presented in the appendix (x).

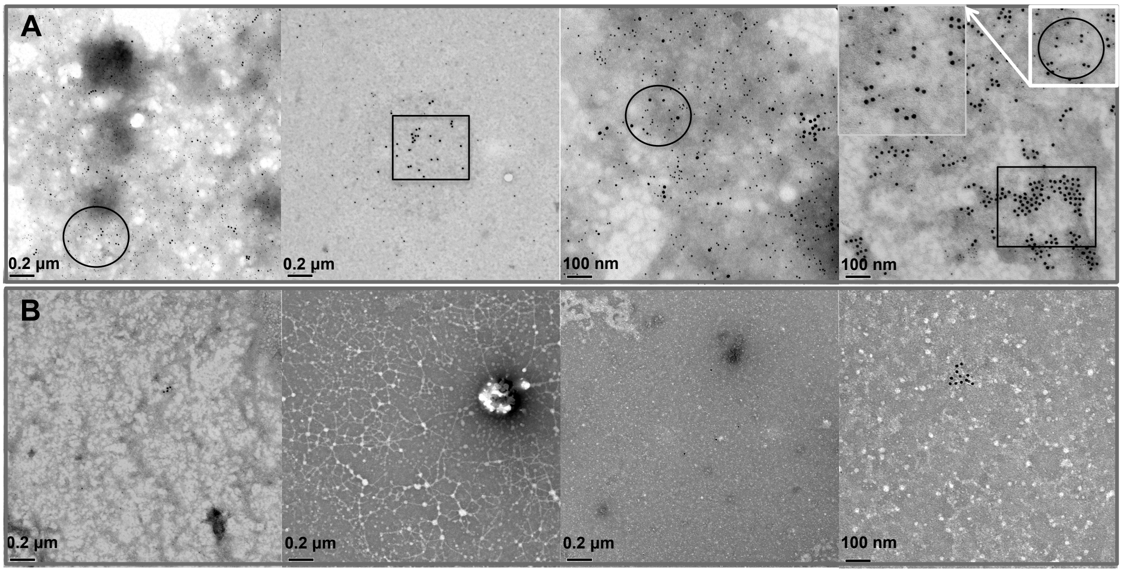

Figure 5-19: Immunogold labelling TEM/negatively stain of cerebrospinal fluid from AD pateints and age matched controls. A) A higher density of dityrosine (labelled with 15 nm) and Aβ (labelled with 5 nm) labelling was observed for CSF from an AD patient (top images) compared to b) age matched control. In CSF of AD patients, we can identify two different areas of labelling, low-density co-localisation (□), and high density co-localisation (O) of dityrosine and Aβ. Inserts show magnified images for further clarity.

5.3 Overall discussion

Results presented here have shown that dityrosine cross-links form in preformed Aβ42 fibrils and in oligomeric Aβ incubated under oxidising conditions in the presence of Cu^{2+} and H_2O_2. It has been shown previously that 1:1 Cu^{2+}: Aβ molar ratios and above are the most efficient ratios to generate dityrosine cross-links (Smith et al. 2007), demonstrating that Cu^{2+}: Aβ molar ratio is a critical factor in controlling the aggregation state of Aβ42. Moreover, it has been shown that both non-aged and aged Aβ42-Cu^{2+} complexes at molar ratio of 1:1 are neurotoxic, whilst Aβ42-Cu^{2+} complexes prepared at sub and supra-equimolar ratios were nontoxic to neuronal cells (Smith et al. 2006a; Smith et al. 2007). Aβ peptide can coordinate with Cu^{2+} to give Aβ-Cu^{2+} complexes (Atwood et al. 2000; Syme et al. 2004), which are redox-active. In turn, these complexes show the ability to induce ROS formation, resulting in oxidative stress (Huang et al. 1999a; Smith et al. 2006a). Cu^{2+} ions coordinate to Aβ via the three histidine residues His6, His13, and His14 and potentially Tyr10 as shown in Figure 5-1 (Atwood et al. 1998; Curtain et al. 2001; Maiti et al. 2008; Tickler et al. 2005) and produce SDS-resistant oligomers (Atwood et al. 2004).

Clioquinol is a potent Cu/Zn chelator and has been shown to significantly reduce Aβ amyloid deposition in an AβPP transgenic mouse (Cherny et al. 2001) and has shown some efficacy in human AD subjects (Ritchie et al. 2003). These studies have been taken to suggest that Cu^{2+} plays a very significant role in Aβ deposition in AD and could imply that dityrosine formation can stabilise deposits.

Here, cell culture experiments show that conditions amenable to Aβ dityrosine cross-linking are also present in a cellular environment and that dityrosine containing Aβ is found around cells and internalised into cells both in lysosomes and occasionally as internalised fibrils. Previously, Serpell and coworkers (Soura et al. 2012) showed that internalised oligomeric Aβ42 leads to accumulation of autophagosomes containing Aβ. Considerable evidence supports the view that intralysosomal Aβ accumulation can induce neuronal death, and that the oligomers and fibrils can be stabilised by dityrosine cross-linking (Gouras et al. 2005; Yu et al. 2005; Zheng et al. 2006). Studies using Aβ42 with the Tyr10 substituted for alanine mutant showed significantly reduced H_2O_2

production and prevented toxicity to primary cortical neurons supporting the view that dityrosine cross-linking may be important in mediating oligomer toxicity (Barnham et al. 2004). Here, electron micrographs show the internalisation of dityrosine cross-linked Aβ fibrillar material into the cytoplasm (Figure 5-14) and into lysosomes (Figure 5-13). The oligomeric Aβ may be stabilised by covalent cross-links.

Oxidative stress has been widely implicated in AD pathogenesis. Sources of ROS, such as H_2O_2, superoxide anion, and hydroxyl radicals, can be formed from different *in vivo* sources (e.g. oxidation, photochemical, and enzymatic reactions) although mitochondria represent the main *in vivo* source of ROS formation (Chance et al. 1979; Loschen et al. 1971). At the same time, mitochondria are the main target of ROS attack (Harman 2002), resulting in the formation of peroxidised, undegradable macromolecules. H_2O_2 can easily diffuse into lysosomes and react with iron ions that are released from the degradation of different metalloproteins during their intralysosomal degradation. The interaction of hydrogen peroxide with iron ions results in the formation of the highly reactive hydroxyl radicals. The latter could attack intralysosomal macromolecules, such as Aβ, causing cross-linking of these materials. The oxidative modification especially cross-linking of autophagocytosed material, is the most probable cause of non-degradability of these materials. The excessive accumulation of these non-digested materials could result in endosomal/lysosomal leakage and as a consequences acid hydrolase enzymes will be released, ultimately leading to cell death (Zheng et al. 2006); (Ditaranto et al. 2001; Yang et al. 1998). Recently, Murakami and Shimizu have clarified the role of cytoplasmic superoxide radical as a possible contributing factor to intracellular Aβ oligomerisation in AD (Murakami and Shimizu 2012). They demonstrated using a human amyloid precursor protein transgenic AD mouse model that lacking SOD1 can accelerate Aβ oligomerisation and also resulted in memory loss, neuro-inflammation, tau phosphorylation, and synaptic loss. This highlights the importance of cytoplasmic superoxide radicals in the pathogenesis of AD, explaining that excessive free radicals in the cytosol could result in conformational changes of intracellular Aβ (Murakami et al. 2010). Supporting the previous result, it is reported that the levels of SOD1 were markedly lower in human AD patients compared with non-AD subjects (Murakami et al. 2011). On the other hand, it has been reported that interaction of intracellular Aβ with SOD1 decreases the activity of SOD1 (Yoon et al. 2009).

It has also been suggested that intraneuronal Aβ oligomers cause neuronal death by activating endoplasmic reticulum stress, endosomal/lysosomal leakage and mitochondria dysfunction (Umeda et al. 2011); (Misonou et al. 2000). Kurz *et al.* have highlighted a close relation between lysosomes and mitochondria, explaining that accumulation of iron inside mitochondria will result in lysosomal iron loading as a consequence of degradation of mitochondria by lysosomal enzymes (Kurz et al. 2008). Moreover, normal production of H_2O_2 by mitochondria results in oxidative stress, which will labilise lysosomes and further oxidative stress could result from degradation of mitochondria by lysosomal enzymes.

We have shown that amyloid plaques in AD brain tissue show extensive dityrosine cross-linking and this may suggest that these highly stable, insoluble deposits are stabilised by covalent cross-linking, resulting in a resistance to degradation. Therefore, the existence of dityrosine may be relevant in AD pathology. Friedrich *et al.* (Friedrich et al. 2010) have shown that Aβ internalised to cultured cells can accumulate and assemble resulting in eventual cell death and thus they suggest that the formation of amyloid plaques might arise from accumulated intracellular Aβ. Therefore, there may be a pathway from the lysosomal/autophagsosome accumulation of dityrosine cross-linked Aβ that we have observed in neuroblastoma cells, to the eventual deposition as amyloid plaques composed of dityrosine cross-linked Aβ observed here in AD tissue.

Interestingly, our preliminary data shows significant increased dityrosine levels in lipofuscin in brain tissue of AD patient compared to healthy aged matched control (Figure 5-17), and that may reflect the important role that is played by oxidative stress in lipofuscin and plaque formation and subsequently AD pathogenesis. It has been found that the level of lipofuscin is markedly elevated in AD brain tissue, thus it is important to understand the mechanism by which lipofuscin is produced and accumulates in brain tissue.

It has been suggested that intraneuronal lipofuscin is intrinsically harmful to neuronal cells (Double et al. 2008). Alternatively, Giaccone *et al.* discussed the role of lipofuscin in the pathogenesis of AD, and proposed that lipofuscin could be harmful to neuronal cells after its release into the extracellular space (Giaccone et al. 2011). However, they reported that lipofuscin contains both Aβ and its precursor and suggested that upon its release into the extracelluar space it may serve as a source of Aβ oligomers for a prolonged period. Results presented here support this hypothesis, showing that lipofuscin in AD brain contains both Aβ and dityrosine.

A few studies have previously attempted to quantify dityrosine in cerebrospinal fluid. Techniques including HPLC with fluorescence detection, HPLC with electrochemical array detection (HPLC-ECD) or fluorescence detection, and liquid chromatography with triple quadrapole mass spectrometric detection have been applied to quantify dityrosine concentrations in CSF sample from both healthy and disease affected subjects (Abdelrahim et al. 1997; Ahmed et al. 2005; Hensley et al. 1998). However, the results of these studies have been conflicting, perhaps due to differences in sample handling and preparation before measuring. Quantitative screening of protein glycation, oxidation and nitration adducts in CSF of AD and healthy age-matched subjects have been taken to suggest that dityrosine concentration does not change in AD patients with respect to control subjects (Ahmed et al. 2005). By contrast, earlier studies using electrochemical detection showed that dityrosine concentration was elevated markedly in CSF of AD patients (Hensley et al. 1998).

Our results have revealed very strong evidence for the presence of both Aβ and dityrosine in the CSF from AD patients. Both Aβ and dityrosine are very rarely observed in CSF from age-matched controls. Therefore, we suggest that dityrosine cross-linked Aβ could represent a potential biomarker for AD.

It has been illustrated that, at equimolar or Cu^{2+}:Aβ molar ratios > 0.3 (Curtain et al. 2001; Smith et al. 2006a) , Aβ coordinates a Cu^{2+} ion and a His bridge forms between Cu^{2+} ions. This His bridge has a marked effect on the formaion of dityrosine adduct, explaining why elimination of the His bridge formation by methylation of the imidazole side chain of the His at either the π or τ position inhibits dityrosine formation significantly. This His bridge can play a significant role in the formation of dityrosine cross-linking by bringing two tyrosine residues in to close approximation and facilitates dityrosine cross-link formation (Smith et al. 2006a).

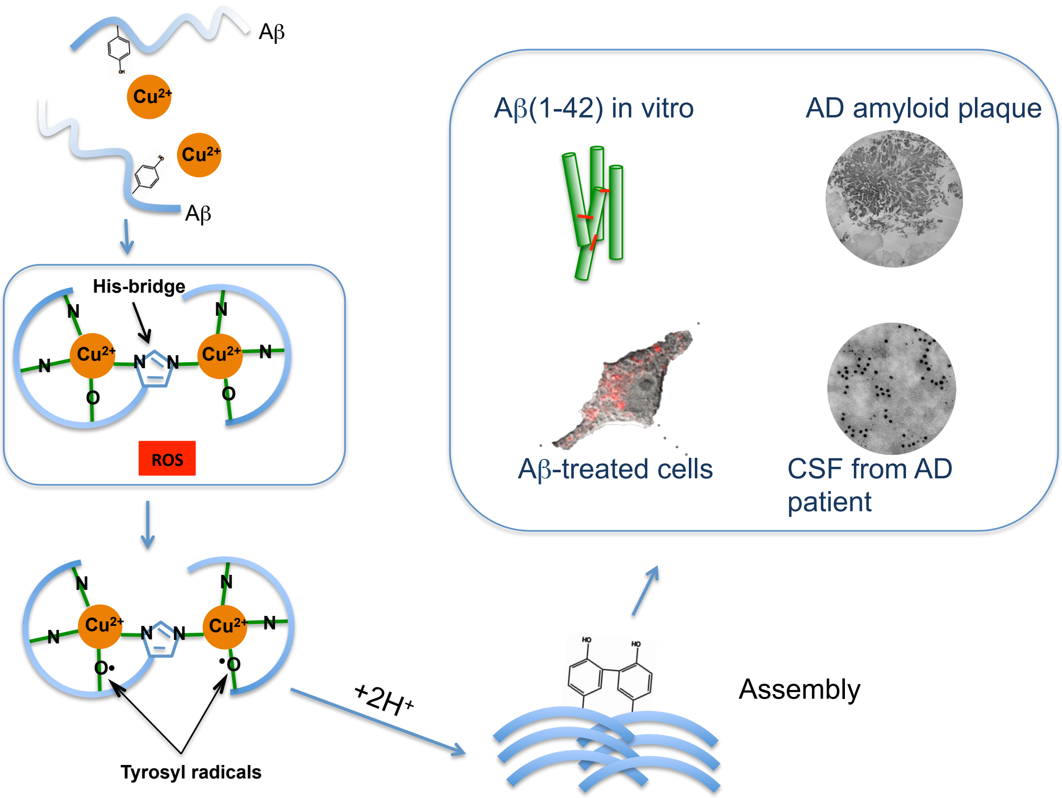

Figure 5-20: Graphic abstract explaining the role of dityrosine cross-link in the pathogenesis of AD.

5.4 Conclusion

At equimolar ratio of Cu^{2+} and Aβ42, Cu^{2+} can catalyse tyrosine oxidation by H_2O_2, leading to dityrosine cross-link generation and the latter can cause Aβ misfolding, resulting in Aβ assembly into oligomers and subsequently into amyloid fibres. It is possible that dityrosine cross-links stabilise Aβ fibres once formed.

Here we present a comprehensive study of *in vivo* and *in vitro* dityrosine cross-linking associated with Aβ. We have revealed the presence of dityrosine cross-links in amyloid plaques in human AD brain, and also in CSF, and identified significant relationships between dityrosine cross-links and amyloid deposit formation. The *in vitro* and *in vivo* results presented here reveal that oligomeric Aβ can undergo oxidative modification in a cellular environment, resulting in cross-linked Aβ through dityrosine, followed by intralysosomal Aβ accumulation that could lead to lysosomal leakage and cell death. Our results show significant accumulation of dityrosine crosslinked Aβ in amyloid plaques, implying a role in stabilisation of these insoluble deposits. We have also proposed a potential new biomarker for AD in CSF, which contains elevated dityrosine cross-linked proteins as well as elevated dityrosine cross-linked Aβ. Our preliminary findings show that dityrosine cross-links were increased in lipofuscin in AD brain, indicating the important role played by dityrosine cross-links in the accumulation of lipofuoscin in higher levels in AD compared to control subjects.

6 Results and Discussion

Aggregation of α-syn induced by Cu^{2+}-catalysed oxidation as a potential mechanism of Lewy body production

6.1 Introduction

PD is the second most common neurodegenerative disease after AD in humans. Recently, it has been proposed that intermediate forms of self-assembled α-syn are the main pathogenic species (Celej et al. 2012; Wright et al. 2009). Oxidative stress has also been implicated in the pathogenesis of a number of neurodegenerative diseases, including AD and PD (Moreira et al. 2007; Zhou et al. 2008). Similar to Aβ, dityrosine cross-links can also be formed *in vitro* via MCO of α-syn under physiological conditions (Cole et al. 2005; Paik et al. 2000), and have been identified as biomarkers of oxidative stress in an MPTP (1-methyl-4-phenyl-1,2,3,6- tetrahydropyridine) mouse model of PD (Pennathur et al. 1999a; Pennathur et al. 1999b). Studying the influence of dityrosine cross-links in the α-syn conformation and during fibrillogenesis would provide insights into the importance of oxidative modification of tyrosine residues in the pathogenesis of PD. In this chapter, the ability of the Cu^{2+} ion to promote the formation of *in vitro* dityrosine cross-linked α-syn was explored and the effect of the Cu^{2+} ion on α-syn fibrillogenesis and conformation was investigated. The role of dityrosine as a covalent cross-linker was revealed using a number of techniques including fluorescence spectroscopy, HPLC, LC-ESIMS/MS, SDS-PAGE, TEM, XRFD and CD.

6.2 **Results and discussion**

6.2.1 **Cu^{2+}-catalysed oxidation of α-syn enhances dityrosine cross-link formation**

Formation of dityrosine cross-linked α-syn was enhanced by incubation of 50 μM recombinant α-syn with 50 μM Cu^{2+}/ 1.25 mM H_2O_2 in 20 mM HEPES buffer pH 7.4 (Figure 6-1, A). Controls were prepared by incubating 50 μM recombinant α-syn in buffer alone and with buffer supplemented with 50 μM Cu^{2+} (Figure 6-1 B and C respectively). The mixtures were incubated for 24 h at 37 °C with agitation of 400 rpm. The incubation of α-syn with Cu^{2+}/H_2O_2 leads to rapid loss of the intrinsic tyrosine fluorescence signal at a wavelength of 305 nm using an excitation wavelength of 280 nm, as seen in Figure 6-1, A. Concomitant with the decrease in tyrosine signal, there was an enhancement in fluorescence emission intensity at wavelength of 410 nm, indicating dityrosine formation (Figure 6-1, A).

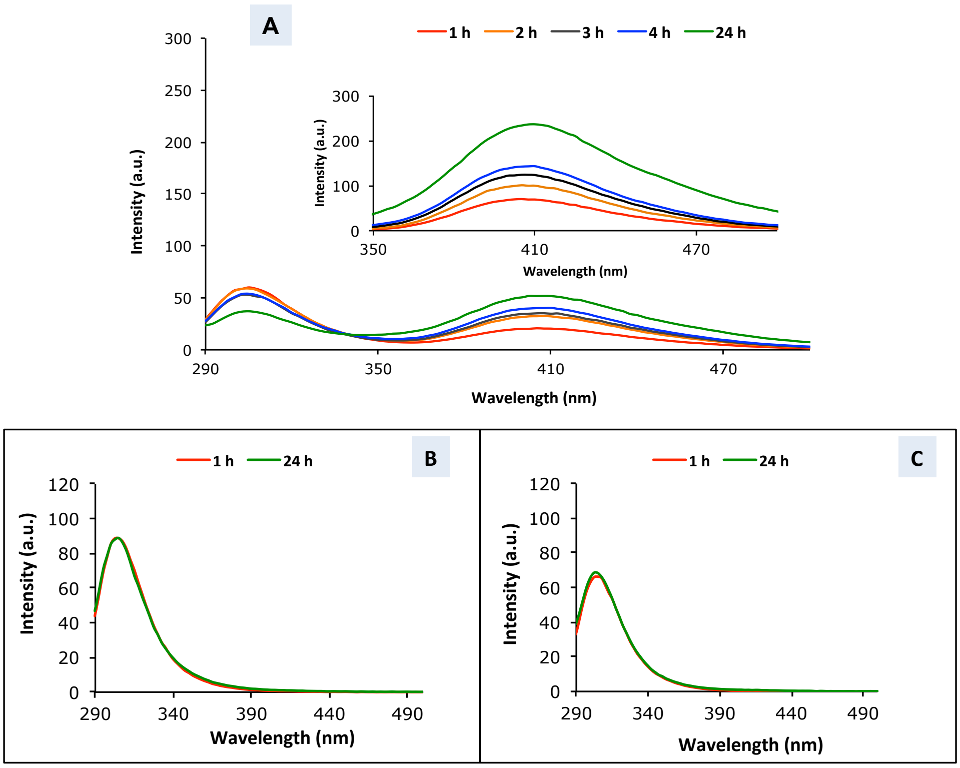

Figure 6-1: Enhanced dityrosine cross-linked α-syn in the presence of Cu^{2+}/H_2O_2. 50 μM of monomeric α-syn was incubated for 24 h with Cu^{2+}/H_2O_2 at 37 °C and agitation 400 rpm (A). After one h of incubation, the tyrosine fluorescence signal was reduced with simultaneous appearance of a new signal at 410 nm, typical of the dityrosine fluorophore. No dityrosine fluorescence signal was obtained over 24 h of incubation of α-syn in HEPES buffer alone (B), and with 50 μM Cu^{2+} (C).

The assignment of the fluorescence to dityrosine was further confirmed using an excitation wavelength of 320 nm and emission at 410 nm as seen in the inset of Figure 6-1, similar to data in Figure 3-9, and also supported by published data obtained at a similar pH (Borsarelli et al. 2012). In addition, LC-ESIMS/MS, which was acquired using MRM mode, was used to further confirm the identity of the resulting dityrosine cross-link (Figure 6-2). As described previously in chapter 3, the detection of the dityrosine was achieved using the most intense ion reaction of *m/z*: 361.1→315. 50 μM of α-syn was oxidised under metal-catalysed oxidation for 24 h, and the reaction was quenched using EDTA. The oxidised peptide was desalted, concentrated and hydrolysed under acidic conditions as described in the method's chapter (2.4.8). The mass chromatogram of α-syn hydrolysate revealed a peak with retention time of 5.8 min, which corresponds to that of authentic dityrosine (Figure 6-2).

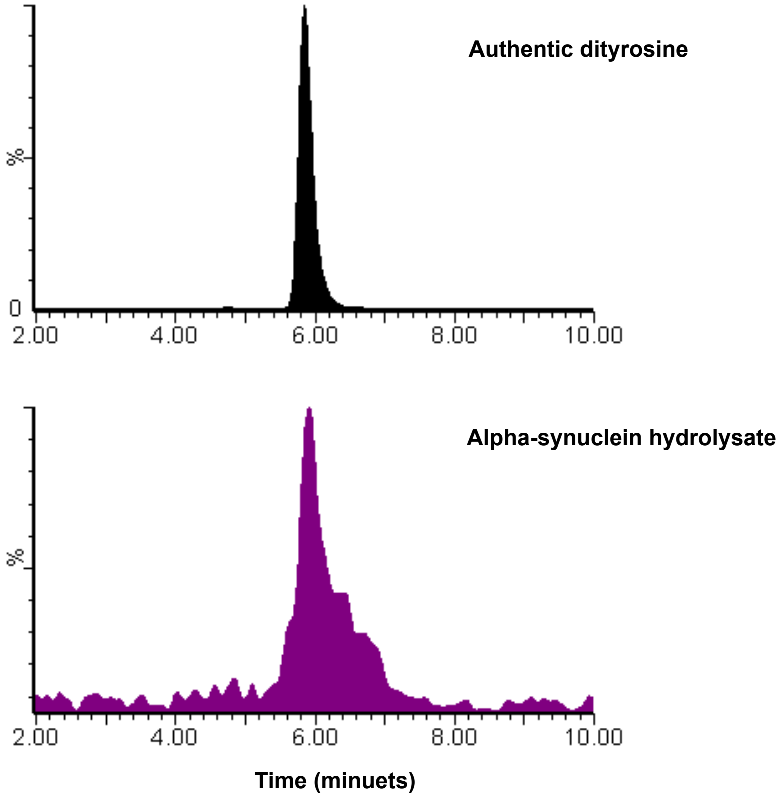

Figure 6-2: LC-ESIMS/MS (MRM) chromatograms showing the presence of dityrosine in the α-syn hydrolysate, which was obtained by acidic hydrolysis of the oxidised α-syn. The oxidised α-syn was obtained by oxidation of (50 μM) monomeric α-syn for 24 h under Cu^{2+}/H_2O_2 *conditions.*

Incubation of 50 µM α-syn in both Cu^{2+}-depleted and Cu^{2+}-containing buffer revealed the remarkable appearance of a fluorescence peak around 410 – 420 nm after 7 days of incubation (Figure 6-3), indicating the possible involvement of dityrosine cross-links in the mechanism underlying the α-syn aggregation and accumulation in PD. At early time points (0-6 days), only the typical tyrosine fluorescence signal at 305 nm was observed, and interestingly after 7 days of incubation in both Cu^{2+}-depleted and Cu^{2+}-containing buffer, a typical dityrosine fluorescence signal at 410 – 420 nm was observed (Figure 6-3, A and B respectively).

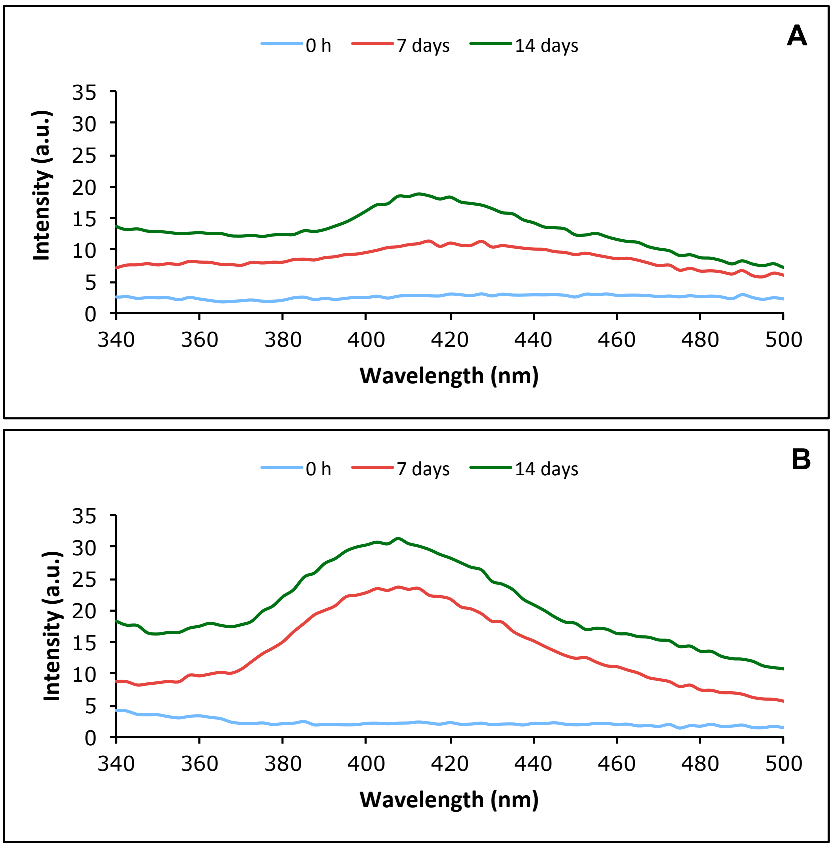

Figure 6-3: Dityrosine formation upon α-syn incubation in HEPES buffer only (A) and with Cu^{2+} (B). Incubation of 50 µM α-syn in both Cu^{2+}-depleted and Cu^{2+}-containing buffer revealed remarkable appearance of dityrosine signal at 410 - 420 nm after 7 days of incubation.

Previous work shows that Cu^{2+} ions play a vital role in α-syn aggregation and fibrillogenesis (Lucas and Lee 2010; Rasia et al. 2005; Uversky et al. 2001; Wang et al. 2010). Preliminary ThT results showed that the ThT signal was significantly enhanced after 13 days of α-syn incubation with 50 µM Cu^{2+} applying 1:1 molar ratio (Figure 6-4, A). The dityrosine and ThT fluorescence data showed an increased intensity after 7 days incubation both with and without Cu^{2+}. This may indicate an important role of

MCO in initiating the α-syn fibrillogenesis process *in vitro*, and perhaps also *in vivo*. It is important to mention that the provided α-syn, which is used in this study, was of high purity and does not show any cysteine mis-incorporation to tyrosine at position 136, which has been observed for about 20% of human α-syn expressed in *Escherichia coli* (Masuda et al. 2006). It has been reported that α-syn mutant Y125W/Y133F/Y136F had showed the same physical properties, including the ability to form fibrils, as wild type α-syn (Kaylor et al. 2005), reflecting the important role played by Y39 in the α-syn fibrillation. A dityrosine fluorescence signal at 410 nm was observed for the mentioned mutant α-syn after 125 h of incubation in only phosphate buffer pH 7.4 with stirring at 37 ºC, explaining that the dityrosine cross-links were intermolecular as there is only one Tyr at position 39 and also it formed only in the soluble late oligomers (Kaylor et al. 2005). Although both α- and β-syn contain four similarly placed tyrosine residues in the C terminus, they display differing abilities to aggregate and, unlike α-syn, β-syn is not found in the Lewy bodies in PD (Biere et al. 2000; Jakes et al. 1994; Spillantini et al. 1997). It has been revealed that *in vitro* exposure of α-syn to nitrating agents resulted in the formation of stable dityrosine cross-linking (Souza et al. 2000). In contrast, β-syn does not form stable dityrosine crosslinks after exposure to nitrating agents, despite the presence of all four conserved tyrosine residues (Souza et al. 2000). This may reflect the importance of dityrosine cross-link formation to enhance α-syn aggregation and its pathological role in PD.

It has been shown that dityrosine forms in α-syn fibrils that have been aged in the absence and presence of Cu^{2+} in an aerobic environment, whilst α-syn aged anaerobically did not show any dityrosine formation (Lucas et al. 2010). Furthermore, incubation of α-syn in solutions that contain methionine and/or EDTA, which help to prevent or reduce the level of protein oxidation, led to lengthened lag times for fibril nucleation (Krishnan et al. 2003). Gathering our results with others indicates that Cu^{2+} ions strongly promote the oxidation of α-syn, resulting in dityrosine cross-linked α-syn formation. Also, it has been found that seeding α-syn with dityrosine cross-linked dimers accelerates α-syn fibrillogenesis, suggesting that the critical rate-limiting step in the nucleation of α-syn fibrils is the formation of dimeric species, dityrosine cross-linked, and their accumulation (Krishnan et al. 2003). Current results are in good agreement with other published data (Krishnan et al. 2003; Lucas et al. 2010; Souza et al. 2000), and support the notion that dityrosine cross-linked α-syn oligomers can serve as a seed in the α-syn fibrillogenesis process. Interestingly, it has been showed that stable α-syn polymers can be generated using nitrating agents and these polymers were highly stabilised due to the formation of dityrosine cross-link (Souza et al. 2000).

To examine whether Cu^{2+}-enhanced α-syn fibrils have a β-sheet conformation, a combination of CD and ThT fluorescence were used to compare the control with Cu^{2+}-enhanced α-syn fibrils. The CD spectra of both α-syn incubated under control (i.e. without Cu^{2+}) and Cu^{2+}-containing buffer conditions did not display a β-sheet structure (Figure 6-4, D and E), which typically has a positive and a negative peak at ~ 196 nm and ~ 216 nm respectively. Instead the CD spectra are consistent with random coil conformation (minimum at 195 nm). In contrast, ThT fluorescence spectrum and TEM micrographs of Cu^{2+}-enhanced α-syn showed fibril formation (Figure 6-4, A and C). These CD results may arise from only the soluble α-syn species that remain in solution in the buffer whilst fibrils were precipitated, leading to the surprising lack of β-sheet signal by CD. Moreover, it could be that the β-sheet CD signal was masked by the signal raised from random coil conformation, which is reported to be much stronger than β-sheet.

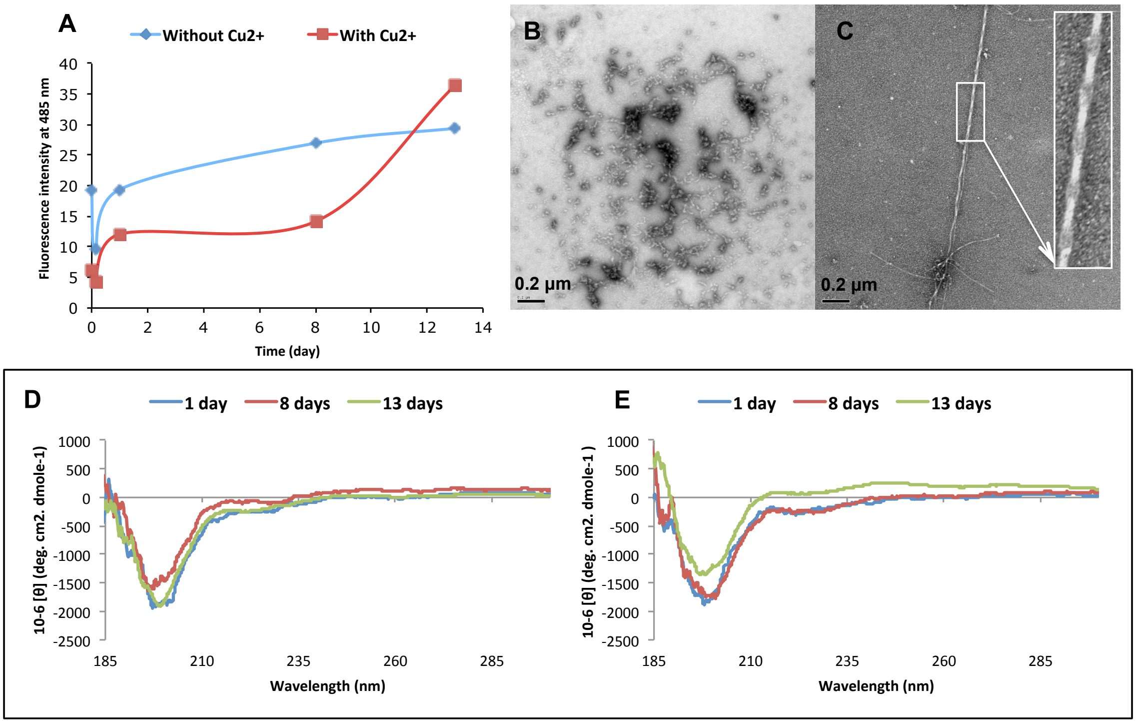

Figure 6-4: Cu^{2+} ion accelerates α-syn fibrillogenesis. Preliminary results showed that the ThT signal was slightly enhanced after 13 days of α-syn incubation with 50 µM Cu^{2+}(A) and this agreed with corresponding TEM micrographs which showed formation of α-syn oligomers in absence of Cu^{2+} (B) compared those incubated with Cu^{2+} (C). The Cu^{2+}-enhanced assemblies display characteristic fibril morphology by negative stain TEM, by contrast spherical aggregation was observed under control condition that corresponds to protofibrils species of α-syn (B). CD spectra of both α-syn fibrils obtained in buffer only (D) and Cu^{2+}-enhanced fibrils (E) revealed a random coil structure that did not change over the incubation time.

TEM micrographs of Cu^{2+}-enhanced α-syn fibrils revealed the formation of relatively uniform, mostly unbranched, and often twisted fibrils (Figure 6-4, C), whereas incubation of α-syn under control conditions for 13 days resulted in α-syn protofibril formation (Figure 6-4, B), indicating that the formation of α-syn fibrils is significantly promoted upon incubation with Cu^{2+}. This finding is in good agreement with previously published data that revealed that various metal ions accelerate α-syn fibrillogenesis (Uversky et al. 2001). Moreover it has been revealed that Cu^{2+} is the most effective ion for inducing α-syn oligomerisation (Paik et al. 1999).

Because the α-syn has four tyrosine residues in its sequence located at 39, 125, 133, 136 (Figure 6-5), this raises the possibility that α-syn oxidation can lead to the formation of intra and inter dityrosine cross-links.

1 MDVFMKGLSK AKEGVVAAAE KTKQGVAEAA GKTKEGVLYV GSKTKEGVVH
51 GVATVAEKTK EQVTNVGGAV VTGVTAVAQK TVEGAGSIAA ATGFVKKDQL
101 GKNEEGATQE GILEDMPVDP DNEAYEMPSE EGYQDYEPEA

Figure 6-5: Amino acid sequence of human α-syn showing the positions of tyrosine residues at 39, 125, 133, and 136 respectively that are highlighted in blue.

In order to characterise which of these tyrosine residues is responsible for the cross-linking formation, HPLC chromatograms of α-syn that had been incubated for 6 h under both control and oxidative conditions were obtained. A C-4 Phenomenex (150X4.6 mm) column was used for HPLC analysis, and α-syn was monitored detecting absorbance at 226 nm. The HPLC chromatogram of non-oxidised α-syn showed a major single peak with a retention time of 9.73 min and maximum absorbance at 226 nm (Figure 6-6, A), indicating the presence of monomeric species of α-syn. The HPLC analysis of oxidised α-syn showed the HPLC profile in Figure 6-6, B. The HPLC chromatogram of oxidised α-syn showed many peaks with retention times between 7.2 – 9.9 min; consequently this makes the comparison of oxidised and non-oxidised α-syn more challenging. Also, the resolution of the peaks that were obtained from oxidised α-syn is very poor, making the fraction collection process difficult. However, the peaks with retention time range of 7.17 – 8.38 min and 8.78 – 9.98 min were collected and labelled fraction 1 and fraction 2 in the figure (Figure 6.6), and then analysed for dityrosine presence using fluorescence spectrophotometry. The fluorescence spectra revealed the appearance of a signal at 410 nm, indicating the presence of dityrosine in fraction 2, whilst fraction 1 did not give a dityrosine fluorescence signal.

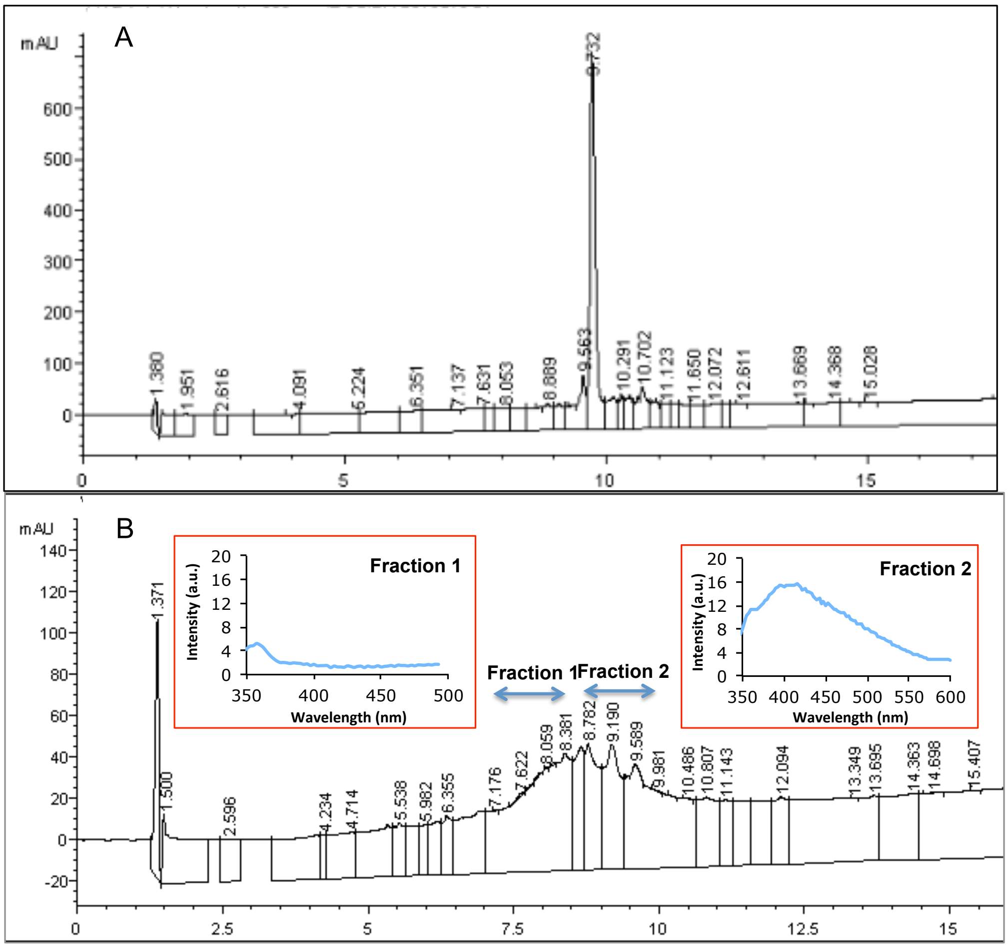

Figure 6-6: HPLC chromatograms showing the profile of oxidised α-syn oligomers. Non-oxidised (A) and oxidised (B) α-syn samples were injected into C–4 Phenomenex (150 X 4.6mm) column with a flow rate was 1 ml/min. 0.1% TFA in water used as solvent A and 0.085% TFA in acetonitrile used as solvent B. α-syn monitored using UV detector at wavelength of 226 nm.

As demonstrated previously, the fluorescence data (Figure 6-1, A) showed that incubating α-syn under oxidation conditions rapidly induces dityrosine cross-linkages in α-syn and 1 h was enough to observe a dityrosine signal with high intensity. Oxidation of α-syn at early time points was examined and analysed by SDS gel electrophoresis and visualised by Coomassie blue and silver staining (Figure 6-7), and showed formation of a dimer after 1 h incubation under oxidation and increasing the oxidation time to 5 h resulted in greater yield of dimer, which is covalently cross-linked through tyrosine-tyrosine coupling. Also, large SDS resistant aggregates that are incapable of entering the gel matrix were observed in all cases, as visualised by silver staining, and this could be due to the presence of these aggregates in the stock solution of α-syn that was used to prepare the desired concentrations and the centrifuging speed was not enough to remove them. Although the fluorescence data showed rapid formation of dityrosine cross-links with high intensity, SDS analysis displayed the presence of high levels of monomeric α-syn with a molecular weight of 14.5 kDa, suggesting that dityrosine cross-linking was more likely intra-α-syn rather than inter-α-syn. Interestingly, SDS analysis revealed an appearance of two adjacent bands after 1 h of oxidation (Figure 6-7), and this could be explained by the formation of two structural forms of dimeric α-syn with different mobilities within the gel. SDS represents one of the compounds that are used as a membrane mimetic (Hunter et al. 2005). Recently, it has been found that α-syn can adopt an α-helical conformation in micelles of SDS (Zibaee 2005), suggesting that the dimeric α-syn species found here may be comprised of two different structural isoforms, i.e. α-helical and another undetermined form, which could be an unfolded form.

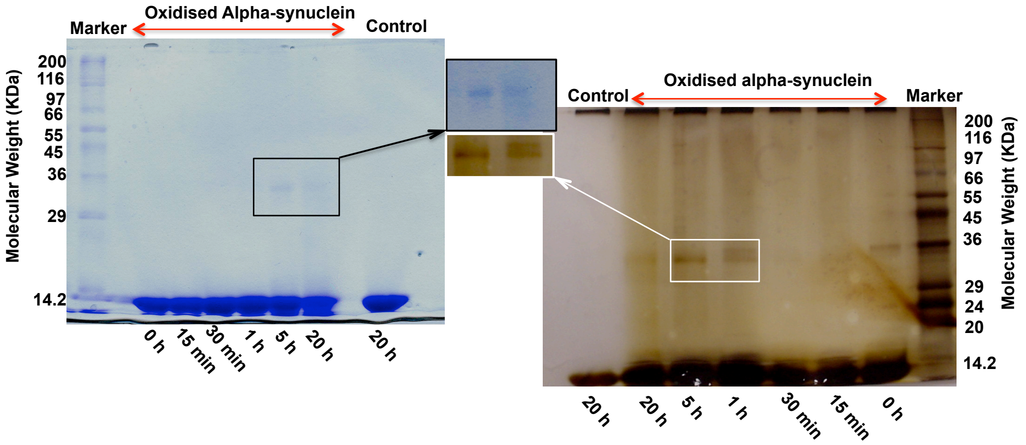

Figure 6-7: SDS-PAGE analysis of α-syn samples as a function of the time of oxidation. 100 µM of purified recombinant human α-syn was oxidised under Cu^{2+}/H_2O_2 conditions in 20 mM HEPES buffer, pH 7.4, at 37 °C with agitation of 400 rpm. Aliquots were removed at time intervals indicated and EDTA was added to quench the oxidation process. SDS-sample buffer added to the samples and then boiled for 5 min at 100 °C, and 10 µl of the boiled sample loaded on 15% Tris-glycine gel. The figure shows the appearance of a new band with molecular weight about 30 kDa after 1 h of oxidation that became more obvious at 5 h of oxidation indicating the presence of a dimer with time.

6.2.2 Identification of dityrosine cross-linked α-syn dimer using LC-MS

To investigate which tyrosine residue(s) may be evolved in the formation of dityrosine cross-links, both intact oxidised and non-oxidised α-syn were analysed using nanoLC-MS (Figure 6-8).

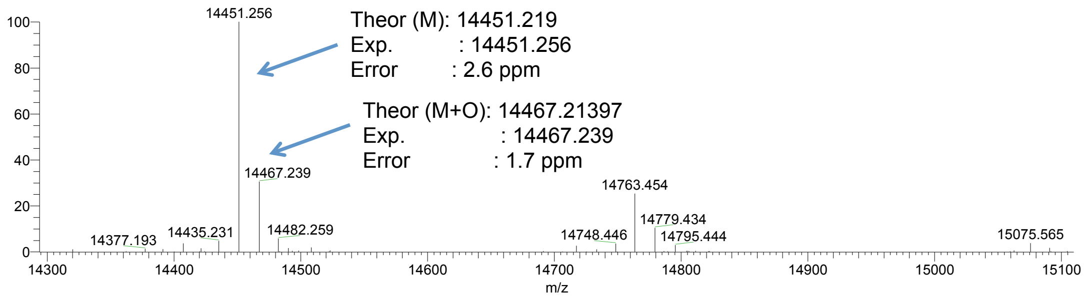

Amino acid sequence of analysed α-syn:
MDVFMKGLSKAKEGVVAAAEKTKQGVAEAAGKTKEGVLYVGSKTKEGVVHGVATVAEKTKEQVTNVGGA
VVTGVTAVAQKTVEGAGSIAAATGFVKKDQLGKNEEGAPQEGILEDMPVDP
DNEAYEMPSEEGYQDYEPEA
Elemental Composition: C627 H1013 N166 O216 S4
Monoisotopic *M/Z* $(M+H^+)$: 14452.22633

Figure 6-8: NanoLC-MS analysis of intact non-oxidised α-syn. 1 pmole/µl of human recombinant α-syn prepared in 0.1% formic acid and then analysed by LTQ orbitrap hybrid FT mass spectrometer. The mass spectrum confirms the identification of the α-syn with the expected mass of 14451.219.

Non-oxidised α-syn (1 pmole/µl of human recombinant α-syn prepared in 0.1% formic acid) was initially used to optimise the nanoLC-MS conditions using a LTQ orbitrap hybrid FT mass spectrometer connected to nanoLC. The mass spectrum revealed the identity of the analysed α-syn and the molecular mass of α-syn was estimated to be *m/z* $(M+H^+)$ 14451.256 and this is consistent with the calculated *m/z* $(M+H^+)$ 14451.219 with precision of 2.6 ppm. The determined primary amino acid sequence (Figure 6-8) was identical with the expected and known sequence of human α-syn (Lucas and Lee 2010; Lucas et al. 2010). To determine the formation of dityrosine cross-linked α-syn dimer, 1 µl aliquot from the α-syn oxidation mixture was injected into nanoLC-MS, and the analysis was performed using the same conditions that were used to identify the non-oxidised α-syn. Unfortunately, it was not possible to detect the α-syn dimer as the signal of monomeric α-syn masked the α-syn dimer signal. The high proportion of monomeric compared to dimeric α-syn dominated the mass spectrum and as a result high signal suppression was observed. These data are consistent with that shown from SDS-PAGE, which revealed a higher concentration of monomeric α-syn compared with α-syn dimer (Figure 6-7). However, many nanoLC-MS attempts were carried out to resolve this problem and to get better resolution, but all of the trials failed to separate the oxidised α-syn mixture.

Coupling of SDS-PAGE with mass spectrometry has been widely used to characterise the post-translational modifications of proteins (Burlingame et al. 1996), and also in protein identification using database searching algorithms (Cohen and Chait 1997). However, nanoLC-MS/MS mapping enabled the determination of a detailed oxidative modification for oxidised α-syn. The oxidised α-syn mixture was successfully separated by SDS-PAGE as demonstrated above (Figure 6-7), and this resolved the problem arising from poor resolution in the LC column and in turn the bad yield in mass spectrometry analysis. In order to gain better insight into the nature of oxidative modification of α-syn catalysed by Cu^{2+} ions, oxidised α-syn mixture was first separated using SDS-PAGE (Figure 6-7), followed by in gel trypsin digestion for the separated bands. Finally, the extracted peptide fragments were analysed by LTQ orbitrap hybrid FT mass spectrometry. To identify the α-syn peptides, the Mascot search engine was used and the search results revealed 100% sequence recovery of α-syn (monomeric) and 89% of α-syn (dimeric) (Figure 6-9 A and B, respectively).

Matched peptides shown in **Bold Red**

A

1 MDVFMKGLSK AKEGVVAAAE KTKQGVAEAA GKTKEGVLYV GSKTKEGVVH
51 GVATVAEKTK EQVTNVGGAV VTGVTAVAQK TVEGAGSIAA ATGFVKKDQL
101 GKNEEGATQE GILEDMPVDP DNEAYEMPSE EGYQDYEPEA

B

1 MDVFMKGLSK AK**EGVVAAAE KTKQGVAEAA GKTK**EGVLYV GSK**TKEGVVH**
51 GVATVAEKTK EQVTNVGGAV VTGVTAVAQK TVEGAGSIAA ATGFVKKDQL
101 GKNEEGATQE GILEDMPVDP DNEAYEMPSE EGYQDYEPEA

Figure 6-9:Identification of tryptic peptides of α-syn using Mascot database search engine. Mascot search results of α-syn digested from the monomeric band (A), and from dimeric band (B).

Interestingly, two regions were not mapped, corresponding to ${}_{7}$GLSKAK${}_{12}$ and ${}_{35}$EGVLYVGSK${}_{43}$ in the α-syn dimer peptides (Figure 6-9, B). The second region contained Y39, and one explanation for the absence of this sequence from all the mass spectrometry data is that Y39 is oxidised and as a result a dityrosine cross-link was formed. As dityrosine exhibits high protease resistance, the mentioned peptide fragment was not released and instead a dimeric form of the ${}_{35}$EGVLYVGSK${}_{43}$ peptide is released, indicating the involvement of Y39 to form homo dimer α-syn. This proposal was confirmed by the appearance of a peak at *m/z* 1179.6127 and identified to be a dimer peptide of ($_{33}$TKEGVLYVGSK$_{43}$) as shown in Figure 6-10.

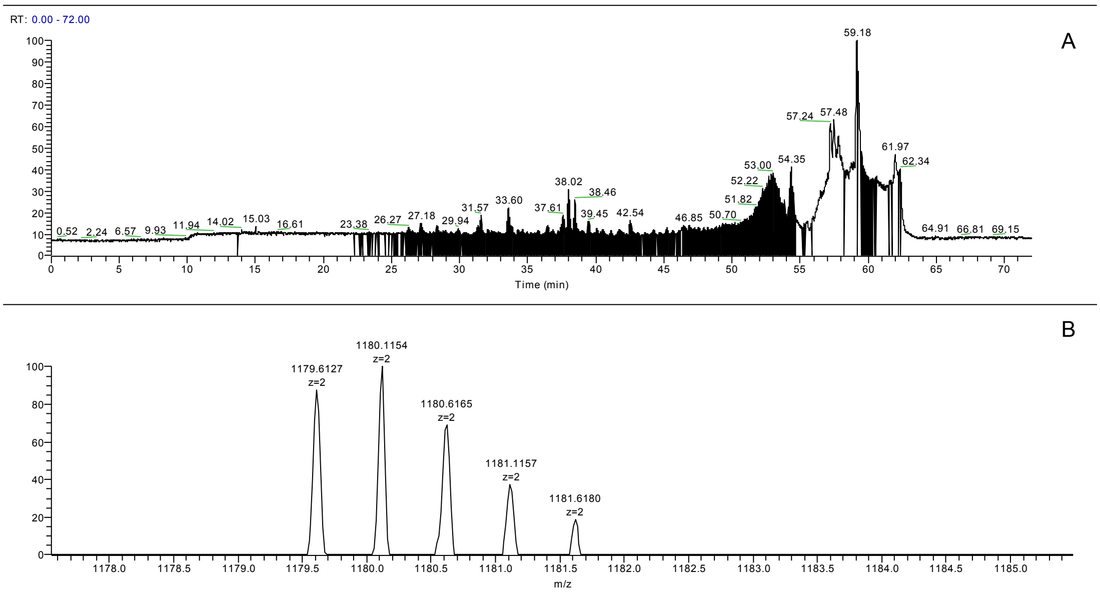

Figure 6-10: NanoLC-MS/MS chromatogram (A) of tryptic digested α-syn dimer that extracted from electrophoresis gel. Mass spectrum (B) showing the appearance of a peak at m/z 1179.6127 that corresponds to the dimer of the peptide with sequence of ($_{33}$TKEGVLYVGSK$_{43}$).

The involvement of Y39 in the formation of hetero dimer, i.e. Y39-Y125, Y39-Y133 or Y136, was also analysed and showed no evidence of formation of these peptide links. Furthermore, the Mascot data showed the presence of the regions that contained Y125, Y133, and Y136 in both monomeric and dimeric α-syn that indicates that α-syn dimer results from crosslinking between Y39 from two molecules to form a dimer.

Quenched hydrogen/deuterium exchange NMR spectroscopy has been used to study the structure of α-syn in its amyloid state and identified five β-strands within the fibril core, comprising residues 35–96 and termed aSβ1, aSβ2, aSβ3, aSβ4 and aSβ5 (Vilar et al. 2008). Tyrosine at position 39 was involved in the formation of aSβ1, while tyrosine residues at 125, 133, and 136 did not contribute towards the formation of any β-strand. Recently, the first region aSβ1, consisting of $_{37}$VLYVGSKT$_{44}$ was studied using XRFD and it was found that at high concentrations the peptide forms nanotubular cross-β assemblies (Morris et al. 2013a). Interestingly, the proposed structural model of these nanotubes revealed that peptide packing and inter-sheet Tyr interactions were involved to stabilise the tape width (Figure 6-11) (Morris et al. 2013a). Also, the model shows that the orientation of the phenol groups of Tyr residues is in agreement with the formation of inter-sheet dityrosine cross-links, however, it is important to keep in mind this may be not true in full length α-syn.

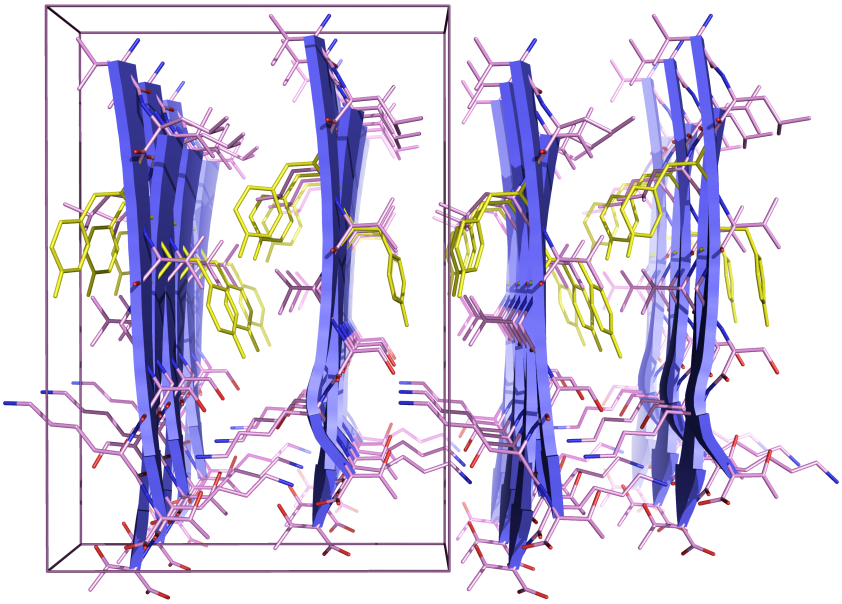

Figure 6-11: The structural model of aSβ1 showing the peptide packing within the fibrils and revealed that inter-sheet Tyr interactions were involved to stabilise the tape width. The model was constructed based on XRFD analysis. Adapted from (Morris et al. 2013a).

Recently, dityrosine cross-linked α-syn oligomers have been formed by PICUP using tris(bipyridine) ruthenium(II) chloride complex as a photosensitiser and these oligomers exhibited high toxicity effects on differentiated neuronal-like SH-SY5Y cells, indicating the importance of the tyrosine residue oxidative modification in the etiology of PD (Borsarelli et al. 2012). Interestingly, using western blot, they showed no intramolecular dityrosine formation in the monomeric band of α-syn and this could be due to the specificity of the PICUP method used to induce dityrosine formation, or the sensitivity of immunochemistry assay. The photo-enhanced α-syn dimer was cross-linked via Y39-Y39 to give homo dimer peptide and Y39-Y125, Y133 and Y136 to give hetero dimer peptide (Borsarelli et al. 2012). The mass spectrometry data in our hands revealed no such hetero dimer peptide formation and could be interpreted as due to the variation in the specificity of the oxidation conditions used to induce the dityrosine formation in α-syn.

6.2.3 α-syn fibrillogenesis and conformation upon incubation with Cu^{2+} ions

Figure 6-3 reveals that incubation of recombinant human α-syn monomers in both the absence and presence of Cu^{2+} ions generate dityrosine cross-links, and that in the case of the presence of Cu^{2+} ions, fibril formation was accelerated. In order to gain insights into the role played by Cu^{2+} ions and to probe both structural and morphological developments of the generated α-syn fibrils, further studies were carried out using 100 and 400 μM α-syn incubated with 100 and 400 μM Cu^{2+} respectively. The samples were then analysed over two weeks using ThT fluorescence, TEM, and CD (Figure 6-12). After one week of incubation, α-syn fibrils formed when incubated in the presence of Cu^{2+}, whereas no α-syn fibrils were detected by TEM or ThT fluorescence in the sample incubated under control conditions, as shown in Figure 6-12. ThT fluorescence spectra of Cu^{2+}-induced α-syn fibrils revealed a significant increase in intensity over the two week incubation period (Figure 6-12, E), revealing α-syn fibril formation after seven days of incubation, and this was further confirmed by observation of fibrils in TEM images (Figure 6-12, D), which showed formation of α-syn fibrils that are of a similar appearance to those formed using 50 μM Cu^{2+} (Figure 6-4, C). This contrasted with the α-syn that was incubated in buffer only, which showed no evidence of fibril formation using both TEM and ThT (Figure 6-12, A and B respectively). Interestingly, after two weeks of incubation, TEM micrographs of Cu^{2+}-induced α-syn fibrils showed distinct morphological changes (Figure 6-12, D), with more dense, short fibrils formed, with needle-like structures. In contrast, α-syn fibrils formed under control condition are similar to those previously seen in other studies (Celej et al. 2012; Serpell et al. 2000a; Wright et al. 2009), which showed a uniform, long and unbranched morphology, with some twisting fibrils (Figure 6-12, A). Fewer fibrils were observed compared with those formed under the Cu^{2+}-containing buffer. To investigate whether α-syn fibrils aged under the Cu^{2+}-containing buffer underwent a conformational development over time, CD spectra were acquired and revealed that after two weeks of incubation assembled α-syn fibrils still have a random coil structure (Figure 6-12, F), and a similar conformation was observed for those aged under control condition (Figure 6-12, C). However, a noticeable decrease in the CD signal at ~ 200 nm was observed for those aged with Cu^{2+} ions (Figure 6-12, F), indicating the presence of less soluble α-syn with random coil structure compared to those aged under control conditions.

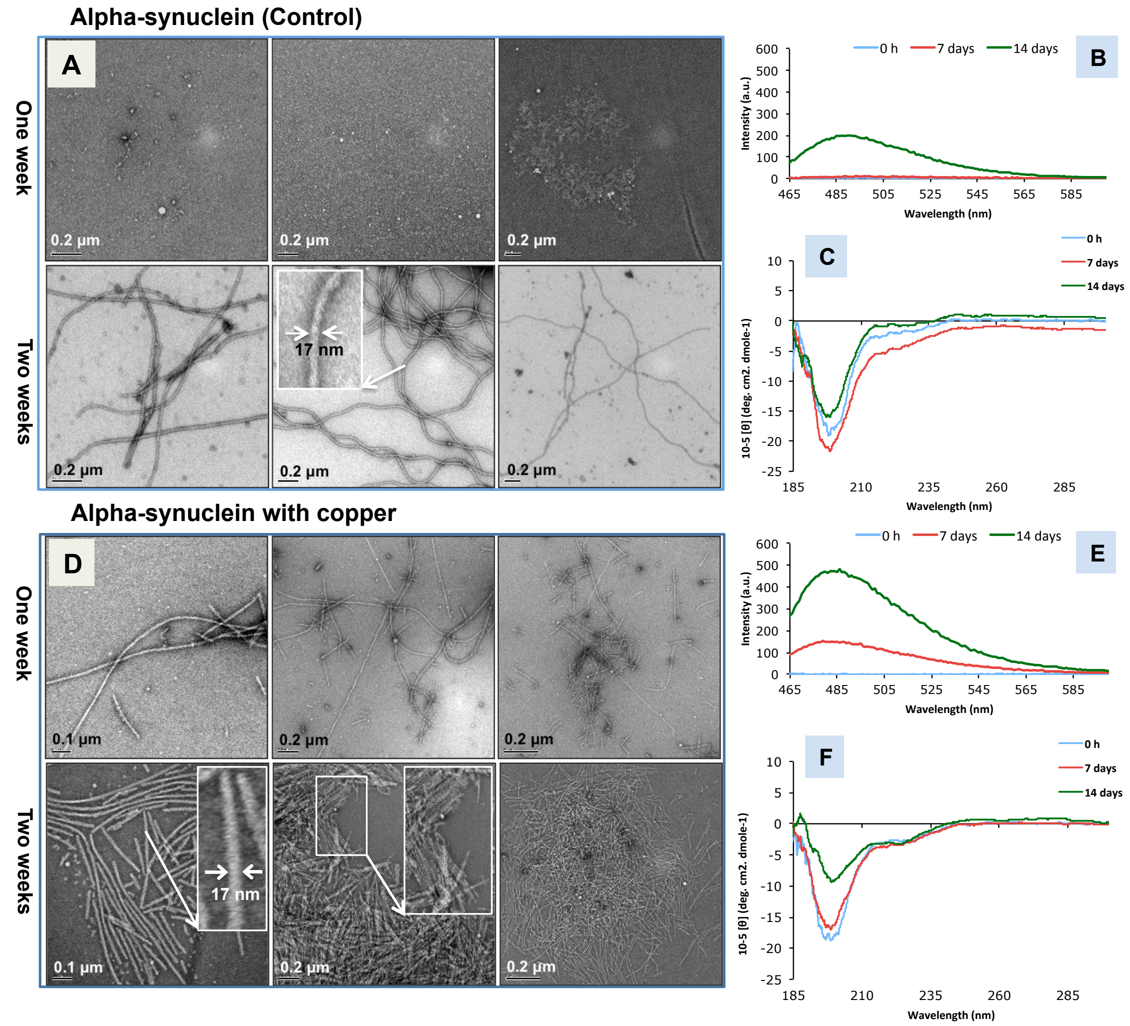

Figure 6-12: 100 µM of monomeric human α-syn incubated in the absence and presence of 100 µM Cu^{2+}in 20 mM HEPES buffer, pH 7.4 at 37 ºC with agitation of 400 rpm. Assembled α-syn fibrils analysed for their growth and structure using ThT, TEM, and CD. TEM micrographs of α-syn fibrils that formed from incubation of α-syn monomers in HEPES buffer only (A) and in Cu^{2+}-containing buffer (D), showing that the presence of Cu^{2+} accelerates the fibril formation. The growth of α-syn fibrils was also monitored using ThT fluorescence in presence (E) and absence (B) of Cu^{2+}. CD spectra of α-syn were recorded upon incubation in HEPES buffer only (C) and in Cu^{2+}-containing buffer (F) and revealed a random coil structure in both cases.

It has been shown that α-syn fibril growth is concentration dependent (Serpell et al. 2000a), where α-syn fibril growth and conformation were assayed using many techniques, including CD, ThT fluorescence, TEM and XRFD. In this current study, fibrillar α-syn was obtained by incubation of 400 µM monomeric recombinant human α-syn in the absence or presence of 400 µM Cu^{2+} using 20 mM HEPES buffer, pH 7.4 with agitation at 450 rpm and a temperature of 37 ºC. Both ThT fluorescence data and TEM images confirmed α-syn fibril formation under control and Cu^{2+}-containing buffer conditions after 120 h of incubation (Figure 6-13), and again revealed that incubation with Cu^{2+} markedly accelerates fibril formation (Figure 6-13, C). A secondary structure measurement of Cu^{2+}-induced α-syn fibrils by CD reveals no significant conformational change over the incubation period (Figure 6-13, D), but, in contrast, the CD spectra from control α-syn fibrils showed a transition from the unfolded conformation, which is characterised by a maximum negative ellipticity at ~ 200 nm, to a β-sheet conformation with a minimum at ~ 218 nm (Figure 6-13, B).

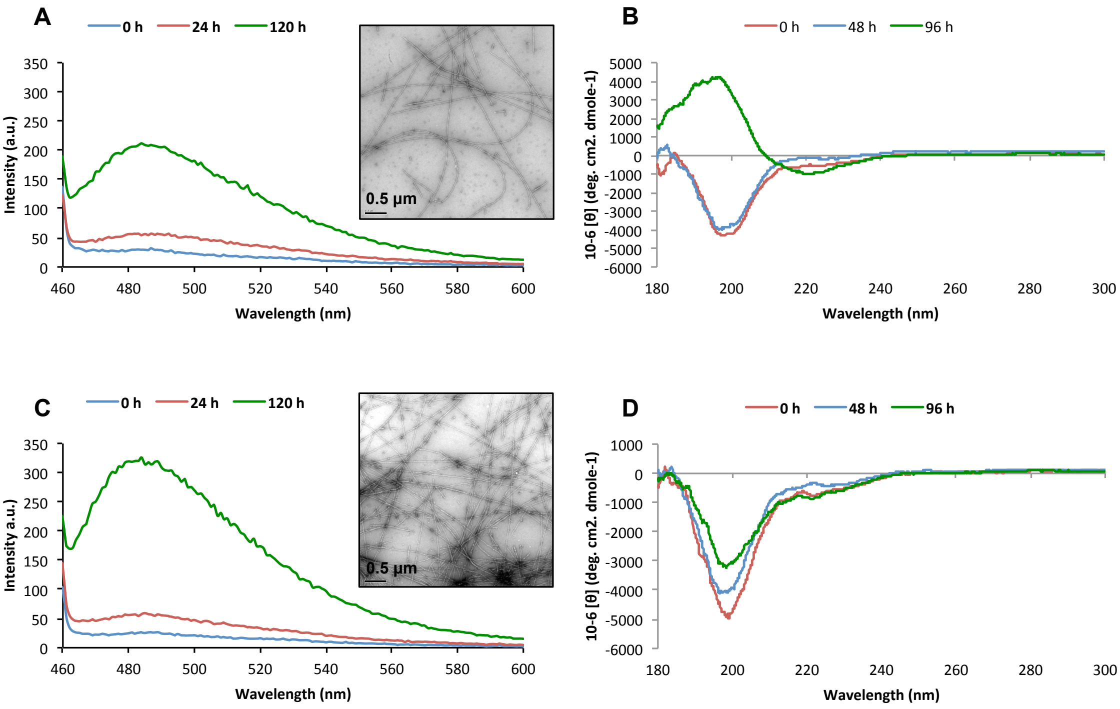

Figure 6-13: Cu^{2+} ions affect α-syn fibril growth and structure. Addition of Cu^{2+} ions to the monomeric α-syn enhanced fibril growth as shown in ThT spectra (C). Cu^{2+}-depleted solution of α-syn shows less fibril content (A). However, TEM images reveal no significant morphological changes over incubation of α-syn with Cu^{2+}, but more fibrils were formed upon incubation. The CD spectra of α-syn fibrils grown in 20 mM HEPES buffer, pH 7.4 with 450 rpm agitation show a conversion from random coil to β sheet structure after 96 h of incubation (B), whereas α-syn fibrils grown in Cu^{2+}-containing buffer did not show this conversion (D), although a significant decline at ~ 200 nm band was obtained after 96 h of incubation.

To verify that the samples contained the expected cross-β amyloid fibrils, XRFD patterns were collected for both α-syn fibrils incubated with Cu^{2+} ions and those which assembled without Cu^{2+} ions following a desalting process by centrifuging for 30 mins at 20,000 g and 4 ºC (see 2.4.12). The XRFD patterns showed the expected cross-β conformation, the characteristic shared feature of both amyloid and amyloid-like fibrils

(Conway et al. 2000; Serpell et al. 1999; Sunde et al. 1997), for both Cu^{2+}-enhanced α-syn fibrils (Figure 6-14, B) and control α-syn fibrils (Figure 6-14, A). Meridional reflections at 4.76 and 2.4 Å were observed in patterns from fibrils assembled under both control (i.e. without Cu^{2+}) and Cu^{2+}-containing conditions. Moreover, a set of reflections at ~ 8.1, 9.5 and 19.4 Å were observed on the equator, similar to those reported in a previous study (Serpell et al. 2000a), confirming the formation of α-syn fibrils with cross-β structure. However, the XRFD for Cu^{2+}-enhanced α-syn fibrils (Figure 6-14, B) revealed a new reflection at ~ 35 Å and also showed more intense reflections attributable to the formation of more aligned fibrils compared to those assemblies incubated under control conditions. TEM micrographs revealed a higher density of Cu^{2+}-enhanced α-syn fibrils that also appeared to have a more ordered, rigid appearance (Figure 6-13, C). This provided more evidence that the Cu^{2+} ion plays a vital role in accelerating α-syn fibril formation and may affect the final structure.

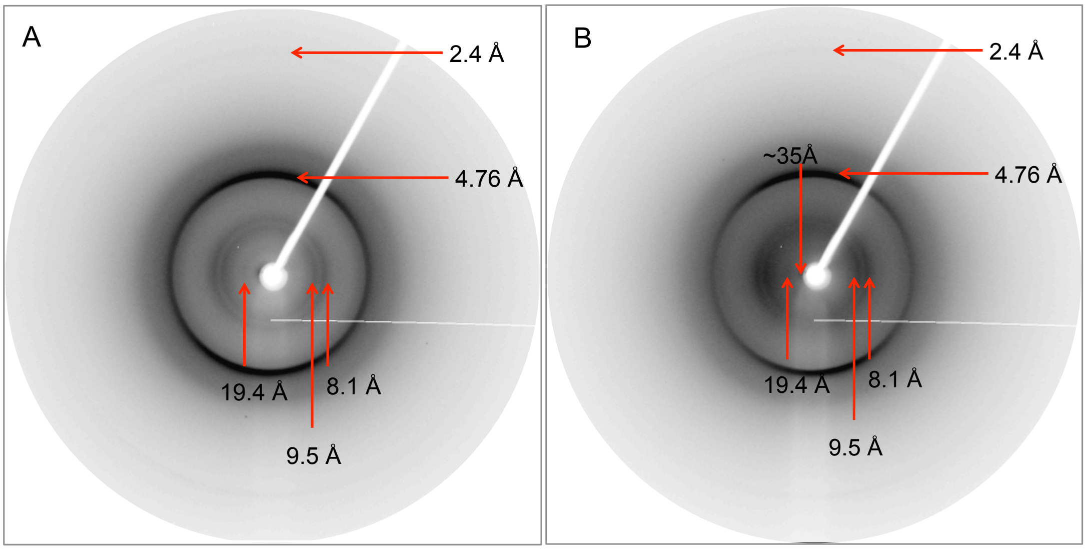

Figure 6-14: X-ray fibre diffraction patterns of α-syn fibrils showing cross-β structure. X-ray fibre diffraction patterns were collected for α-syn fibrils formed by incubation of 400 µM recombinant α-syn monomer in 20 mM HEPES buffer, pH 7.4 alone (A) and in 20 mM HEPES containing 400 µM Cu^{2+} (B).

The cross-β diffraction pattern was first shown for insect silk (Geddes et al. 1968), and it demonstrated that the cross-β reflections consist of a meridional reflection at ~ 4.7 Å corresponding to the inter-chain spacing, and an equatorial reflection located in the 5 - 10 Å region, which represents the spacing between the β-sheets. This distance is dependent upon the size of the side chains (Figure 6-15). The assembly properties and secondary structure features of recombinant α-syn have been assessed using XRFD, CD and electron diffraction (Serpell et al. 2000a), which showed that α-syn assemblies display a cross-β conformation characteristic of amyloids. It is clear from the XRFD pattern of Cu^{2+}-enhanced α-syn fibrils (Figure 6-13, C) that those fibrils showed a cross-β conformation contrasted to their CD spectra that revealed a random coil structure corresponding to the negative band at ~ 200 nm (Figure 6-13, D). However, the decline in the 200 nm signal observed upon incubation time would suggest that those fibrils precipitated out of the buffer and the CD was recorded just for the buffer-soluble α-syn aggregates.

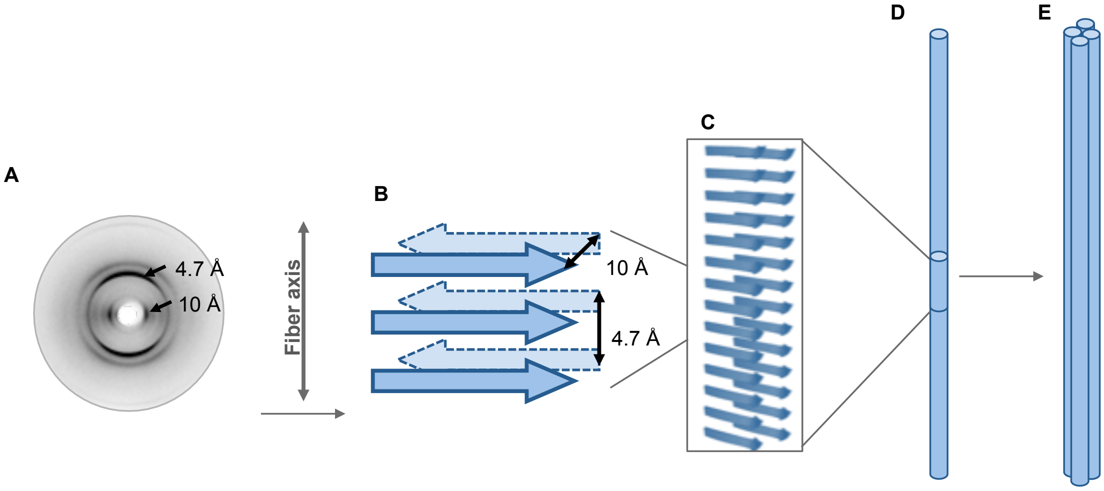

Figure 6-15: Schematic diagram illustrating the X-ray fibril diffraction analysis. Provided by Prof. Louise Serpell.

6.3 **Conclusion**

PD is the second most common neurodegenerative disease after AD among the ageing human population (Tanner and Goldman 1996). Copper has been found to decrease in the substantia nigra and increase in the CSF of PD patients (Barnham and Bush 2008; Pall et al. 1987). A large body of data shows that α-syn is a metalloprotein and can bind Cu^{2+} and that Cu^{2+} can promote α-syn aggregation efficiently (Ahmad et al. 2012; Binolfi et al. 2006; Rasia et al. 2005). In addition, a role was suggested for Cu^{2+} in the catalysis of oxidative oligomerisation and subsequent α-syn aggregation in the presence of H_2O_2 (Paik et al. 2000). Oxidative stress is implicated in the pathogenesis of PD. Oxidative modification of tyrosine residues plays a vital role in the α-syn aggregation via protein cross-linking. In this chapter, *in vitro* dityrosine cross-linked α-syn, which is formed through coupling of two tyrosyl radicals, was formed under oxidative stress conditions of Cu^{2+}/H_2O_2, which are more physiologically relevant than other conditions used to oxidise the α-syn, such as PICUP. The covalently cross-linked dimer was isolated and characterised to contain dityrosine. The mass spectrometry analysis showed that dityrosine dimer was formed via the coupling of Y39-Y39 to give homo dimer peptide. Incubation of α-syn in both Cu^{2+}-depleted and Cu^{2+}-containing buffer revealed a remarkable appearance of dityrosine signal at 410 – 420nm, indicating the possible involvement of dityrosine cross-links in the mechanism underlying α-syn aggregation and accumulation in PD. The suggested role played by these dityrosine oligomers in the aggregation and fibrillogenesis of α-syn is explained in the schematic diagram below, and it is proposed that dityrosine cross-linked α-syn dimers could serve as nuclei to initiate the polymerisation of α-syn monomers resulting in α-syn fibril formation (Figure 6-16).

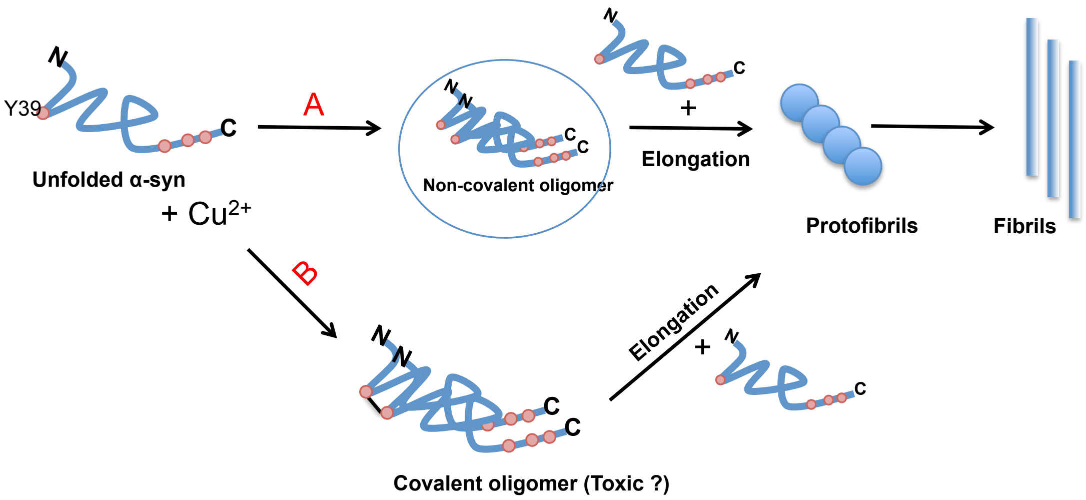

Figure 6-16: Schematic of a proposed mechanism explaining the suggested role of dityrosine cross-linked α-syn dimers in the fibrillation of α-syn. Fibrillation of α-syn was demonstrated as a nucleation-dependent process (Fernandez et al. 2004). In vitro, at high concentrations of α-syn, the non-covalent aggregates provide seeds to initiate the polymerisation of α-syn to form fibrils as shown in path A. By contrast, at low concentration of α-syn these non-covalent oligomers become less available and thus the fibrillation of α-syn takes longer to develop. Formation of covalent oligomers represents an alternative mechanism (path B) that may be important at low concentrations. These covalent oligomers are represented by Y39-Y39 coupling, which is formed as a consequence of oxidative stress, could represent the toxic forms of α-syn, and also serve as a nucleus for α-syn fibrillation.

7 Discussion and Future work

The work presented here describes the importance of oxidative modification of tyrosine residues to form dityrosine cross-links in a range of amyloidogenic peptides/proteins from naturally derived to designer, and eventually establishes the role of dityrosine cross-links in the pathogenesis of AD and PD. It has been revealed that oxidative stress may play a vital role in the pathogenesis of many neurodegenerative diseases including AD and PD. High levels of oxidative stress can be produced as a consequence of metal-protein interactions leading to protein misfolding and cross link formation. Increasing evidence points to the pivotal role of the Cu^{2+} ion in Aβ and α-syn misfolding and aggregation. However, no previous comprehensive *in vitro* and *in vivo* study has been carried out to establish the role played by dityrosine cross-links in amyloid fibril formation and to explain the link between dityrosine cross-links and misfolding of amyloidogenic proteins, such as Aβ and α-syn, leading to amyloid assembly. The research aims here were firstly, synthesis of dityrosine as a standard for comparison, as it is commercially not available. Secondly, testing the Cu^{2+}/H_2O_2 oxidation system using two short peptides as model system, which can provide more information about the nature of oxidative modification under Cu^{2+}/H_2O_2 oxidation system. Finally, *in vitro* and *in vivo* investigation of dityrosine cross-links in Aβ and α-syn examined the affects on fibril stability and morphology providing more details to enhance our understanding of the putative role played by dityrosine cross-links in Aβ and α-syn misfolding and subsequently in the pathogenesis of AD and PD. Furthermore, the work included testing the possibility of using dityrosine cross-linked Aβ as a biomarker of oxidative stress in AD and to detect the early stages of AD.

In this work, authentic dityrosine was synthesised chemically and enzymatically and identified using different analytical techniques including RP-HPLC, mass spectrometry, fluorescence spectrophotometry, and NMR spectroscopy. Later on it was used in the rest of our study as a standard. Moreover, LC-ESIMS/MS method using MRM mode, which has high sensitivity and selectivity, was used in order to detect dityrosine cross-linking in samples of interest.

A fine balance of conditions will be required for optimising the production of dityrosine cross-links. In the current study, the oxidative modification of two short peptides, HYFNIF and VIYKI, using Cu^{2+}/H_2O_2 oxidation system was explored, and also the morphological and conformational changes of these amyloid fibrils over the oxidation process was studied. Both HYFNIF and VIYKI serve as useful and worthwhile model systems to examine the ability of Cu^{2+}/H_2O_2 to induce tyrosine residue modifications and to form dityrosine cross-links. Both HYFNIF and VIYKI have been previously structurally characterised using many biophysical techniques (Morris et al. 2013b), and therefore provide excellent starting point for further study. The results and conclusions drawn demonstrate how these models can provide a wealth of information on what drives the formation of dityrosine cross-links. Many factors can significantly affect the oxidation process using Cu^{2+}/H_2O_2 and the most important are buffer composition and pH. Phosphate buffer appears to be more suited for the oxidation than HEPES, and this can be explained in context of Cu^{2+}/ peptide complex stability. It has been found that Cu^{2+}ions can form more stable complexes in HEPES buffer (Tougu et al. 2008), and this can affect the free radical generation. The pH of the oxidation environment has a strong influence on the dityrosine production and this is due to the net peptide charge. It is important to generate a neutral or negatively charged peptide to facilitate the coordination with Cu^{2+} ions. At pH 7.4, HYFNIF and VIYKI peptide have more neutral net charge (0.1 and 0.8 respectively) than that in water (1.2 for HYFNIF and 1.1 for VIYKI), where the pH is more acidic (the pI of HYFNIF and VIYKI fibrils are 8.0 and 10.3 respectively). As a result, Cu^{2+}-peptide complexes can be easily generated at pH 7.4, subsequently these complexes can catalyse the tyrosine cross-linking and that may explain why a lower dityrosine yield was obtained at acidic pH in water compared to more efficient dityrosine formation at pH 7.4.

The presence of dityrosine in oxidised fibrils was confirmed using LC-ESIMS/MS following acid hydrolysis of the oxidised VIYKI and HYFNIF fibrils. It appears that once dityrosine cross-links form they do not revert back to monomers, indicating that they are very stable. Several studies reported that dityrosine exhibits protease resistance, supporting our results that the dityrosine cross-link is stable (Amado et al. 1984; Giulivi and Davies 1994).

The results showed that VIYKI fibrils have a greater ability than HYFNIF fibrils to oxidise and produce dityrosine cross-links, and also demonstrated that the preorganised fibrils can enhance dityrosine formation by bringing two tyrosine residues close enough to cross-link covalently. The results are in good agreement with XRFD models of HYFNIF and VIYKI fibrils from a previous study (Morris et al. 2013b), which revealed that phenolic groups of the tyrosine residues in VIYKI fibrils are packing closely together (Figure 4-19) and become close in proximity that allows tyrosine cross-linking to be more favorable (Morris et al. 2013b). In contrast, the structural model of HYFNIF fibrils revealed that side chain of tyrosine residues are organised away from each other (Figure 4-19) and as a consequence, dityrosine formation was more restricted. Although the CD and TEM data of the oxidised fibrils revealed interesting structural and morphological changes upon the oxidation processes, no dityrosine characteristic signal was observed in CD.

Both Aβ and α-syn can undergo modification to yield species that are toxic and also these modifications can facilitate the conversion of Aβ and α-syn from non-amyloidogenic to an amyloidogenic state. The fundamental questions are; what is the identity of the toxic species and what is the mechanism that underlies the formation of amyloid fibrils? These questions can be possibly answered through the oxidative modification of Aβ and α-syn that leads to protein cross-linking.

The *in vitro* experimental model presented here can help to understand the early events leading to chemical, structural and conformational modifications before the conversion of soluble Aβ and α-syn to insoluble amyloid fibrils and eventually the formation of senile plaques in AD and Lewy bodies in PD respectively. In turn, this could help to design a new inhibitor (e.g. antioxidant) for Aβ and α-syn deposition process and identify a potential biomarker for early AD and PD. Herein, we have explored the role of Cu^{2+} ions in the formation of dityrosine cross-links in Aβ and α-syn using many different techniques, including fluorescence spectrophotometry, HPLC, mass spectrometry, transmission electron microscopy, immunogold labelling, and CD.

In chapter 5, I present a comprehensive study of *in vivo* and *in vitro* dityrosine cross-linking associated with Aβ. We have revealed for the first time the presence of dityrosine cross-links in amyloid plaques in human AD brain, and also in CSF, and identified significant relationships between dityrosine cross-links and amyloid deposit formation. The *in vitro* and *in vivo* results presented here reveal that oligomeric Aβ can undergo oxidative modifications in a cellular environment, resulting in cross-linked Aβ through dityrosine followed by intralysosomal Aβ accumulation that could lead to lysosomal leakage and cell death. Our results show the significant accumulation of dityrosine crosslinked Aβ in amyloid plaques, implying a role in stabilisation of these insoluble deposits. This hypothesis was confirmed *in vitro* by testing the stability of Aβ fibrils induced under Cu^{2+}/H_2O_2 conditions and showed higher stability compared with that formed in control conditions. We have also shown a potential biomarker for AD in CSF, which contains elevated dityrosine crosslinked proteins as well as elevated dityrosine crosslinked Aβ. Our preliminary findings show that dityrosine crosslinks were increased in lipofuscin in AD brain, indicating the important role played by dityrosine crosslinks in the accumulation of lipofuoscin in higher levels in AD compared to control subjects. Also, our results have revealed very strong evidence for the presence of both Aβ and dityrosine in CSF from AD patients and both Aβ and dityrosine are very rarely observed in CSF from age-matched controls. Therefore, we suggest that this could represent a potential biomarker for AD. A few studies have previously attempted to quantify dityrosine in cerebrospinal fluid. Techniques including HPLC with fluorescence detection, HPLC with electrochemical array detection (HPLC-ECD) or fluorescence detection, and liquid chromatography with triple quadrapole mass spectrometric detection (LC-MS/MS) have been applied to quantify dityrosine concentrations in CSF sample from both healthy and disease affected subjects (Abdelrahim et al. 1997; Ahmed et al. 2005; Hensley et al. 1998). However, the results of these studies have been conflicting, perhaps due to differences in sample handling and preparation before measuring. Quantitative screening of protein glycation, oxidation and nitration adducts in CSF of AD and healthy age-matched subjects have been taken to suggest that dityrosine concentration does not change in AD patients with respect to control subjects (Ahmed et al. 2005). By contrast, earlier studies using electrochemical detection showed that dityrosine concentration was elevated markedly in CSF of AD patients (Hensley et al. 1998).

The plausibility of dityrosine cross-linking has been illustrated as a possible mechanism for the formation of Aβ aggregates (Atwood et al. 2004), thus dityrosine would be highly localised with Aβ at plaque sites. Many studies focused on measuring the dityrosine levels in whole brain section in AD, and their results conflicted. While some showed elevated dityrosine levels in AD affected brain (Hensley et al. 1998), others failed to show any significant elevation (Bucknall 2006). Plaques represent only a small proportion of whole AD affected brain, so dityrosine cross-linked protein in whole brain might not be measurably elevated. In this work, we have revealed a novel observation of the presence of dityrosine cross-links in amyloid plaques in human AD brain. This observation provides strong evidence of implying of dityrosine in the Aβ aggregation and subsequently plaque formation in the brain of AD patients.

The ability of the Cu^{2+} ion to promote the formation of *in vitro* dityrosine cross-linked α-syn was explored and the effect on α-syn fibrillogenesis and conformation that is induced by the Cu^{2+} ion was investigated. The role of dityrosine as a covalent cross-linker was revealed using a number of techniques including fluorescence spectroscopy, HPLC, LC-ESIMS/MS, SDS-PAGE, TEM, XRFD and CD. *In vitro* dityrosine cross-linked α-syn, which formed through coupling of two tyrosyl radicals, was formed under oxidative stress condition of Cu^{2+}/H_2O_2. The covalently cross-linked dimer was isolated by SDS-PAGE and characterised by nanoLC-MS/MS following tryptic digestion to be dityrosine. The mass analysis showed that dityrosine dimer was formed via the coupling of Y39-Y39 to give a homo dimer peptide. Incubation of α-syn in both Cu^{2+}-depleted and Cu^{2+}-containing buffers revealed the remarkable appearance of a dityrosine signal at 410 – 420 nm, indicating the possible involvement of dityrosine cross-links in the mechanism underlying the α-syn aggregation and accumulation in PD. α-syn fibrillogenesis is a nucleus dependent process. Thus the dityrosine cross-linked α-syn dimers can serve as nuclei to initiate the polymerisation of α-syn monomers resulting in α-syn fibril formation. This hypothesis is supported by finding that dityrosine cross-linked α-syn dimer formation is the critical rate-limiting step for α-synuclein fibrillogenesis in PD (Krishnan et al. 2003).

For a long time, it was believed that insoluble Aβ fibrillar deposition found in extracellular amyloid plaques initiated the neurodegenerative cascades of AD. However, a recent view is that prefibrillar soluble oligomeric Aβ species are the key intermediates in AD-related the observed synaptic disorder (Caughey and Lansbury 2003; Klein 2006). Various amyloidogenic proteins, such as Aβ and α-syn, can produce toxic soluble oligomers, proposing that soluble oligomeric species are the general key factors in various amyloidosis diseases such as AD and PD (Haass and Selkoe 2007; Kayed et al. 2003; Sorgjerd et al. 2008). However, both Aβ and α-syn oligomers can be formed through interactions between two tyrosine residues to form dityrosine cross-links and this may represent one of the pathways by which stable oligomers are generated.

Further work in the area of dityrosine cross-linked Aβ measurement in the AD brain using LC-MS/MS should focus on extracted plaques rather than whole brain tissues and measurement of the dityrosine levels. Isolation and identification of dityrosine cross-linked Aβ using various techniques such as western blot or mass spectrometry would further confirm our results, however, it is important to keep in mind that the plaque isolation process can affect the chemical and biochemical structure of plaques and that in turn could affect analysis of the samples. On the other hand, the immunogold-labelling procedure reduces the possibility of artifacts from the isolation procedure and enables the examination of the *in vivo* dityrosine cross-linked species as they are, to provide a clearer, more physiologically relevant view. Further toxicity studies with early stage oligomeric species and fibrils that may provide a better understanding about the identity of the toxic species. Testing some compounds that inhibit the dityrosine cross-link formation using a model AD or PD would give more a clear view about the importance of dityrosine cross-linking in the etiology of neurodegenerative diseases. The potential use of dityrosine as a biomarker of oxidative stress in AD and PD remains unresolved, but work is currently aiming to confirm this using immunogold labelling quantification, particularly in early cases of AD and also would surely bring us closer to confirming that by quantification using LC-MS. In addition, it would be ideal to estimate the limit of detection for dityrosine using LC-MS.

Although many studies demonstrated that dityrosine cross-linked α-syn species reduce the yield of amyloid fibrils (Borsarelli et al. 2012; Ruf et al. 2008), dityrosine formation has been described to be the critical rate-limiting step in α-syn fibrillogenesis (Krishnan et al. 2003). These results appear to be in conflict and this could be interpreted by the variation of the *in vitro* oxidative stress conditions that have been used to form the dityrosine cross-link. Also, there are many factors that can affect the lag duration such as α-syn concentration, buffer composition and pH, and temperature (Fink 2006; Lee et al. 2007a; Roberti et al. 2009). In order to gain better understanding of the relationship between dityrosine oligomer formation and α-syn fibrillogenesis, it would be ideal to use *in vitro* oxidative stress conditions that mimic the *in vivo* conditions. Also, it would be very important to detect dityrosine cross-linked α-syn *in vivo* using a similar method we have used for dityrosine cross-linked Aβ in brain and CSF samples of AD, and also try to isolate it from Lewy bodies in PD.

More structural measurement, e.g. LD, can be applied to discover whether dityrosine has a unique LD signal and consequently enhance our understanding of the structural role for dityrosine as a cross-linker in the protein. Moreover, more precise details could be gained by using a pure dityrosine cross-linked peptide. As dityrosine is intrinsically fluorescent, more evidence can be gained using confocal microscopy about whether the dityrosine can be intra- or inter fibrils. Thereby dityrosine cross-linked protein could potentially be monitored in the cell using confocal microscopy.

Bibliography

Abdelrahim, M., et al. (1997), 'Liquid chromatographic assay of dityrosine in human cerebrospinal fluid', *Journal of Chromatography B,* 696 (2), 175-82.

Abe, H. and Nakanishi, H. (2003), 'Novel observation of a circular dichroism band originating from amyloid fibril', *Anal Sci,* 19 (1), 171-3.

Adamec, E., et al. (2000), 'Up-regulation of the lysosomal system in experimental models of neuronal injury: Implications for Alzheimer's disease', *Neuroscience,* 100 (3), 663-75.

Agholme, L., et al. (2012), 'Amyloid-beta secretion, generation, and lysosomal sequestration in response to proteasome inhibition: involvement of autophagy', *J Alzheimers Dis,* 31 (2), 343-58.

Ahmad, A., et al. (2012), 'Peculiarities of copper binding to alpha-synuclein', *J Biomol Struct Dyn,* 29 (4), 825-42.

Ahmed, N., et al. (2005), 'Protein glycation, oxidation and nitration adduct residues and free adducts of cerebrospinal fluid in Alzheimer's disease and link to cognitive impairment', *Journal of Neurochemistry,* 92 (2), 255-63.

Al-Hilaly, Y., et al. (2013), 'A central role for dityrosine crosslinking of Amyloid-beta in Alzheimer's disease', *Acta Neuropathologica Communications,* 1 (1), 83.

Ali, F. E., et al. (2003), 'Copper catalysed oxidation of amino acids and Alzheimer's disease', *Letters in Peptide Science,* 10 (5-6), 405-12.

Ali, F. E., et al. (2004), 'Metal catalyzed oxidation of tyrosine residues by different oxidation systems of copper/hydrogen peroxide', *Journal of Inorganic Biochemistry,* 98 (1), 173-84.

Ali, F. E., et al. (2005), 'Methionine regulates copper/hydrogen peroxide oxidation products of Abeta', *J Pept Sci,* 11 (6), 353-60.

Alzheimer, A. (1904), *Histologische Studien zur Differentialdiagnose der progressiven Paralyse* (G. Fischer).

Alzheimer, A., et al. (1995), 'An English translation of Alzheimer's 1907 paper, "Uber eine eigenartige Erkankung der Hirnrinde"', *Clin Anat,* 8 (6), 429-31.

Amado, R., Aeschbach, R., and Neukom, H. (1984), 'Dityrosine - Invitro Production and Characterization', *Methods in Enzymology,* 107, 377-88.

Amdursky, N., Erez, Y., and Huppert, D. (2012), 'Molecular Rotors: What Lies Behind the High Sensitivity of the Thioflavin-T Fluorescent Marker', *Accounts of Chemical Research,* 45 (9), 1548-57.

Amiry-Moghaddam, M. and Ottersen, O. P. (2013), 'Immunogold cytochemistry in neuroscience', *Nat Neurosci,* 16 (7), 798-804.

Andersen, S. O. (1964), 'Cross-Links in Resilin Identified as Dityrosine & Trityrosine', *Biochimica Et Biophysica Acta,* 93 (1), 213-15.

Andreyev, A. Y., Kushnareva, Y. E., and Starkov, A. A. (2005), 'Mitochondrial metabolism of reactive oxygen species', *Biochemistry (Mosc),* 70 (2), 200-14.

Anfinsen, C. B. (1973), 'Principles that govern the folding of protein chains', *Science,* 181 (96), 223-30.

Atwood, C. S., et al. (2000), 'Characterization of copper interactions with Alzheimer amyloid beta peptides: Identification of an attomolar-affinity copper binding site on amyloid beta 1-42', *Journal of Neurochemistry,* 75 (3), 1219-33.

Atwood, C. S., et al. (1998), 'Dramatic Aggregation of Alzheimer AŒ≤ by Cu(II) Is Induced by Conditions Representing Physiological Acidosis', *Journal of Biological Chemistry,* 273 (21), 12817-26.

Atwood, C. S., et al. (2004), 'Copper mediates dityrosine cross-linking of Alzheimer's amyloid-beta', *Biochemistry,* 43 (2), 560-8.

Bailey, A. J. (1991), 'The chemistry of natural enzyme-induced cross-links of proteins', *Amino Acids,* 1 (3), 293-306.

Balbach, J. J., et al. (2002), 'Supramolecular structure in full-length Alzheimer's beta-amyloid fibrils: evidence for a parallel beta-sheet organization from solid-state nuclear magnetic resonance', *Biophys J,* 83 (2), 1205-16.

Banerjee, S. and Mazumdar, S. (2012), 'Electrospray ionization mass spectrometry: a technique to access the information beyond the molecular weight of the analyte', *International journal of analytical chemistry,* 2012, 282574.

Barnham, K. J. and Bush, A. I. (2008), 'Metals in Alzheimer's and Parkinson's diseases', *Curr Opin Chem Biol,* 12 (2), 222-8.

Barnham, K. J., et al. (2004), 'Tyrosine gated electron transfer is key to the toxic mechanism of Alzheimer's disease beta-amyloid', *Faseb J,* 18 (12), 1427-9.

Barrow, C. J., et al. (1992), 'Solution conformations and aggregational properties of synthetic amyloid β-peptides of Alzheimer's disease: Analysis of circular dichroism spectra', *Journal of Molecular Biology,* 225 (4), 1075-93.

Bartlett, A. I. and Radford, S. E. (2009), 'An expanding arsenal of experimental methods yields an explosion of insights into protein folding mechanisms', *Nat Struct Mol Biol,* 16 (6), 582-8.

Bayse, G. S., Michaels, A. W., and Morrison, M. (1972), 'The peroxidase-catalyzed oxidation of tyrosine', *Biochim Biophys Acta,* 284 (1), 34-42.

Biere, A. L., et al. (2000), 'Parkinson's Disease-associated α-Synuclein Is More Fibrillogenic than β- and γ-Synuclein and Cannot Cross-seed Its Homologs', *Journal of Biological Chemistry,* 275 (44), 34574-79.

Binolfi, A., et al. (2006), 'Interaction of alpha-synuclein with divalent metal ions reveals key differences: a link between structure, binding specificity and fibrillation enhancement', *J Am Chem Soc,* 128 (30), 9893-901.

Binolfi, A., et al. (2010), 'Bioinorganic chemistry of Parkinson's disease: structural determinants for the copper-mediated amyloid formation of alpha-synuclein', *Inorg Chem,* 49 (22), 10668-79.

Bitan, G., et al. (2003), 'Amyloid beta -protein (Abeta) assembly: Abeta 40 and Abeta 42 oligomerize through distinct pathways', *Proc Natl Acad Sci U S A,* 100 (1), 330-5.

Bodaness, R. S. and Zigler, J. S., Jr. (1983), 'The rapid H2O2-mediated nonphotodynamic crosslinking of lens crystallins generated by the heme-undecapeptide from cytochrome C: potential implications for cataractogenesis in man', *Biochem Biophys Res Commun,* 113 (2), 592-7.

Bollag, D.M. and Edelstein, S.J. (1991), *Protein methods* (Wiley-Liss).

Borsarelli, C. D., et al. (2012), 'Biophysical properties and cellular toxicity of covalent crosslinked oligomers of α-synuclein formed by photoinduced side-chain tyrosyl radicals', *Free Radical Biology and Medicine,* 53 (4), 1004-15.

Bothwell, M. and Giniger, E. (2000), 'Alzheimer's disease: neurodevelopment converges with neurodegeneration', (102), 271-73.

Brockwell, D. J. and Radford, S. E. (2007), 'Intermediates: ubiquitous species on folding energy landscapes?', *Curr Opin Struct Biol,* 17 (1), 30-7.

Brown, D. R. (2009), 'Brain proteins that mind metals: a neurodegenerative perspective', *Dalton Transactions,* (21), 4069-76.

Bruggink, K. A., et al. (2013), 'Amyloid-beta oligomer detection by ELISA in cerebrospinal fluid and brain tissue', *Anal Biochem,* 433 (2), 112-20.

Brunk, U. T. (1989), 'On the Origin of Lipofuscin - the Iron Content of Residual Bodies, and the Relation of These Organelles to the Lysosomal Vacuome - a Study on Cultured Human Glial-Cells', *Lipofuscin and Ceroid Pigments,* 266, 313-22.

Brunk, U. T. and Terman, A. (2002), 'Lipofuscin: Mechanisms of age-related accumulation and influence on cell function', *Free Radical Biology and Medicine,* 33 (5), 611-19.

Bucknall, M.P. (2006), *Dityrosine as a Biomarker of Free Radical Induced Oxidative Damage in Diseases of Ageing* (University of New South Wales).

Bulheller, B. M., Rodger, A., and Hirst, J. D. (2007), 'Circular and linear dichroism of proteins', *Phys Chem Chem Phys,* 9 (17), 2020-35.

Burlingame, A. L., Boyd, R. K., and Gaskell, S. J. (1996), 'Mass spectrometry', *Anal Chem,* 68 (12), 599R-651R.

Bush, A. I. (2003a), 'Copper, zinc, and the metallobiology of Alzheimer disease', *Alzheimer Dis Assoc Disord,* 17 (3), 147-50.

Bush, A. I. (2003b), 'The metallobiology of Alzheimer's disease', *Trends in Neurosciences,* 26 (4), 207-14.

Bush, A. I. and Curtain, C. C. (2008), 'Twenty years of metallo-neurobiology: where to now?', *Eur Biophys J,* 37 (3), 241-5.

Bush, A. I., et al. (1994a), 'Modulation of A beta adhesiveness and secretase site cleavage by zinc', *J Biol Chem,* 269 (16), 12152-8.

Bush, A. I., et al. (1994b), 'Rapid Induction of Alzheimer a-Beta Amyloid Formation by Zinc', *Science,* 265 (5177), 1464-67.

Butterfield, D. A. (2002), 'Amyloid beta-peptide (1-42)-induced oxidative stress and neurotoxicity: implications for neurodegeneration in Alzheimer's disease brain. A review', *Free Radic Res,* 36 (12), 1307-13.

Calloni, G., et al. (2008), 'Structure and dynamics of a partially folded protein are decoupled from its mechanism of aggregation', *J Am Chem Soc,* 130 (39), 13040-50.

Campioni, S., Monsellier, E., and Chiti, F. (2010), 'Why Proteins Misfold', *Protein Misfolding Diseases* (John Wiley & Sons, Inc.), 1-20.

Caughey, B. and Lansbury, P. T. (2003), 'Protofibrils, pores, fibrils, and neurodegeneration: separating the responsible protein aggregates from the innocent bystanders', *Annu Rev Neurosci,* 26, 267-98.

Celej, M. S., et al. (2012), 'Toxic prefibrillar alpha-synuclein amyloid oligomers adopt a distinctive antiparallel beta-sheet structure', *Biochem J,* 443 (3), 719-26.

Cerpa, R., Cohen, F. E., and Kuntz, I. D. (1996), 'Conformational switching in designed peptides: The helix/sheet transition', *Folding & Design,* 1 (2), 91-101.

Cerpa, W., et al. (2005), 'Is there a role for copper in neurodegenerative diseases?', *Molecular Aspects of Medicine,* 26 (4–5), 405-20.

Chakraborty, M., et al. (2010), 'Structure and conformational studies on dityrosine formation in the DNA binding domain of RFX5', *Biophys Chem,* 149 (3), 92-101.

Chamberlain, A. K., et al. (2000), 'Ultrastructural organization of amyloid fibrils by atomic force microscopy', *Biophys J,* 79 (6), 3282-93.

Chance, B, Sies, H, and Boveris, A (1979), 'Hydroperoxide metabolism in mammalian organs', *Physiological Reviews,* 59 (3), 527-605.

Cherny, R. A., et al. (2001), 'Treatment with a copper-zinc chelator markedly and rapidly inhibits beta-amyloid accumulation in Alzheimer's disease transgenic mice', *Neuron,* 30 (3), 665-76.

Chiti, F. and Dobson, C. M. (2006), 'Protein misfolding, functional amyloid, and human disease', *Annu Rev Biochem,* 75, 333-66.

Ciccotosto, G. D., et al. (2004), 'Enhanced toxicity and cellular binding of a modified amyloid beta peptide with a methionine to valine substitution', *J Biol Chem,* 279 (41), 42528-34.

Clayton, D. F. and George, J. M. (1999), 'Synucleins in synaptic plasticity and neurodegenerative disorders', *J Neurosci Res,* 58 (1), 120-9.

Cohen (1982), *Electron Microscopy of Protein* (3).

Cohen, A. S. (1986), *General introduction and a breif history of the amyloid fibril*, ed. Van Rijswijk MH Marrink J (Amyloidosis; Dordrecht, The Netherlands: Martinus Nijhoff).

Cohen, A. S. and Calkins, E. (1959), 'Electron microscopic observations on a fibrous component in amyloid of diverse origins', *Nature,* 183 (4669), 1202-3.

Cohen, S. L. and Chait, B. T. (1997), 'Mass spectrometry of whole proteins eluted from sodium dodecyl sulfate-polyacrylamide gel electrophoresis gels', *Analytical Biochemistry,* 247 (2), 257-67.

Cole, N. B., et al. (2005), 'Metal-catalyzed oxidation of alpha-synuclein: helping to define the relationship between oligomers, protofibrils, and filaments', *J Biol Chem,* 280 (10), 9678-90.

Collins, V. P., et al. (1980), 'Phagocytosis and degradation of rat liver mitochondria by cultivated human glial cells', *Lab Invest,* 42 (2), 209-16.

Colon, W. and Kelly, J. W. (1992), 'Partial denaturation of transthyretin is sufficient for amyloid fibril formation in vitro', *Biochemistry,* 31 (36), 8654-60.

Connors, L. H., et al. (1985), 'In vitro formation of amyloid fibrils from intact β2-microglobulin', *Biochemical and Biophysical Research Communications,* 131 (3), 1063-68.

Conway, K. A., Harper, J. D., and Lansbury, P. T., Jr. (2000), 'Fibrils formed in vitro from alpha-synuclein and two mutant forms linked to Parkinson's disease are typical amyloid', *Biochemistry,* 39 (10), 2552-63.

Cox, D. M., et al. (2005), 'Multiple reaction monitoring as a method for identifying protein posttranslational modifications', *Journal of Biomolecular Techniques,* 16 (2), 83-90.

Cruts, M. and Van Broeckhoven, C. (1998), 'Presenilin mutations in Alzheimer's disease', *Hum Mutat,* 11 (3), 183-90.

Curtain, C. C., et al. (2001), 'Alzheimer's disease amyloid-beta binds copper and zinc to generate an allosterically ordered membrane-penetrating structure containing superoxide dismutase-like subunits', *J Biol Chem,* 276 (23), 20466-73.

Cutillas, P., R. and Timms, J., F. (2010), 'LC-MS/MS in Proteomics: Methods and Applications', *Lc-Ms/Ms in Proteomics: Methods and Applications,* 658, 1-357.

Dai, X. L., Sun, Y. X., and Jiang, Z. F. (2006), 'Cu(II) potentiation of Alzheimer Abeta1-40 cytotoxicity and transition on its secondary structure', *Acta biochimica et biophysica Sinica,* 38 (11), 765-72.

Dalsgaard, T. K., et al. (2011), 'Dityrosine, 3,4-dihydroxyphenylalanine (DOPA), and radical formation from tyrosine residues on milk proteins with globular and flexible structures as a result of riboflavin-mediated photo-oxidation', *J Agric Food Chem,* 59 (14), 7939-47.

Davidson, W. S., et al. (1998), 'Stabilization of alpha-synuclein secondary structure upon binding to synthetic membranes', *J Biol Chem,* 273 (16), 9443-9.

Davidsson, A., Norden, B., and Seth, S. (1980), 'Measurement of oriented circular dichroism', *Chemical Physics Letters,* 70 (2).

Davie, C. A. (2008), 'A review of Parkinson's disease', *British Medical Bulletin,* 86 (1), 109-27.

De Strooper, B. (2007), 'Loss-of-function presenilin mutations in Alzheimer disease. Talking Point on the role of presenilin mutations in Alzheimer disease', *EMBO Rep,* 8 (2), 141-6.

DeLano (2002), 'ThePyMol Molecular Graphics System'.

DiMarco, T. and Giulivi, C. (2007), 'Current analytical methods for the detection of dityrosine, a biomarker of oxidative stress, in biological samples', *Mass Spectrom Rev,* 26 (1), 108-20.

Ding, Y., et al. (2013), 'Photo-cross-linking approach to engineering small tyrosine-containing peptide hydrogels with enhanced mechanical stability', *Langmuir,* 29 (43), 13299-306.

Ditaranto, K., Tekirian, T. L., and Yang, A. J. (2001), 'Lysosomal membrane damage in soluble A beta-mediated cell death in Alzheimer's disease', *Neurobiol Dis,* 8 (1), 19-31.

Doan, N. D., et al. (2008), 'Effectiveness of the Suzuki-Miyaura cross-coupling reaction for solid-phase peptide modification', *Journal of Combinatorial Chemistry,* 10 (1), 44-51.

Dobson, C. M. (2003), 'Protein folding and misfolding', *Nature,* 426 (6968), 884-90.

Dobson, C. M. (2004), 'Experimental investigation of protein folding and misfolding', *Methods,* 34 (1), 4-14.

Dobson, C. M. (2013), 'The Amyloid Phenomenon and Its Significance', *Amyloid Fibrils and Prefibrillar Aggregates* (Wiley-VCH Verlag GmbH & Co. KGaA), 1-19.

Double, K. L., et al. (2008), 'The comparative biology of neuromelanin and lipofuscin in the human brain', *Cellular and Molecular Life Sciences,* 65 (11), 1669-82.

Drew, S., et al. (2013), 'Cu2+ Coordination of Covalently Cross-linked Beta Amyloid Dimers', *Applied Magnetic Resonance*, 1-13.

Dusa, A., et al. (2006), 'Characterization of oligomers during alpha-synuclein aggregation using intrinsic tryptophan fluorescence', *Biochemistry,* 45 (8), 2752-60.

Dyrks, T, et al. (1992), 'Amyloidogenicity of beta A4 and beta A4-bearing amyloid protein precursor fragments by metal-catalyzed oxidation', *Journal of Biological Chemistry,* 267 (25), 18210-17.

Dyrks, T., et al. (1993), 'Amyloidogenicity of rodent and human Œ≤A4 sequences', *Febs Letters,* 324 (2), 231-36.

Eakin, C. M., et al. (2004), 'Oligomeric assembly of native-like precursors precedes amyloid formation by beta-2 microglobulin', *Biochemistry,* 43 (24), 7808-15.

Eichner, T. and Radford, S. E. (2011), 'A diversity of assembly mechanisms of a generic amyloid fold', *Mol Cell,* 43 (1), 8-18.

Eliezer, D., et al. (2001), 'Conformational properties of alpha-synuclein in its free and lipid-associated states', *J Mol Biol,* 307 (4), 1061-73.

Elleder, M. (1981), *Chemical characterization of pigment*, ed. R. S. Sohal (Age pigment; Amsterdam: Elsevier).

Elliott, K. A. (1932), 'Milk peroxidase: Its preparation, properties, and action with H(2)O(2) on metabolites. With a method for determining small amounts of H(2)O(2) in complex mixtures', *Biochem J,* 26 (1), 10-24.

Ellis, C. E., et al. (2001), 'alpha-Synuclein is phosphorylated by members of the Src family of protein-tyrosine kinases', *Journal of Biological Chemistry,* 276 (6), 3879-84.

Eskici, G. and Axelsen, P. H. (2012), 'Copper and oxidative stress in the pathogenesis of Alzheimer's disease', *Biochemistry,* 51 (32), 6289-311.

Fandrich, M., Meinhardt, J., and Grigorieff, N. (2009), 'Structural polymorphism of Alzheimer Abeta and other amyloid fibrils', *Prion,* 3 (2), 89-93.

Fasman, Edited by Gerald D. (1996), *Circular Dichroism and the Conformational Analysis of Biomolecules*.

Fenaille, F., et al. (2004), 'Quantitative determination of dityrosine in milk powders by liquid chromatography coupled to tandem mass spectrometry using isotope dilution', *Journal of Chromatography A,* 1052 (1-2), 77-84.

Fenn, J. B., et al. (1989), 'Electrospray ionization for mass spectrometry of large biomolecules', *Science,* 246 (4926), 64-71.

Fernandez, C. O., et al. (2004), 'NMR of alpha-synuclein-polyamine complexes elucidates the mechanism and kinetics of induced aggregation', *EMBO J,* 23 (10), 2039-46.

Ferrone, F. (1999), 'Analysis of protein aggregation kinetics', *Methods Enzymol,* 309, 256-74.

Fetterer, R. H., Rhoads, M. L., and Urban, J. F., Jr. (1993), 'Synthesis of tyrosine-derived cross-links in Ascaris suum cuticular proteins', *J Parasitol,* 79 (2), 160-6.

Fink, A. L. (2006), 'The aggregation and fibrillation of alpha-synuclein', *Accounts of Chemical Research,* 39 (9), 628-34.

Fitzpatrick, A. W., et al. (2013), 'Atomic structure and hierarchical assembly of a cross-beta amyloid fibril', *Proceedings of the National Academy of Sciences of the United States of America,* 110 (14), 5468-73.

Foerder, C. A. and Shapiro, B. M. (1977), 'Release of ovoperoxidase from sea urchin eggs hardens the fertilization membrane with tyrosine crosslinks', *Proc Natl Acad Sci U S A,* 74 (10), 4214-8.

Fowler, D. M., et al. (2006), 'Functional amyloid formation within mammalian tissue', *PLoS Biol,* 4 (1), e6.

Friedlich, A. L., et al. (2004), 'Neuronal zinc exchange with the blood vessel wall promotes cerebral amyloid angiopathy in an animal model of Alzheimer's disease', *J Neurosci,* 24 (13), 3453-9.

Friedrich, R. P., et al. (2010), 'Mechanism of amyloid plaque formation suggests an intracellular basis of Abeta pathogenicity', *Proceedings of the National Academy of Sciences of the United States of America,* 107 (5), 1942-7.

Fujimoto, D. (1975), 'Occurrence of Dityrosine in Cuticlin, a Structural Protein from Ascaris Cuticle', *Comparative Biochemistry and Physiology B-Biochemistry & Molecular Biology,* 51 (2), 205-07.

Galeazzi, L., et al. (1999), 'In vitro peroxidase oxidation induces stable dimers of beta-amyloid (1-42) through dityrosine bridge formation', *Amyloid-International Journal of Experimental and Clinical Investigation,* 6 (1), 7-13.

Gazit, E. (2002), 'A possible role for pi-stacking in the self-assembly of amyloid fibrils', *Faseb J,* 16 (1), 77-83.

Geddes, A. J., et al. (1968), '"Cross-β" conformation in proteins', *Journal of Molecular Biology,* 32 (2), 343-58.

George, J. M. (2002), 'The synucleins', *Genome Biol,* 3 (1), REVIEWS3002.

Gething, M. J. and Sambrook, J. (1992), 'Protein folding in the cell', *Nature,* 355 (6355), 33-45.

Giaccone, G., et al. (2011), 'Lipofuscin hypothesis of Alzheimer's disease', *Dementia and geriatric cognitive disorders extra,* 1 (1), 292-6.

Giancotti, V., Fonda, M., and Crane-Robinson, C. (1977), 'Tyrosine fluorescence of two tryptophan-free proteins: histones H1 and H5', *Biophys Chem,* 6 (3), 379-83.

Giancotti, V., et al. (1980), 'Fluorescence of buried tyrosine residues in proteins', *Biochimica et Biophysica Acta (BBA) - Protein Structure,* 624 (1), 60-65.

Giasson, B. I., et al. (2001), 'A hydrophobic stretch of 12 amino acid residues in the middle of alpha-synuclein is essential for filament assembly', *Journal of Biological Chemistry,* 276 (4), 2380-86.

Giulian, D., et al. (1998), 'The HHQK domain of beta-amyloid provides a structural basis for the immunopathology of Alzheimer's disease', *J Biol Chem,* 273 (45), 29719-26.

Giulivi, C. and Davies, K. J. (1993), 'Dityrosine and tyrosine oxidation products are endogenous markers for the selective proteolysis of oxidatively modified red blood cell hemoglobin by (the 19 S) proteasome', *The Journal of biological chemistry,* 268 (12), 8752-9.

Giulivi, C. and Davies, K. J. (1994), 'Dityrosine: a marker for oxidatively modified proteins and selective proteolysis', *Methods in enzymology,* 233, 363-71.

Giulivi, C. and Davies, K. J. (2001), 'Mechanism of the formation and proteolytic release of H2O2-induced dityrosine and tyrosine oxidation products in hemoglobin and red blood cells', *J Biol Chem,* 276 (26), 24129-36.

Giulivi, C., Traaseth, N. J., and Davies, K. J. (2003), 'Tyrosine oxidation products: analysis and biological relevance', *Amino Acids,* 25 (3-4), 227-32.

Glatzel, M., et al. (2005), 'Human prion diseases: molecular and clinical aspects', *Arch Neurol,* 62 (4), 545-52.

Glenner, G. G. and Wong, C. W. (1984), 'Alzheimer's disease: initial report of the purification and characterization of a novel cerebrovascular amyloid protein', *Biochem Biophys Res Commun,* 120 (3), 885-90.

Glusker, J. P., Katz, A. K., and Bock, C. W. (1999), 'METAL IONS IN BIOLOGICAL SYSTEMS', *The Rigaku Journal,* 16 (2), 8-16.

Goldsbury, C., et al. (1999), 'Watching amyloid fibrils grow by time-lapse atomic force microscopy', *J Mol Biol,* 285 (1), 33-9.

Goldsbury, C. S., et al. (2000), 'Studies on the in vitro assembly of a beta 1-40: implications for the search for a beta fibril formation inhibitors', *J Struct Biol,* 130 (2-3), 217-31.

Gordon, D. J., Tappe, R., and Meredith, S. C. (2002), 'Design and characterization of a membrane permeable N-methyl amino acid-containing peptide that inhibits A beta(1-40) fibrillogenesis', *Journal of Peptide Research,* 60 (1), 37-55.

Gouras, G. K., Almeida, C. G., and Takahashi, R. H. (2005), 'Intraneuronal Abeta accumulation and origin of plaques in Alzheimer's disease', *Neurobiology of Aging,* 26 (9), 1235-44.

Granata, A., et al. (2007), 'Tyrosinase-generated quinones induce covalent modification, unfolding, and aggregation of human holo-myoglobin', *Biomacromolecules,* 8 (10), 3214-23.

Gray, D. A., and Woulfe, J. (2005), 'Lipofuscin and Aging: A Matter of Toxic Waste', *Science of Aging Knowledge Environment,* 2005 (5), re1.

Greenfield, N. J. (1996), 'Methods to estimate the conformation of proteins and polypeptides from circular dichroism data', *Anal Biochem,* 235 (1), 1-10.

Griffiths, Gareth (1993), 'An Overview of Techniques for Labelling at the EM Level', *Fine Structure Immunocytochemistry* (Springer Berlin Heidelberg), 446-49.

Griffiths, Gareth, Burke, Brian, and Lucocq, John (1993), *Fine structure immunocytochemistry* (Berlin ; New York: Springer-Verlag) xxi, 459 p.

Gross, A. J. and Sizer, I. W. (1955), 'Synthesis of dityrosine', *Proc Int Con Biochem abstract number 29.*

Gross, A. J. and Sizer, I. W. (1959), 'The oxidation of tyramine, tyrosine, and related compounds by peroxidase', *J Biol Chem,* 234 (6), 1611-4.

Gross, J.H. and Roepstorff, P. (2011), *Mass Spectrometry: A Textbook* (Springer).

Gross, M. L., Chen, G., and Pramanik, B. N. (2012), *Protein and peptide mass spectrometry in drug discovery* (Hoboken, N.J.: Wiley) xvii, 464 p.

Gugiu, B. G., et al. (2005), 'Proteomic and ultrastructural analyses of human lipofuscin', *Investigative Ophthalmology & Visual Science,* 46.

Guo, Z. W., et al. (1997), 'Enzymatic oxidative phenolic coupling', *Journal of Organic Chemistry,* 62 (20), 6700-01.

Gupta, A. and Pansari, K. (2003), 'Inflammation and Alzheimer's disease', *Int J Clin Pract,* 57 (1), 36-9.

Gupta M, Bagaria A, Mishra A, Mathur P, Basu A, Ramakumar S, Chauhan VS (2007), 'Self-Assembly of a Dipeptide- Containing Conformationally Restricted Dehydrophenylalanine Residue to Form Ordered Nanotubes', *Advanced Materials,* 19 (6), 858-61.

Gutteridge, John M. C. (1984), 'Age pigments: Role of iron and copper salts in the formation of fluorescent lipid complexes', *Mechanisms of Ageing and Development,* 25 (1–2), 205-14.

Haass, C. and Selkoe, D. J. (2007), 'Soluble protein oligomers in neurodegeneration: lessons from the Alzheimer's amyloid beta-peptide', *Nat Rev Mol Cell Biol,* 8 (2), 101-12.

Haber, F. and Weiss, J. (1934), 'The Catalytic Decomposition of Hydrogen Peroxide by Iron Salts', *Proceedings of the Royal Society of London. Series A - Mathematical and Physical Sciences,* 147 (861), 332-51.

Haeffner, F., et al. (2005), 'Model studies of cholesterol and ascorbate oxidation by copper complexes: Relevance to Alzheimer's disease beta-amyloid metallochemistry', *Journal of Inorganic Biochemistry,* 99 (12), 2403-22.

Hanft, F. and Koehler, P. (2005), 'Quantitation of dityrosine in wheat flour and dough by liquid chromatography-tandem mass spectrometry', *Journal of Agricultural and Food Chemistry,* 53 (7), 2418-23.

Hardy, J. and Selkoe, D. J. (2002), 'The amyloid hypothesis of Alzheimer's disease: progress and problems on the road to therapeutics', *Science,* 297 (5580), 353-6.

Hardy, J., et al. (2009), 'The genetics of Parkinson's syndromes: a critical review', *Curr Opin Genet Dev,* 19 (3), 254-65.

Hardy, J. and Higgins, G. A. (1992), 'Alzheimer's disease: the amyloid cascade hypothesis', *Science,* 256 (5054), 184-5.

Harman, D. (2002), 'Aging: A Theory Based on Free Radical and Radiation Chemistry', *Science of Aging Knowledge Environment,* 2002 (37), cp14.

Harper, J. D., et al. (1997), 'Observation of metastable Abeta amyloid protofibrils by atomic force microscopy', *Chem Biol,* 4 (2), 119-25.

Harper, J. D., et al. (1999), 'Assembly of A beta amyloid protofibrils: An in vitro model for a possible early event in Alzheimer's disease', *Biochemistry,* 38 (28), 8972-80.

Harris, J. R. (2005), 'The Contribution of Microscopy to the Study of Alzheimer's Disease, Amyloid Plaques and Aβ Fibrillogenesis', in J. Robin Harris and Falk Fahrenholz (eds.), *Alzheimer's Disease* (Subcellular Biochemistry, 38: Springer US), 1-44.

Harrison, R. S., et al. (2007), 'Amyloid peptides and proteins in review', in S. G. Amara, et al. (eds.), *Reviews of Physiology, Biochemistry and Pharmacology* (Reviews of Physiology, Biochemistry and Pharmacology, 159: Springer Berlin Heidelberg), 1-77.

Hartl, F. U. and Hayer-Hartl, M. (2009), 'Converging concepts of protein folding in vitro and in vivo', *Nat Struct Mol Biol,* 16 (6), 574-81.

Hartley, D. M., et al. (2008), 'Transglutaminase induces protofibril-like amyloid beta-protein assemblies that are protease-resistant and inhibit long-term potentiation', *J Biol Chem,* 283 (24), 16790-800.

Hayden, E. Y. and Teplow, D. B. (2013), 'Amyloid beta-protein oligomers and Alzheimer's disease', *Alzheimers Res Ther,* 5 (6), 60.

Head, E., et al. (2001), 'Oxidation of Abeta and plaque biogenesis in Alzheimer's disease and Down syndrome', *Neurobiol Dis,* 8 (5), 792-806.

Heinecke, J. W. (2002), 'Tyrosyl radical production by myeloperoxidase: a phagocyte pathway for lipid peroxidation and dityrosine cross-linking of proteins', *Toxicology,* 177 (1), 11-22.

Heinecke, J. W., et al. (1993), 'Tyrosyl radical generated by myeloperoxidase catalyzes the oxidative cross-linking of proteins', *Journal of Clinical Investigation,* 91 (6), 2866-72.

Hensley, K., et al. (1998), 'Electrochemical analysis of protein nitrotyrosine and dityrosine in the Alzheimer brain indicates region-specific accumulation', *J Neurosci,* 18 (20), 8126-32.

Hicks, D. A., Nalivaeva, N. N., and Turner, A. J. (2012), 'Lipid rafts and Alzheimer's disease: protein-lipid interactions and perturbation of signaling', *Front Physiol,* 3, 189.

Hicks, M. R., Kowalski, J., and Rodger, A. (2010), 'LD spectroscopy of natural and synthetic biomaterials (vol 39, pg 3380, 2010)', *Chemical Society Reviews,* 39 (12), 5069-69.

High, A.A. (2003), *The Analysis of Proteins and Peptides by Mass Spectrometry: From the Whole Cell Proteome to Small Protein Complexes* (University of Virginia).

Hill, A. F., Antoniou, M., and Collinge, J. (1999), 'Protease-resistant prion protein produced in vitro lacks detectable infectivity', *J Gen Virol,* 80 (Pt 1), 11-4.

Ho, C. S., et al. (2003), 'Electrospray ionisation mass spectrometry: principles and clinical applications', *Clin Biochem Rev,* 24 (1), 3-12.

Horwitz, J., Strickland, E. H., and Billups, C. (1970), 'Analysis of the vibrational structure in the near-ultraviolet circular dichroism and absorption spectra of tyrosine derivatives and ribonuclease-A at 77 degrees K', *J Am Chem Soc,* 92 (7), 2119-29.

Hozumi, I., et al. (2010), 'High Levels of Copper, Zinc, Iron and Magnesium, but not Calcium, in the Cerebrospinal Fluid of Patients with Fahr's Disease', *Case Rep Neurol,* 2 (2), 46-51.

http://physics.stackexchange.com.

http://www.alz.co.uk/research/world-report-2013.

http://www.alzheimers.org.uk.

http://www.hk-phy.org/atomic_world/tem/tem02_e.html.

http://www.hopkinsmedicine.org/.

http://www.isa.au.dk/facilities/astrid/beamlines/cd1/cd1_3.asp.

http://www.lifesci.sussex.ac.uk/home/Julian_Thorpe/immuno4.htm.

http://www.mhhe.com/physsci/chemistry/carey/student/olc/ch13ms.html.

http://www.pathology.vcu.edu/education/.

http://www.proteinchemist.com/cd/cdspec.html.

http://www.virtualmedstudent.com/links/neurological/parkinsons.html.

Huang, X., et al. (1999a), 'The A beta peptide of Alzheimer's disease directly produces hydrogen peroxide through metal ion reduction', *Biochemistry,* 38 (24), 7609-16.

Huang, X., et al. (2004a), 'Redox-Active Metals, Oxidative Stress, and Alzheimer's Disease Pathology', *Annals of the New York Academy of Sciences,* 1012 (1), 153-63.

Huang, X., et al. (2004b), 'Trace metal contamination initiates the apparent auto-aggregation, amyloidosis, and oligomerization of Alzheimer‚Äôs AŒ≤ peptides', *JBIC Journal of Biological Inorganic Chemistry,* 9 (8), 954-60.

Huang, X., et al. (1999b), 'Cu(II) Potentiation of Alzheimer Aβ Neurotoxicity: CORRELATION WITH CELL-FREE HYDROGEN PEROXIDE PRODUCTION AND METAL REDUCTION', *Journal of Biological Chemistry,* 274 (52), 37111-16.

Hueck, W. (1912), 'Pigmentstudien ', *Beitr. Pathol. Anat.,* 54, 68-232.

Huggins, T. G., et al. (1993), 'Formation of O-Tyrosine and Dityrosine in Proteins during Radiolytic and Metal-Catalyzed Oxidation', *Journal of Biological Chemistry,* 268 (17), 12341-47.

Hunter, H. N., et al. (2005), 'The interactions of antimicrobial peptides derived from lysozyme with model membrane systems', *Biochim Biophys Acta,* 1668 (2), 175-89.

Hutton, C. A. and Skaff, O. (2003), 'A convenient preparation of dityrosine via Miyaura borylation-Suzuki coupling of iodotyrosine derivatives', *Tetrahedron Letters,* 44 (26), 4895-98.

Ischiropoulos, H. and Al-Mehdi, A. B. (1995), 'Peroxynitrite-mediated oxidative protein modifications', *Febs Letters,* 364 (3), 279-82.

Issaq, H. J. and Blonder, J. (2009), 'Electrophoresis and liquid chromatography/tandem mass spectrometry in disease biomarker discovery', *J Chromatogr B Analyt Technol Biomed Life Sci,* 877 (13), 1222-8.

Iwata, K., et al. (2006), '3D structure of amyloid protofilaments of beta2-microglobulin fragment probed by solid-state NMR', *Proc Natl Acad Sci U S A,* 103 (48), 18119-24.

Jacob, J. S., et al. (1996), 'Human phagocytes employ the myeloperoxidase-hydrogen peroxide system to synthesize dityrosine, trityrosine, pulcherosine, and isodityrosine by a tyrosyl radical-dependent pathway', *Journal of Biological Chemistry,* 271 (33), 19950-56.

Jahn, T. R., et al. (2006), 'Amyloid formation under physiological conditions proceeds via a native-like folding intermediate', *Nat Struct Mol Biol,* 13 (3), 195-201.

Jahn, T. R., et al. (2010), 'The common architecture of cross-beta amyloid', *J Mol Biol,* 395 (4), 717-27.

Jakes, R., Spillantini, M. G., and Goedert, M. (1994), 'Identification of two distinct synucleins from human brain', *FEBS Lett,* 345 (1), 27-32.

Jarrett, J. T., Berger, E. P., and Lansbury, P. T. (1993), 'The Carboxy Terminus of the Beta-Amyloid Protein Is Critical for the Seeding of Amyloid Formation - Implications for the Pathogenesis of Alzheimers-Disease', *Biochemistry,* 32 (18), 4693-97.

Jean, L., et al. (2008), 'Structural elements regulating amyloidogenesis: a cholinesterase model system', *PLoS ONE,* 3 (3), e1834.

Jenko Kokalj, S., et al. (2007), 'Essential role of proline isomerization in stefin B tetramer formation', *J Mol Biol,* 366 (5), 1569-79.

Ji, T. H. and Urry, D. W. (1969), 'Correlation of light scattering and absorption flattening effects with distortions in the circular dichroism patterns of mitochondrial membrane fragments', *Biochemical and Biophysical Research Communications,* 34 (4), 404-11.

Jiang, D. L., et al. (2007), 'Redox reactions of copper complexes formed with different beta-amyloid peptides and their neuropathalogical relevance', *Biochemistry,* 46 (32), 9270-82.

Jimenez, J. L., et al. (2001), 'Structural diversity of ex vivo amyloid fibrils studied by cryo-electron microscopy', *J Mol Biol,* 311 (2), 241-7.

Jimenez, J. L., et al. (2002), 'The protofilament structure of insulin amyloid fibrils', *Proc Natl Acad Sci U S A,* 99 (14), 9196-201.

Johnson, H. and Eyers, C. E. (2010), 'Analysis of Post-translational Modifications by LC-MS/MS', *Lc-Ms/Ms in Proteomics: Methods and Applications,* 658, 93-108.

Jomova, K., et al. (2010), 'Metals, oxidative stress and neurodegenerative disorders', *Mol Cell Biochem,* 345 (1-2), 91-104.

Juban, M., Javadpour, M., and Barkley, M. (1997), 'Circular Dichroism Studies of Secondary Structure of Peptides', in WilliamM Shafer (ed.), *Antibacterial Peptide Protocols* (Methods In Molecular Biology™, 78: Humana Press), 73-78.

Jungblut, P. R. (2012), 'Protein and Peptide Mass Spectrometry in Drug Discovery. Edited by Michael L. Gross, Guodong Chen and Birendra N. Pramanik', *ChemMedChem,* 7 (12), 2241-42.

Kanwar, R. and Balasubramanian, D. (1999), 'Structure and stability of the dityrosine-linked dimer of gamma B-crystallin', *Experimental Eye Research,* 68 (6), 773-84.

Kanwar, R. and Balasubramanian, D. (2000), 'Structural studies on some dityrosine-cross-linked globular proteins: Stability is weakened, but activity is not abolished', *Biochemistry,* 39 (48), 14976-83.

Karpinar, D. P., et al. (2009), 'Pre-fibrillar alpha-synuclein variants with impaired beta-structure increase neurotoxicity in Parkinson's disease models', *EMBO J,* 28 (20), 3256-68.

Karran, E., Mercken, M., and De Strooper, B. (2011), 'The amyloid cascade hypothesis for Alzheimer's disease: an appraisal for the development of therapeutics', *Nat Rev Drug Discov,* 10 (9), 698-712.

Kato, Y., Uchida, K., and Kawakishi, S. (1994), 'Aggregation of collagen exposed to UVA in the presence of riboflavin: a plausible role of tyrosine modification', *Photochem Photobiol,* 59 (3), 343-9.

Kato, Y., et al. (2001), 'The hydrogen peroxide/copper ion system, but not other metal-catalyzed oxidation systems, produces protein-bound dityrosine', *Free Radical Biology and Medicine,* 31 (5), 624-32.

Kato, Y., et al. (1998), 'Immunohistochemical detection of dityrosine in lipofuscin pigments in the aged human brain', *Febs Letters,* 439 (3), 231-34.

Kato, Y., et al. (2000), 'Immunochemical detection of protein dityrosine in atherosclerotic lesion of apo-E-deficient mice using a novel monoclonal antibody', *Biochemical and biophysical research communications,* 275 (1), 11-5.

Kaur, D., et al. (2003), 'Genetic or pharmacological iron chelation prevents MPTP-induced neurotoxicity in vivo: a novel therapy for Parkinson's disease', *Neuron,* 37 (6), 899-909.

Kayed, R. and Lasagna-Reeves, C. A. (2013), 'Molecular mechanisms of amyloid oligomers toxicity', *Journal of Alzheimer's Disease,* 33 (SUPPL. 1), S67-S78.

Kayed, R., et al. (2003), 'Common structure of soluble amyloid oligomers implies common mechanism of pathogenesis', *Science,* 300 (5618), 486-9.

Kaylor, J., et al. (2005), 'Characterization of oligomeric intermediates in alpha-synuclein fibrillation: FRET studies of Y125W/Y133F/Y136F alpha-synuclein', *J Mol Biol,* 353 (2), 357-72.

Kehrer, J. P. (2000), 'The Haber-Weiss reaction and mechanisms of toxicity', *Toxicology,* 149 (1), 43-50.

Kelenyi, G. (1967), 'On the histochemistry of azo group-free thiazole dyes', *J Histochem Cytochem,* 15 (3), 172-80.

Kelly, J. W. (1996), 'Alternative conformations of amyloidogenic proteins govern their behavior', *Curr Opin Struct Biol,* 6 (1), 11-7.

Kelly, S. M. and Price, N. C. (2000), 'The use of circular dichroism in the investigation of protein structure and function', *Curr Protein Pept Sci,* 1 (4), 349-84.

Kelly, S. M., Jess, T. J., and Price, N. C. (2005), 'How to study proteins by circular dichroism', *Biochim Biophys Acta,* 1751 (2), 119-39.

Kenche, V. B. and Barnham, K. J. (2011), 'Alzheimer's disease & metals: therapeutic opportunities', *Br J Pharmacol,* 163 (2), 211-9.

Khurana, R., et al. (2005), 'Mechanism of thioflavin T binding to amyloid fibrils', *J Struct Biol,* 151 (3), 229-38.

Kienzl, E., et al. (1995), 'The role of transition metals in the pathogenesis of Parkinson's disease', *J Neurol Sci,* 134 Suppl, 69-78.

Kihara, M., et al. (2006), 'Conformation of amyloid fibrils of beta2-microglobulin probed by tryptophan mutagenesis', *J Biol Chem,* 281 (41), 31061-9.

Kim, J., Basak, J. M., and Holtzman, D. M. (2009), 'The role of apolipoprotein E in Alzheimer's disease', *Neuron,* 63 (3), 287-303.

Kim, W. and Hecht, M. H. (2008), 'Mutations enhance the aggregation propensity of the Alzheimer's A beta peptide', *J Mol Biol,* 377 (2), 565-74.

Kitteringham, N. R., et al. (2009), 'Multiple reaction monitoring for quantitative biomarker analysis in proteomics and metabolomics', *J Chromatogr B Analyt Technol Biomed Life Sci,* 877 (13), 1229-39.

Kiyonami, R. and Domon, B. (2010), 'Selected Reaction Monitoring Applied to Quantitative Proteomics', *Lc-Ms/Ms in Proteomics: Methods and Applications,* 658, 155-66.

Klein, W. (2006), 'Cytotoxic Intermediates in the Fibrillation Pathway: Aβ Oligomers in Alzheimer’s Disease as a Case Study', in VladimirN Uversky and AnthonyL Fink (eds.), *Protein Misfolding, Aggregation, and Conformational Diseases* (Protein Reviews, 4: Springer US), 60-81.

Kozlowski, H., et al. (2006), 'Metal Ion Binding Properties of Proteins Related to Neurodegeneration', *Neurodegenerative Diseases and Metal Ions* (John Wiley & Sons, Ltd), 61-87.

Kozlowski, H., et al. (2012), 'Copper, zinc and iron in neurodegenerative diseases (Alzheimer's, Parkinson's and prion diseases)', *Coordination Chemistry Reviews,* 256 (19,Äì20), 2129-41.

Krishnan, S., et al. (2003), 'Oxidative dimer formation is the critical rate-limiting step for parkinson's disease α-synuclein fibrillogenesis', *Biochemistry,* 42 (3), 829-37.

Kruger, R., et al. (1998), 'Ala30Pro mutation in the gene encoding alpha-synuclein in Parkinson's disease', *Nature Genetics,* 18 (2), 106-08.

Krysmann, M. J., et al. (2008), 'Self-assembly and hydrogelation of an amyloid peptide fragment', *Biochemistry,* 47 (16), 4597-605.

Kuo, Y. M., et al. (1996), 'Water-soluble Abeta (N-40, N-42) oligomers in normal and Alzheimer disease brains', *The Journal of biological chemistry,* 271 (8), 4077-81.

Kurz, T., et al. (2008), 'Lysosomes and oxidative stress in aging and apoptosis', *Biochimica et Biophysica Acta - General Subjects,* 1780 (11), 1291-303.

Kushioka, K. (1983), 'Catalytic Activity of Copper(Ii)-Ethylenediamine Complexes in Autoxidation of Phenols', *Journal of Organic Chemistry,* 48 (25), 4948-50.

Kushioka, K., Tanimoto, I., and Maruyama, K. (1989), 'Oxidation of 2,4-Di-T-Butylphenol with T-Butyl Hydroperoxide Catalyzed by Copper(Ii)-Ethylenediamine Complexes', *Journal of the Chemical Society-Perkin Transactions 2,* (9), 1303-08.

Labella, F., et al. (1967), 'Evidence for Dityrosine in Elastin', *Biochemical and Biophysical Research Communications,* 26 (6), 748-&.

Lakowicz, J.R. (1999), *Principles of Fluorescence Spectroscopy Second Edition* (Kluwer Academic/Plenum).

Lakowicz, J.R. (2007), *Principles of Fluorescence Spectroscopy* (Springer) 980.

Lashuel, H. A., et al. (2000), 'Protofilaments, filaments, ribbons, and fibrils from peptidomimetic self-assembly: implications for amyloid fibril formation and materials science', *J Am Chem Soc,* 122 (22), 5262-77.

Lavedan, C. (1998), 'The synuclein family', *Genome Res,* 8 (9), 871-80.

Lee, C. C., et al. (2007a), 'A three-stage kinetic model of amyloid fibrillation', *Biophys J,* 92 (10), 3448-58.

Lee, D. I., et al. (2011a), 'Large-scale production of N,N '-diBoc-dityrosine and dityrosine by HRP-catalyzed N-Boc-L-tyrosine oxidation and one-step chromatographic purification', *Process Biochemistry,* 46 (1), 142-47.

Lee, D. I., et al. (2008), 'A convenient preparation of dityrosine via Mn(III)-mediated oxidation of tyrosine', *Process Biochemistry,* 43 (9), 999-1003.

Lee, J., et al. (2011b), 'Amyloid-beta forms fibrils by nucleated conformational conversion of oligomers', *Nat Chem Biol,* 7 (9), 602-9.

Lee, J. C., et al. (2006), 'Protein Folding, Misfolding, and Disease', *Neurodegenerative Diseases and Metal Ions* (John Wiley & Sons, Ltd), 9-60.

Lee, J. Y., et al. (2002), 'Contribution by synaptic zinc to the gender-disparate plaque formation in human Swedish mutant APP transgenic mice', *Proc Natl Acad Sci U S A,* 99 (11), 7705-10.

Lee, S., Fernandez, E. J., and Good, T. A. (2007b), 'Role of aggregation conditions in structure, stability, and toxicity of intermediates in the Abeta fibril formation pathway', *Protein Sci,* 16 (4), 723-32.

Leeuwenburgh, C., et al. (1996), 'Massive increase in protein-bound dityrosine in LDL isolated from human atherosclerotic aorta: Implications for the role of tyrosyl radical in atherogenesis', *Circulation,* 94 (8), 2332-32.

Leeuwenburgh, C., et al. (1997a), 'Mass spectrometric quantification of markers for protein oxidation by tyrosyl radical, copper, and hydroxyl radical in low density lipoprotein isolated from human atherosclerotic plaques', *Journal of Biological Chemistry,* 272 (6), 3520-26.

Leeuwenburgh, Christiaan, et al. (1997b), 'Caloric Restriction Attenuates Dityrosine Cross-Linking of Cardiac and Skeletal Muscle Proteins in Aging Mice', *Archives of Biochemistry and Biophysics,* 346 (1), 74-80.

Lenvinthal, C. (1968), 'Are there pathways for proetin folding?', *Chimie Physique et de Physico-Chimie Biologique* 65, 44–45.

Leslie, A. G. W. (1992), 'Recent changes to the MOSFLM package for processing film and image plate data', *oint CCP4 + ESF-EAMCB Newsletter on Protein Crystallography,* 26.

Lesné, S. E., et al. (2013), 'Brain amyloid-β oligomers in ageing and Alzheimer's disease', *Brain,* 136 (5), 1383-98.

LeVine, H., 3rd (1993), 'Thioflavine T interaction with synthetic Alzheimer's disease beta-amyloid peptides: detection of amyloid aggregation in solution', *Protein Sci,* 2 (3), 404-10.

LeVine, H. (1999), 'Quantification of beta-sheet amyloid fibril structures with thioflavin T', *Methods Enzymol,* 309, 274-84.

Lewis, J., et al. (2001), 'Enhanced neurofibrillary degeneration in transgenic mice expressing mutant tau and APP', *Science,* 293 (5534), 1487-91.

Li, J., Hodgeman, B. A., and Christensen, B. M. (1996), 'Involvement of peroxidase in chorion hardening in Aedes aegypti', *Insect Biochem Mol Biol,* 26 (3), 309-17.

Lipton, M.S. and Paša-Tolic, L. (2009), *Mass Spectrometry of Proteins and Peptides: Methods and Protocols, Second Edition* (Humana Press).

Liu, C., Sawaya, M. R., and Eisenberg, D. (2011), 'beta(2)-microglobulin forms three-dimensional domain-swapped amyloid fibrils with disulfide linkages', *Nat Struct Mol Biol,* 18 (1), 49-55.

Loschen, G., Flohe', L., and Chance, B. (1971), 'Respiratory chain linked H(2)O(2) production in pigeon heart mitochondria', *Febs Letters,* 18 (2), 261-64.

Lovell, M. A., et al. (1998), 'Copper, iron and zinc in Alzheimer's disease senile plaques', *Journal of the Neurological Sciences,* 158 (1), 47-52.

Lu, J. X., et al. (2013), 'Molecular Structure of beta-Amyloid Fibrils in Alzheimer's Disease Brain Tissue', *Cell,* 154 (6), 1257-68.

Lucas, H. R. and Lee, J. C. (2010), 'Effect of dioxygen on copper(II) binding to alpha-synuclein', *Journal of Inorganic Biochemistry,* 104 (3), 245-49.

Lucas, H. R., et al. (2010), 'Evidence for copper-dioxygen reactivity during α-synuclein fibril formation', *Journal of the American Chemical Society,* 132 (19), 6636-37.

Luhrs, T., et al. (2005), '3D structure of Alzheimer's amyloid-beta(1-42) fibrils', *Proc Natl Acad Sci U S A,* 102 (48), 17342-7.

Maiti, N. C., et al. (2008), 'Mechanistic studies of Cu(II) binding to amyloid-beta peptides and the fluorescence and redox behaviors of the resulting complexes', *Journal of Physical Chemistry B,* 112 (28), 8406-11.

Maji, S. K., et al. (2009), 'Functional amyloids as natural storage of peptide hormones in pituitary secretory granules', *Science,* 325 (5938), 328-32.

Makin, O. S. and Serpell, L. C. (2005), 'Structures for amyloid fibrils', *Febs J,* 272 (23), 5950-61.

Makin, O. S., Sikorski, P., and Serpell, L. C. (2006), 'Diffraction to study protein and peptide assemblies', *Curr Opin Chem Biol,* 10 (5), 417-22.

Malencik, D. A. and Anderson, S. R. (1991), 'Fluorometric Characterization of Dityrosine - Complex-Formation with Boric-Acid and Borate Ion', *Biochemical and Biophysical Research Communications,* 178 (1), 60-67.

Malencik, D. A. and Anderson, S. R. (1996), 'Dityrosine formation in calmodulin: Cross-linking and polymerization catalyzed by Arthromyces peroxidase', *Biochemistry,* 35 (14), 4375-86.

Malencik, D. A., et al. (1996), 'Dityrosine: Preparation, Isolation, and Analysis', *Analytical Biochemistry,* 242 (2), 202-13.

Malinchik, S. B., et al. (1998), 'Structural analysis of Alzheimer's beta(1-40) amyloid: protofilament assembly of tubular fibrils', *Biophys J,* 74 (1), 537-45.

Manary, M. J., Leeuwenburgh, C., and Heinecke, J. W. (2000), 'Increased oxidative stress in kwashiorkor', *J Pediatr,* 137 (3), 421-4.

Manning, M. C., Illangasekare, M., and Woody, R. W. (1988), 'Circular dichroism studies of distorted alpha-helices, twisted beta-sheets, and beta turns', *Biophys Chem,* 31 (1-2), 77-86.

Mao, D. and Wallace, B. A. (1984), 'Differential light scattering and absorption flattening optical effects are minimal in the circular dichroism spectra of small unilamellar vesicles', *Biochemistry,* 23 (12), 2667-73.

Mariani, E., et al. (2005), 'Oxidative stress in brain aging, neurodegenerative and vascular diseases: an overview', *J Chromatogr B Analyt Technol Biomed Life Sci,* 827 (1), 65-75.

Marques, O. and Outeiro, T. F. (2012), 'Alpha-synuclein: from secretion to dysfunction and death', *Cell Death Dis,* 3, e350.

Marquez, L. A. and Dunford, H. B. (1995), 'Kinetics of oxidation of tyrosine and dityrosine by myeloperoxidase compounds I and II. Implications for lipoprotein peroxidation studies', *The Journal of biological chemistry,* 270 (51), 30434-40.

Marshall, K. E. and Serpell, L. C. (2009), 'Structural integrity of beta-sheet assembly', *Biochem Soc Trans,* 37 (Pt 4), 671-6.

Marshall, K. E. and Serpell, Louise C. (2010), 'Insights into the Structure of Amyloid Fibrils~!2009-04-21~!2009-07-09~!2010-01-02~!', *The Open Biology Journal,* 2 (2), 185-92.

Marshall, K. E., et al. (2010), 'Characterizing the assembly of the Sup35 yeast prion fragment, GNNQQNY: structural changes accompany a fiber-to-crystal switch', *Biophys J,* 98 (2), 330-8.

Marshall, K. E., et al. (2011), 'Hydrophobic, aromatic, and electrostatic interactions play a central role in amyloid fibril formation and stability', *Biochemistry,* 50 (12), 2061-71.

Masters, C. L., et al. (1985), 'Amyloid plaque core protein in Alzheimer disease and Down syndrome', *Proc Natl Acad Sci U S A,* 82 (12), 4245-9.

Masuda, M., et al. (2006), 'Cysteine misincorporation in bacterially expressed human alpha-synuclein', *FEBS Lett,* 580 (7), 1775-9.

Maurer-Stroh, S., et al. (2010), 'Exploring the sequence determinants of amyloid structure using position-specific scoring matrices', *Nature Methods,* 7 (3), 237-U109.

Maury, C. P. (2009), 'The emerging concept of functional amyloid', *J Intern Med,* 265 (3), 329-34.

Maynard, C. J., et al. (2002), 'Overexpression of Alzheimer's disease amyloid-beta opposes the age-dependent elevations of brain copper and iron', *Journal of Biological Chemistry,* 277 (47), 44670-76.

McParland, V. J., et al. (2000), 'Partially unfolded states of beta(2)-microglobulin and amyloid formation in vitro', *Biochemistry,* 39 (30), 8735-46.

Meinhardt, J. and Fandrich, M. (2009), '[Structure of amyloid fibrils]', *Pathologe,* 30 (3), 175-81.

Meinhardt, J., et al. (2009), 'Abeta(1-40) fibril polymorphism implies diverse interaction patterns in amyloid fibrils', *J Mol Biol,* 386 (3), 869-77.

Misonou, H., Morishima-Kawashima, M., and Ihara, Y. (2000), 'Oxidative stress induces intracellular accumulation of amyloid beta protein (AB) in human neuroblastoma cells', *Biochemistry,* 39 (23), 6951-59.

Moore, T. and Wang, Y. L. (1947), 'Formation of Fluorescent Pigment in Vitamin-E Deficiency', *British Journal of Nutrition,* 1 (1), 53-64.

Moreira, Paula I., et al. (2007), 'Chapter 12 - The key role of oxidative stress in alzheimer's disease', in G. Ali Qureshi and S. Hassan Parvez (eds.), *Oxidative Stress and Neurodegenerative Disorders* (Amsterdam: Elsevier Science B.V.), 267-81.

Morris, K. L. and Serpell, L. (2010), 'From natural to designer self-assembling biopolymers, the structural characterisation of fibrous proteins & peptides using fibre diffraction', *Chemical Society Reviews,* 39 (9), 3445-53.

Morris, K. L. and Serpell, L. C. (2012), 'X-ray fibre diffraction studies of amyloid fibrils', *Methods Mol Biol,* 849, 121-35.

Morris, K. L. and Serpell, L. C. (2013), 'From Molecular to Supramolecular Amyloid Structures: Contributions from Fiber Diffraction and Electron Microscopy', *Amyloid Fibrils and Prefibrillar Aggregates* (Wiley-VCH Verlag GmbH & Co. KGaA), 63-84.

Morris, K. L., et al. (2013a), 'The Structure of Cross-β Tapes and Tubes Formed by an Octapeptide, αSβ1', *Angewandte Chemie International Edition,* 52 (8), 2279-83.

Morris, K. L., et al. (2013b), 'Exploring the sequence-structure relationship for amyloid peptides', *Biochem J,* 450 (2), 275-83.

Murakami, K. and Shimizu, T. (2012), 'Cytoplasmic superoxide radical: a possible contributing factor to intracellular Abeta oligomerization in Alzheimer disease', *Commun Integr Biol,* 5 (3), 255-8.

Murakami, K., et al. (2011), 'SOD1 (Copper/Zinc Superoxide Dismutase) Deficiency Drives Amyloid beta Protein Oligomerization and Memory Loss in Mouse Model of Alzheimer Disease', *Journal of Biological Chemistry,* 286 (52), 44557-68.

Murakami, K., et al. (2010), 'Monoclonal Antibody Against the Turn of the 42-Residue Amyloid β-Protein at Positions 22 and 23', *ACS Chemical Neuroscience,* 1 (11), 747-56.

Murphy, R. M. (2007), 'Kinetics of amyloid formation and membrane interaction with amyloidogenic proteins', *Biochim Biophys Acta,* 1768 (8), 1923-34.

Nair, N. G., et al. (2010), 'NMR Studies of Zinc, Copper, and Iron Binding to Histidine, the Principal Metal Ion Complexing Site of Amyloid-beta Peptide', *Journal of Alzheimers Disease,* 20 (1), 57-66.

Nakamura, T., et al. (2001), 'Activated Fyn phosphorylates alpha-synuclein at tyrosine residue 125', *Biochemical and Biophysical Research Communications,* 280 (4), 1085-92.

Naylor, R., Hill, A. F., and Barnham, K. J. (2008), 'Neurotoxicity in Alzheimer's disease: is covalently crosslinked A beta responsible?', *Eur Biophys J,* 37 (3), 265-8.

Negro, A., et al. (2002), 'Multiple phosphorylation of alpha-synuclein by protein tyrosine kinase Syk prevents eosin-induced aggregation', *FASEB J,* 16 (2), 210-2.

Nelson, R., et al. (2005), 'Structure of the cross-beta spine of amyloid-like fibrils', *Nature,* 435 (7043), 773-8.

Nielsen, J. T., et al. (2009), 'Unique identification of supramolecular structures in amyloid fibrils by solid-state NMR spectroscopy', *Angew Chem Int Ed Engl,* 48 (12), 2118-21.

Nilsson, M. R. (2004), 'Techniques to study amyloid fibril formation in vitro', *Methods,* 34 (1), 151-60.

Nishiyama, S., Kim, M. H., and Yamamura, S. (1994), 'Syntheses of Isodityrosine, Dityrosine and Related-Compounds by Phenolic Oxidation of Tyrosine and Phenylglycine Derivatives Using an Electrochemical Method', *Tetrahedron Letters,* 35 (45), 8397-400.

Norden, B., Rodger, A., and Dafforn, T. (2010), 'Linear Dichroism and Circular Dichroism: A Textbook on Polarized Light Spectroscopy', *Linear Dichroism and Circular Dichroism: A Textbook on Polarized Light Spectroscopy*, 1-+.

O'Brien, R. J. and Wong, P. C. (2011), 'Amyloid precursor protein processing and Alzheimer's disease', *Annu Rev Neurosci,* 34, 185-204.

Onuchic, J. N. and Wolynes, P. G. (2004), 'Theory of protein folding', *Curr Opin Struct Biol,* 14 (1), 70-5.

Opazo, C., et al. (2002), 'Metalloenzyme-like activity of Alzheimer's disease beta-amyloid. Cu-dependent catalytic conversion of dopamine, cholesterol, and biological reducing agents to neurotoxic H(2)O(2)', *J Biol Chem,* 277 (43), 40302-8.

Orhan, H., Coolen, S., and Meerman, J. H. N. (2005), 'Quantification of urinary o,o '-dityrosine, a biomarker for oxidative damage to proteins, by high performance liquid chromatography with triple quadrupole tandem mass spectrometry - A comparison with ion-trap tandem mass spectrometry', *Journal of Chromatography B-Analytical Technologies in the Biomedical and Life Sciences,* 827 (1), 104-08.

Orpiszewski, J. and Benson, M. D. (1999), 'Induction of beta-sheet structure in amyloidogenic peptides by neutralization of aspartate: A model for amyloid nucleation', *Journal of Molecular Biology,* 289 (2), 413-28.

Outten, C. E. and O'Halloran, T. V. (2001), 'Femtomolar sensitivity of metalloregulatory proteins controlling zinc homeostasis', *Science,* 292 (5526), 2488-92.

Paik, S. R., Shin, H. J., and Lee, J. H. (2000), 'Metal-catalyzed oxidation of alpha-synuclein in the presence of Copper(II) and hydrogen peroxide', *Arch Biochem Biophys,* 378 (2), 269-77.

Paik, S. R., et al. (1999), 'Copper(II)-induced self-oligomerization of alpha-synuclein', *Biochem J,* 340 (Pt 3), 821-8.

Pall, H. S., et al. (1987), 'RAISED CEREBROSPINAL-FLUID COPPER CONCENTRATION IN PARKINSON'S DISEASE', *The Lancet,* 330 (8553), 238-41.

Paravastu, A. K., et al. (2008), 'Molecular structural basis for polymorphism in Alzheimer's beta-amyloid fibrils', *Proc Natl Acad Sci U S A,* 105 (47), 18349-54.

Pastor, M. T., et al. (2008), 'Amyloid toxicity is independent of polypeptide sequence, length and chirality', *Journal of Molecular Biology,* 375 (3), 695-707.

Patel, R. N., et al. (2002), 'Potentiometric and spectrometric study: Copper(II), nickel(II) and zinc(II) complexes with potentially tridentate and monodentate ligands', *Journal of Chemical Sciences,* 114 (2), 115-24.

Pawar, A. P., et al. (2005), 'Prediction of "aggregation-prone" and "aggregation-susceptible" regions in proteins associated with neurodegenerative diseases', *J Mol Biol,* 350 (2), 379-92.

Pennathur, S., et al. (1999a), 'Marked elevations of 3-nitrotyrosine and dityrosine in mice with MPTP-induced Parkinson's Disease', *Free Radical Biology and Medicine,* 27, S141-S41.

Pennathur, S., et al. (1999b), 'Mass spectrometric quantification of 3-nitrotyrosine, ortho-tyrosine, and o,o'-dityrosine in brain tissue of 1-methyl-4-phenyl-1,2,3, 6-tetrahydropyridine-treated mice, a model of oxidative stress in Parkinson's disease', *The Journal of biological chemistry,* 274 (49), 34621-8.

Pepys, M. B. (2006), 'Amyloidosis', *Annu Rev Med,* 57, 223-41.

Petkova, A. T., Yau, W. M., and Tycko, R. (2006), 'Experimental constraints on quaternary structure in Alzheimer's beta-amyloid fibrils', *Biochemistry,* 45 (2), 498-512.

Petkova, A. T., et al. (2004), 'Solid state NMR reveals a pH-dependent antiparallel beta-sheet registry in fibrils formed by a beta-amyloid peptide', *J Mol Biol,* 335 (1), 247-60.

Petkova, A. T., et al. (2005), 'Self-propagating, molecular-level polymorphism in Alzheimer's beta-amyloid fibrils', *Science,* 307 (5707), 262-5.

Petkova, A. T., et al. (2002), 'A structural model for Alzheimer's beta -amyloid fibrils based on experimental constraints from solid state NMR', *Proc Natl Acad Sci U S A,* 99 (26), 16742-7.

Pitt, J. J. (2009), 'Principles and applications of liquid chromatography-mass spectrometry in clinical biochemistry', *Clin Biochem Rev,* 30 (1), 19-34.

Porta, E. A. (2002), 'Pigments in aging: an overview', *Ann N Y Acad Sci,* 959, 57-65.

Puglielli, L., et al. (2005), 'Alzheimer disease beta-amyloid activity mimics cholesterol oxidase', *J Clin Invest,* 115 (9), 2556-63.

Radford, S. E. (2000), 'Protein folding: progress made and promises ahead', *Trends in Biochemical Sciences,* 25 (12), 611-18.

Radford, S. E. and Dobson, C. M. (1999), 'From computer simulations to human disease: emerging themes in protein folding', *Cell,* 97 (3), 291-8.

Rambaran, R. N. and Serpell, L. C. (2008), 'Amyloid fibrils: abnormal protein assembly', *Prion,* 2 (3), 112-7.

Rashed, M. S., et al. (1997), 'Screening blood spots for inborn errors of metabolism by electrospray tandem mass spectrometry with a microplate batch process and a computer algorithm for automated flagging of abnormal profiles', *Clin Chem,* 43 (7), 1129-41.

Rasia, R. M., et al. (2005), 'Structural characterization of copper(II) binding to alpha-synuclein: Insights into the bioinorganic chemistry of Parkinson's disease', *Proc Natl Acad Sci U S A,* 102 (12), 4294-9.

Raven, D. J., Earland, C., and Little, M. (1971), 'Occurrence of Dityrosine in Tussah Silk Fibroin and Keratin', *Biochimica Et Biophysica Acta,* 251 (1), 96-&.

Recchia, A., et al. (2004), 'Alpha-synuclein and Parkinson's disease', *FASEB J,* 18 (6), 617-26.

Reimer, L., and Kohl, H. (2008), *Transmission electron microscopy : physics of image formation* (5th edn., Springer series in optical sciences; New York, NY: Springer) xvi, 587 p.

Relini, A., Marano, N., and Gliozzi, A. (2014), 'Misfolding of Amyloidogenic Proteins and Their Interactions with Membranes', *Biomolecules,* 4 (1), 20-55.

Reynolds, Wanda F., et al. (1999), 'Myeloperoxidase Polymorphism Is Associated with Gender Specific Risk for Alzheimer's Disease', *Exp Neurol,* 155 (1), 31-41.

Richardson, J. C., et al. (2003), 'Ultrastructural and behavioural changes precede amyloid deposition in a transgenic model of Alzheimer's disease', *Neuroscience,* 122 (1), 213-28.

Ritchie, C. W., et al. (2003), 'Metal-protein attenuation with iodochlorhydroxyquin (clioquinol) targeting Abeta amyloid deposition and toxicity in Alzheimer disease: a pilot phase 2 clinical trial', *Arch Neurol,* 60 (12), 1685-91.

Robbins, K. J., et al. (2012), 'Conformational analysis of thioflavin T bound to the surface of amyloid fibrils', *Langmuir,* 28 (48), 16490-95.

Roberti, M. J., et al. (2009), 'Quantum Dots As Ultrasensitive Nanoactuators and Sensors of Amyloid Aggregation in Live Cells', *Journal of the American Chemical Society,* 131 (23), 8102-07.

Roberts, B. R., et al. (2012), 'The role of metallobiology and amyloid-beta peptides in Alzheimer's disease', *J Neurochem,* 120 Suppl 1, 149-66.

Rochet, J. C., Conway, K. A., and Lansbury, P. T., Jr. (2000), 'Inhibition of fibrillization and accumulation of prefibrillar oligomers in mixtures of human and mouse alpha-synuclein', *Biochemistry,* 39 (35), 10619-26.

Rodger, A. (2010), 'Circular and Linear Dichroism of Drug-DNA Systems', *Drug-DNA Interaction Protocols, Second Edition,* 613, 37-54.

Rodger, A., et al. (2006), 'Looking at long molecules in solution: what happens when they are subjected to Couette flow?', *Phys Chem Chem Phys,* 8 (27), 3161-71.

Rogers, J. T., et al. (2002), 'An iron-responsive element type II in the 5'-untranslated region of the Alzheimer's amyloid precursor protein transcript', *J Biol Chem,* 277 (47), 45518-28.

Roher, A. E., et al. (1996), 'Morphology and Toxicity of AŒ≤-(1-42) Dimer Derived from Neuritic and Vascular Amyloid Deposits of Alzheimer's Disease', *Journal of Biological Chemistry,* 271 (34), 20631-35.

Rolinski, O. J., Amaro, M., and Birch, D. J. (2010), 'Early detection of amyloid aggregation using intrinsic fluorescence', *Biosens Bioelectron,* 25 (10), 2249-52.

Romano, A., et al. (2003), 'Neuronal fibrillogenesis: amyloid fibrils from primary neuronal cultures impair long-term memory in the crab Chasmagnathus', *Behavioural Brain Research,* 147 (1-2), 73-82.

Roychaudhuri, R., et al. (2009), 'Amyloid Beta-Protein Assembly and Alzheimer Disease', *Journal of Biological Chemistry,* 284 (8), 4749-53.

Ruf, R. A., et al. (2008), 'Alpha-Synuclein conformation affects its tyrosine-dependent oxidative aggregation', *Biochemistry,* 47 (51), 13604-9.

Sabate, R. and Saupe, S. J. (2007), 'Thioflavin T fluorescence anisotropy: an alternative technique for the study of amyloid aggregation', *Biochem Biophys Res Commun,* 360 (1), 135-8.

Sabate, Raimon, et al. (2013), 'Thioflavin-T excimer formation upon interaction with amyloid fibers', *Chemical Communications,* 49 (51), 5745-47.

Sakono, M. and Zako, T. (2010), 'Amyloid oligomers: formation and toxicity of Abeta oligomers', *FEBS J,* 277 (6), 1348-58.

Salazar, G., et al. (2009), 'SLC30A3 (ZnT3) Oligomerization by Dityrosine Bonds Regulates Its Subcellular Localization and Metal Transport Capacity', *Plos One,* 4 (6).

Sarell, C. J., Wilkinson, S. R., and Viles, J. H. (2010), 'Substoichiometric Levels of Cu2+ Ions Accelerate the Kinetics of Fiber Formation and Promote Cell Toxicity of Amyloid-beta from Alzheimer Disease', *Journal of Biological Chemistry,* 285 (53), 41533-40.

Sasaki, A., et al. (2002), 'Amyloid cored plaques in Tg2576 transgenic mice are characterized by giant plaques, slightly activated microglia, and the lack of paired helical filament-typed, dystrophic neurites', *Virchows Arch,* 441 (4), 358-67.

Savenkova, M. I., Mueller, D. M., and Heinecke, J. W. (1994), 'Tyrosyl radical generated by myeloperoxidase is a physiological catalyst for the initiation of lipid peroxidation in low density lipoprotein', *Journal of Biological Chemistry,* 269 (32), 20394-400.

Sawada, T., Mihara, H., and Serizawa, T. (2013), 'Peptides as New Smart Bionanomaterials: Molecular-Recognition and Self-Assembly Capabilities', *The Chemical Record,* 13 (2), 172-86.

Sawaya, M. R., et al. (2007), 'Atomic structures of amyloid cross-beta spines reveal varied steric zippers', *Nature,* 447 (7143), 453-7.

Sayre, L. M., et al. (2000), 'In situ oxidative catalysis by neurofibrillary tangles and senile plaques in Alzheimer's disease: a central role for bound transition metals', *J Neurochem,* 74 (1), 270-9.

Scheinost, J. C., et al. (2010), 'Role of Oxidative Stress in Protein Misfolding and/or Amyloid Formation', *Protein Misfolding Diseases* (John Wiley & Sons, Inc.), 615-30.

Schellman (1975), 'Circular Dicroism and Optical Rotation', *Chemical Reviews,* 75 (3), 323-31.

Seidel, C., Orth, A., and Greulich, K. O. (1993), 'Electronic effects on the fluorescence of tyrosine in small peptides', *Photochem Photobiol,* 58 (2), 178-84.

Selkoe, D. J. (1991), 'The molecular pathology of Alzheimer's disease', *Neuron,* 6 (4), 487-98.

Selkoe, D. J. (2000), 'The genetics and molecular pathology of Alzheimer's disease: roles of amyloid and the presenilins', *Neurologic clinics,* 18 (4), 903-22.

Serpell, L. C. (2000), 'Alzheimer's amyloid fibrils: structure and assembly', *Biochim Biophys Acta,* 1502 (1), 16-30.

Serpell, L. C. and Smith, J. M. (2000), 'Direct visualisation of the beta-sheet structure of synthetic Alzheimer's amyloid', *J Mol Biol,* 299 (1), 225-31.

Serpell, L. C., Sunde, M., and Blake, C. C. (1997), 'The molecular basis of amyloidosis', *Cell Mol Life Sci,* 53 (11-12), 871-87.

Serpell, L. C., Fraser, P. E., and Sunde, M. (1999), 'X-ray fiber diffraction of amyloid fibrils', *Methods Enzymol,* 309, 526-36.

Serpell, L. C., et al. (2000a), 'Fiber diffraction of synthetic alpha-synuclein filaments shows amyloid-like cross-beta conformation', *Proc Natl Acad Sci U S A,* 97 (9), 4897-902.

Serpell, L. C., et al. (2000b), 'The protofilament substructure of amyloid fibrils', *J Mol Biol,* 300 (5), 1033-9.

Shankar, G. M., et al. (2008), 'Amyloid-beta protein dimers isolated directly from Alzheimer's brains impair synaptic plasticity and memory', *Nature medicine,* 14 (8), 837-42.

Sharma, M. and Jain, R. (1998), 'Isolation and analysis of dityrosine from enzyme-catalyzed oxidation of tyrosine and X-irradiated peptide and proteins', *Chemico-Biological Interactions,* 108 (3), 171-85.

Sian-Hulsmann, J., et al. (2011), 'The relevance of iron in the pathogenesis of Parkinson's disease', *J Neurochem,* 118 (6), 939-57.

Sisodia, S. S. and Gallagher, M. (1998), 'A role for the beta-amyloid precursor protein in memory?', *Proc Natl Acad Sci U S A,* 95 (21), 12074-6.

Skaff, O., Jolliffe, K. A., and Hutton, C. A. (2005), 'Synthesis of the side chain cross-linked tyrosine oligomers dityrosine, trityrosine, and pulcherosine', *Journal of Organic Chemistry,* 70 (18), 7353-63.

Smail, E. H., et al. (1995), 'Candida-Albicans Cell-Walls Contain the Fluorescent Cross-Linking Amino-Acid Dityrosine', *Infection and Immunity,* 63 (10), 4078-83.

Smith, D. P., et al. (2007), 'Concentration dependent Cu2+ induced aggregation and dityrosine formation of the Alzheimer's disease amyloid-beta peptide', *Biochemistry,* 46 (10), 2881-91.

Smith, D. P., et al. (2006a), 'Copper-mediated amyloid-beta toxicity is associated with an intermolecular histidine bridge', *J Biol Chem,* 281 (22), 15145-54.

Smith, J. F., et al. (2006b), 'Characterization of the nanoscale properties of individual amyloid fibrils', *Proc Natl Acad Sci U S A,* 103 (43), 15806-11.

Smith, M. A., et al. (1997), 'Widespread peroxynitrite-mediated damage in Alzheimer's disease', *J Neurosci,* 17 (8), 2653-7.

Smith, M. A., et al. (1996), 'Oxidative damage in Alzheimer's', *Nature,* 382 (6587), 120-1.

Sorgjerd, K., et al. (2008), 'Prefibrillar transthyretin oligomers and cold stored native tetrameric transthyretin are cytotoxic in cell culture', *Biochemical and Biophysical Research Communications,* 377 (4), 1072-78.

Soto, C., et al. (1995), 'Fibrillogenesis of synthetic amyloid-beta peptides is dependent on their initial secondary structure', *Neurosci Lett,* 200 (2), 105-8.

Soura, V., et al. (2012), 'Visualization of co-localization in Abeta42-administered neuroblastoma cells reveals lysosome damage and autophagosome accumulation related to cell death', *Biochem J,* 441 (2), 579-90.

Souza, J. M., et al. (2000), 'Dityrosine cross-linking promotes formation of stable alpha-synuclein polymers - Implication of nitrative and oxidative stress in the pathogenesis of neurodegenerative synucleinopathies', *Journal of Biological Chemistry,* 275 (24), 18344-49.

Spillantini, M. G., et al. (1997), 'Alpha-synuclein in Lewy bodies', *Nature,* 388 (6645), 839-40.

Sreerama, N., et al. (1999), 'Tyrosine, phenylalanine, and disulfide contributions to the circular dichroism of proteins: circular dichroism spectra of wild-type and mutant bovine pancreatic trypsin inhibitor', *Biochemistry,* 38 (33), 10814-22.

Stankiewicz, J., et al. (2007), 'Iron in chronic brain disorders: imaging and neurotherapeutic implications', *Neurotherapeutics,* 4 (3), 371-86.

Starck, C. S. and Sutherland-Smith, A. J. (2010), 'Cytotoxic aggregation and amyloid formation by the myostatin precursor protein', *PLoS One,* 5 (2), e9170.

Stefanis, L. (2012), 'alpha-Synuclein in Parkinson's disease', *Cold Spring Harb Perspect Med,* 2 (2), a009399.

Streltsov, V. A., et al. (2008), 'The structure of the amyloid-beta peptide high-affinity copper II binding site in Alzheimer disease', *Biophysical Journal,* 95 (7), 3447-56.

Strickland, E. H. (1974), 'Aromatic contributions to circular dichroism spectra of proteins', *CRC Crit Rev Biochem,* 2 (1), 113-75.

Stromer, T. and Serpell, L. C. (2005), 'Structure and morphology of the Alzheimer's amyloid fibril', *Microsc Res Tech,* 67 (3-4), 210-7.

Strozyk, D., and Bush, A. I. (2006), 'The Role of Metal Ions in Neurology. An Introduction', *Neurodegenerative Diseases and Metal Ions*, 1-7.

Stsiapura, V. I., et al. (2008), 'Thioflavin T as a Molecular Rotor: Fluorescent Properties of Thioflavin T in Solvents with Different Viscosity', *Journal of Physical Chemistry B,* 112 (49), 15893-902.

Suh, S. W., et al. (2000), 'Histochemically-reactive zinc in amyloid plaques, angiopathy, and degenerating neurons of Alzheimer's diseased brains', *Brain Research,* 852 (2), 274-8.

Sunde, M., et al. (1997), 'Common core structure of amyloid fibrils by synchrotron X-ray diffraction', *J Mol Biol,* 273 (3), 729-39.

Syme, C. D., et al. (2004), 'Copper binding to the amyloid-beta (A beta) peptide associated with Alzheimer's disease - Folding, coordination geometry, pH dependence, stoichiometry, and affinity of A beta-(1-28): Insights from a range of complementary spectroscopic techniques', *Journal of Biological Chemistry,* 279 (18), 18169-77.

Szweda, P. A., et al. (2003), 'Aging, lipofuscin formation, and free radical-mediated inhibition of cellular proteolytic systems', *Ageing Research Reviews,* 2 (4), 383-405.

Takasaki, S., et al. (2005), 'Effects of peroxidase and hydrogen peroxide on the dityrosine formation and the mixing characteristics of wheat-flour dough', *Bioscience Biotechnology and Biochemistry,* 69 (9), 1686-92.

Tanner, C. M. and Goldman, S. M. (1996), 'Epidemiology of Parkinson's disease', *Neurol Clin,* 14 (2), 317-35.

Tattum, M. H., et al. (2006), 'Elongated oligomers assemble into mammalian PrP amyloid fibrils', *Journal of Molecular Biology,* 357 (3), 975-85.

Terman, A. and Brunk, U. T. (1998a), 'Ceroid/lipofuscin formation in cultured human fibroblasts: the role of oxidative stress and lysosomal proteolysis', *Mech Ageing Dev,* 104 (3), 277-91.

Terman, Alexei and Brunk, Ulf T. (1998b), 'Lipofuscin: Mechanisms of formation and increase with age', *APMIS,* 106 (1-6), 265-76.

Terman, Alexei and Brunk, Ulf T. (2004), 'Lipofuscin', *The International Journal of Biochemistry & Cell Biology,* 36 (8), 1400-04.

Thorpe, J. R. (1999), 'The Application of LR Gold Resin for Immunogold Labeling', *Electron Microscopy Methods and Protocols,* 117, 99-110.

Thorpe, J. R., Morley, S. J., and Rulten, S. L. (2001), 'Utilizing the peptidyl-prolyl cis-trans isomerase Pin1 as a probe of its phosphorylated target proteins: Examples of binding to nuclear proteins in a human kidney cell line and to tau in Alzheimer's diseased brain', *Journal of Histochemistry and Cytochemistry,* 49 (1), 97-107.

Thorpe, J. R., et al. (2004), 'Shortfalls in the peptidyl-prolyl cis-trans isomerase protein Pin1 in neurons are associated with frontotemporal dementias', *Neurobiol Dis,* 17 (2), 237-49.

Tickler, A. K., et al. (2005), 'Methylation of the imidazole side chains of the Alzheimer disease amyloid-beta peptide results in abolition of superoxide dismutase-like structures and inhibition of neurotoxicity', *J Biol Chem,* 280 (14), 13355-63.

Tilley, M., et al. (2004), 'Nonenzymatic preparative-scale synthesis of dityrosine and 3-bromotyrosine', *Analytical Biochemistry,* 334 (1), 193-95.

Tinker, D. A., et al. (1988), 'Synthetic beta-turn peptides as substrates for a tyrosine protein kinase', *J Biol Chem,* 263 (11), 5024-6.

Touchette, J. C., et al. (2010), 'Probing the amyloid-beta(1-40) fibril environment with substituted tryptophan residues', *Archives of Biochemistry and Biophysics,* 494 (2), 192-97.

Tougu, V., Karafin, A., and Palumaa, P. (2008), 'Binding of zinc(II) and copper(II) to the full-length Alzheimer's amyloid-beta peptide', *Journal of Neurochemistry,* 104 (5), 1249-59.

Turner, P. R., et al. (2003), 'Roles of amyloid precursor protein and its fragments in regulating neural activity, plasticity and memory', *Prog Neurobiol,* 70 (1), 1-32.

Ulrih, N. P., Barry, C. H., and Fink, A. L. (2008), 'Impact of Tyr to Ala mutations on alpha-synuclein fibrillation and structural properties', *Biochim Biophys Acta,* 1782 (10), 581-5.

Umeda, T., et al. (2011), 'Intraneuronal amyloid beta oligomers cause cell death via endoplasmic reticulum stress, endosomal/lysosomal leakage, and mitochondrial dysfunction in vivo', *Journal of neuroscience research,* 89 (7), 1031-42.

Uversky, V. N. and Fink, A. L. (2004), 'Conformational constraints for amyloid fibrillation: the importance of being unfolded', *Biochim Biophys Acta,* 1698 (2), 131-53.

Uversky, V. N., Li, Jie, and Fink, Anthony L. (2001), 'Metal-triggered Structural Transformations, Aggregation, and Fibrillation of Human α-Synuclein: A possible molecular link between Parkinson's disease and heavy metal exposure', *Journal of Biological Chemistry,* 276 (47), 44284-96.

Uversky, V. N., Fernández, Ariel, and Fink, AnthonyL (2006a), 'Structural and Conformational Prerequisites of Amyloidogenesis', in VladimirN Uversky and

AnthonyL Fink (eds.), *Protein Misfolding, Aggregation, and Conformational Diseases* (Protein Reviews, 4: Springer US), 1-20.

Uversky, V. N., Kabanov, A. V., and Lyubchenko, Y. L. (2006b), 'Nanotools for megaproblems: probing protein misfolding diseases using nanomedicine modus operandi', *J Proteome Res,* 5 (10), 2505-22.

Vabulas, R. M., et al. (2010), 'Protein folding in the cytoplasm and the heat shock response', *Cold Spring Harb Perspect Biol,* 2 (12), a004390.

Valiente-Gabioud, A. A., et al. (2012), 'Structural basis behind the interaction of Zn(2)(+) with the protein alpha-synuclein and the Abeta peptide: a comparative analysis', *J Inorg Biochem,* 117, 334-41.

Van Der Vliet, A., et al. (2000), 'Myeloperoxidase and protein oxidation in cystic fibrosis', *Am J Physiol Lung Cell Mol Physiol,* 279 (3), L537-46.

Vassar, P. S. and Culling, C. F. (1959), 'Fluorescent stains, with special reference to amyloid and connective tissues', *Arch Pathol,* 68, 487-98.

Vilar, M., et al. (2008), 'The fold of α-synuclein fibrils', *Proceedings of the National Academy of Sciences,* 105 (25), 8637-42.

Viles, J. H. (2012), 'Metal ions and amyloid fiber formation in neurodegenerative diseases. Copper, zinc and iron in Alzheimer's, Parkinson's and prion diseases', *Coordination Chemistry Reviews,* 256 (19-20), 2271-84.

Virchow, R. (1854), 'Zur Cellulose —Frage', *Archiv für pathologische Anatomie und Physiologie und für klinische Medicin,* 6 (3), 416-26.

Wallace, B. A. (2009), 'Protein characterisation by synchrotron radiation circular dichroism spectroscopy', *Q Rev Biophys,* 42 (4), 317-70.

Wallace, B. A. and Janes, R. W. (2009), *Modern techniques for circular dichroism and synchrotron radiation circular dichroism spectroscopy* (Advances in biomedical spectroscopy,; Amsterdam ; Washington, DC: IOS Press) xii, 231 p.

Walsh, D. M. and Selkoe, D. J. (2007), 'A beta oligomers - a decade of discovery', *J Neurochem,* 101 (5), 1172-84.

Walsh, D. M., et al. (1997), 'Amyloid beta-protein fibrillogenesis. Detection of a protofibrillar intermediate', *J Biol Chem,* 272 (35), 22364-72.

Walsh, D. M., et al. (2002), 'Naturally secreted oligomers of amyloid Œ≤ protein potently inhibit hippocampal long-term potentiation in vivo', *Nature,* 416 (6880), 535-39.

Wang, H., et al. (2012), 'Immunogold labeling and X-ray fluorescence microscopy reveal enrichment ratios of Cu and Zn, metabolism of APP and amyloid-beta plaque formation in a mouse model of Alzheimer's disease', *Metallomics,* 4 (10), 1113-8.

Wang, X., et al. (2010), 'Copper binding regulates intracellular alpha-synuclein localisation, aggregation and toxicity', *J Neurochem,* 113 (3), 704-14.

Wasmer, C., et al. (2008), 'Infectious and noninfectious amyloids of the HET-s(218-289) prion have different NMR spectra', *Angew Chem Int Ed Engl,* 47 (31), 5839-41.

Waters, W., A. (1952), *Organic chemsitry* (IV; H. Gilman. New York: John Wiley and Sons, Inc.).

Watson, J. Throck and Sparkman, O. David (2007), 'Mass Spectrometry/Mass Spectrometry', *Introduction to Mass Spectrometry* (John Wiley & Sons, Ltd), 173-228.

Watson, J. Throck and Sparkman, O. David (2008), 'Front Matter', *Introduction to Mass Spectrometry* (John Wiley & Sons, Ltd), i-xxiv.

Waykole, P. and Heidemann, E. (1976), 'Dityrosine in Collagen', *Connective Tissue Research,* 4 (4), 219-22.

Wegiel, J., et al. (2003), 'Origin and turnover of microglial cells in fibrillar plaques of APPsw transgenic mice', *Acta Neuropathol,* 105 (4), 393-402.

Wegiel, J., et al. (2002), 'Vascular fibrosis and calcification in the hippocampus in aging, Alzheimer disease, and Down syndrome', *Acta Neuropathol,* 103 (4), 333-43.

Wegiel, J., et al. (2001), 'The role of microglial cells and astrocytes in fibrillar plaque evolution in transgenic APP(SW) mice', *Neurobiol Aging,* 22 (1), 49-61.

Wells-Knecht, M. C., et al. (1993), 'Oxidized amino acids in lens protein with age. Measurement of o-tyrosine and dityrosine in the aging human lens', *The Journal of biological chemistry,* 268 (17), 12348-52.

Westermark, P. (2005), 'Amyloidosis and Amyloid Proteins: Brief History and Definitions', *Amyloid Proteins* (Wiley-VCH Verlag GmbH), 2-27.

Westermark, P., et al. (2007), 'A primer of amyloid nomenclature', *Amyloid,* 14 (3), 179-83.

White, H. E., et al. (2009), 'Globular Tetramers of beta(2)-Microglobulin Assemble into Elaborate Amyloid Fibrils', *J Mol Biol.*

Williams, D. B. and Carter, C. B. (2008), *Transmission electron microscopy : a textbook for materials science*, 4 vols. (2nd edn.; New York: Springer).

Williams, T. L., Day, I. J., and Serpell, L. C. (2010), 'The effect of Alzheimer's Abeta aggregation state on the permeation of biomimetic lipid vesicles', *Langmuir,* 26 (22), 17260-8.

Williams, T. L., et al. (2011), 'Abeta42 oligomers, but not fibrils, simultaneously bind to and cause damage to ganglioside-containing lipid membranes', *Biochem J,* 439 (1), 67-77.

Winner, B., et al. (2011), 'In vivo demonstration that alpha-synuclein oligomers are toxic', *Proceedings of the National Academy of Sciences of the United States of America,* 108 (10), 4194-99.

Wood, S. P., et al. (1975), 'The relation of conformation and association of insulin to receptor binding; x-ray and circular-dichroism studies on bovine and hystricomorph insulins', *Eur J Biochem,* 55 (3), 531-42.

Woody, R. W. (1978), 'Aromatic side-chain contributions to the far ultraviolet circular dichroism of peptides and proteins', *Biopolymers,* 17 (6), 1451-67.

Woody, R. W. (1994), 'Contributions of tryptophan side chains to the far-ultraviolet circular dichroism of proteins', *Eur Biophys J,* 23 (4), 253-62.

Wright, J. A., Wang, X., and Brown, D. R. (2009), 'Unique copper-induced oligomers mediate alpha-synuclein toxicity', *FASEB J,* 23 (8), 2384-93.

Wu, C., et al. (2009), 'Binding Modes of Thioflavin-T to the Single-Layer beta-Sheet of the Peptide Self-Assembly Mimics', *Journal of Molecular Biology,* 394 (4), 627-33.

Xia, W., et al. (2000), 'Presenilin complexes with the C-terminal fragments of amyloid precursor protein at the sites of amyloid beta-protein generation', *Proceedings of the National Academy of Sciences of the United States of America,* 97 (16), 9299-304.

Xue, W. F., Homans, S. W., and Radford, S. E. (2008), 'Systematic analysis of nucleation-dependent polymerization reveals new insights into the mechanism of amyloid self-assembly', *Proc Natl Acad Sci U S A,* 105 (26), 8926-31.

Yamin, G., et al. (2003), 'Certain metals trigger fibrillation of methionine-oxidized alpha-synuclein', *J Biol Chem,* 278 (30), 27630-5.

Yang, A. J., et al. (1998), 'Loss of endosomal/lysosomal membrane impermeability is an early event in amyloid A beta 1-42 pathogenesis', *Journal of Neuroscience Research,* 52 (6), 691-98.

Yoburn, J. C., et al. (2003), 'Dityrosine cross-linked Abeta peptides: fibrillar beta-structure in Abeta(1-40) is conducive to formation of dityrosine cross-links but a dityrosine cross-link in Abeta(8-14) does not induce beta-structure', *Chemical research in toxicology,* 16 (4), 531-5.

Yoon, E. J., et al. (2009), 'Intracellular amyloid beta interacts with SOD1 and impairs the enzymatic activity of SOD1: implications for the pathogenesis of amyotrophic lateral sclerosis', *Exp Mol Med,* 41 (9), 611-7.

Youdim, M. B., Fridkin, M., and Zheng, H. (2004), 'Novel bifunctional drugs targeting monoamine oxidase inhibition and iron chelation as an approach to neuroprotection in Parkinson's disease and other neurodegenerative diseases', *J Neural Transm,* 111 (10-11), 1455-71.

Younan, N. D., et al. (2011), 'Copper(II)-induced secondary structure changes and reduced folding stability of the prion protein', *J Mol Biol,* 410 (3), 369-82.

Yu, W. H., et al. (2005), 'Macroautophagy--a novel Beta-amyloid peptide-generating pathway activated in Alzheimer's disease', *The Journal of cell biology,* 171 (1), 87-98.

Zhang, H., et al. (2012), 'Proteolytic processing of Alzheimer's beta-amyloid precursor protein', *J Neurochem,* 120 Suppl 1, 9-21.

Zhang, H., et al. (2004), 'The carbonate radical anion-induced covalent aggregation of human copper, zinc superoxide dismutase, and alpha-synuclein: intermediacy of tryptophan- and tyrosine-derived oxidation products', *Free Radic Biol Med,* 36 (11), 1355-65.

Zheng, L., et al. (2006), 'Autophagy of amyloid beta-protein in differentiated neuroblastoma cells exposed to oxidative stress', *Neuroscience letters,* 394 (3), 184-9.

Zhou, C., Huang, Y., and Przedborski, S. (2008), 'Oxidative stress in Parkinson's disease: a mechanism of pathogenic and therapeutic significance', *Ann N Y Acad Sci,* 1147, 93-104.

Zhu, W., et al. (2007), 'Prevention and restoration of lactacystin-induced nigrostriatal dopamine neuron degeneration by novel brain-permeable iron chelators', *FASEB J,* 21 (14), 3835-44.

Zibaee, S. (2005), 'The amyloidogenic proensity of alpha-synuclein ', (University of Cambridge).

Appendix

i. ^{1}H NMR spectrum of 3-iodo-L-tyrosine derivative

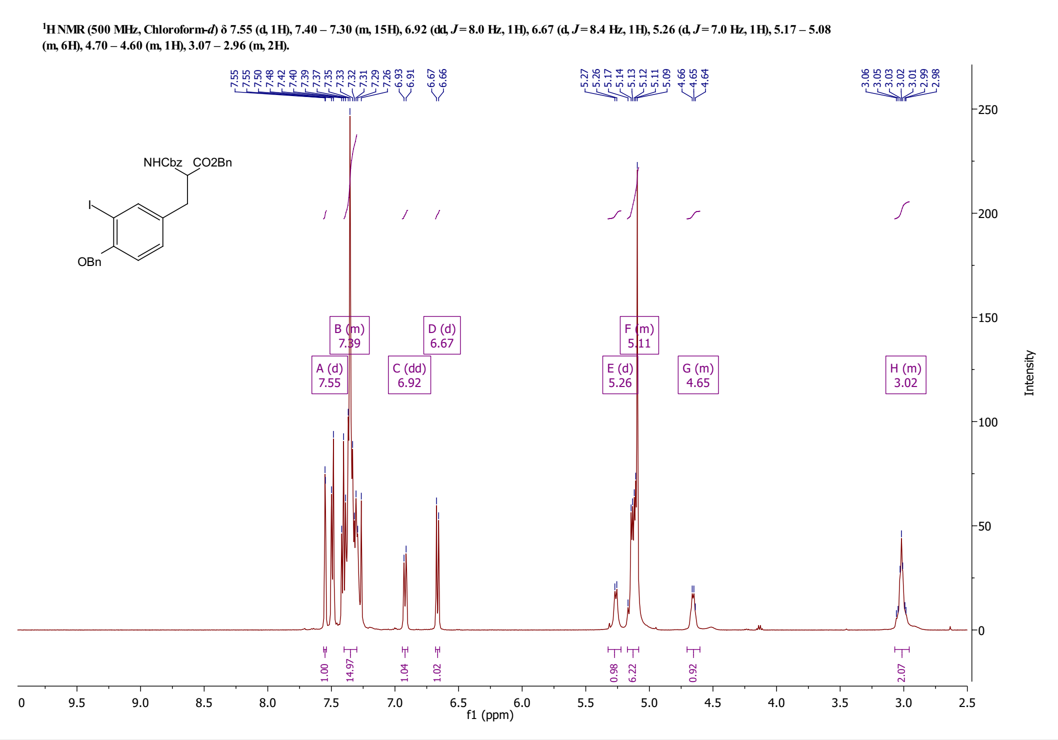

^{1}H NMR (500 MHz, Chloroform-*d*) δ 7.55 (d, 1H), 7.40 – 7.30 (m, 15H), 6.92 (dd, *J* = 8.0 Hz, 1H), 6.67 (d, *J* = 8.4 Hz, 1H), 5.26 (d, *J* = 7.0 Hz, 1H), 5.17 – 5.08 (m, 6H), 4.70 – 4.60 (m, 1H), 3.07 – 2.96 (m, 2H).

ii. ^{13}C NMR spectrum of 3-iodo-L-tyrosine derivative

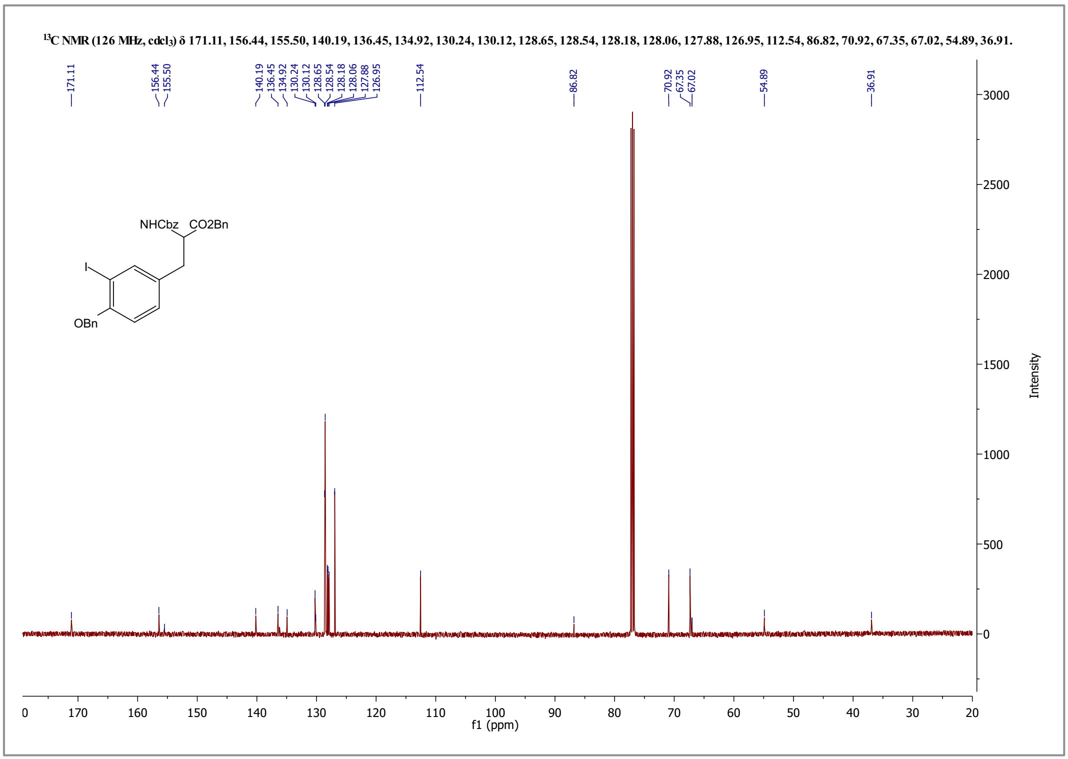

^{13}C NMR (126 MHz, cdcl$_3$) δ 171.11, 156.44, 155.50, 140.19, 136.45, 134.92, 130.24, 130.12, 128.65, 128.54, 128.18, 128.06, 127.88, 126.95, 112.54, 86.82, 70.92, 67.35, 67.02, 54.89, 36.91.

iii. ^{1}H NMR spectrum of protected dityrosine

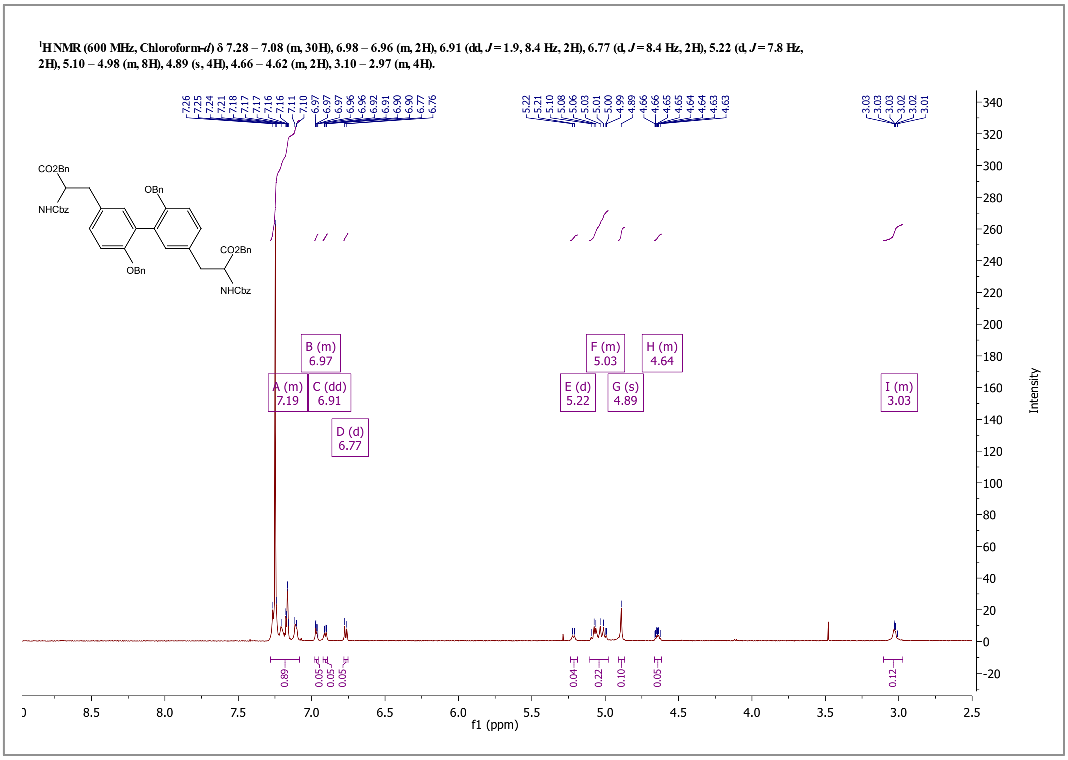

^{1}H NMR (600 MHz, Chloroform-*d*) δ 7.28 – 7.08 (m, 30H), 6.98 – 6.96 (m, 2H), 6.91 (dd, J = 1.9, 8.4 Hz, 2H), 6.77 (d, J = 8.4 Hz, 2H), 5.22 (d, J = 7.8 Hz, 2H), 5.10 – 4.98 (m, 8H), 4.89 (s, 4H), 4.66 – 4.62 (m, 2H), 3.10 – 2.97 (m, 4H).

iv. ^{13}C NMR spectrum of protected dityrosine

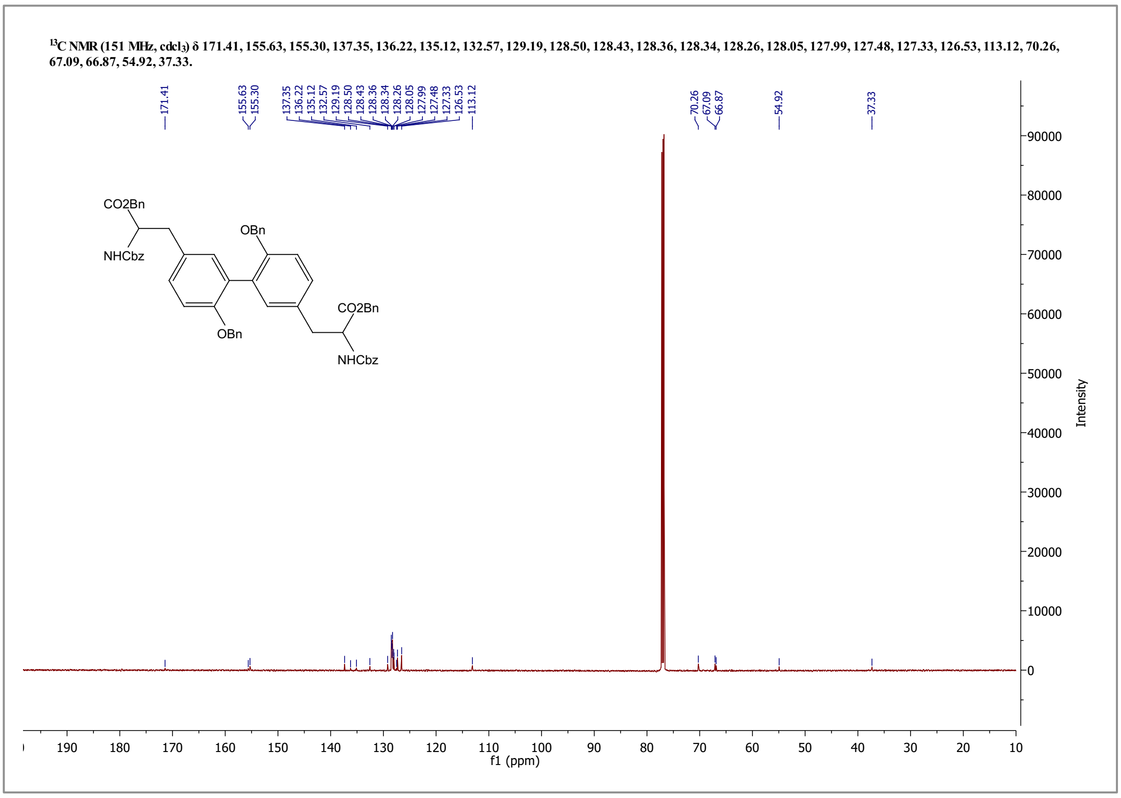

^{13}C NMR (151 MHz, cdcl$_3$) δ 171.41, 155.63, 155.30, 137.35, 136.22, 135.12, 132.57, 129.19, 128.50, 128.43, 128.36, 128.34, 128.26, 128.05, 127.99, 127.48, 127.33, 126.53, 113.12, 70.26, 67.09, 66.87, 54.92, 37.33.

v. ^{1}H NMR spectrum of diiodo diacetyl dityrosine

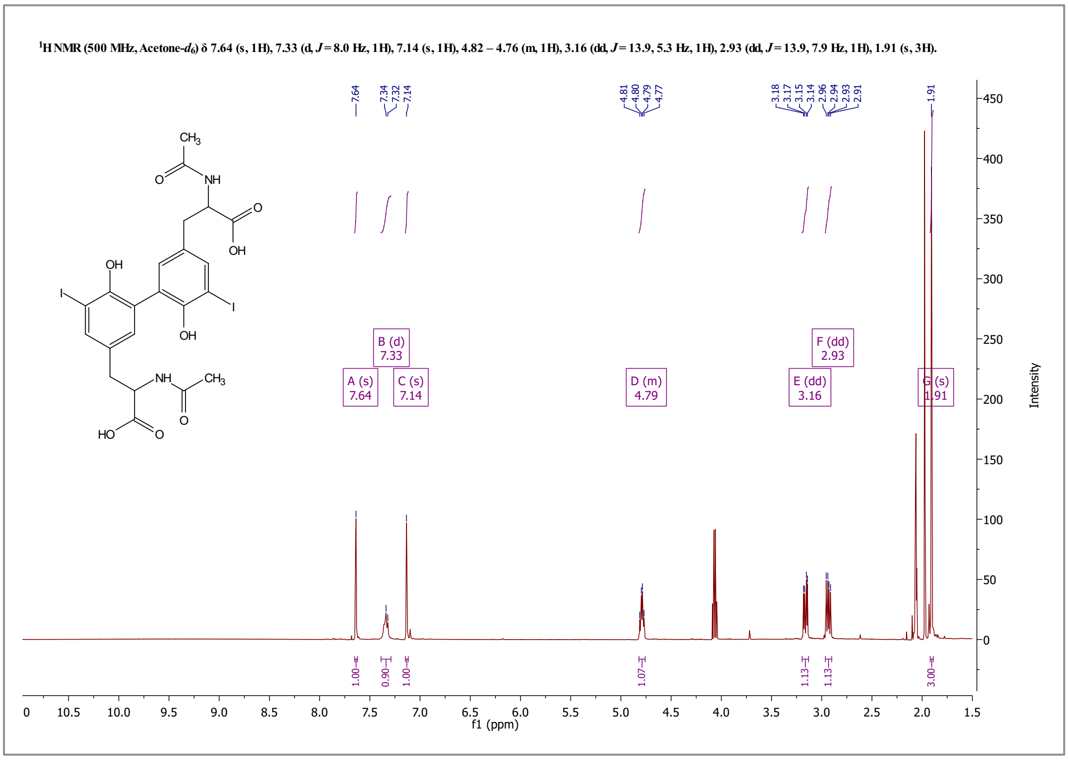

^{1}H NMR (500 MHz, Acetone-d_6) δ 7.64 (s, 1H), 7.33 (d, J = 8.0 Hz, 1H), 7.14 (s, 1H), 4.82 – 4.76 (m, 1H), 3.16 (dd, J = 13.9, 5.3 Hz, 1H), 2.93 (dd, J = 13.9, 7.9 Hz, 1H), 1.91 (s, 3H).

vi. ^{13}C NMR spectrum of diiodo diacetyl dityrosine

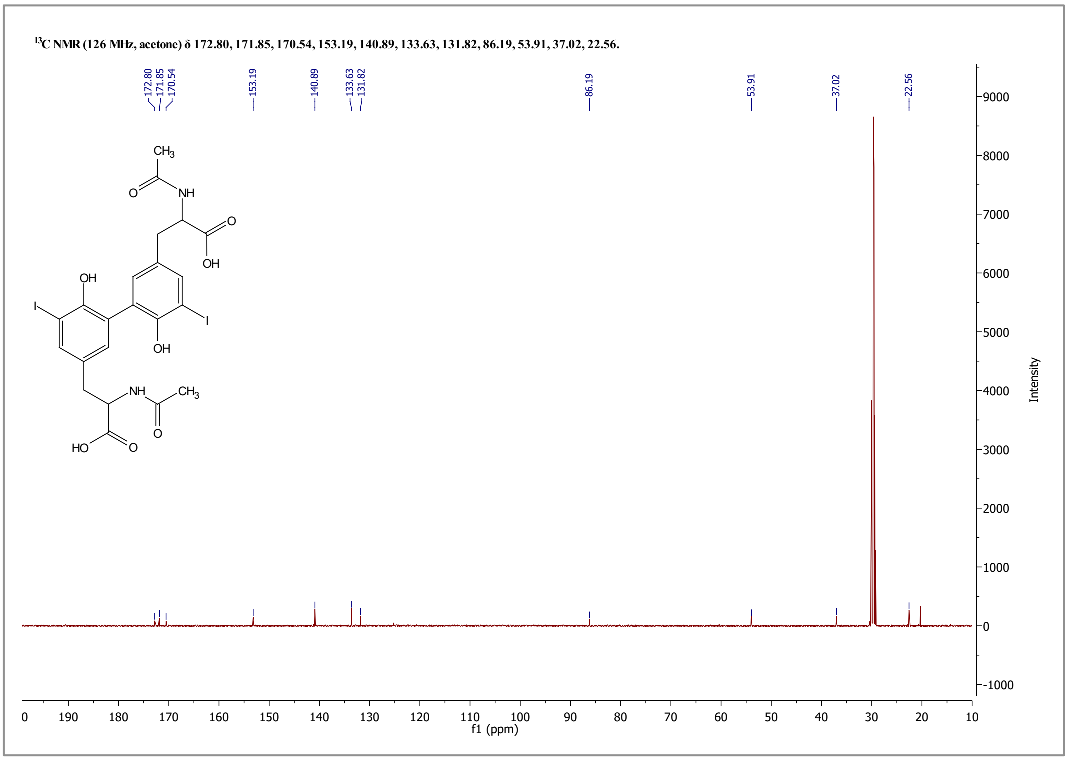

^{13}C NMR (126 MHz, acetone) δ 172.80, 171.85, 170.54, 153.19, 140.89, 133.63, 131.82, 86.19, 53.91, 37.02, 22.56.

vii. TEM immunogold labelling of dityrosine in oxidised Aβ42 fibrils

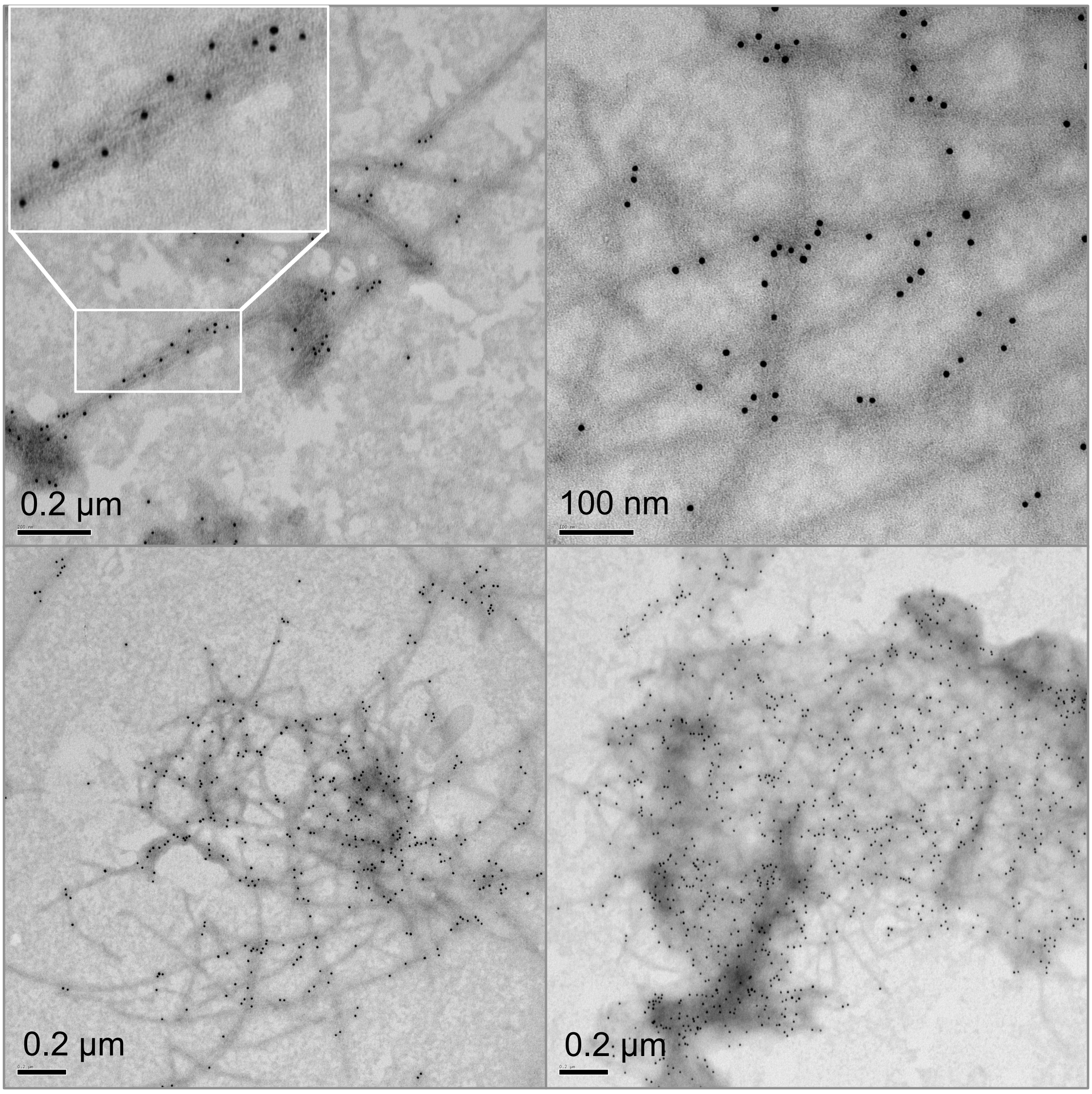

viii. Immunogold labelling TEM imagesshowing showing neuroblastoma cells treated with oligomeric Aβ

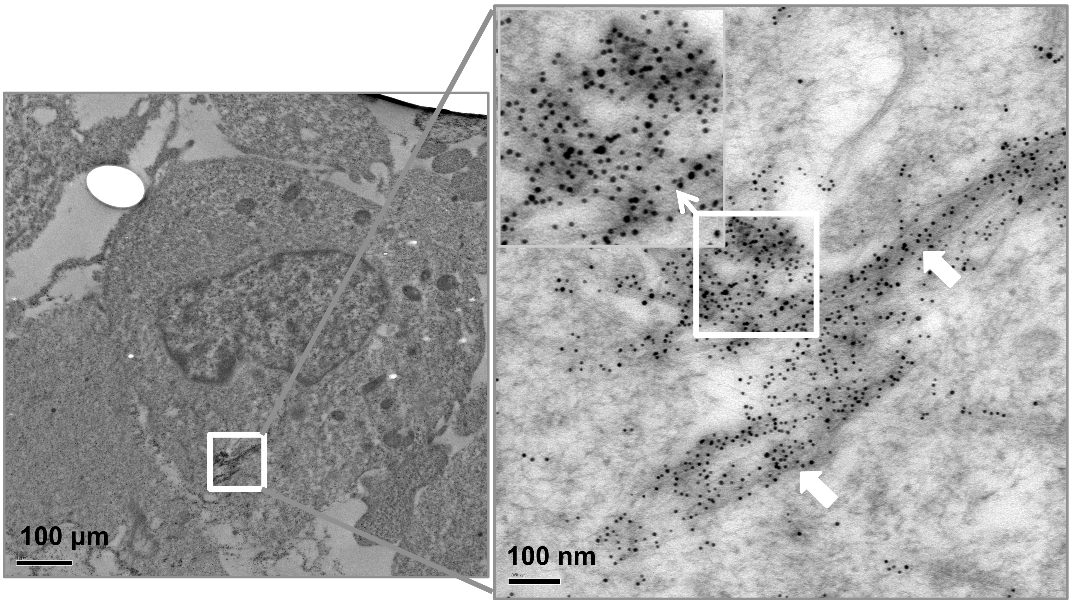

ix. TEM image of negative immunogold labelling control

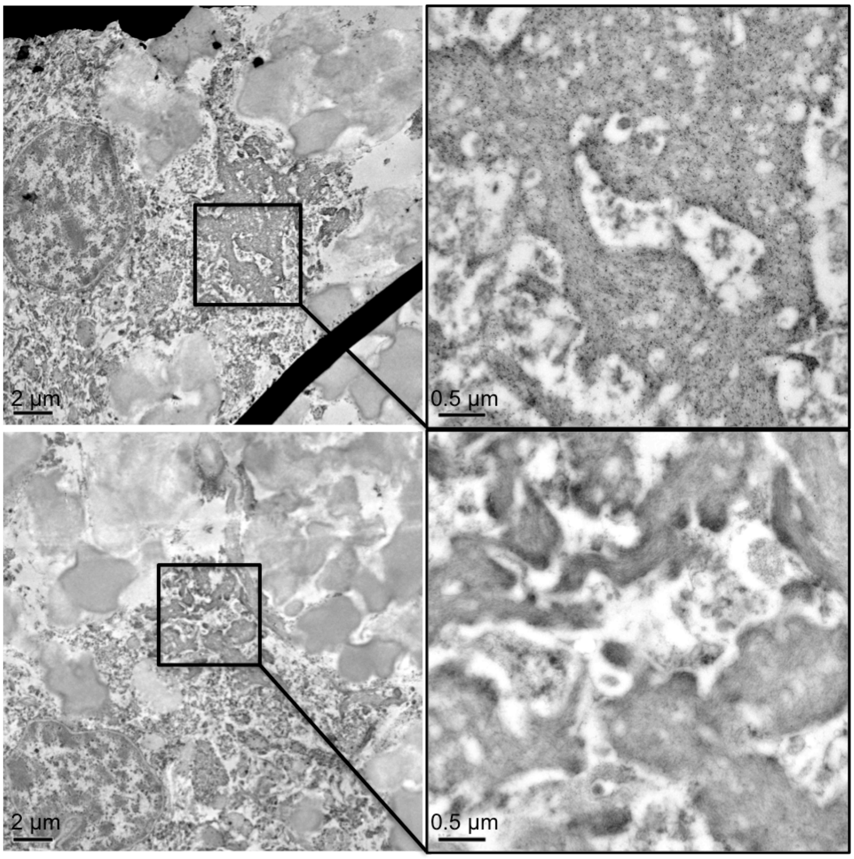

x. *Immunogold labelling TEM images of dityrosine in CSF*

CSF from AD affected patient

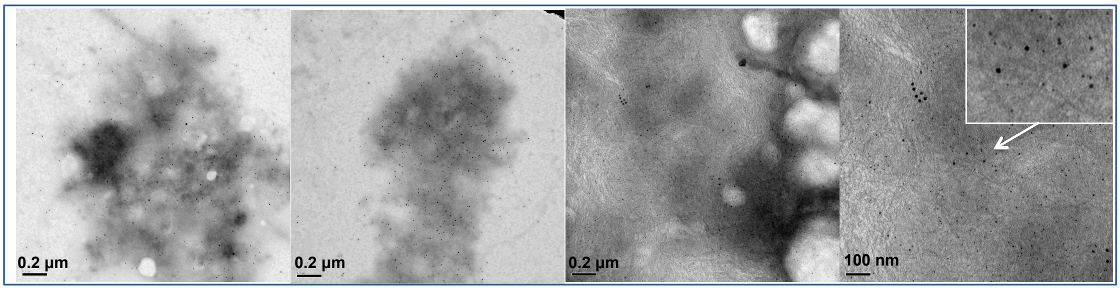

CSF from age matched control